QUANTIFYING ICE NUCLEATION BY SILVER IODIDE AEROSOLS

PAUL JUDSON DEMOTT

Colorado State University

DEPARTMENT OF ATMOSPHERIC SCIENCE

PAPER NO. 466

QUANTIFYING ICE NUCLEATION BY SILVER IODIDE AEROSOLS

By

Paul Judson DeMott

This report was prepared with support provided by National Science Foundation Grants ATM-8519370 and ATM-8813345. Principal Investigator Lewis O. Grant

Department of Atmospheric Science
Colorado State University
Fort Collins, Colorado

May 1990

Atmospheric Science Paper No. 466

ABSTRACT

QUANTIFYING ICE NUCLEATION BY SILVER IODIDE AEROSOLS

Laboratory studies of artificial ice nucleating aerosols used for weather modification by cloud seeding have generally been inadequate for describing their complex action in the varied temperature, pressure humidity, and cloud conditions that can be encountered in the atmosphere. This study provides a quantitative framework for predicting ice formation by aerosol particles based on experiments which specifically target currently accepted mechanisms by which ice can form. A physical system for reproducing realistic atmospheric cloud conditions, the Colorado State University dynamic (controlled expansion) cloud chamber, is described. Physical simulations of adiabatic cloud formation and growth are demonstrated. Methodologies were also formulated to use the cloud chamber and other available intrumentation to isolate the action of ice nucleating aerosols by accepted primary ice nucleation modes. These methods were applied to the study of two chemically different silver iodide (AgI)-type aerosols, generated in the exact form in which they have been used for seeding natural clouds. The results were formulated as a function of basic thermodynamic quantities and particle size. An available one dimensional numerical cloud model with microphysical detail was adapted for the equivalent simulation of experiments performed in the cloud

chamber. The model was utilized as a diagnostic tool to estimate water supersaturation in association with experiments and it was used for comparison of the predictions of new ice nucleus formulations with observations from generalized seeding simulations conducted in the cloud chamber. The nucleant and mode-specific formulations represent vast improvements compared to available formulations for "pure" AgI. The general implications of these new results were tested by using the model to simulate a few common seeding situations in the atmosphere, and the transferability of results was evaluated by modeling two actual seeding experiments conducted in summertime cumuli. Within the limitations of the cloud model used, agreement with the atmospheric results was very good. The results of this study should be most useful for designing standard and better methods for the quantitative study of ice nucleation by artificially generated and natural aerosols, and for evaluating cloud seeding methodologies and potential seeding effects using more complex microphysical-dynamic cloud models.

Paul Judson DeMott
Atmospheric Science Department
Colorado State University
Fort Collins, CO 80523
Spring 1990

ACKNOWLEDGEMENTS

Various stages of this research were conducted under National Science Foundation Grants ATM-8519370 and ATM-8813345. Facility improvements were also made possible with the past support of the U.S. Air Force and the Alberta Research Council of Canada. This manuscript culminates several years of research, so there are numerous individuals to thank. First, to Professor Lewis O. Grant for his guidance and for giving me the responsibility and opportunity to freely pursue my ideas. To Dr. William G. Finnegan for his early guidance, for stimulating the interest that I will always have in nucleation, and for the lasting inspiration of his acute curiosity and unbound ideas. Very special thanks go to Dr. David C. Rogers for his ready conversations and assistance in data reduction. The scheme for deconvoluting ice crystal measurements was entirely the result of his resourcefulness. Also, very special thanks to Mr. Brian Jesse for his invaluable technical assistance at the Cloud Simulation and Aerosol Laboratory. Thanks also to Dr. William Cotton and Dr. Branka Ladanyi for their careful readings of the manuscript and suggestions made. Thanks are due to Mr. Randy Horn for design of many of the instrumentation and data acquisition systems, and numerous discussions regarding these after his departure from CSU; Dr. Jeffrey Stith of the University of North

Dakota, for discussions of the field data used and for providing additional information on these observation; Mrs. Lucy McCall for special drafting; Mr. Mark Branson, for performing much of the rapid expansion experimental series; Mrs. Janis Davis for her help in detailing the manuscript. Finally, I want to thank my parents, John and Tina DeMott, for their enduring support of my pursuits.

TABLE OF CONTENTS

LIST OF TABLES

LIST OF FIGURES

I. INTRODUCTION

1.1 Background

The research reported in this dissertation has been conducted to define and quantify important fundamental aspects of ice nucleation by artificial ice nuclei in supercooled clouds. Experiments have shown that temperature and water vapor supersaturation are of primary importance for the formation of ice (e.g., Grant, 1971; Gagin, 1972; Vali, 1975;1976). It is also known that the chemical composition, the mechanisms (modes) of nucleation, and the history of the nucleating particles can be of primary importance (Edwards and Evans, 1971; Cooper, 1974; Gerber, 1976; Schaller and Fukuta, 1979; Rogers, 1982; DeMott et al., 1983; Blumenstein et al., 1987), but descriptions of these aspects are far from complete. In addition, it is not clear to planners of weather modification programs whether to or how to implement the evolving understanding of the complex function of ice nuclei into decision making; ie., what seeding agent to use for specific cloud characteristics and how, when, and where to deliver it for optimum effect (Hindman, 1985; Braham, 1985; AMS, 1986).

Seeding a cloud with a silver iodide (AgI) containing nucleant aerosol is expected to result in the production of ice crystals in the supercooled parts of the cloud. The assumption is made that the nuclei will function to form a specified concentration of ice crystals if delivered to the appropriate cloud location in a known concentration.

The seeding effect on ice crystal concentrations is expected to follow the estimate of the nucleating activity of the seeding agent, which has historically been determined for a variety of generation devices by tests in an isothermal cloud chamber (Grant and Steele, 1966; Garvey, 1975). For most cloud seeding programs, this approach does not adequately consider the differences between the conditions in the real cloud and the environmental conditions in the cloud chamber where the nucleant was characterized. This has been a necessary simplification, since there is not enough known about the differences in nuclei response to ambient conditions, transport through warm cloud, or seeding method. A complete description of these effects is not available for even one nucleant.

Cloud models can play an important role in answering questions concerning the consequences of seeding a supercooled cloud with an ice nucleating aerosol, but model descriptions of nucleation processes must be derived from experimental evidence, because adequate descriptive theories do not exist. An example of an experimental and model interactive study was demonstrated by the incorporation into computer simulations by Lamb et al. (1981) of mathematical descriptions of secondary ice formation processes derived from laboratory studies of this phenomenon by Hallett and Mossop (1974). The characteristics of clouds which form by simple lifting over short time periods (orographic clouds, cumulus clouds and some stratiform clouds) can be closely simulated with computer models. However, mathematical parameterizations or simplifications based on analogy are often used in models in place of physical laws, in order to circumvent limits of computer power and cost or when theory and understanding are insufficient or incomplete.

The tacit assumption is made that these simplifications are close enough to reality that the results of the simulation will represent the atmospheric situation correctly. Such assumptions are typically crude, at best, and frequently not basically adequate. This is the case for many aspects of ice nucleation in clouds.

Uncertainties about ice nucleus activity and nucleation mechanisms are reflected in the way they are incorporated into computer simulations. Nucleation mechanisms are usually differentiated in microphysical models (e.g., Young, 1974a; Cotton et al., 1986), and some regions of cloud are theoretically expected to favor some mechanisms of nucleation over others. For example, Young (1974b) has shown theoretically that contact-freezing nucleation would proceed faster in an evaporating cloud because of enhanced thermophoretic collection of aerosol and because of evaporative cooling of cloud drops; however, there is little experimental evidence of this preferential activity. For a particular type of ice nucleating aerosol, there is as yet no theoretical basis for differentiating between its ability to act by, respectively, condensation-freezing or immersion-freezing modes of nucleation. This needs to be determined experimentally. Likewise, the difference in nucleating activity of an aerosol which can arrive in a supercooled cloud by several different thermodynamic paths is largely unresolved; there exists little theoretical or experimental information to infer any difference in ice nucleus function. Matthews et al. (1972) theoretically predicted ice nucleating aerosols would have short lifetimes within cloud droplets because they would dissolve; however, this was not evident in preliminary studies by DeMott et al. (1985).

With the development of the CSU dynamic (controlled expansion) cloud chamber (DCC) some of the severe limitations of the laboratory study of ice nuclei have been removed or ameliorated. No substrate is needed to capture or support the ice nucleating particles (as for membrane filters). Gradients in temperature and supersaturation are controlled so that conditions in the chamber are nearly uniform, unlike conditions in static or laminar flow chambers. Furthermore, cloud formation rates are comparable with those in many natural clouds, and cloud condensation temperatures and pressures can be controlled over most of the atmospheric range. The different environmental paths by which nuclei arrive at a certain point in a cloud can also be simulated in the cloud chamber. As will be discussed, cooling rates and particulars of the ice crystal detection system introduce some complexities, but these are surmountable. All of the factors affecting nucleation can be measured and independently controlled in cloud chamber experiments and in theoretically based computer model simulations. Experiments of this type have not been done before.

1.2 Objectives of Research

The general objectives of this research program were to design a series of experiments to study the ice forming processes of artificial ice nuclei under a variety of well-defined cloud environmental conditions (equivalent to conditions in atmospheric clouds) in the laboratory; to compare results of these laboratory experiments with the best descriptions currently available for use in numerical cloud models; to provide experimentally determined descriptions of ice formation which can be incorporated in conceptual and quantitative

models; to provide information for direct comparison of laboratory and model results with atmospheric clouds; and to provide information for planning cloud seeding research and operations.

These general objectives can be separated into seven specific objectives for this research. These are:

1. Define and demonstrate appropriate experiments for using a continuous expansion cloud chamber and other available tools to assess the separate and combined roles of the four hypothesized primary modes of ice nucleation (deposition, condensation-freezing, immersion-freezing, and contact-freezing, as defined in Chapter 4) for any ice nucleating aerosol.

2. Using defined experimental methods, determine the efficiencies, nucleation rates and mechanisms of two commonly used, chemically different ice nucleating aerosols, as they relate to cloud temperature, supersaturation and droplet concentration. The effect that condensation temperature and parcel history of temperature and humidity have on the nucleation modes, efficiencies and rates are also assessed.

3. Perform numerical cloud model simulations using the same initialization criteria and expansion rates as cloud chamber experiments. An existing detailed microphysical model (Young 1974a) is used. Areas where current descriptions of artificial ice nuclei function are unsatisfactory are identified, based on comparing the model results with those from the cloud chamber.

4. Develop functional, quantitative descriptions of the ice nucleating behavior of the aerosols under varying conditions of cloud temperature, saturation, and droplet characteristics based on experimental results.

5. Explore the implications and validity of the new descriptions of ice nucleant behavior to specific cloud conditions. This is initiated by incorporating them into Young's. Comparisons are made to experimental data and some simulations relevant to summer and winter cloud seeding are performed.

6. Compare simulations of seeded summertime clouds using the one-dimensional Young model to special field measurements for cases where one of the aerosols studied was utilized.

7. Final specific objectives are to define a minimum experimental effort for describing the action of any ice nucleant in atmospheric clouds and suggest procedures for evaluating these results in seeding field experiments and operational programs.

1.3 General Approach

The approach to experiments was mechanistic, as defined by Vali (1985). In this approach, the total nucleation activity is considered to be the sum of the contributions from deposition, contact-freezing, immersion-freezing and condensation-freezing nucleation modes. A clarification is needed in this regard. The terminology nucleation mode or nucleation mechanism will be used throughout this dissertation,

since this is an accepted terminology. It should be quite clear, however, that this terminology truly refers to the macroscopic process (sometimes multi-stage) by which an ice crystal forms, and not the microscopic mechanism that describes how the ice phase first appears or is ordered on a particle surface. Experiments were designed to systematically isolate nucleation mechanisms operative by direct measurement and subtraction methods, primarily using continuous expansions experiments. For the two nucleants employed, certain nucleation mechanisms are favored or dominant under some cloud conditions because of chemical and physical properties and the history of environmental exposure. Flexibility was inherent in the approach, but not in the basic framework.

In all experiments, the ice nucleating aerosol, generated in the same way as in operational weather modification projects, was sampled and diluted as needed with dry air before injection into the DCC. Two types of seeding materials were used. These were AgI-AgCl and AgI-AgCl-NaCl aerosols. These aerosols represent the most efficient AgI-type aerosols actively used for weather modification, based on current knowledge. Most experiments utilized narrow size cuts of particles, in order to differentiate particle size effects. When such nearly monodisperse nuclei were desired, the sample was first transferred to a particle size classifier. The aerosols were injected directly into the DCC before or after cloud formation, depending on the desired measurement conditions. Total aerosol concentrations were measured beforehand. Two particle sizes were generated for the experiments: distributions of particles closely centered at 0.03 μm and 0.07 μm diameter. This covered a sufficient range of dry particle mobility and

expected size effects for nucleation. Experiments were also performed with the full polydisperse particle size distributions for comparison.

Comparisons made between cloud chamber experiments and numerical model simulations were made "equivalent" in the sense that temperature, pressure, humidity and ascent rate were identical. Cloud condensation nuclei activity was controlled in the laboratory experiments and specified in the model simulations. Items which were not simulated were considered to be of secondary importance in these experiments. They include turbulent mixing, interactions with precipitation size particles, radiation effects, and electric field and particle charging effects. Additionally, some aspects related to the long term residence of ice nuclei in the atmosphere, namely photodeactivation and potential reactivation following evaporation, were not studied.

Comparative field experimental data were obtained from tracer/seeding experiments conducted in North Dakota cumulus clouds (Stith et al., 1990). These experiments used AgI-AgCl aerosols. Specific experimental plans are outlined in chapter 4, and are discussed further in Chapter 5.

1.4 Expected Utility of Results

The results of this research should have a number of applications, as enumerated here.

1. It is important to compare laboratory experiments and computer model simulations and to evaluate how well the results can be extrapolated to real atmospheric situations. The results from this work should provide a more valid description of the early

stages of cloud seeding than is currently available, and they will provide some comparisons between laboratory results and computer model simulations of cloud and ice nucleation for well defined experimental conditions.

2. The results will serve the needs of conceptual models and computer models for accurate descriptions of ice nucleating behavior along different paths into and through clouds.

3. The results will provide information to be applied as guidance in operational weather modification programs, for choosing seeding agents and seeding methods. This is useful for planning experimental tests and for evaluating program effectiveness.

4. The results provide a data base for comparing to existing theories, or for formulating new ones, for ice nucleation by aerosols.

5. Establish simple general procedures for characterizing any ice nucleant, natural or artificial.

II. BASIS FOR RESEARCH

2.1 Status of Experimental Knowledge of Ice Nuclei Function

Standard terminology for the nucleation modes by which ice can form have been given by Vali (1985). These are,

> "*Deposition nucleation*. The formation of ice in a (supersaturated) vapor environment."
>
> "*Condensation freezing*. The sequence of events whereby a cloud condensation nucleus (CCN) initiates freezing of the condensate"
>
> "*Contact freezing*. Nucleation of a supercooled droplet subsequent to an aerosol particle's comming into contact with it."
>
> "*Immersion freezing*. Nucleation of supercooled water by a nucleus suspended in the body of water."

Vali pointed out that "broader, narrower, or perhaps altogether different definitions might be needed at times". This is true for this study, as will be made clear in Chapter 4. Regardless of the exact terminology used, there is much laboratory evidence (Edwards and Evans, 1960; Langer et al., 1978; Schaller and Fukuta, 1979; Tomlinson, 1980; Rogers, 1982; DeMott et al., 1983; DeMott et al., 1984a,b; Blumenstein et al., 1987, DeMott, 1988; Feng and Finnegan, 1989) that artificial ice nucleus aerosols will function by all of these various nucleation modes and can nucleate ice at different rates, depending on the chemical and physical properties of the nuclei and on the environmental conditions (temperature, saturation ratio and droplet concentration).

Discussion here is limited to AgI-type ice nucleants to be most relevant to the present study. For AgI-type nucleants, at least until recently, there has clearly been a dearth of studies isolating the action of specific nucleation mechanisms for aerosols as they are produced in actual cloud seeding. Instead, most earlier studies were done using thermally produced AgI (for example, heating AgI on metal wire). Presumably, this was done because studies were motivated by the desire for a basic understanding of ice nucleation processes, so direct relevance to cloud seeding was not an important requirement. Nevertheless, these studies demonstrate some of the characteristics of the different nucleation modes for AgI aerosols.

Studies of nucleation of ice from the vapor phase onto AgI aerosols have shown this mechanism to be the least efficient of all, but it possesses a strong dependence on particle size. Using small particles ($< 0.01\mu m$ radius) produced by reacting iodine vapor with silver aerosol deposited onto a gold surface and exposed to relative humidity near 98%, Edwards and Evans (1960) found less than 0.5% of these to form ice down to a temperature of -18.5°C. For polydisperse thermally produced AgI in free suspension in ice-thermal diffusion chambers, both Schaller and Fukuta (1979) and Detwiler and Vonnegut (1981) inferred nucleation from the vapor as warm as -6°C and found activity to be related at all temperatures to ice supersaturation. Schaller and Fukuta noted nucleation activities as high as 6.4% of the particles present ($0.3\mu m$ median diameter) below -12°C, while Detwiler and Vonnegut ($0.1\mu m$ median diameter particles) noted 1% activation for a similar range of ice supersaturation and temperatures.

Various studies have differed on the degree of water supersaturation required to trigger condensation-freezing nucleation by AgI aerosols, or to cause the immersion of a particle in a cloud droplet that might freeze at some colder temperature. Edwards and Evans (1960) showed that supersaturation had to exceed 10% for condensation alone on their small particles. Langer et al. (1978) claimed similar results for nearly monodisperse "pure" AgI particles with diameters between 0.02 and 0.12μm. When condensation was forced on these AgI aerosols, nucleation activity was as much as 100 times the activity by deposition. In contrast, Schaller and Fukuta (1979) found condensation-freezing to readily operate at small finite water supersaturations, increasing sharply with higher supersaturations.

Contact-freezing nucleation appears to be a very efficient nucleation mode for AgI aerosols, rate limited by the collision process with cloud droplets. This mechanism has been examined by allowing droplets to settle through an aerosol cloud or by using very high cloud droplet concentrations in mixing chambers. Typically, it has been found that the activity by contact-freezing exceeds the activity by immersion-freezing at similar temperatures (Ghokale and Goold , 1968; Langer et al., 1978). In the study by Ghokale and Goold, the surface nucleation of millimeter-sized droplets was found to occur even at -5°C, while the purposeful submersion of the particles in drops did not lead to efficient nucleation at this warm temperature. Contact-freezing activity has been found to increase with particle size and decreasing temperature. Sax and Goldsmith (1972) showed fractional activation to approach 1 at -18°C for polydisperse (0.02 to 0.03μm diameter) thermally generated AgI. They also demonstrated that the

occurence of collisions at cloud temperatures warmer than 0°C did not significantly reduce the activity of the AgI, at least at tempertures below -10°C. Their experiments did not have the proper sensitivity at warmer temperatures.

A complete quantitative characterization of an ice nucleus should include descriptions of its action to form ice crystals by all of the potential nucleation modes. Only a few studies have been performed with this intent, most notably those of Langer et al. (1978) and Schaller and Fukuta (1979). Unfortunately, these most comprehensive of studies performed previously suffer from their lack of relevance for the actual aerosols used in weather modification. Both studies noted generated pure AgI thermally. This is not a method used operationally. Most relevant to the research reported in this dissertation are studies of nucleation by AgI aerosols produced by the solution combustion method operationally employed for both ground-based and airborne aerosol generation. In this method, solutions of AgI, acetone, water and some type of solubilizing agent for the AgI are burned. Although these aerosols can act to form ice by all of the defined nucleation modes, the predominant mode is influenced by the particular solution chemistry. When the solubilizing agent is ammonium iodide (NH_4I), the NH_4I is destroyed by combustion and the resultant nucleant is simply AgI, with little hygroscopic character (St. Amand et al., 1971). Other chemicals can be added to this solution to cause the formation of mixed or composite nucleus aerosols and to synergystically influence the efficiency of ice nucleation without changing the essentially hydrophobic character of the nuclei. An example is the AgI-AgCl ice nucleant studied by DeMott et al. (1983), which is generated by

combustion of $AgI \cdot NH_4I$-acetone-water solutions containing ammonium perchlorate (30 mole % with respect to AgI was found to be optimal). Both the AgI and AgI-AgCl nuclei produced by solution combustion have been shown to function primarily and preferentially as contact-freezing nuclei in the high concentration, water saturated, conditions in the CSU isothermal cloud chamber. Other experiments conducted at saturation ratios between ice saturation and water saturation in the CSU dynamic cloud chamber have demonstrated that these nuclei can initiate ice formation by a deposition mechanism, at least at temperatures colder than about -16°C (DeMott et al., 1984b). Size effects were not investigated in these preliminary studies. Feng et al. (1989) have also observed nucleation by these aerosols in cloudless air, as warm as -10°C. However, humidity was not well controlled in their study. Finnegan and Pitter (1988) have also shown that the AgI-AgCl aerosols may act very rapidly by a condensation-freezing nucleation mode when introduced directly into cloud, due to high supersaturations generated with the addition of water vapor from combustion. Comprehensive quantitative descriptions of these results for AgI-AgCl aerosols have not been developed.

Solution combustion type ice nuclei generators can be made to produce aerosols that form ice preferentially by condensation-freezing or immersion-freezing nucleation mechanisms. One means by which this occurs is when a complexing and solubilizing reagent such as sodium iodide (NaI) is used together with AgI (Mossop and Jayaweera, 1969). Blumenstein et al. (1987) have demonstrated that the widely used AgI•NaI aerosols nucleate ice by two different condensation-freezing modes; one acts quickly (within seconds) in the presence of a transient

supersaturation with respect to water, and the other, at water saturation, is much slower (minutes). DeMott et al. (1983) had previously distinguished these potential mechanisms as condensation to aqueous embryos followed by freezing, and condensation to droplets followed by freezing.

A method for generating more efficient condensation-freezing ice nuclei (AgI-AgCl-xNaCl) has been described by Feng and Finnegan (1985; 1989) and has come into use in the operational weather modification community over the past few years. Results of experiments in the dynamic cloud chamber (DeMott, 1988) show that the activity of a polydisperse aerosol of this composition is insensitive to large changes in ambient droplet concentrations for equivalent injections into expansion-formed clouds; i.e., the nuclei function predominately by condensation-freezing or at least form cloud/haze drops before droplet-nuclei contact has time to occur. Below water saturation, Feng et al. (1989) found these aerosols to be several times to 10 times as efficient in apparently nucleating ice by deposition, compared to AgI-AgCl aerosols.

Preliminary experiments in the CSU dynamic cloud chamber have also suggested that nuclei aerosol injection prior to warm cloud condensation influences both the mode and rate of formation of ice by AgI-AgCl aerosols (DeMott et al., 1984a). AgI-AgCl-4NaCl aerosols showed no apparent sensitivity to their time history in cloudy air.

2.2 Descriptions of Ice Nuclei Behavior in Cloud Models

Nucleation mechanisms, rates and effectivities can directly and indirectly influence the nature of numerical cloud model results. Lamb

et al. (1981), developed a model to study dynamic seeding effects in deep convection over Florida. This model predicted that glaciation ultimately occurred due to natural secondary processes (ice multiplication), but seeding initiated these mechanisms earlier. In seeded cases the timing of latent heat release depended on the mechanism of action of the nuclei (i.e., faster for deposition, slower for contact freezing). Orville et al. (1984) found unexpected dynamic effects in AgI seeding simulations of stratus clouds. This clearly related to the presumed nucleation ativity and rates of ice crystal formation (instantaneous). Orville et al. noted the potential inadequacy of the nucleation scheme employed and its importance in the quantitative results.

Numerical cloud models have been used to simulate the effects of various seeding techniques in different types of clouds. The ice nucleation schemes employed by the models vary widely. They are usually based on a combination of theory and laboratory results that are not necessarily compatible. Due to the lack of information, the schemes are seldom nuclei-specific. Young (1974a) included both deposition and contact nucleation (via Brownian and phoretic transport processes) in a detailed microphysical cloud parcel model. Only contact-freezing nucleation was used in the published seeding simulations (Young, 1974c), and the nucleus effectivity spectrum employed was not representative of most that have been measured. Hsie et al. (1980) simulated both contact-freezing and deposition nucleation in a study of seeding effects in continental cumulus clouds using a 2-D time-dependent model. The nucleation mechanisms were applied to the laboratory-measured effectivity spectra of a nucleus for which the

mechanisms were not known. The relative contribution to ice crystal formation by each mechanism was based on the theoretical work of Cooper (1974) which has not been directly verified. More common and simplistic schemes (e.g., Plooster and Fukuta, 1975) use the laboratory-measured effectivity spectra to specify the number of ice crystals formed, with no regard to mechanism or a consideration of the potential time required for nucleation. None of the above mentioned models explicitly include condensation-freezing or consider differences in nuclei response with thermodynamic path.

Blumenstein et al.(1987) developed time and temperature dependent empirical expressions from experimental data obtained in the CSU isothermal cloud chamber and applied these in Rauber's (1981) two dimensional orographic cloud model. Her laboratory study demonstrated slow and fast (rates) condensation-freezing nucleation processes by AgI•NaI aerosols. Near water saturation, the freezing of droplets grown on aerosols determined the rate at which ice crystals formed in the isothermal chamber. This rate was expressed as a first order rate law with a temperature dependent rate coefficient. The process was slow (up to 100 minutes for completion), but the rate coefficient increased with colder temperatures. In contrast, for water supersaturations, the values of which were not defined, the nucleation of ice proceeded very rapidly (within seconds), such that crystal diffusion growth and crystal sedimentation rates determined the rate of collection of ice crystals. Also, nucleation activity increased in the supersaturated case. DeMott (1988) has shown that, at least for cloud parcels undergoing moderate expansion rates (2.5 m s^{-1} equivalent updraft) in which sustained supersaturation with respect to water might reasonably

be expected, the fast mechanism seems to prevail. The slow and fast nucleation processes in the Blumenstein analysis yielded large differences in the amount and targeting of seeded snowfall in model simulations.

2.3 Ice Nuclei Function in Real Clouds

There are few atmospheric seeding tests from which the rates and mechanisms of nucleation can be deduced. One such study is that of Davis (1974). He studied ice nucleation effectiveness and rates of ice crystal formation for combustion-produced AgI aerosols in the CSU isothermal chamber and in Elk Mountain (Wyoming) cap clouds. The relatively simple clouds used and the ground access to sampling sites at different cloud temperatures provided an effective outdoor laboratory for testing the transfer of cloud chamber results to general atmospheric clouds. Excellent agreement was found between the ice nucleation yields (g^{-1} AgI) in the laboratory studies and in the cap clouds for aerosols produced from AgI•NH_4I-acetone-water solutions. This agreement was realized after assuming that contact-freezing nucleation was the dominant nucleation mode in both the laboratory and the field clouds, then adjusting the field data (based on the particle sizes and the cloud droplet size distribution observed) to determine the yield that would have been realized at any temperature if the nuclei had resided at that temperature for infinite time. Davis correctly inferred that contact-freezing was the dominant nucleation mode for these AgI aerosols in the isothermal cloud chamber. However, he did not conduct experiments to determine the potential contributions of other mechanisms. Additionally, there are inherent limits to the

type of field experiment he conducted. Primarily, the continuous production of airborne ice crystals from blowing snow near a mountain surface competes with seeding and is an uncontrollable factor (Rogers and Vali, 1988). Finally, it is worth noting that Davis found that AgI•NaI aerosols also continuously nucleated fresh ice crystals with time in the cap clouds. This suggests that the fast condensation-freezing mechanism measured by Blumenstein et al. (1987) does not occur in these weakly dynamic (and probably very low water supersaturated) clouds.

Recently, some careful observations of the evolution of ice in seeded cumulus clouds have been conducted that are of direct relevance to the studies reported in this dissertation. In these experiments, the concentrations of sulfur hexaflouride tracer and ice crystals formed by AgI-AgCl aerosols released simultaneously into cumulus clouds in North Dakota have been measured as a function of time after seeding (Stith et al., 1990). This permitted estimates to be made of the active fractions of ice nucleating aerosols versus time and temperature. The time evolution of ice crystals formed (fractions of aerosols nucleating) have been shown to crudely agree with predictions based on the results of DeMott et al. (1983), and a predominance of the contact-freezing nucleation mode (Stith et al., 1990). No attempt was made to make a more exact comparison using an appropriate numerical model to account for aerosol scavenging rates as a function of the observed cloud droplet size distribution. Also, the possibility of the function of other nucleation mechanisms was not considered.

Other field studies have produced results which indicate important distinctions between the nucleating aerosols employed. For example,

English and Marwitz (1981), Marwitz and Stewart (1982) and Kochtubajda and Rogers (1984) reported the continuing production of small ice crystals in cumulus clouds that had been seeded with AgI containing nucleant aerosols generated by pyrotechnic combustion. They attributed this to continuing nucleation by the AgI aerosol. This seeding effect was quite different from CO_2 seeded clouds which contained small ice crystals for only the first few minutes following seeding. Precipitation from AgI seeded clouds also persisted much longer than from CO_2 seeded clouds (English et al., 1984). Differences like this might occur in similar situations where the ice nuclei function is not well defined, but it is assumed that the seeding effect is a constant; differences in outcome (such as radar echo features or precipitation location or characteristics), which could be caused by ice nucleation processes, could be incorrectly attributed to some other cause.

Recent field studies in orographic clouds in Colorado and Montana that clearly establish that artificial IN can be transported over a target (by ground or air) in sufficient quantities to induce observable microphysical effects (Holdroyd et al., 1988, Super and Heimbach, 1988; Super and Boe, 1988, Super et al., 1988) have also confirmed that potential ice nucleation activity is not instantly achieved at seeded temperatures. Holdroyd et al. made crude estimates of nucleus concentrations potentially "active" based on aircraft measurements with an NCAR ice nucleus counter above ground seeding locations. The level of quantification in the study is not justified because the actual ice nucleus counter used was not calibrated versus an absolute standard (ie., a CN counter or CSU isothermal cloud chamber) for the exact aerosols used (AgI from $AgI \cdot NH_4I$-acetone-water combustion). A careful

study by Sackiw et al. (1984) clearly showed that NCAR counters (operating at -20°C) only detected about 10% of the ice crystals detected from the same aerosol sample in the CSU isothermal cloud chamber, even after applying the correction for ice particle losses because of instrument design given by Langer (1973). Therefore, the potential nuclei were probably underestimated. Even so, the recent orographic cloud studies found only a "small fraction" of the available AgI nucleated ice crystals. They suggested that this may be due to the long time dependence of contact nucleation as discussed by DeMott et al. (1983).

Finally, there is evidence that the complex behavior of ice nucleating aerosols can impact the targetting of seeding effects. Observations have shown statistically significant increases in precipitation in regions downwind of seeding target areas, such as observed by Super and Heimbach (1983) for Montana orographic clouds. This program used both AgI and AgI•NaI nuclei at different times.

III. THE CLOUD CHAMBER FACILITY

3.1 Dynamic Cloud Chamber

The dynamic cloud chamber has been described by DeMott (1988) and DeMott and Rogers (1990). It is shown in the schematics in Figure 3.1. It consists of a 2.0 m^3 stainless steel outer pressure vessel which houses a thin (low thermal mass) cylindrical inner copper liner open to the pressure vessel by small holes in the top and bottom plates. Total experimental working volume is 1.19 m^3. In operation, air is evacuated at a controlled rate from the pressure vessel (using a vacuum pump and a stepping-motor-driven control valve connected to the pressure vessel) to produce expansion cooling of the sample air. The space between the pressure vessel and the inner vessel acts as an expansion plenum which helps to dampen changes in flow rate out of the inner vessel as the pressure control valve cycles. The evacuation rate is controlled by computer, based on specified initial conditions of temperature, pressure, humidity and ascent rate. The simulated ascents are based on equations for dry adiabatic ascent to cloud point and moist adiabatic ascent thereafter. The program allows for a high degree of flexibility regarding initial chamber conditions and accounts for latent heat release at the lifting condensation level. Computed air parcel coefficients are output to an ascent profile memory system that is triggered when the desired initial conditions have been physically

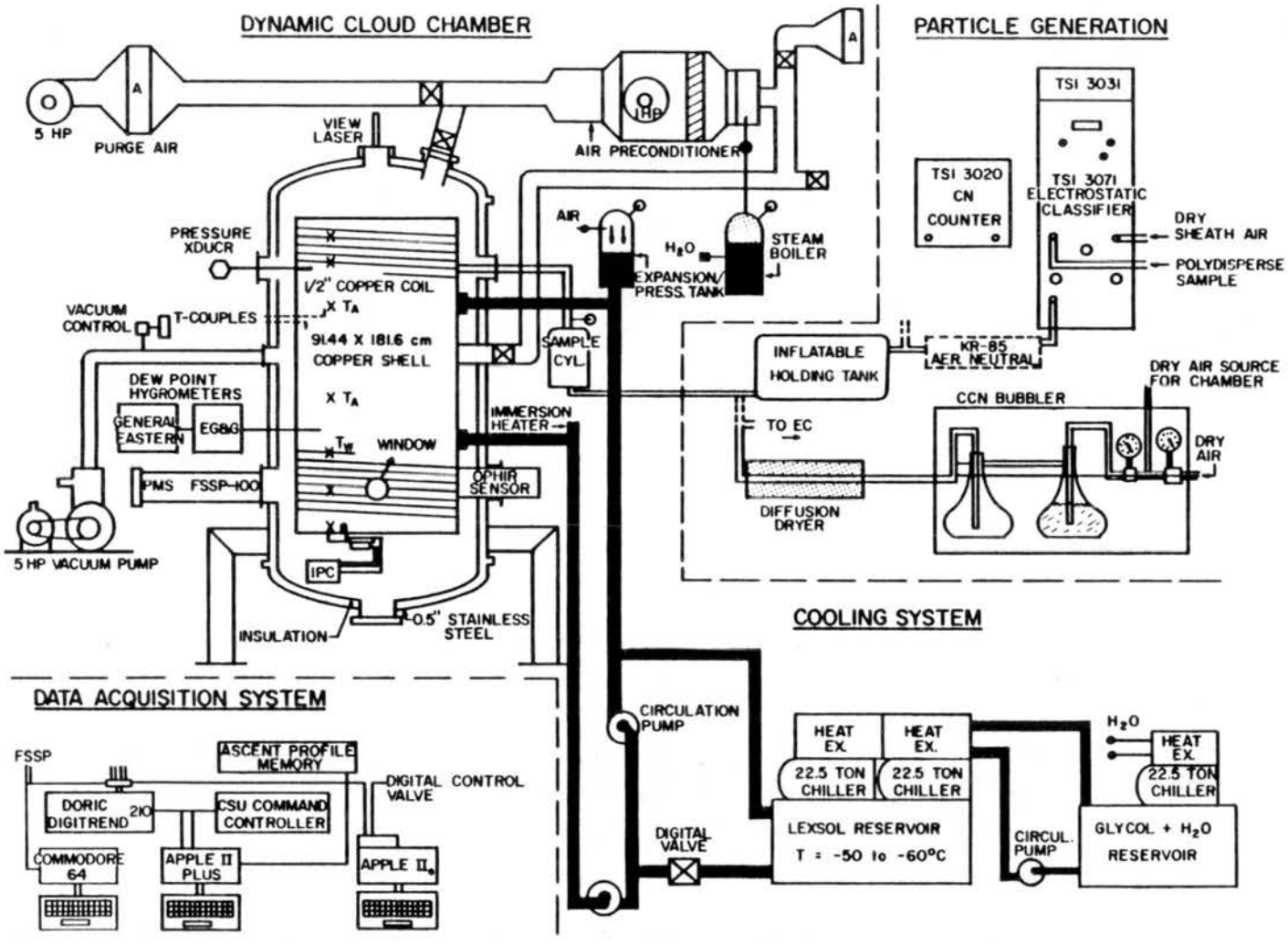

Figure 3.1 Schematic diagram of the CSU dynamic cloud chamber and its support systems. Various details are referred to and discussed in the text.

achieved (using an air preconditioning system and forced cooling of the inner liner). Wall temperature effects (heat transfer) are mimimized by cooling the inner liner to match the calculated mean air temperature. This is accomplished by circulating fluid (LEXSOL) through spiral-wound copper tubing which is soldered to the copper liner. Large compressors are used to cool the fluid, and the rate of introduction of the cooled fluid to the circulating fluid loop is regulated by a computer-controlled digital valve. A software program was developed to use measured versus programmed wall temperatures in time to empirically drive adjustments to valve position, as needed. A homogeneous working volume, free from large thermal or vapor gradients is thus made to simulate a wide range of air parcel and cloud conditions. An example of a particular experimental versus programmed ascent profile is shown in Figure 3.2. The usable working ranges and system tolerances of the dynamic cloud chamber are:

temperature	+40°C to -55°C ± 0.2°C
pressure	90kpa to < 10kpa ± 0.5mb
relative humidity	0.1% to > 100%
simulated vertical velocity	0.2 m s^{-1} to 20 m s^{-1}

Cloud droplet sizes and concentrations are measured with a Particle Measuring Systems (PMS) FSSP-100. A small funnel shaped glass tube protrudes 10 cm into the cloud volume and draws cloud air into the FSSP. The sample inlet necks down to 0.65 mm, and with a sampling rate of 0.4 L min^{-1}, the flow accelerates to 20 m s^{-1}. This stream is combined with an isokinetic sheath flow and is directed through the

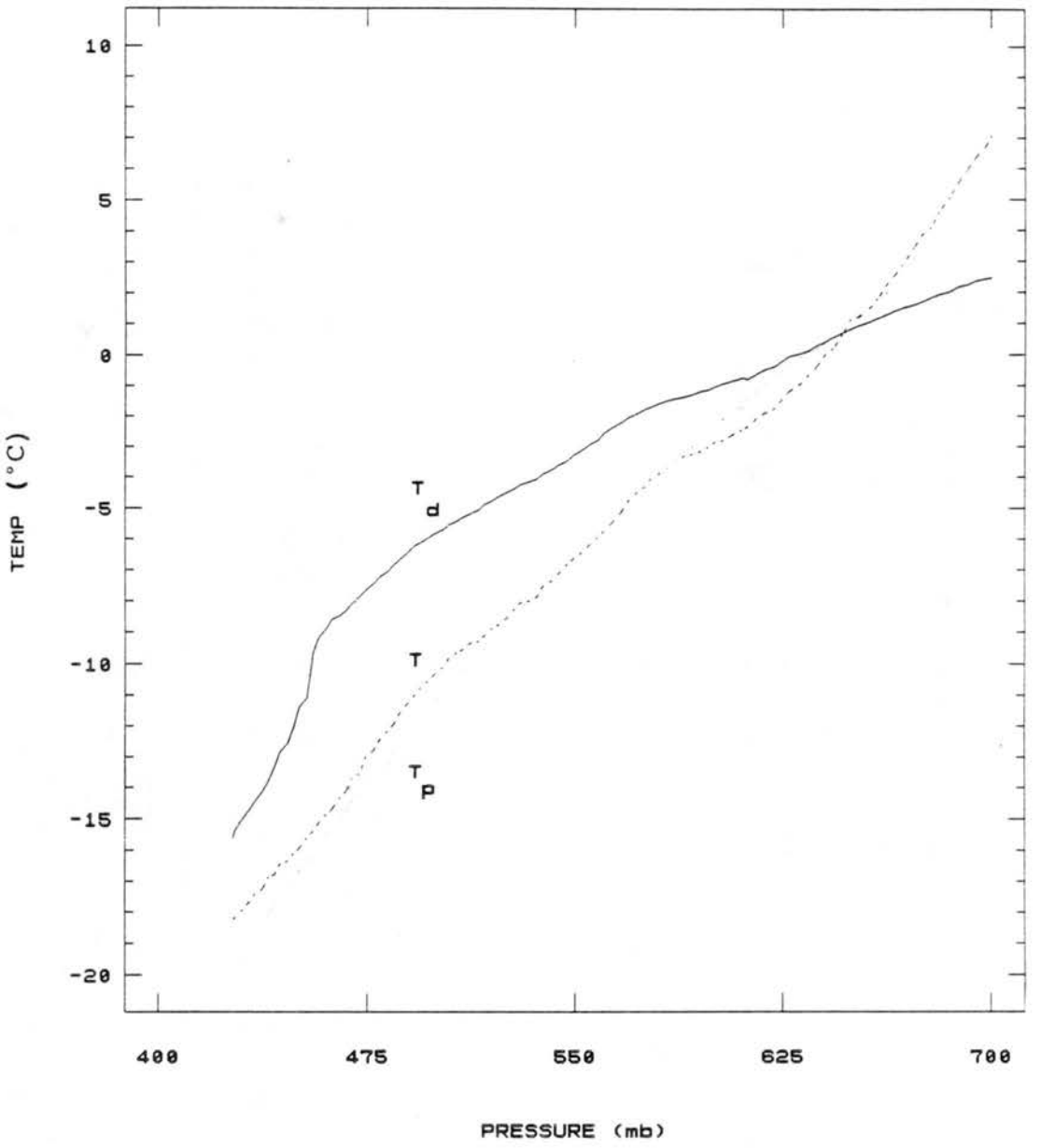

Figure 3.2 An example of a programmed (T_p versus P) versus the simulated ascent profile experimentally observed (T versus P) in the dynamic cloud chamber. Dewpoint temperature as measured by the optical condensation-type hygrometer is also shown.

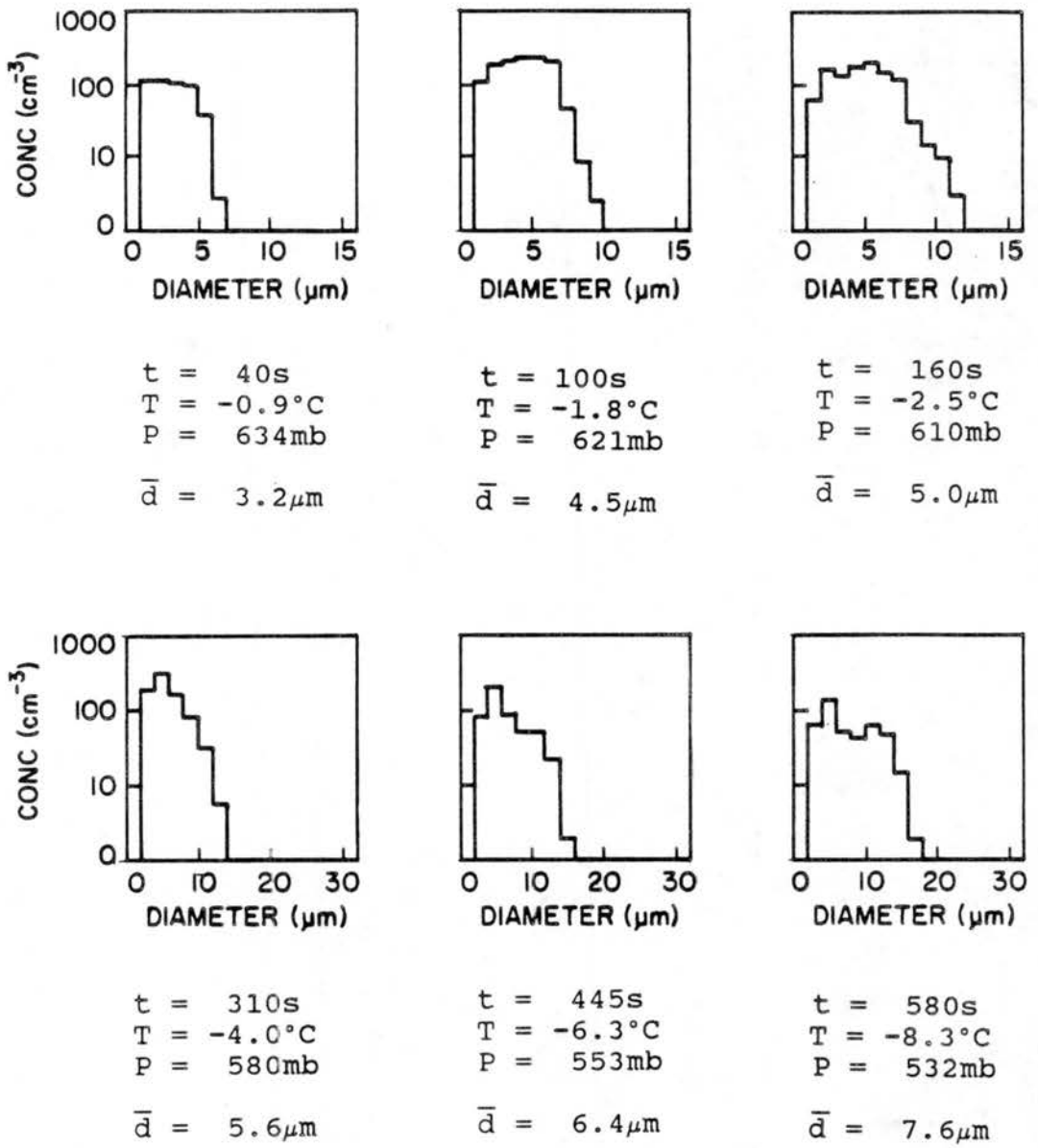

Figure 3.3 FSSP Cloud droplet spectra observed at various times after the thermodynamic cloud point indicated in Figure 3.2.

center of the laser beam. This sampling system has a number of advantages and avoids some the measurement problems associated with these instruments when they sample the free air stream from aircraft (Dye and Baumgardner, 1984; Baumgardner et al., 1985; Cooper, 1988). The sample volume in our FSSP system is determined by the size of the laser beam (constant ~0.2mm), the depth of field (DOF), and the air speed (constant). In aircraft FSSP systems, the DOF and the air speed can vary: the DOF is determined with a combination of optics and electronics and is typically 2 to 3mm. With an FSSP sampling in the free stream, there are many droplets outside the DOF, and they can produce significant coincidence errors in the droplet size measurements (Cooper, 1988). However, in our system, the DOF is defined by the size of the airstream (0.65mm) carrying the droplets. This air stream is centered in the optical DOF; there are no droplets outside the DOF. The isokinetic sheath flow keeps the edges of the droplet stream intact. This was verified with smoke tests. The particle stream velocity is higher than the minimum required, yet is well below the velocity where size corrections become necessary for this factor (Cerni, 1983). At the same time, the volume sample rate of approximately 1 cm^3 s^{-1} results in particle transit rates of 1 to 10^3 s^{-1} in most experiments, well below the 10^5 s^{-1} value for which coincidence errors become important to measuring concentrations (Dye and Baumgardner, 1984; Baumgardner et al., 1985; Cooper, 1988). There are unavoidable inherent sizing uncertainties for all FSSP probes which particularly occur in the 1 to 10μm range of particle sizes due to the behavior of the Mie scattering function there (Pinnick and Auvermann, 1979). Multiple Mie peaks for droplets below 10μm can lead to

uncertainties as large as a factor of 2 to 3 in diameter. An example of cloud droplet spectra at various times after cloud formation point are shown in Figure 3.3.

Ice crystals are detected by a laser-based detection device similar to that of Lawson and Stewart (1983). A primary difference, however, is that the instrument described by Lawson and Stewart uses transmission/depolarization to detect ice crystals and rolls off to near zero response for particles smaller than about 75μm. Our device was configured instead to detect single particles by extinction in a laser beam. Ice crystals which fall through a 3.8mm diameter hole on the bottom of the copper liner are collected by a converging air stream which flows into a funnel-shaped glass sample tube (10mm o.d. inlet, 0.7mm o.d. outlet, flow 15 cm^3 s^{-1}). This air stream crosses a HeNe laser beam (0.7mm diameter), which falls on a fast response solid state photodetector. The extinction signal should be approximately proportional to the particle cross section area. Experiments have shown that the technique responds to cloud droplets, ice particles, and electronic noise. A threshold circuit is used to discriminate against both noise and small cloud droplets. Cloud droplets rarely reach diameters larger than 20 to 25μm before settling out of the chamber, so the threshold is first calibrated coarsely to detect glass beads of 35μm, but not 15μm; finer adjustments were made to discriminate against droplets in warm cloud formation tests, in which droplets have long growth lifetimes. The largest droplets in the experiments described here were 15μm diameter, so it is unlikely that droplets were seen as ice particles. Other evidence also supports this conclusion (i.e., the FSSP measurements collected simultaneously with ice formation).

Calibration of the ice particle counts was made versus "ground truth" collections onto microscope slides. From numerous calibrations, it was found that the standard deviation in ice particle counts was about 30% of the total, independent of temperature or ice crystal habit. The total ice crystal number settled from the chamber was determined by multiplying the ice particle count by the ratio of liner bottom surface area to the sample hole area.

A slight measurement lag in detecting freshly nucleated ice crystals occurs because crystals must grow and settle to the bottom of the chamber. "Instantaneous" pulse nucleation tests in the chamber using liquid CO_2 and dry ice injections into supercooled water clouds have shown a nearly Gaussian response, peaking 30 to 75 s after nucleation, depending on temperature and pressure (which affect crystal growth rate and fall velocity). A deconvolution procedure is used to obtain the true response from the measured ice crystal signal (Mage and Noghrey, 1972). The finite difference approximation to the Laplace transform which describes the relation between the instantaneous rate (s^{-1}) of ice crystal formation (R) and the actual nucleation response (X) is given by,

$$R(t) = \sum_{n=1}^{n=\tau/\Delta t} C(n)\, X(t - n\Delta t)\, \Delta t \qquad (3.1)$$

where the coefficients C(n) represent a transfer function describing the response to a unit impulse of ice crystals, τ is the total time

required for the unit impulse to settle from the chamber, and Δt is a small increment of time.

The transfer function for the procedure in this work is based on pulse nucleation results in clouds cooling in the -7 to -12°C temperature range. Injection of CO_2 at the top inlet to the chamber was controlled so as not to overnucleate the clouds. A small mixing fan was used to mix the small crystals throughout the cloud volume for a few seconds. Thus, crystals always grew in a water saturated environment. The ice crystal signal for a particular pulse nucleation test and the transfer function fit to the data from several of these experiments are shown in Figure 3.4. This result is quite consistent with expectations based on ice crystal growth and fall velocities. The crystal growth and fall equations of Rogers and Vali (1987) can be used to estimate how long it takes for growing crystals to fall out of the cloud chamber. For example, typical observed cloud droplet size extremes, 1μm and 15μm diameter, may be used to bracket initial ice crystal sizes after nucleation at any point in the cloud chamber. These crystals are allowed to grow and settle in a water saturated environment at -10°C and 600mb. The 15μm particle falls 180cm from the top to the bottom of the chamber 58s later as a skeletal plate crystal 70μm in diameter (the change from spherical to plate habit is assumed to occur at 20μm). The 1μm particle takes 70s and is 68μm in diameter. If these ice crystals start from the middle of the chamber, the fall times are 37 and 50s, and the crystal lengths at the bottom are 50 and 49μm. These model results suggest that the crystals should be of detectable size, and if they all nucleated at once, they should be detected between about 30 and 80s. These times are very similar to the times for crystal

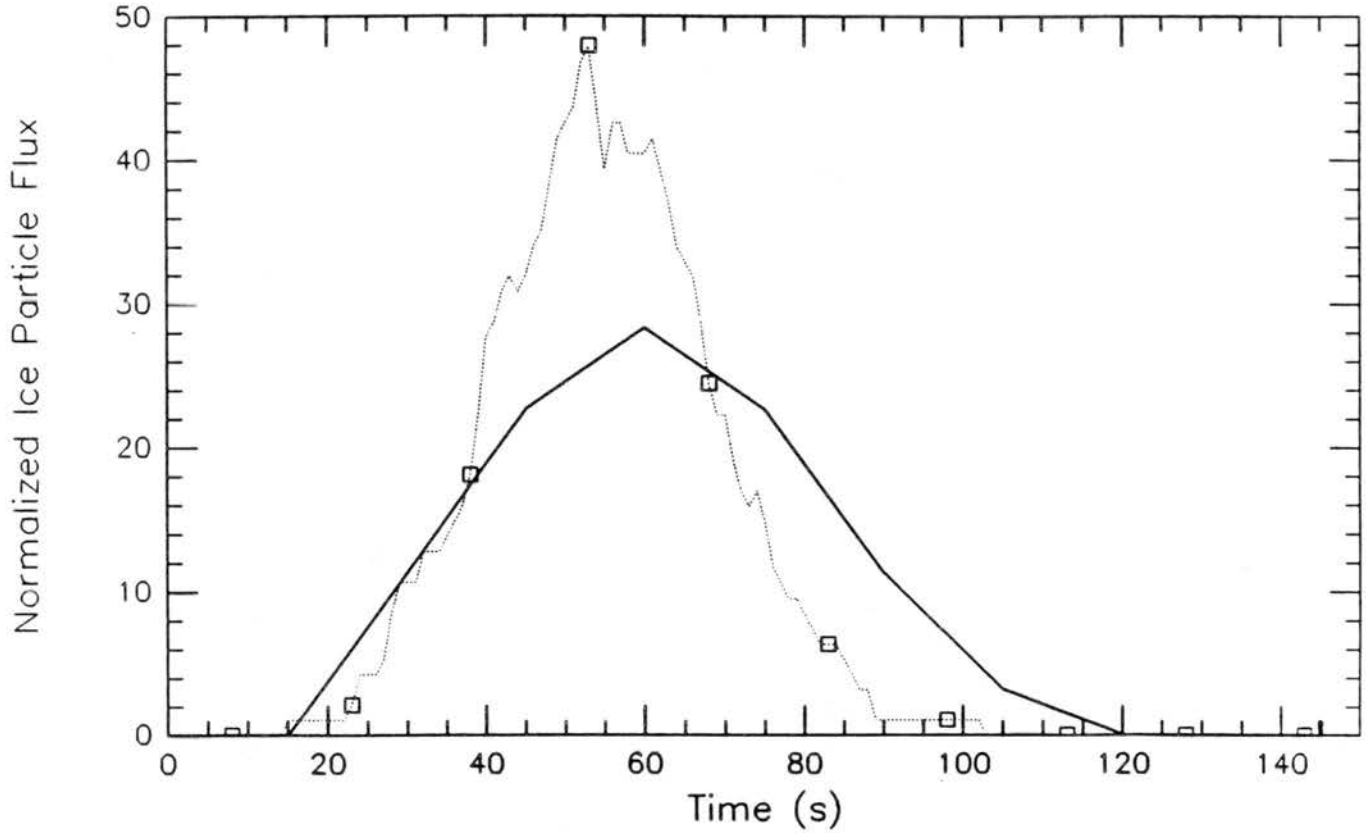

Figure 3.4 Plot of the shape of the unit transfer function formulated for the required deconvolution of ice data (see text). Also shown are ice crystal numbers measured versus time following one of the instantaneous nucleation experiments (using liquid CO_2 in the dynamic cloud chamber) used to define it.

growth and sedimentation in the experiments where the transfer function was defined. At this time, observations of the crystal sizes or habits in the cloud chamber are not available, although a microscope video camera will be installed to provide this information in the future.

The transfer function has not been determined exactly for the types of crystals and conditions existing at all temperatures. Clearly, the form of the transfer function will depend on temperature, pressure, and saturation ratio, since these all affect ice crystal growth and sedimentation rates. An estimate of the errors involved by using the single transfer function (Figure 3.4) at all temperatures employed in this study can be made by comparing the transfer function to fallout data obtained from 0 to -20°C in dry ice seeding tests in the isothermal cloud chamber (Morrison, 1989). The cloud chambers are similar in size. The only differences involve the crystal growth rate dependence on vapor diffusivity (which varies with pressure) and fall speed dependence on pressure. These should be minor influences. It is also presumed that the dry ice experiments were not overseeded. The cumulative ice crystal signals at various isothermal temperatures in Morrison's experiments are presented for comparison to the cumulative form of the function used to deconvolute dynamic chamber experimental data in Figure 3.5. The transfer function well characterizes the average ice crystal appearance rate for the temperature range of experiments performed in this study (-5 to -20°C). In this range, Figure 3.5 shows that the median time for detection of an instantaneous ice crystal nucleation signal may be overestimated or underestimated by a maximum of up to 15s, depending on temperature. The same effect goes

for the initial time to detect a signal. This maximum error is one data record (Δt = 15s in this study), and is equivalent to an error in nucleation temperature of 0.25°C in a 2.5 m s^{-1} equivalent updraft experiment. Studies are underway to implement a temperature dependent transfer function based on Morrison's data and further DCC pulse nucleation experiments (Rogers and DeMott, 1990).

The results of using the deconvolution procedure on some experimental data are shown in Figure 3.6. In this experiment, ice nucleus aerosols were injected directly into cloud at -8°C. After normalizing the ice crystal numbers measured falling from the chamber in time to the total number of aerosols injected, these values were smoothed with a binomial filter; typically a nine point filter was used. This was done to keep the technique numerically stable. The raw ice signal and the smoothed signal are shown in Figure 3.6a. The deconvoluted signal produced after the application of the transfer function is shown in Figure 3.6b. The deconvoluted signal was sometimes smoothed with a 5 point binomial filter prior to further analysis for nucleation rates. This smoothed signal is also shown in Figure 3.6b. Whenever smoothing was performed, the initial signal was always truncated so as not to create artificial data before ice formation was initially observed.

The primary measurement of humidity in the experiments performed was made using two optical condensation type dew point hygrometers. A prototype infrared transmittance hygrometer manufactured by the Ophir Corporation (Nelson, 1982; Kahan, 1989) was also installed in the chamber. This particular sensor and its performance characteristics have been described by DeMott and Rogers (1989). Its potential use as

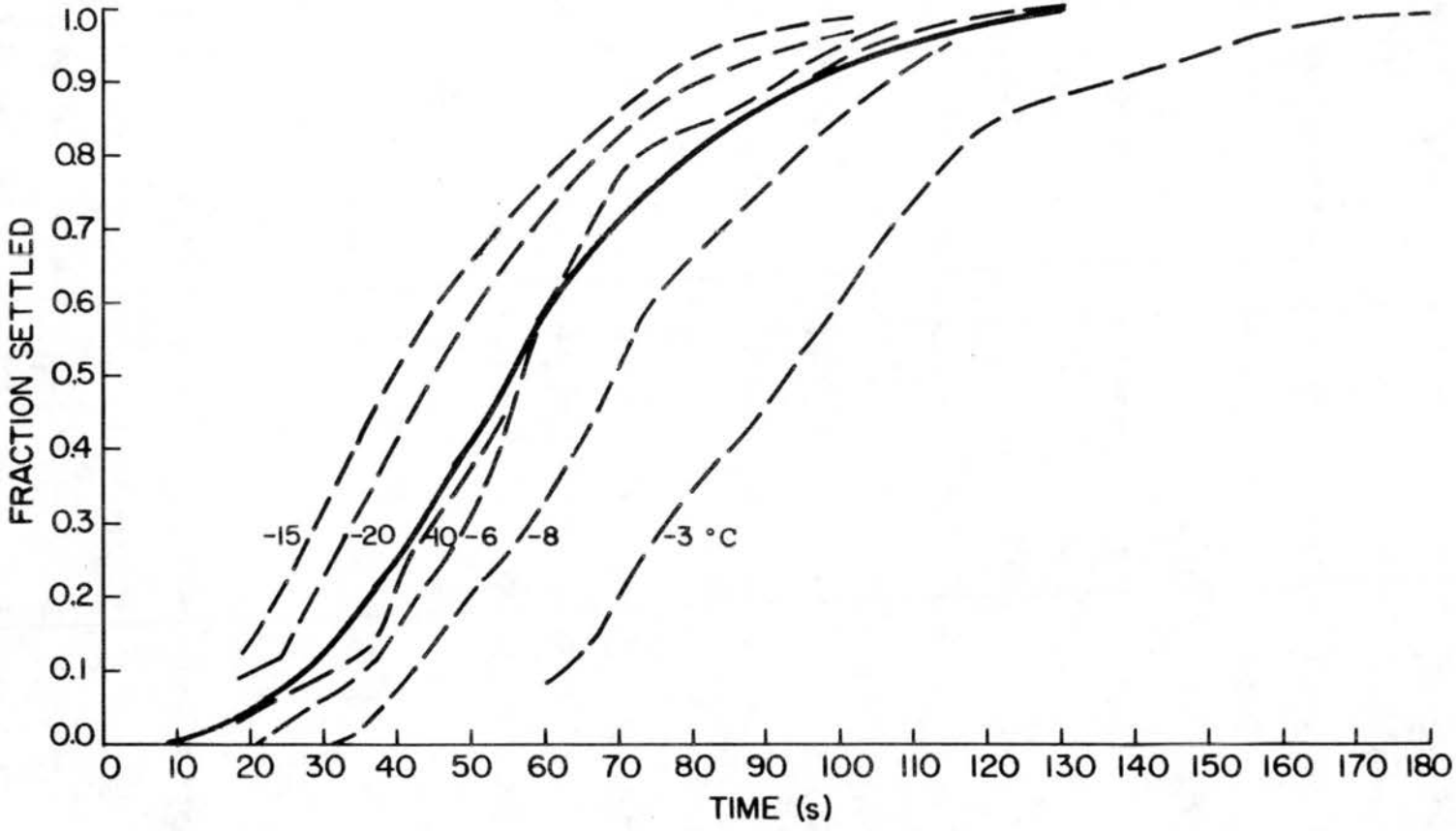

Figure 3.5 Temporal rates of ice crystal formation versus temperature measured following instantaneous nucleation using dry ice. Data are from experiments conducted in the CSU isothermal cloud chamber by Morrison (1989). The solid line is the unit transfer function used in this study.

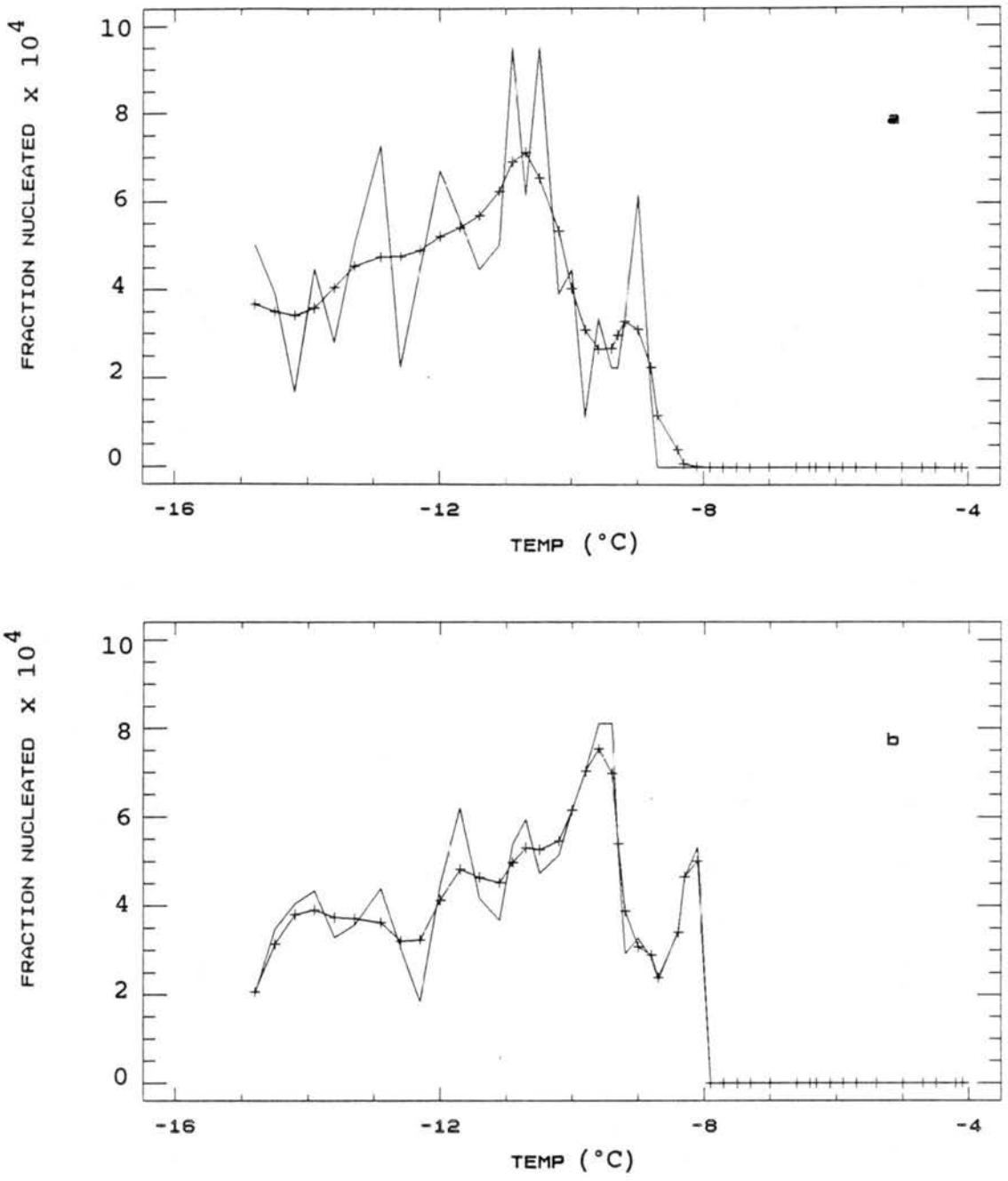

Figure 3.6 Example of the result of applying the deconvolution procedure to real experimental data. The raw (lines) and smoothed (- + -) numbers of crystals settling from the cloud (per s) as a fraction of ice nucleus aerosols injected versus temperature are shown in (a). The deconvoluted and smoothed-deconvoluted signals are given in (b).

an indicator of water supersaturation within cloud will not be realized without further technological developments. It is unfortunate that the cloud physics field lacks an instrument to measure this most important quantity, particularly as it influences ice nucleation. Without such a measurement, it was necessary in this study to estimate supersaturation using numerical model techniques, as discussed in the following chapters. The primary uses of the normal humidity measurements are to set initial experimental conditions and anticipate the onset time of cloud formation.

Temperature is measured continuously using an array of ten copper-Constantan thermocouples (0.508 mm wire) located on the inner liner and two faster response (0.0254 mm wire) thermocouples (TA1, TA2 in Figure 3.1) located 25 cm into the air volume from the inner wall. Temperature uncertainty is 0.2°C. Pressure is measured with strain guage type transducers. The Setra transducer included with the infrared hygrometer served as the primary indicator for experiments. Sensitivity is 0.5 mb at room pressure (~850 mb).

Two APPLE II computers are used to control expansion, to set the coolant flow rate, and to control the acquisition, display and recording of measurements of cloud and wall temperatures, pressure, humidity, cloud drop concentration, liquid water content, and ice crystal formation. Selected real-time printed data are generated and all data are stored on floppy disks. A COMMODORE 64 computer is separately devoted to the acquisition, real time display and recording of cloud droplet size and concentration data from the FSSP. Data analyses are performed on an NCR PC-8, with the aid of special PASCAL

and FORTRAN 77 programs and a statistical graphics package, after data are converted to compatible ASCII formats and transfered through one of the CSU CYBER 206's. A new data system based about a single 386 PC machine will soon replace the old data system (DeMott and Rogers, 1990). Improvements in ice detection systems will also be made.

3.2 Isothermal Cloud Chamber

The CSU isothermal cloud chamber (ICC) has been described previously by Garvey (1975), and DeMott et al. (1983). The chamber is a closed cylindrical double shell with an inner shell of 0.64 cm aluminum, 1.37 m in diameter and 1.52 m high. The outer shell of 10 gage steel is 1.68 m in diameter, and the annular space between the shells is filled with polyurethane insulation. Cooling is achieved by a two-phase Freon flow in a system of 1.5 cm tubes welded to the outside of the inner shell at 15 cm spacings. These features were designed to maintain wall temperature within +/- 0.1°C around the chamber walls. The inner shell of the chamber is fitted with a black velvet liner about 15 cm from the walls. Originally installed to minimize frost accumulation and shattering, the liner has proved important in maintaining an experimental volume with an acceptable cloud density gradient.

The cloud is introduced using the system shown schematically in Figure 3.7, from DeMott et al.(1983). Cloud droplets are generated continuously by the atomization of distilled water with an ultrasonic humidifier (Monaghan 670). They are then mixed with cold air and allowed to equilibrate with the chamber while rising through a standing tube in its center. By varying dilution airflow, the liquid water

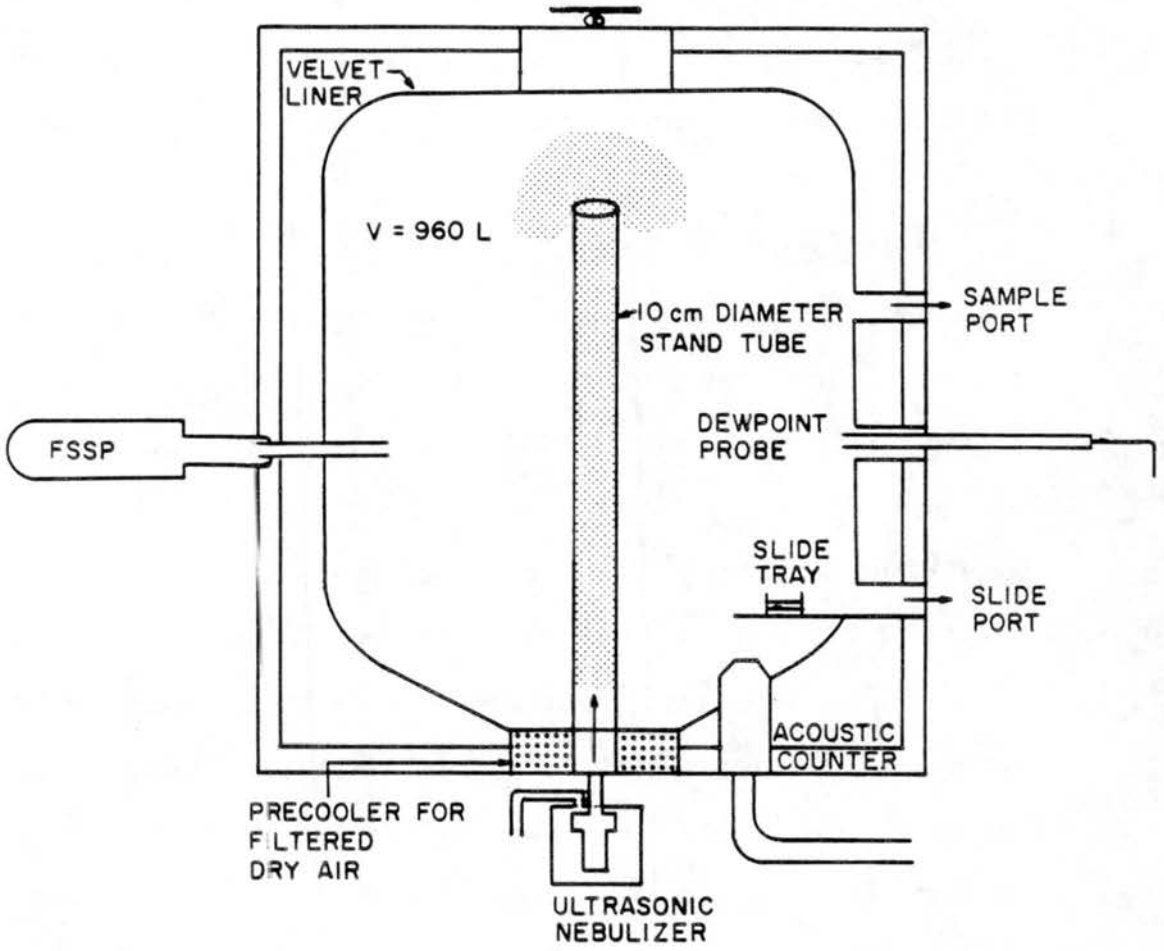

Figure 3.7 Schematic diagram of the CSU isothermal cloud chamber. The FSSP was temporarily mounted in the chamber to obtain droplet size distributions. Further description is provided in the text.

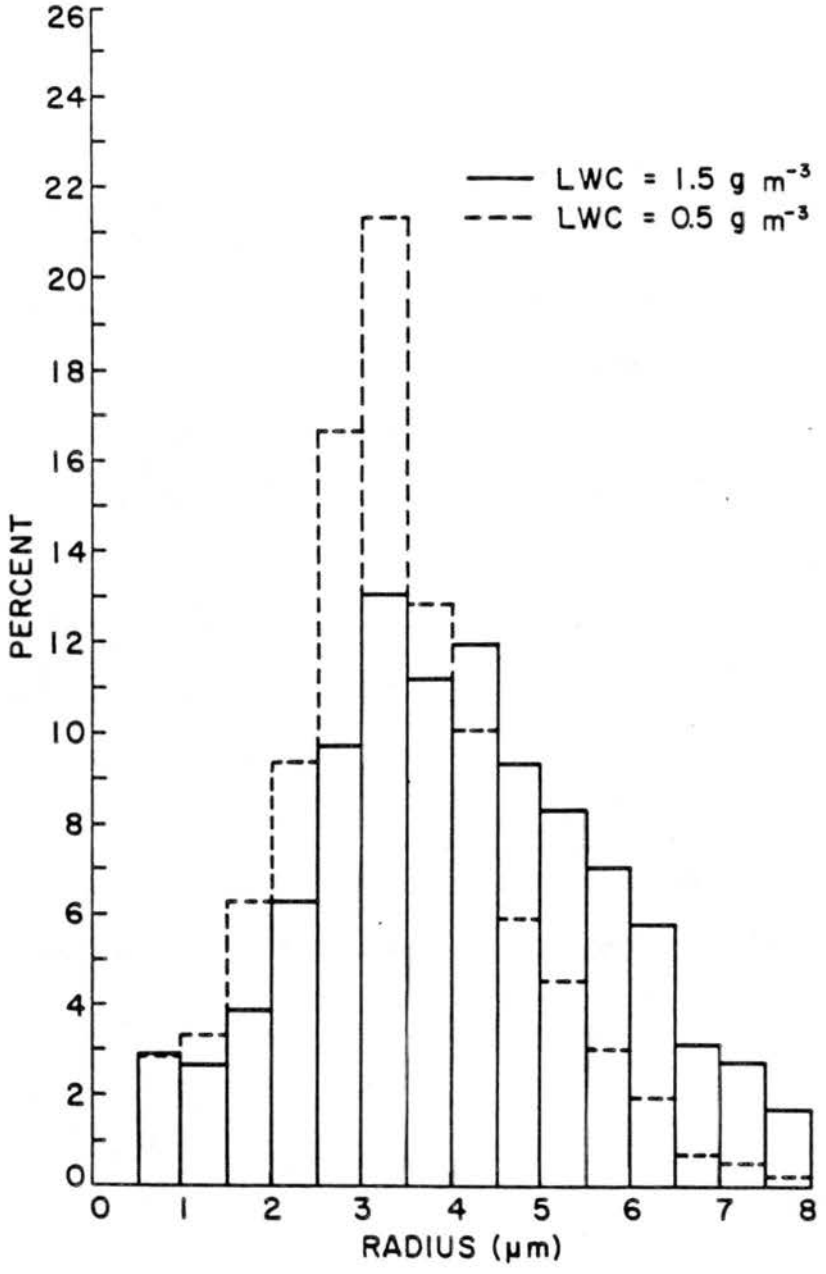

Figure 3.8 Isothermal cloud chamber droplet spectra measured at two liquid water contents at -12°C using the FSSP. Data are 5 minute averages. Average droplet concentrations represented are 4300 cm^{-3} (——) and 2100 cm^{-3} (---).

content (LWC) can be varied from 0.3 to 3.0 g m^3 without changing the droplet size appreciably. Temperature within the 1 m^3 experimental volume can be maintained to within +/- 0.3°C of the setpoint over a range from 0 to -25°C.

The cloud density is continuously monitored by means of a Cambridge Systems dewpoint hygrometer. The technique employed is to evaporate a cloud sample and measure its dewpoint; the difference between the saturation mixing ratio corresponding to the dewpoint temperature and that corresponding to the cloud temperature is taken as the liquid water content. Temperatures throughout the system are measured by thermocouples and are recorded continuously. Droplet sizes have been measured using soot-coated slides with a device patterned after that of Squires and Gillespie (1952) and using a Particle Measuring Systems Forward Scattering Spectrometer Probe (FSSP-100) (DeMott et al., 1983). Mean droplet diameters range between 6 and 9 μm on all occasions. Representative mean droplet concentrations are 2100 cm^{-3} at 0.5 g m^{-3} and 4300 cm^{-3} at 1.5 g m^{-3} LWC. Representative cloud droplet spectra are shown in Figure 3.8. The cloud simulates a slowly settling fog or stratus cloud at water saturation, and its quasi-steady-state nature allows nucleation and ice crystal growth to be studied as a function of time.

Ice crystals settling from the cloud after injection of artificial ice nucleating aerosols are collected on microscope slides and are counted using a cold-box microcope. Slides are sampled from the chamber periodically until nucleation ceases. The uncertainty in this procedure is about 30% based on past results. Counts are typically converted to numbers effective per gram of nucleant dispersed (= Yield), but for

this study fractions active were determined with the aid of the condensation nucleus counter, considered to give an estimate of total (Aitken) particles. This is discussed further in the following section.

3.3 Aerosol Generation

Cloud condensation and ice nuclei for experimentation are generated outside the dynamic cloud chamber and can be injected at any point prior to or during an expansion. A small fan is used to induce mixing. Polydisperse or nearly monodisperse CCN particles of various compositions can be generated from aqueous solution using a bubbler system. These solution droplets are dried in a diffusion type drier before input directly into the chamber or into a Thermo Systems Incorporated (TSI) Electrostatic Classifier (Model 3071). Particle concentrations in the DCC prior to injection are typically controlled to be < 0.1 cm^{-3}. The activity of the CCN aerosols used are relatively well behaved and can be predicted theoretically (Fitzgerald, 1975). CCN concentration can be adjusted over the range 10 to 10^4 cm^{-3}. Total condensation nucleus concentration was not monitored in every experiment; rather, equivalent timed injections were used for this study, based on measurements of bubbler output usinga TSI Condensation Nucleus Counter (Model 3020).

Ice nucleating aerosols were generated in a repeatable manner by solution combustion within a large vertical dilution tunnel. Samples of ice nuclei were taken directly from the tunnel just before injection time and were stored in flexibe, electrically conductive bags (Velostat). When polydisperse aerosols were to be injected, this required dilution with -30°C dewpoint air, due to the high

concentrations present in the tunnel. When monodisperse aerosols were required, sampling was done directly from the tunnel into the electrostatic classifier. The classifier design also assured a "dry" sample. The monodisperse aerosols were stored in the Velostat bags mentioned previously. Injection into the dynamic cloud chamber was achieved by venting the bag through the sample inject port, using the pressure differential between bag and chamber. For isothermal chamber injections, the sample was transfered from the velostat bag to a 4 L sample syringe for manual injection. Size distributions and total particle concentrations of ice nuclei aerosols are obtained by using the classifier in series with the condensation nucleus counter.

IV. EXPERIMENTAL DESIGN

4.1 Laboratory Experiments

Development of the laboratory experimental design was in itself a primary goal and an obstacle for this research program. These types of studies had never been performed before. The ideal design is described along with the actual procedures used here, as they were compromised by the limitations of available physical facilities and time. Ice nucleation is quantified in the framework of well founded macroscopic conceptual models of the various processes that can lead to ice formation. Standard definitions of these have been given in Chapter 2. Again, it is important to note that this is not a study of the nature of the different mechanisms, only of their consequences. The microscopic details related to each mechanism are not well known, but are not important for this study. The macroscopic details are important because they help define the experiments necessary to isolate the contributions of different modes for different atmospheric conditions. In this regard, the working definitions of the nucleation modes differ slightly from the standard definitions, and from the definitions given by DeMott et al. (1983). For example, any nucleation occurring below water saturation is included as deposition nucleation, since the role of liquid condensation cannot be discerned. The current definitions are

also too ambiguous in explaining the difference between condensation-freezing and immersion-freezing. For this study, condensation-freezing is distinguished from immersion-freezing by the requirement that ice crystal formation occurs instantly in response to a given water supersaturation and temperature, and the lack of requirement for the activation of a macroscopic cloud droplet. In fact, nucleation that follows from predicted cloud droplet activation is termed a form of immersion-freezing. Nucleation due to water supersaturation in excess of the immersion-freezing fraction is termed condensation-freezing. These working definitions can be further clarified by considering the history of a particle in a condensing environment, as is done next.

As the schematic in Fig. 4.1 shows, the four nucleation modes actually present five different pathways by which ice can form when heterogeneous ice nuclei are present or are introduced into ice supersaturated or cloudy air below 0°C. Deposition nucleation requires only that the saturation ratio with respect to ice exceed 1. Then, at any temperature (T_1) and time (t_1), some fraction of the aerosol (F_1) will act to form ice (lowest path in Figure 4.1). At a constant temperature and ice supersaturation (S_{i1}), the fraction F_1 may vary with time, expressing the kinetic rate of ice crystal formation.

When saturation with respect to water (S_{w1}) is approached and exceeded, some fraction (F_2) of the ice nucleating aerosol may hydrate, form a liquid haze particle, or activate as a solution droplet (middle pathway in Figure 4.1). This will depend primarily on the chemical hygroscopic characteristics of the aerosol, and the peak S_{w1} achieved. At temperatures T_1 below 0°C, the instantaneous freezing of the condensing liquid phase is referred to as condensation-freezing

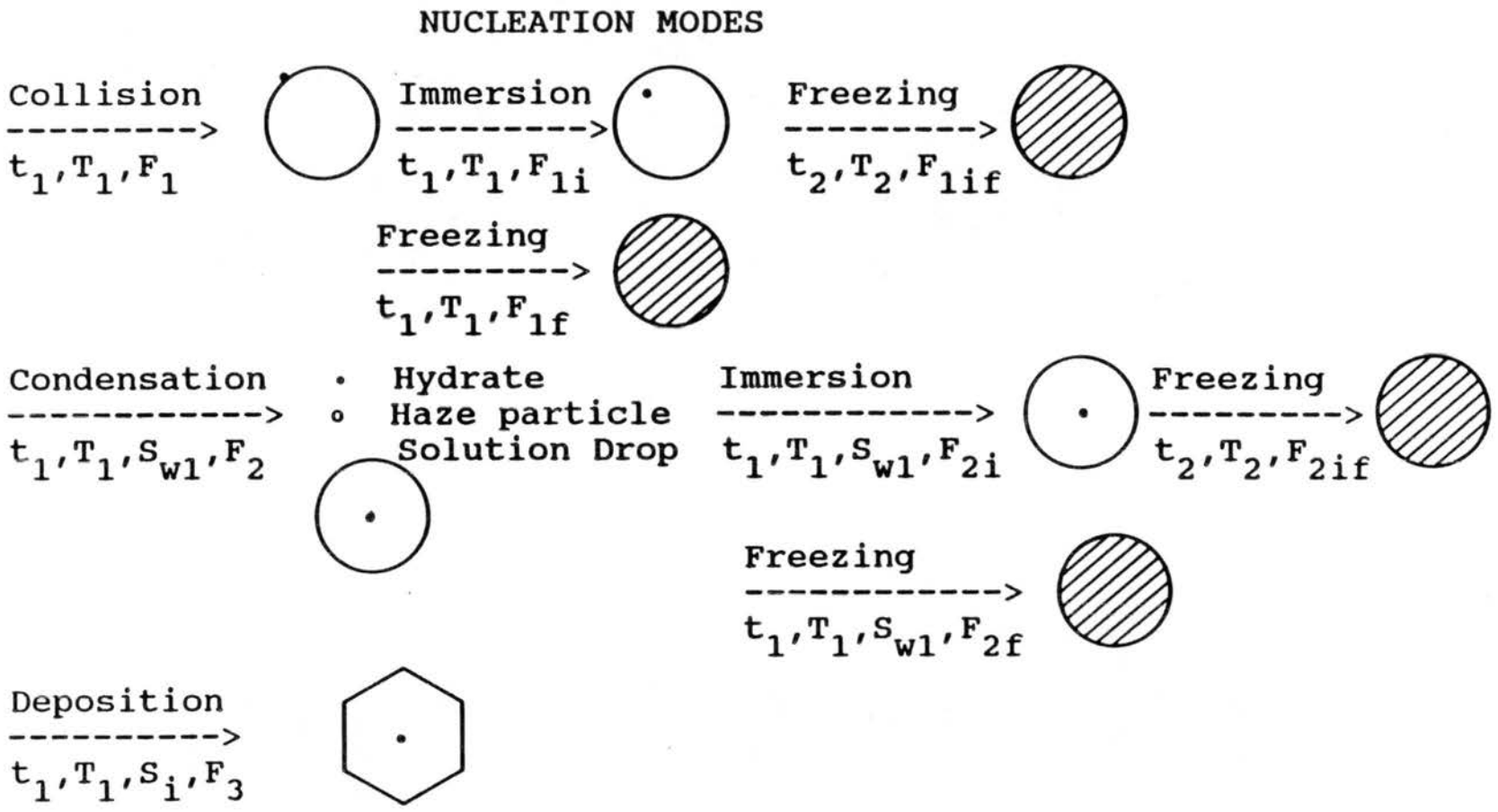

Figure 4.1 Schematic diagram of the mechanisms by which ice crystals can form in a cooling cloud parcel. Ice particles are indicated by shading and the various symbols describing rates and nucleating fractions are discussed in the text.

nucleation. The existence of a rate constant at sustained T_1 and S_{w1} could not be examined here. Aerosols or unactivated droplets may also nucleate ice by this mechanism at colder cloud temperatures than the initial formation point where lower water supersaturations may be necessary. If nucleation does not occur rapidly, but a macroscopic droplet forms and freezes upon cooling to a lower cloud temperature (T_2), nucleation no longer bears any relationship to water supersaturation and is rightly a form of immersion-freezing.

Whenever cloud is present, transport processes (brownian motion, differential aerodynamic fall speeds, phoretic forces) will cause some fraction (F_3) of the aerosol to be collected by cloud droplets. At some supercooled cloud temperature (T_1), some fraction of these collected particles (F_{1f}) will cause ice nucleation instantly after collision by contact-freezing nucleation (top pathway in Figure 4.1). If freezing does not occur instantaneously, some fraction (F_{1if}) of the immersed fraction (F_{1i}) may freeze at a colder temperature (T_2). This latter mechanism is again a form of immersion-freezing.

Some processes are not represented in Fig 4.1 and were not within the scope of this study. These include the potential dissolution of nuclei over time within droplets, the nature of renucleation following the evaporation of droplets or ice crystals containing AgI aerosols, and photolytic effects on the aerosol character and its ability to nucleate ice. These processes should not have been at play in the experiments performed due to the short time scales and the nature of the experiments themselves.

4.1.1 Deposition Nucleation Experiments

The approach to the deposition studies was to perform continuous expansions to water saturation in the dynamic chamber at a slow ascent rate, to cover the range of humidities between ice saturation and water saturation for temperatures between -5°C and -20°C. In this way, nucleation of freezing of the liquid phase was limited from influencing the results. A thermodynamic path for such an expansion is demonstrated in Fig. 4.2. The measured cumulative ice crystal flux settling from the cloud could be related to a given temperature and percent ice supersaturation (S_i). S_i was determined from the humidity measurements, with verification provided by the observed thermodynamic cloud point. This approach assumes that once the critical supersaturation is exceeded, nucleation occurs instantaneously; and the time response of the experiment is limited by ice crystal growth and fallout. Only Anderson and Hallett (1976) have noted a finite delay before the onset of nucleation at some defined temperature and supersaturation. Edwards and Evans (1960) and Schaller and Fukuta (1979) did not find this delay and neither study observed any nucleation to occur after initial ice formation. To evaluate such potential effects in the dynamic cloud chamber, one could conduct intermittent expansion experiments in which a set of conditions are established and held to measure the nucleation rate and the ultimate number of ice crystals that formed, followed by another brief expansion to produce a higher value of S_i, at a slightly colder temperature. This has not been done due to the additional time that would be needed to implement the special coolant control procedure required.

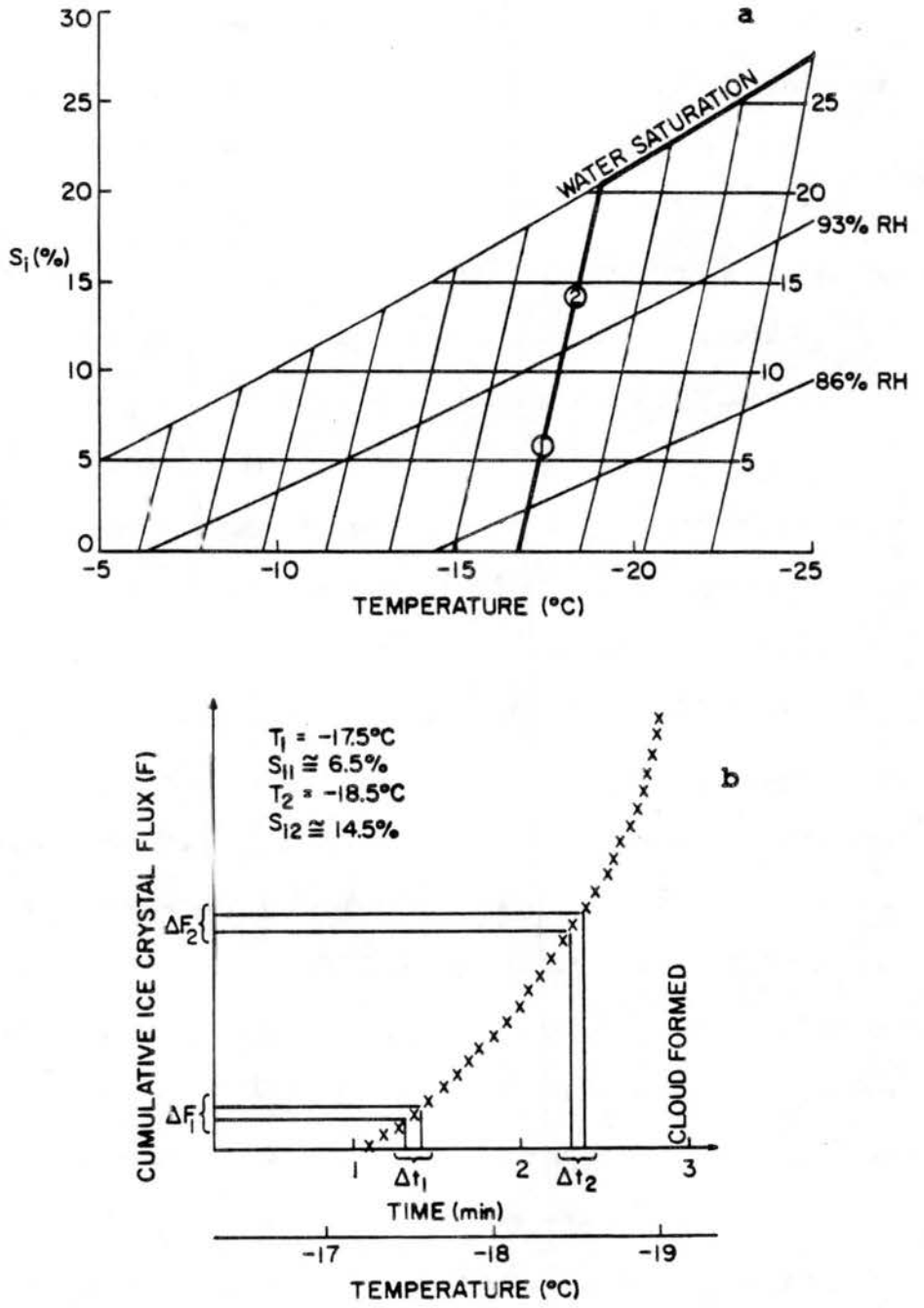

Figure 4.2 Schematic of the thermodynamic history of a parcel between ice and water saturation (a) during expansion-cooling, representing a pathway over which deposition nucleation can be measured. Computation of the nucleation rate at two points is shown in (b).

For deposition, results for nucleation activity are expressed by an active site density D_{dep} (cm^{-2}) parameter. This quantity is computed using the cumulative fraction of the aerosols nucleating ice by deposition (F_{dep}) and the aerosol sizes (r_a^2), by way of the equation,

$$F_{dep} = 1 - EXP\ (-4\ \pi\ r_a^2\ D_{dep}) \qquad (4.1)$$

This method provides a way for quantifying nucleation size effects. The method shows that deposition nucleation rate should directly depend on the surface area of the aerosol particle because it assumes that nucleating sites are uniformly distributed with surface area. This method was used by Schaller and Fukuta (1979), although they did not use monodisperse aerosols in their studies to test the primary assumption. The validity of this approach is tested for the AgI aerosols used in this study. A polynomial (multiplicative) function of ice supersaturation is fit to the computed site density, just as Huffman (1973) did for ice nucleus concentrations measured versus ice supersaturation in an ice-thermal gradient diffusion chamber.

4.1.2 Contact-Freezing Nucleation Experiments

The technique used to quantify contact-freezing nucleation activity of the ice nucleus aerosols employed the isothermal cloud chamber. These experiments utilized the steady state and long time response characteristics of this cloud chamber that are ideal for studying this clearly time dependent mechanism. As previously described, droplet concentrations are maintained in this chamber by continuous supply at a fixed temperature. Tests with known injected

quantities (measured with the CN counter) of monodisperse and polydisperse nuclei were done to quantify size dependence, and total droplet concentrations (N_d) were varied between 2100 and 4300 cm^{-3} nominal values. Such experiments had previously shown that AgI-AgCl-4NaCl nuclei display little or no activity as contact-freezing nuclei, due to their hygroscopicity. This was noted by the insensitivity of the ice crytal nucleation kinetics to changes in cloud characteristics. Therefore, the isothermal chamber experiments were performed for AgI-AgCl aerosols only. The primary results are identified in terms of the cumulative fractions of aerosol active as ice nuclei (F_{ctf}) and active site densities (D_{ctf}) for contact-freezing versus particle size and temperature. F_{ctf} is determined from the cumulative amount of ice formed over time divided by the particle number injected. F_{ctf} values were already available from DeMott et al. (1983) for polydisperse AgI-AgCl from the same (stoichiometric) solutions burned with the same cloud seeding generator. Equation (4.1) can be used to compute D_{ctf} after substituting F_{ctf} for F_{dep} and D_{ctf} for D_{dep}. A multiplicative function of temperature or ice supersaturation can be fit to D_{ctf}. Before computing D_{ctf}, F_{ctf} was first adjusted for the artificial dilution process that occurs simultaneously with ice crystal formation in the isothermal chamber due to the forced-air introduction (and expulsion) of cloud droplets. This is described in DeMott et al. (1983). This correction required that the kinetic rate constant (k) for ice crystal formation be computed, again as described in DeMott et al.. Using the kinetic rate constant, corrected for artificial dilution processes, approximate scavenging collection kernels versus aerosol size can also be computed for comparison to theoretical values

(calculated using equations from Young (1974b), which are also included in Appendix A). Presumably, scavenging in the ICC is dominated by Brownian motion (collection kernel K_B), since the ICC cloud is approximately water saturated. Phoretic effects should not be important, unless the nuclei concentration is initially too high, leading to depletion of saturation ratio by the Bergeron process. This has never been tested for the ICC in an exact sense, as is possible with monodisperse colliders. The relation between the approximate collection kernel (K_B) and kinetic rate constant is given by,

$$K_B \simeq \frac{k}{N_d} \tag{4.2}$$

Equation (4.2) is strictly an equality if droplets are monodisperse. For theoretical calculations, the actual droplet spectrum previously measured from the ultrasonic nebulizer in the ICC was used, and the net collection kernel versus size was determined as the sum of fractional contributions by each droplet size.

Continuous slow expansions in the DCC at 2.5 m s^{-1} (~ 1°C min^{-1} in cloud), particularly at temperatures warmer than about -12°C, where contact-freezing nucleation is expected to be much more active than deposition or immersion (Cooper, 1974; Vali, 1975), afforded the opportunity to differentiate the cumulative ice formation curve to obtain the instantaneous nucleation rate. Experimental rates are again compared with theoretical values calculated assuming contact-freezing as the only mechanism. In this way, the relevance of the ICC results to DCC expansions could be evaluated, before the contact-freezing results were used in a predictive manner to allow differentiation of the contributions of other mechanisms.

Contact-freezing can still be a contributing mode for AgI-AgCl-4NaCl aerosols, although there is no way to address this due to the dominance of other modes in any experiment that could be performed, or conditions that can exist. To quantify this mode for the hygroscopic aerosol some fair assumptions and approximations were made. First, "free" aerosol (those not activated as cloud droplets or scavenged by existing droplets) sizes were adjusted to be their equilibrium droplet size at water saturation (approximate average condition whenever cloud is present) based on Howell (1949). Howell gave equations and computations of droplet growth versus humidity and moles of solute in hygroscopic particles. Rather than use explicit equations here, haze particle size versus the moles of soluble material has been described empirically. Essentially, at water saturation, the $\log_{10}$ [moles of soluble material] can be described as a linear function of the $\log_{10}$ [haze particle radius] with a slope of 2.0 and an intercept of -7.56. This is depicted in Fig. 4.3. The soluble fraction of the dry particles was assumed to follow the stoichiometric ratio, independent of particle size. Fractional activity for contact-freezing was then assumed to be the same as for AgI-AgCl of the same initial dry aerosol size.

4.1.3 Immersion-Freezing Nucleation Experiments

To characterize the immersion-freezing activity of the aerosols studied, continuous expansion tests were done to form clouds on the ice nucleus aerosols used as CCN. No ammonium sulfate CCN were used in these experiments. Clouds were typically formed at temperatures of -6°C

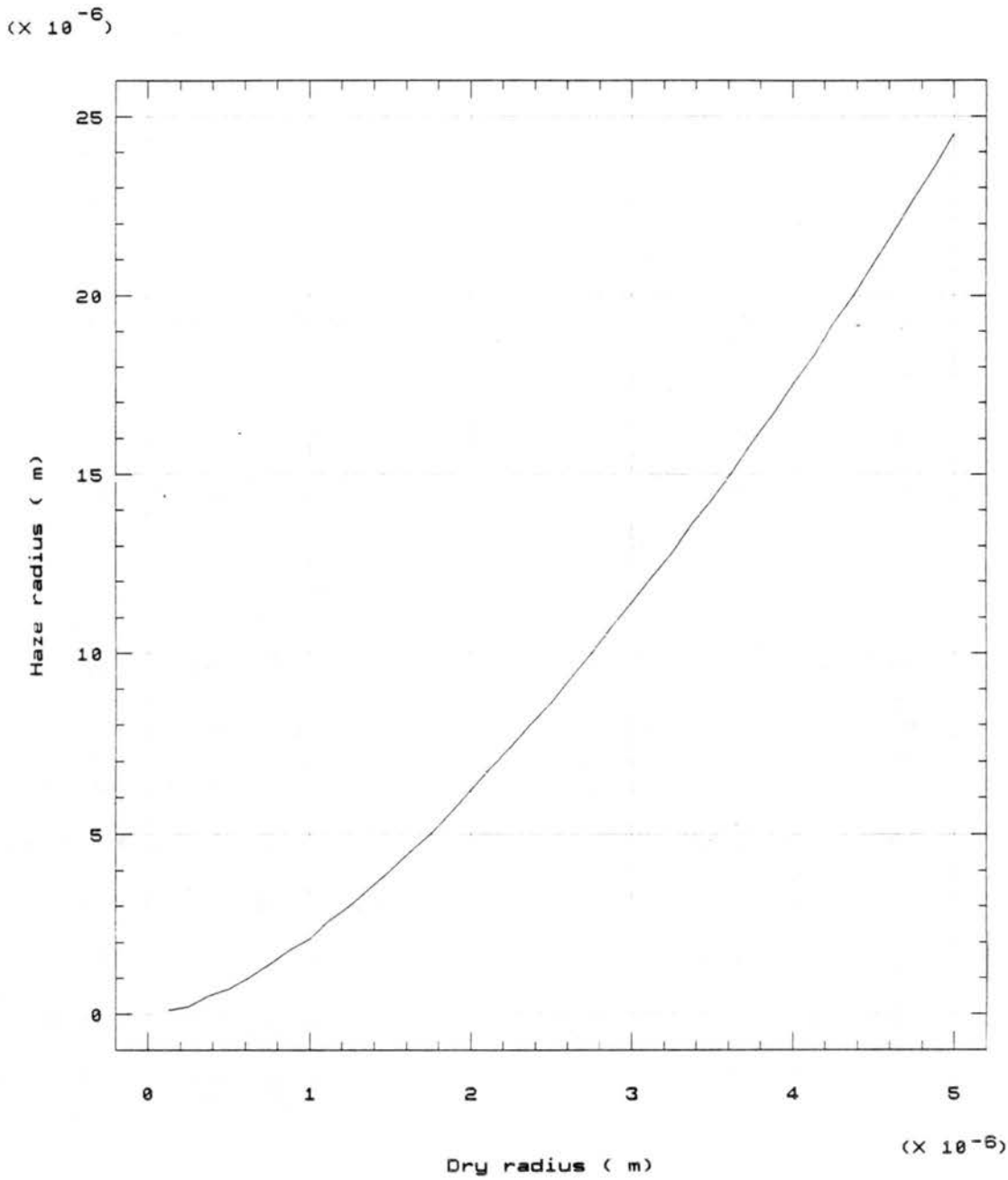

Figure 4.3 Dry particle size versus equivalent haze particle size of AgI-AgCl-4NaCl aerosols at water saturation, computed empirically as described in the text.

and warmer, thereby biasing against the condensation-freezing mode contributing to the signal. Higher ascent rates were used to nucleate as many monodisperse aerosols as possible. The total fraction of aerosols immersed in drops was known from the measured droplet concentrations formed versus the measured aerosol concentrations injected. Freezing fractions of this population were then measured as clouds cooled, subtracting the separately determined fractions expected to nucleate by deposition and contact-freezing nucleation (for the aerosols not immersed in drops). By immersing 50% or more of the aerosols in drops initially and by nucleating low concentrations (<400 cm^{-3}), the potential contribution of free aerosols immersed due to collection by droplets was minimized. Total fractions potentially effective as immersion-freezing nuclei were computed by adjusting the fraction frozen during each data record for the fraction still immersed. The results are presented as cumulative active fraction by immersion-freezing (F_{imf}) versus temperature for aerosols that have become immersed in droplets, and after incorporation of aerosol size, as immersion-freezing active site density (D_{imf}). The latter quantity is computed from F_{imf} using an equation of the form of (4.1). A simple multiplicative fit for D_{imf} with temperature is sought.

In order to extend such results to any particular cloud situation, it is necessary to quantify the means by which these aerosols enter droplets. Scavenging mechanisms are fairly well known. The condensation nucleation activity of the aerosols at the higher supersaturations typical of the immersion-freezing experiments was compared to the supersaturation estimated by performing comparative simulations with the cloud model. The condensation nucleation activity at the the lower

supersaturations more typical of atmospheric clouds was determined by using a static thermal gradient diffusion chamber (Mee Industries Model 130). By thermoelectrically cooling parallel plates to different temperatures and providing a vapor source, a defined supersaturation profile between the plates is created by this instrument (due to the non-linear dependence of saturation vapor pressure on temeprature). It is assumed that aerosols immersed from collision (F_{imc}) have the same nucleation activity by immersion-freezing as those particles which act as CCN. In model simulations (Chapter 6), the fractions of aerosol that are immersed by cloud droplet nucleation and by collision at any time are summed, and the fraction that will act by immersion-freezing is obtained by multiplying by $F_{imf}(T)$.

4.1.4 Condensation-Freezing Nucleation Experiments

Two separate techniques were employed to investigate the condensation-freezing nucleation behavior of the aerosols used. In both methods, monodisperse or polydisperse ice nucleating aerosols were injected and mixed into particle-free air in the dynamic cloud chamber. The sample was slowly cooled by expansion to conditions between ice and water saturation. Then, one of two methods was employed, as described in the following paragraphs.

In the primary method employed to study condensation-freezing, particularly at the lower supersaturations typical of most atmospheric clouds, expansions were made with other CCN present to form cloud at succesively colder (supercooled) temperatures, as was done for contact-freezing experiments. Also, simulated updraft was varied to cause varying water supersaturations (S_w) at cloud point, and different

steady-state S_w in cloud. This method is termed the continuous expansion method. Cloud model simulations using the adiabatic cloud model (see section 4.2) were done to estimate the supersaturation profile in each experiment. Then, predicted aerosol fractions nucleating ice by deposition, immersion-freezing (initial number in drops based on peak supersaturation) and contact-freezing nucleation (scavenging based on measured drop concentrations and sizes) were computed at each time step (defined by 15 s data records) and subtracted from the total observed fraction nucleated as ice. The residual, when there was one, was taken as the net condensation-freezing activity (F_{cdf}). As for the other nucleation mechanisms, F_{cdf} was used to compute active site density for condensation-freezing (D_{cdf}), following an equation of the form of (4.1). A simple multiplicative fit for D_{cdf} as a function of temperature and water supersaturation was sought. This method has a large uncertainty, since each mechanistic contribution has about a 30% error associated with it, and model predicted water supersaturation is likely accurate to no more than a few tenths of a percent. As it turned out, a few tenths of a percent water supersaturation are all that are needed to cause large fraction of aersosol to act as condensation-freezing nuclei under some circumstances. There was no way around this problem.

A second experimental technique was used that is most suitable for determining the condensation-freezing activity at relatively high supersaturations. This is termed the rapid expansion method. In these experiments, the expansion was halted prior to cloud point. Then, rapid 10 to 20 mb expansions were used to produce water supersaturations for a few seconds, sometimes followed by a rapid compression to evaporate

the water cloud, but leave the environment ice supersaturated. Thus, any ice crystals which formed continued to grow to detectable size, but contact nucleation was prevented. This defined the effect of supersaturation on ice nucleus activity. Successive cycles of expansion-compression achieved different values of water supersaturation and temperature. The total activity was the sum of condensation-freezing and deposition. The deposition contribution is calculated based on the results of the separate experiments discussed and can be subtracted from the net ice crystal signal.

The rapid expansions were achieved either by using the maximum capacity of the vacuum pump system or by equilibrating pressure between the DCC and an evacuated 30 liter tank ported to the pressure vessel by a manual release valve. In the first case, a new pressure was entered into the pressure controller and the vacuum system would adjust as fast as it could. The changes of pressure and temperature with time were monitored using analog signals printed on a strip chart. The nature of the control system would always cause an "overshoot" of the specified pressure. The pressure decrease achieved by venting the external tank to the DCC depended on the initial pressure in the DCC and the pressure to which the external tank had been evacuated. Peak supersaturation was estimated in either case with a version of the cloud model of Nimitz and Plooster (1980) and Plooster (1985). This model was designed for the zero gravity environment of a space-based cloud physics laboratory. It also contains no ice physics. Neither of these factors preclude its use for comparison to the DCC experiments described because nucleation is instantaneous, so gravity is of no concern, and because the peak supersaturation is achieved rapidly, before ice has grown to a size

that influences the water balance. This model may be run in a continuous expansion (continuous updraft) mode from some initial temperature and humidity, as for the Young cloud model that will be discussed in Section 4.2, but there is also and option to specify a pressure versus time profile. This is the particular utility of the model for predicting supersaturation for these specific experiments.

Following expansion, the cloud would typically evaporate due to thermal adjustment, since a means has not yet been designed to force cool the walls to match the air in rapid expansions. In the case of system controlled expansions, pressure would initially fall to a value below that specified (due to response time of pressure control), but would adjust back to the planned final pressure within 20 to 30s. When cloud persisted, compression to ice supersaturated, but water undersaturated, conditions was achieved by introducing compressed air into the pressure vessel, between the liners.

The rapid expansion method was a highly exploratory method. Presumably, with the new data and control systems being installed and with further developments in cooling control algorithms, it will be possible to program such expansions. This will require a prior estimate of the expansion-cooling that will occur, so that the wall cooling can be initiated prior to the initiation of the expansion cooling to adjust for thermal lag and equilibration.

Although rate constants may be associated with condensation-freezing, there was no means for establishing and holding a stable set of temperature and water supersaturated conditions in the DCC. This is more aptly achieved in a continuous flow ice thermal diffusion chamber, such as the one described by Rogers (1988). The flow chamber would need

to be long in extent along the transit path, to give sufficient time resolution to the measurements. Since time could not be treated for this mechanism in the DCC, it was assumed that the instantaneous activity at a set of temperature and supersaturation conditions was the net activity. Some justification for this exists from the studies of Schaller and Fukuta (1979). They found that increments in water supersaturation led to increments in ice nucleus activity for pure AgI that did not change with time, within the limits of their semi-quantitative measurements.

The condensation-freezing mode was thus quantified only as a function of temperature (or ice supersaturation), water supersaturation and aerosol size. For the continuous expansion method experiments, if additional condensation-freezing activity occurred at a lower temperature and at a lower supersaturation than the peak value achieved at cloud point temperature, then it was assumed that all particles which had previously acted by condensation-freezing would act instanteously at the new set of conditions if introduced at this later point.

4.1.5 Other Experiments and Experimental Summary

Besides experiments to isolate specific nucleation modes, a number of other general experiments were performed for which any or all of the modes might be operative. In some of these tests, aerosols were introduced directly into cloud, when steady state supersaturations were low. In other cases, aerosols were injected prior to the formation of clouds at temperatures of 0°C and warmer. Also, a number of tests were done with polydisperse aerosol size distributions. All of these

additional experiments served as tests of the size dependent descriptions of nucleation formulated from the results of mode-specific experiments. They also provided comparative tests of different cloud seeding methodologies.

During this research project, a total of 226 experiments were performed in the DCC. A full scale continuous expansion, including initialization of conditions, takes about one and a half hours. Table 4.1 shows the number and variety of experiments that were performed, stratified by aerosol size, aerosol chemistry, expansion rate, seeding

Table 4.1

Number and Type of Experiments Performed
in the Dynamic (Expansion) Cloud Chamber

attribute	# experiments
aerosol size	
polydisperse	20
0.03μm diameter	86
0.07μm diameter	80
chemisty of AgI aerosol	
AgI-AgCl	96
AgI-AgCl-4NaCl	90
expansion rate (updraft)	
1.5 m s^{-1}	10
2.5 m s^{-1}	75
3.5 m s^{-1}	10
5.0 m s^{-1}	32
"rapid expansion"	59
seeding before cloud formation	160
seeding into supercooled cloud	26
temperature at cloud condensation	
warmer than 0°C	50
colder than 0°C	136
calibration experiments	40

method, and seeding temperature. Some 40 "calibration experiments" were performed during the course of research. These involved the formation of clouds with no ice nuclei to test for contamination or to check the operation of the FSSP-100, and ice nucleation tests to check the calibration of the ice particle counter. In addition to the experiments listed in Table 4.1, 22 experiments were performed in the ICC for the elucidation of the contact-freezing mode.

4.2 Cloud Model Simulations

An adiabatic parcel model was desired for use in comparison to cloud chamber experiments and for evaluation of the effect of new ice nucleus formulations. Therefore, it was desired to have a model with,

1. Sufficient physical detail and information with regard to the specific ice nucleation modes to be studied, and/or the ability to modify the model to include such details.

2. The ability to explicitly quantify the fate of ice nucleus aerosols in time, in terms of their scavenging by cloud particles, and for nucleation by different ice nucleation modes as a function of their size.

An adiabatic parcel model was not developed for comparison and evaluation of experimental data because one was made available which sufficiently filled the desired criteria. This is the model of Young (1977). This model essentially contains the same physics as appear in Young (1974a), but the newer version was adapted to a one-dimensional

framework and newer data were used to quantify parameters related to nucleation. The model simulates the formation of precipitation with a minimum of parameterization of the microphysical processes. Further details of the cloud model, particularly the pre-existing mechanistic descriptions for ice nucleation, are presented in Appendix A.

The adiabatic cloud model was used both as an analytical tool for estimating water supersaturations and scavenging, and it was used for predicting ice formation in comparison to experiments. Original model versions of ice nucleation were first used in comparitive simulations. After new quantitative descriptions of nucleation are derived based on the experiments described in section 4.1, the model is used for "blind" comparison to experiments and for examining the behavior of the nucleants in a variety of atmospheric cloud conditions (see Chapter 6). In Chapter 7, specific comparisons are made to some seeding experiments conducted in atmospheric clouds in the summertime.

4.3 Ice Nucleating Aerosols

The generation of AgI-AgCl aerosols by solution combustion has been described in detail by DeMott (1982). Basically, the addition of ammonium perchlorate (NH_4ClO_4) in small quantities to the standard AgI-acetone - ammonium iodide - water solution used to produce AgI results in the formation of some AgCl upon combustion. This AgCl becomes intimately mixed with AgI in the particles formed. A form of chemical synergism occurs in that the ice nuclei activity of these mixed particles is enhanced over that of pure AgI. This synergism was optimized for between 20 and 30 mole% NH_4ClO_4 with respect to AgI in the solution. The 30 mole% value was used to generate aerosols for this

research. AgI is present in solutions at 2% by weight. The particle size distribution produced by burning these solutions in the CSU statndard laboratory generator is shown in Figure 4.4. These results are from the scanning electron microscopy studies reported by DeMott et al. (1983).

Following Finnegen et al. (1984), AgI-AgCl-4NaCl aerosols were produced from the same solutions used to produce AgI-AgCl aerosols, but sodium perchlorate ($NaClO_4$) was added in a 4 to 1 mole ratio with respect to AgI. Particle size distribution following combustion was estimated using the electrostatic classifier in series with the condensation nucleus counter (to get total particle count of polydisperse aerosol). The measured distribution is shown in Figure 4.5 (double-hatched area). This size distribution must be corrected for the size dependent efficiency for charging aerosols prior to electrostatic collection and for particles which receive more than a single elementary charge and are thus undersized. This correction follows the linear inversion technique of Hagen and Alofs (1983).

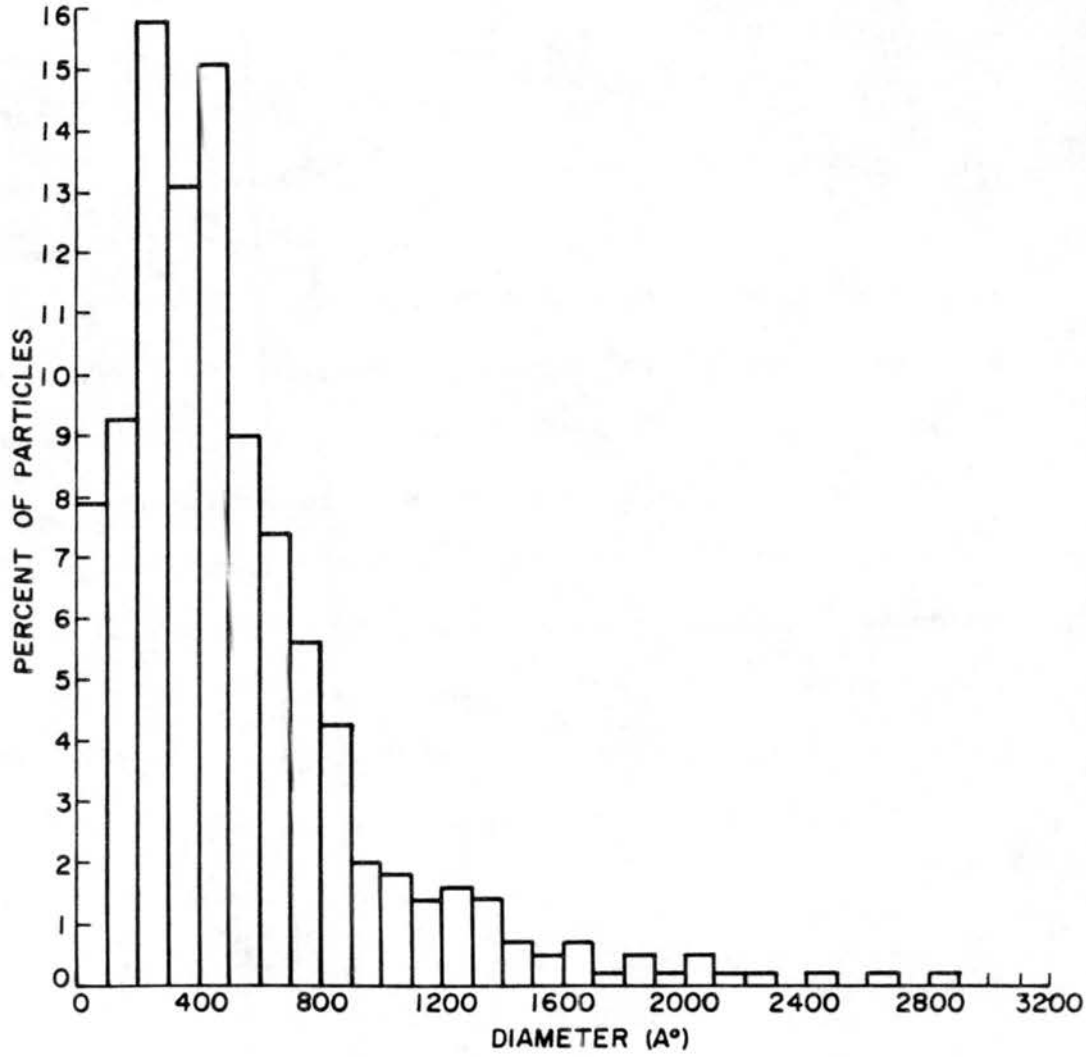

Figure 4.4 Size distribution of AgI-AgCl aerosols from the CSU standard generator, determined by scanning electron microscopy.

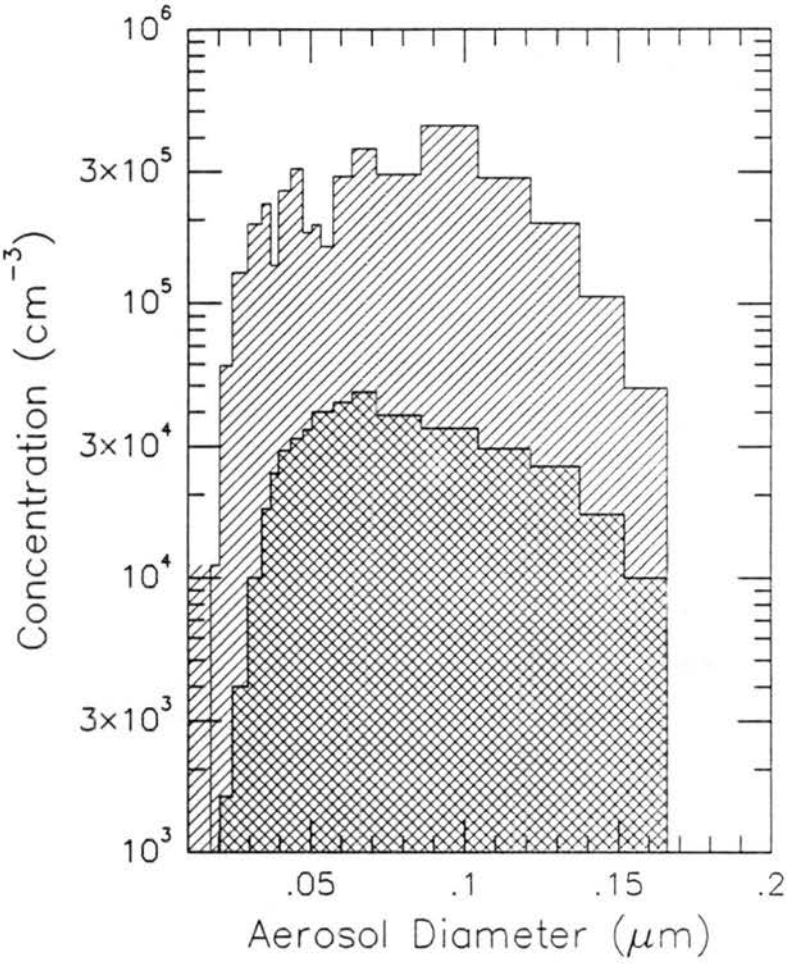

Figure 4.5 Size distribution of AgI-AgCl-4NaCl aerosols produced by the CSU standard generator, determined by electrostatic classification. The double hatched distribution gives the raw measurements, while the single hatched area is the distribution after correction for charging efficiency and multiple charging effects (see text).

V. NUCLEATION MODE-SPECIFIC EXPERIMENTAL RESULTS

5.1 Deposition Nucleation

5.1.1 AgI-AgCl aerosols

Results from two deposition nucleation experiments are shown in Figure 5.1. Raw and deconvoluted ice flux (s^{-1}) signals are shown in relation to cloud formation temperature in Figure 5.1a. The experiments show ice formation preceding cloud formation in both cases. In the colder cloud test (experiment 1789), ice was detected at the same time that cloud initially appeared. Due to the time required for crystals to grow to the size required to fall from the chamber and be detected, this means that nucleation and growth started in ice supersaturated air, well before cloud formed. The deconvoluted ice signal shows this clearly. In the warmer cloud test (experiment 9388), ice was detected during the second cloud record. The deconvoluted flux signal shows that ice was forming 2 records, or 30 s, prior to cloud formation. Figure 5.1b shows the cumulative ice signal versus ice supersaturation and demonstrates most of the features of the deposition nucleation experiments taken as a unit. These features are that ice nucleation rate increases with ice supersaturation, is higher at a colder temperature for the same saturation ratio, and the increase in nucleation rate with supersaturation slows as a parcel approaches water

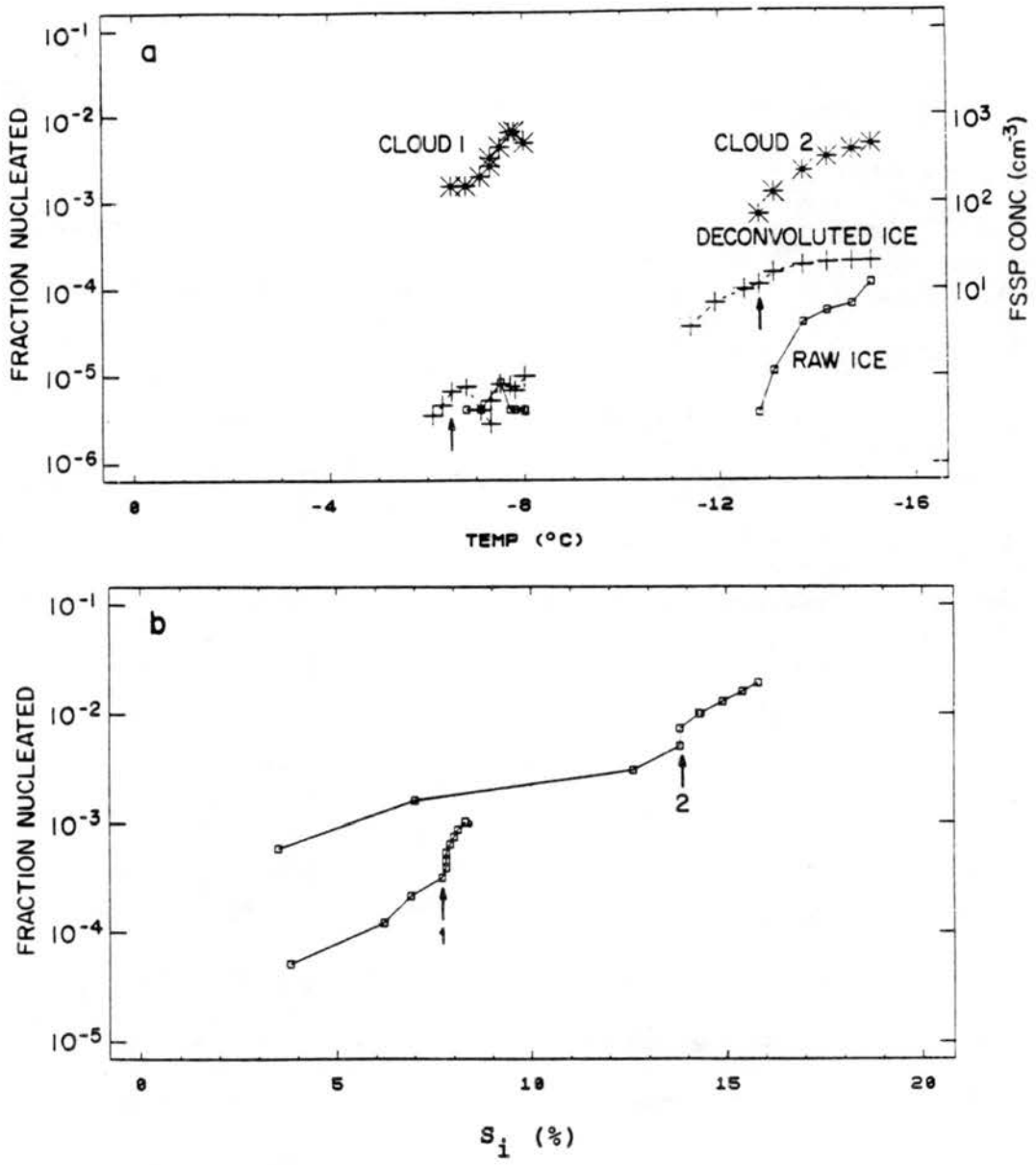

Figure 5.1 Ice formation with respect to cloud formation point in two experiments used in the analysis of deposition nucleation by AgI-AgCl aerosols. The raw (□) and deconvoluted (+) ice fractions nucleated (s^{-1}) versus temperature are shown in part (a). Cloud droplet concentrations (✳) are also indicated. The deconvoluted cumulative ice fractions nucleated are compared versus ice supersaturation in part (b). Cloud formation points are indicated by arrows.

saturation. This last feature was also noted in the study of Schaller and Fukuta (1979), who also provided some theoretical basis for this behavior. The increase in nucleation rate by other mechanisms besides deposition is clearly also noted in coincidence with the formation of cloud. The deposition experiments for AgI-AgCl aerosols are summarized in Figure 5.2, where the temporal paths of fractional activity versus ice supersaturation are shown.

The analyses of the deposition data for AgI-AgCl and for AgI-AgCl-4NaCl proceeded as described in Chapter 4. The active site parameter D_{dep} was computed by assuming time-independent nucleation (dependent only on supersaturation and temperature). This is displayed in Figure 5.3, along with a power law fit,

$$D_{dep} = a(S_i)^b \qquad (5.1)$$

with $a = 8.93 \times 10^4$ and $b = 1.923$. This simple fit is adequate ($r = 0.77$). However, the size-coded points in the figure indicate that there will be a tendency for (5.1) to overestimate the nucleation activity of larger aerosols and underestimate the activity of smaller ones. This shows that a surface area dependence for nucleation rate was not clearly realized in the experiments. This is shown in Figure 5.4, where the observed active fractions versus ice supersaturation are compared with the values predicted using (5.1) in (4.1). A size dependence for active fraction is apparent in the data, but a fit based on surface area exaggerates this. Considering that most particles in the polydisperse distribution of sizes produced by the combustion generator are between the sizes quantified, the formulation given in (5.1) may be

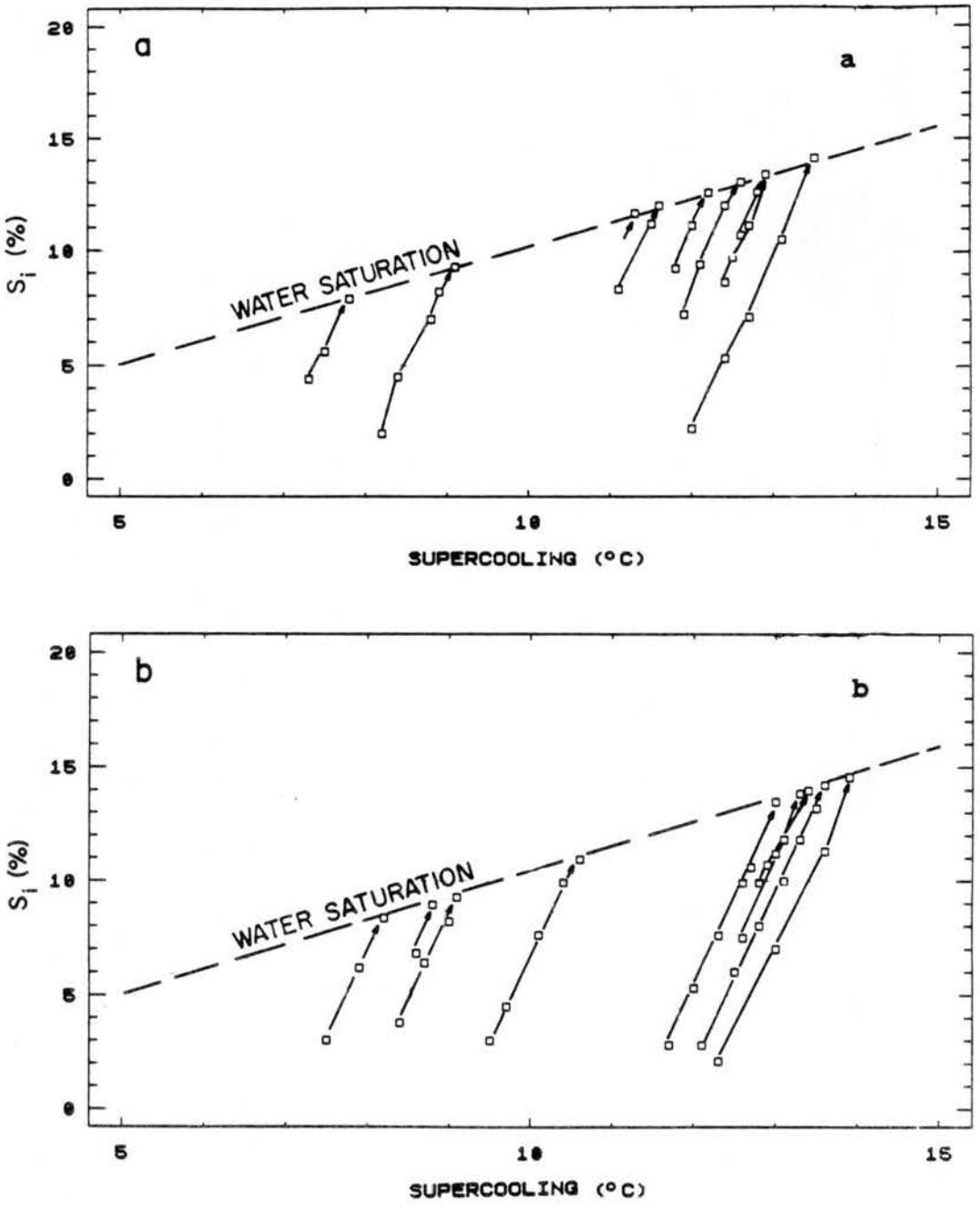

Figure 5.2 Summary of the thermodynamic history of data records indicating ice formation before cloud point in a number of experiments used to quantify deposition nucleation for AgI-AgCl (a) and AgI-AgCl-4NaCl aerosols.

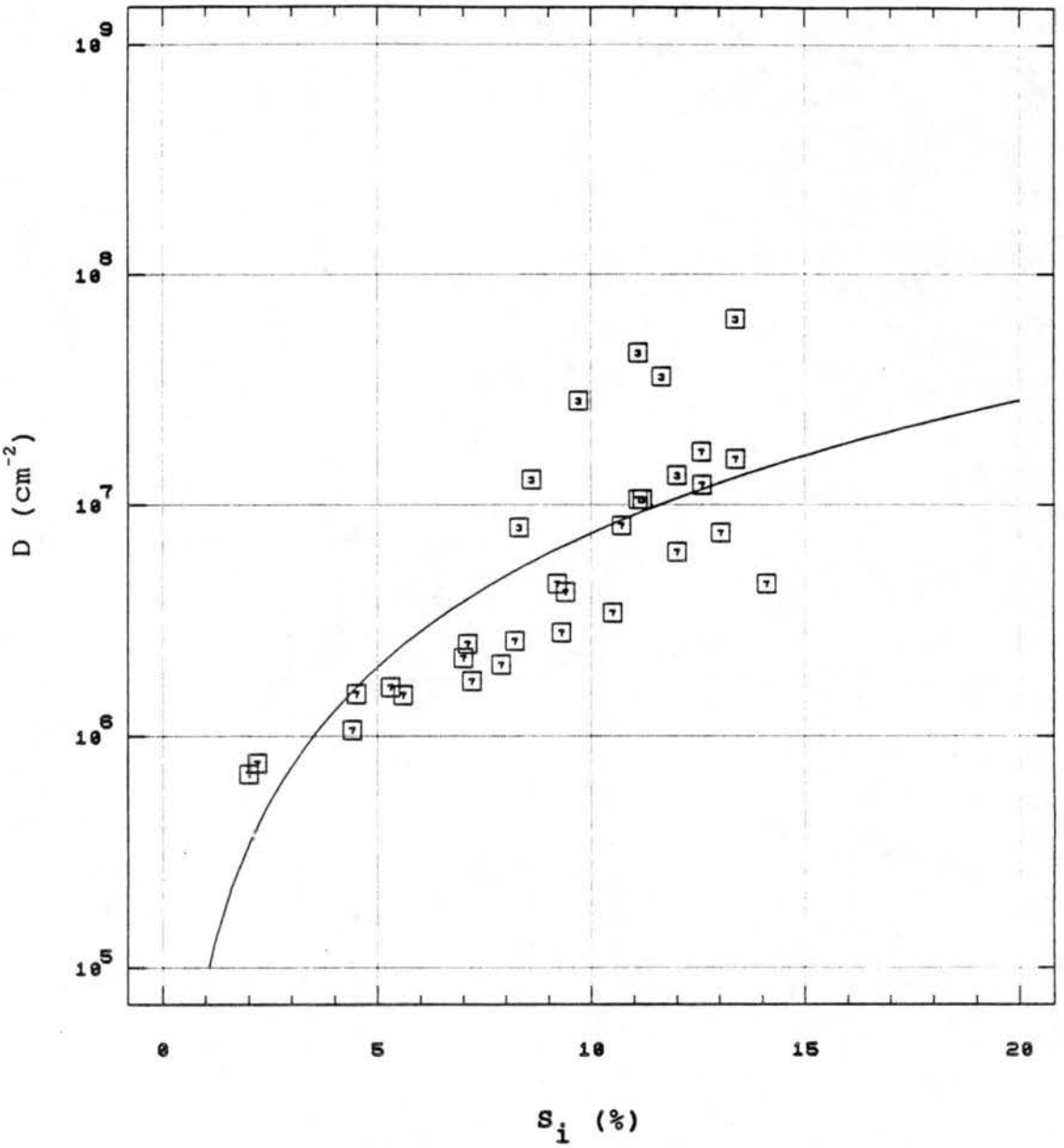

Figure 5.3 Active site density by deposition versus supersaturation with respect to ice for AgI-AgCl aerosols. A power law fit to the data using (5.1) is indicated. Data points are coded to be 100 times the aerosol diameter in microns.

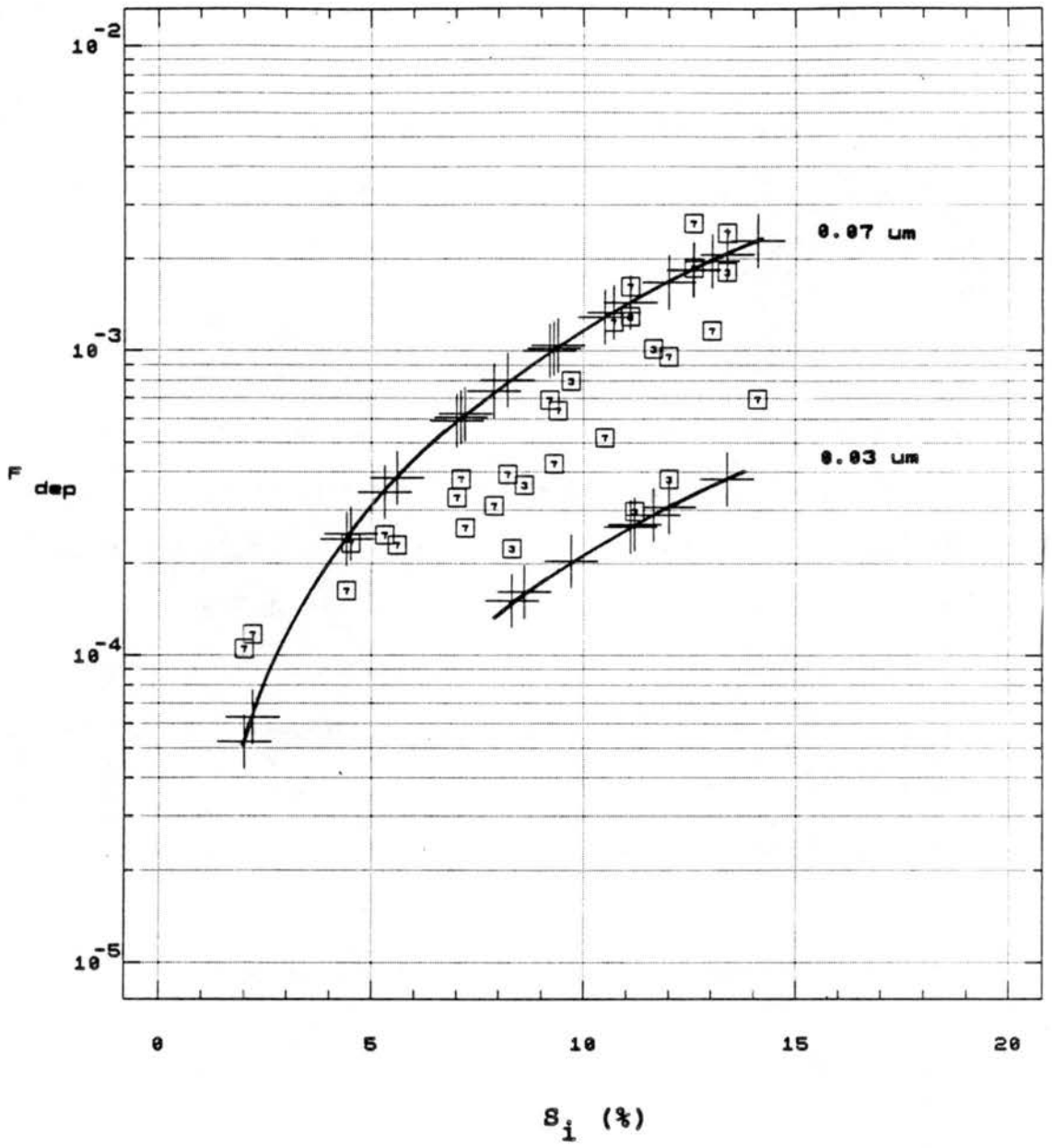

Figure 5.4 Fractions of AgI-AgCl aerosols effective by deposition for AgI-AgCl aerosols. Points are coded as in Figure 5.3, and the lines through the crosses indicate values computed for 0.07 and 0.03μm diameter sizes using (5.1).

a better method for quantifying deposition than Figure 5.4 initially suggests. It is also possible that a size independent formulation for deposition may do just as well. For example, directly formulating the fraction active by deposition (F_{dep}) versus ice supersatuation gives a correlation coefficient of 0.817 ($a = 2.30 \times 10^{-5}$; $b = 1.477$).

The variation in D_{dep} or F_{dep} with both temperature and ice supersaturation noted in Figure 5.1 can be quantified by formulating a dependence on (S_w) in place of temperature. This is how the deposition results of Fukuta and Schaller (1976) were quantified for the original version of AgI nucleation used in the adiabatic cloud model (see Appendix A). Figure 5.5 shows the positions of various D_{dep} values on the plane of ice supersaturation versus temperature. Equation 5.1 would characterize deposition with horizontal lines of constant D_{dep}, as shown by the dotted lines in Figure 5.5.

The solid lines that appear in Figure 5.5 come from the equation,

$$D_{dep} = a(S_i - 0.65(S_w) - 5)^b \qquad (5.2)$$

where $a = 5.018 \times 10^5$ and $b = 1.493$. This S_w dependence is taken to only be valid for $S_w > -8\%$. At lower values, only S_i is raised to the power b. Lines of negative slope toward water saturation are somewhat better supported by the data. Equation 5.2 is the final version of deposition nucleation quantified for AgI-AgCl aerosols for use in the adiabatic cloud model. Similar adjustments could be made to the size independent formulation for deposition.

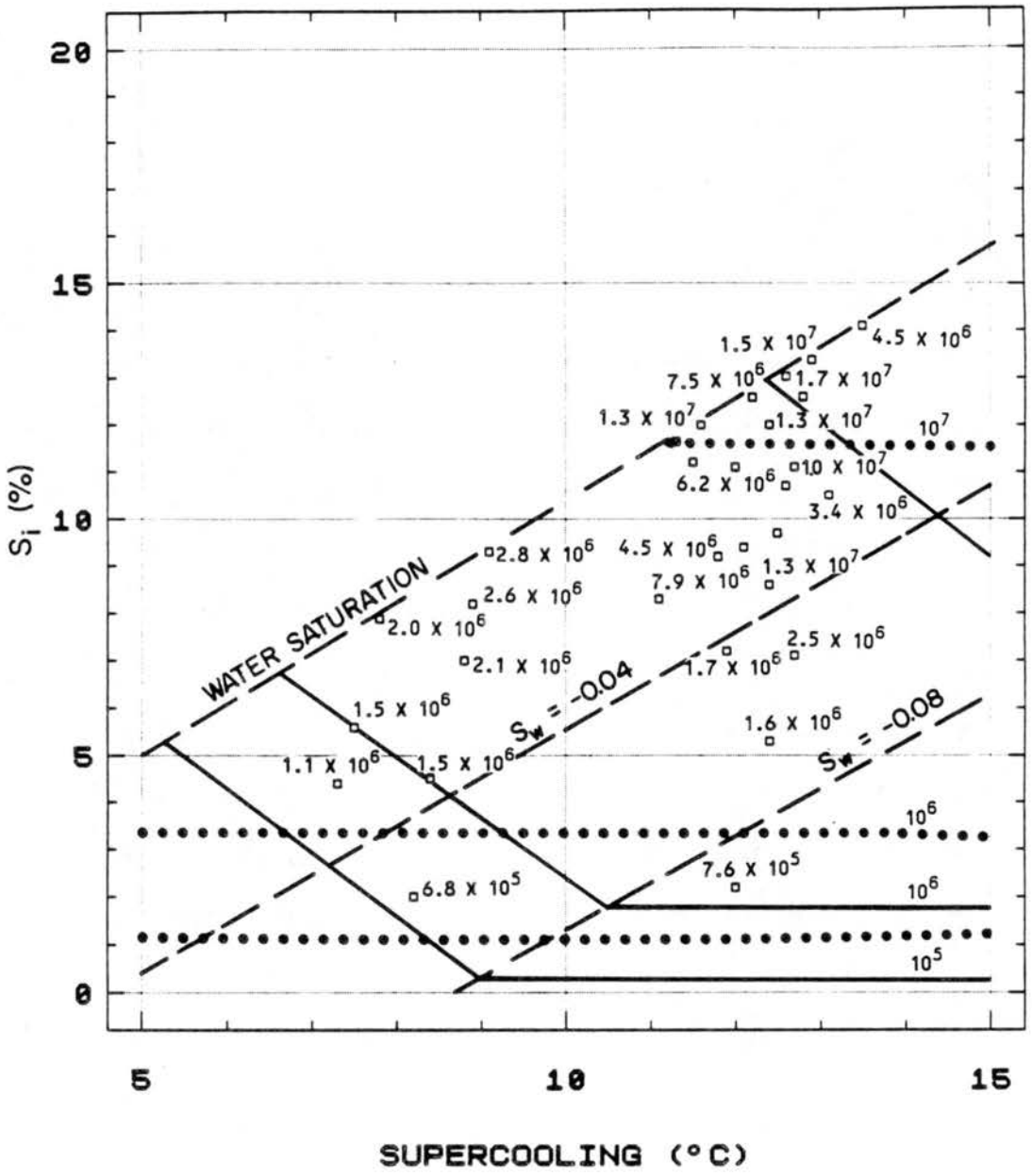

Figure 5.5 Experimental D_{dep} values for AgI-AgCl aerosols on an ice supersaturation-temperature plane. Lines of constant S_w on the S_i-T plane are also indicated. Values predicted by (5.1)[i] are shown by the dotted lines, while those predicted by (5.3) are shown by the solid lines.

5.1.2 AgI-AgCl-4NaCl aerosols

Deposition nucleation experimental paths for tests of AgI-AgCl-4NaCl aerosols are summarized in Figure 5.2b. The ranges of temperature and supersaturation covered are adequate. Active fraction as a function of particle size, computed using a simple multiplicative fit versus ice supersaturation for active site density, is shown by the solid lines in Figure 5.6 ($a = 2.46 \times 10^6$, $b = 1.467$, $r = 0.66$). A size effect is more apparent than for AgI-AgCl aerosols and seems better fit by the simple ice supersaturation dependent active site density formulation. It can also be noted that the activity by deposition is higher for AgI-AgCl-4NaCl aerosols than for AgI-AgCl. This seems reasonable, considering their greater affinity for water. In fact, it is possible that the nucleation is really not deposition in the classical sense for these aerosols, but more a form of freezing of liquid layers. The simple S_i fit (dotted lines) and the fit including sensitivity of D_{dep} to S_w (solid lines) are shown on the supersaturation-temperature plane for AgI-AgCl-4NaCl aerosols in Figure 5.7. Again, as for AgI-AgCl aerosols, the introduction of the S_w dependence ($a = 5.8655 \times 10^6$, $b = 1.3462$, $c = 2$) provides better agreement with the observed results, particularly at the warmest temperatures.

5.2 Contact-freezing Nucleation

The results of contact-freezing nuceation experiments performed for AgI-AgCl aerosols in the isothermal cloud chamber are summarized in Table 5.1. Included are the results of tests with nearly monodisperse aerosols (0.03 and 0.07μm diameter), and polydisperse aerosol results based on tests reported by DeMott et al. (1983). The polydisperse

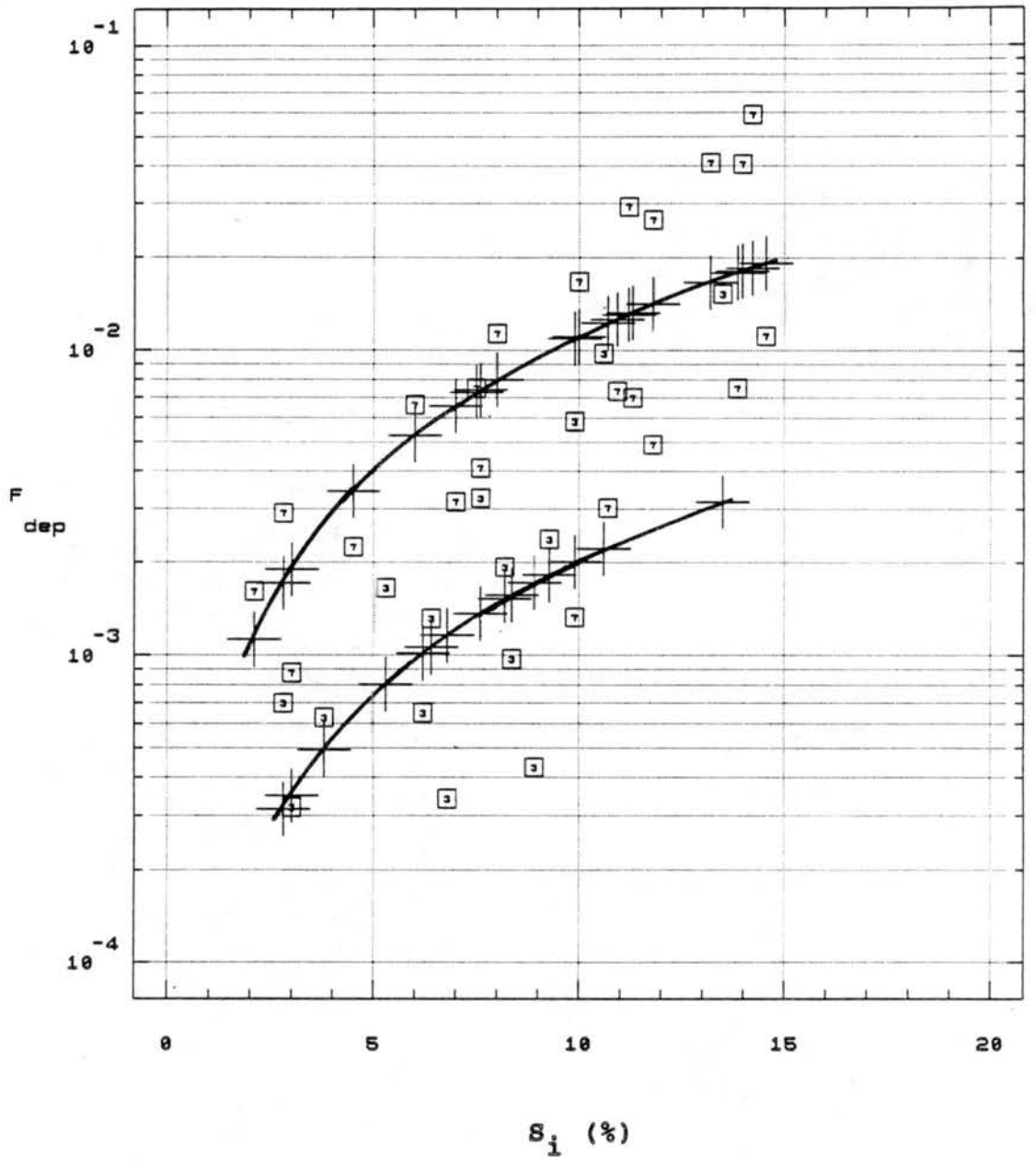

Figure 5.6 Deposition fractions effective, as in Figure 5.4, but for AgI-AgCl-4NaCl aerosols.

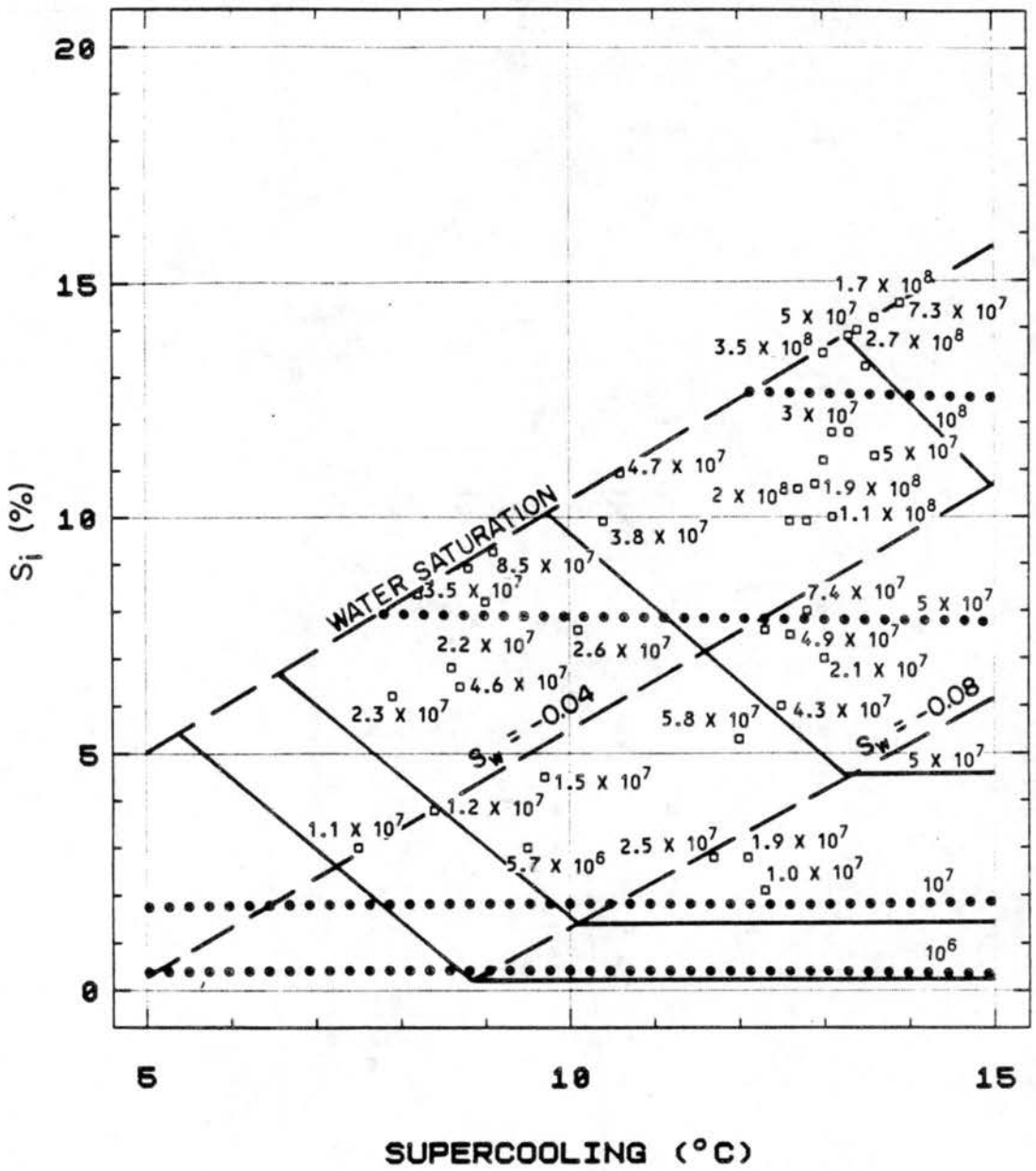

Figure 5.7 D_{dep} for AgI-AgCl-4NaCl on the S_i-T plane. Lines are given as in Figure 5.5.

aerosol is characterized by an average size of 0.052μm diameter. These results will now be explained.

The values for the rate constant k and the fraction active F_{ctf} given in Table 5.1 are the values that have been corrected for the artificial dilution effect which exists in the ICC. As shown in Section 4.1.2, K_B is computed from k and N_d using 4.2, and D_{ctf} is computed from F_{ctf} and r_a using 4.1. For the nearly monodisperse aerosols, each line of data in Table 5.1 represents an average of 2 to 3 experiments. Polydisperse aerosol data are averages of 5 to 7 experiments.

The rate constants were determined from the analysis of the ice crystal formation kinetics plots shown in Figures 5.8, 5.9, 5.11 and 5.12. The nature of such plots and their use have been discussed by DeMott et al. (1983), but will be briefly reviewed here. The vertical scale in the plots is the natural logarithm of the percentage fraction of the total aerosol number effective as ice nuclei (at the particular cloud temperature) which remain at time t. For the raw data plotted, the total aerosol number effective is taken as the total number of ice crystals counted until the sensitivity of the measurement prevents further detection in the chamber. A linear plot implies a pseudo-first order process, and the negative slope of the plot is the rate constant. A collision-dependent nucleation process will be pseudo-first order in the ICC because droplet concentrations and saturation ratio are nearly constant in each experiment. These tests provide a unique and almost unambiguous opportunity to quantitatively confirm the conclusion by DeMott et al. (1983) that contact-freezing is by far the predominant nucleation mode for AgI-AgCl aerosols in the dense ICC clouds.

Table 5.1

Contact-freezing Nucleation Experiments in Isothermal Cloud Chamber

T(°C)	r_a(μm)	N_d(cm^{-3})	k(min^{-1})	K_B(cm^3 s^{-1})	F_{ctf}	S_i(%)	D_{ctf}(cm^{-2})
-6	0.015	4300	---	---	0.0004	5.99	1.41E+07
-6	0.026	4300	---	---	0.0036	5.99	4.25E+07
-6	0.035	4300	---	---	0.0020	5.99	1.30E+07
-8	0.015	4300	0.149	5.76E-07	0.066	8.10	2.41E+09
-8	0.026	4300	0.114	4.22E-07	0.066	8.10	8.04E+08
-8	0.035	4300	0.078	2.89E-07	0.398	8.10	3.45E+09
-10	0.015	4300	0.185	7.17E-07	0.122	10.24	4.51E+09
-10	0.026	4300	0.159	5.89E-07	0.210	10.24	2.78E+09
-10	0.035	4300	0.094	3.19E-07	0.546	10.24	5.35E+09
-10	0.015	2100	0.123	8.91E-07	0.090	10.24	3.53E+09
-10	0.035	2100	0.065	4.71E-07	0.522	10.24	5.11E+09
-12	0.015	4300	0.213	8.25E-07	0.243	12.37	9.14E+09
-12	0.026	4300	0.141	5.22E-07	0.390	12.37	5.82E+09
-12	0.035	4300	0.118	4.37E-07	0.458	12.37	6.91E+09
-12	0.015	2100	0.139	9.85E-07	0.133	12.37	5.29E+09
-12	0.026	2100	0.076	5.51E-07	0.296	12.37	4.13E+09
-12	0.035	2100	0.088	6.37E-07	0.284	12.37	2.17E+09
-16	0.015	4300	0.212	7.85E-07	0.344	16.86	1.51E+10
-16	0.026	4300	0.182	6.74E-07	0.450	16.86	7.04E+09
-16	0.035	4300	0.092	3.43E-07	0.650	16.86	6.89E+09

Narrow size ranges of ice nucleating aerosols were not available for the earlier studies.

All of the kinetics plots are very nearly linear, as the linear regression correlation coefficients (listed in each figure caption) indicate. The decay of particle number by air flowing out of the chamber is also a first order process, but fortunately of a smaller magnitude than the nucleation process. This dilution rate is superimposed on the true contact-freezing nucleation rate and must be subtracted. The exact magnitude of the dilution rate varies with cloud density and temperature, subject to the operator's subjective assessment that cloud density is at the appropriate value and

temperatures throughout the chamber are within an acceptable degree of equivalence. A consistent value was always used for equivalent experiments. For example, in the experiments performed with 0.03μm aerosols at -8°C and N_d = 4300 cm^{-3} (Figure 5.8), the dilution flow was 26.9 *l* min^{-1}. Dividing this value by the chamber volume gives the rate constant for dilution (k_{dil}) as 0.028 min^{-1}. Subtracting k_{dil} from the apparent rate constant k_{app} (= 0.177 min^{-1}) gives the actual rate constant **k** (= 0.149 min^{-1}), as demonstrated in Figure 5.8. For 0.07μm particles in the same cloud and dilution conditions, k_{app} = 0.106 min^{-1}, so **k** = 0.078 min^{-1}.

The same relationship between rate constant and particle size is also noted at -16°C, as shown in Figure 5.9. The magnitudes are slightly different (see also Table 5.1), but in both cases, the rate constant increases nearly inversely with particle size. Reassuringly, the rate constant for the polydisperse particle size distribution falls between those of the two nearly monodisperse sizes. Theoretically, assuming a contact-freezing nucleation process dominated by Brownian collection, the rate constant for 0.03μm particles should be 2.7 times the rate constant for 0.07μm particles. This is shown in Figure 5.10, where the theroretical collection kernels for Brownian coagulation between monodisperse particles and the droplet distributions present in the ICC are plotted. These theoretical values were computed using the scavenging equations from Young (1974b), also listed in Appendix A. Collection kernels (K_B) calculated from the rate constants determined in Figures 5.8 and 5.9 are also plotted in Figure 5.10. The ratios between measured K_B for 0.03 and 0.07μm particles at -8 and -16°C are 2.0 and 2.3, respectively. For all the average data listed in Table 5.1

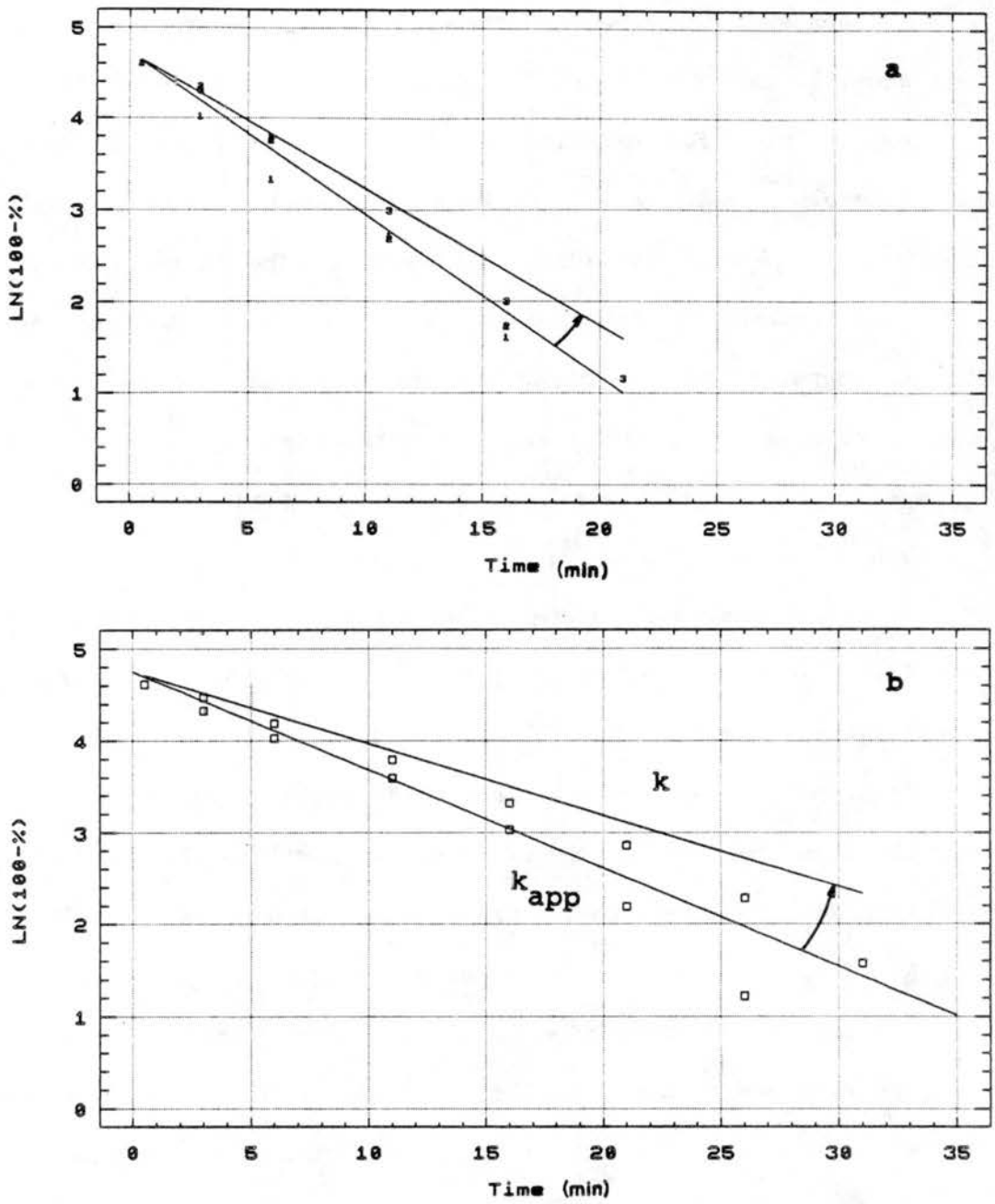

Figure 5.8 Ice crystal formation kinetics plot for 0.03μm (a) and 0.07μm (b) AgI-AgCl aerosols at -8°C in the isothermal cloud chamber. Plotting convention is discussed in the text. Numbered symbols in (a) indicate specific experiments to which an average linear regression was fit (r^2 = 0.98). In (b), r^2 = 0.94. Correction to the regressions for dilution during the experiments is indicated by the arrows. Cloud droplet concentration was 4300 cm^{-3}.

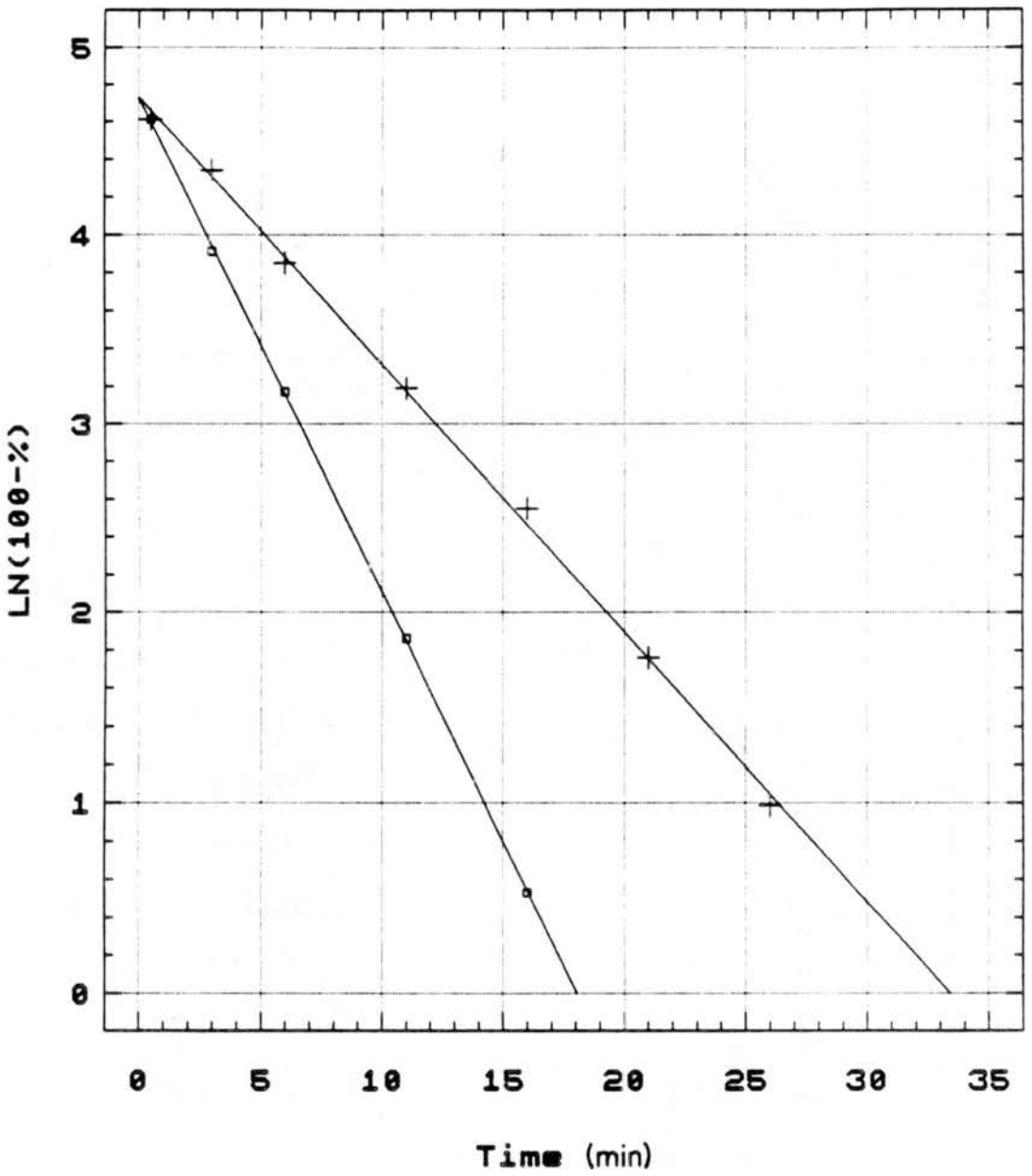

Figure 5.9 Isothermal cloud chamber kinetics plot for AgI-AgCl aerosols at -16°C. Results for 0.03μm aerosols are given by + symbols, while 0.07μm results are given by □ symbols. Linear correlation coefficients are > 0.99 in each case.

and plotted in Figure 5.10, the ratio is 2.0 for these particle sizes. This is a reasonably good agreement between experiment and theory. However, the actual magnitudes of experimental K_B are higher than the theoretical values. Contributing to the apparent discrepancy are the uncertainties in experimental values. The sources of uncertainty are the droplet concentration values and the ice crystal counting process. The uncertainty in both of these factors has been estimated as 30% (see Chapter 3). Thus, the net uncertainty in K_B is up to 60%. This uncertainty applied to the average value of K_B (not the uncertainty of the average) versus size is indicated in Figure 5.10. This average uncertainty very nearly takes in the theoretical values. Still, it seems apparent that some other factors are enhancing the experimental collection kernel in the ICC, so the assumption of the dominance of Brownian coagulation is probably not valid. For example, the influence of thermo-, diffusio- or electrophoretic forces would simply be linearly additive to the Brownian rate constant (DeMott et al., 1983). An enhancement from the net effects of diffusiophoresis and thermophoresis could only occur if water subsaturation exists at least locally in the ICC. A subsaturation of 7% with respect to water would have to exist to bring the theoretical collection kernel in line with the average value observed, based on computations made with the scavenging model. This is probably unreasonable for the experiments performed, although some cloud depletion is always noted, particularly at the onset of nucleation, when most of the ice is produced. There is no way to measure this subsaturation. Electrophoresis could play a role, since the ultrasonic nebulizer technique for droplet atomization can place small charges on droplets. This was not investigated further,

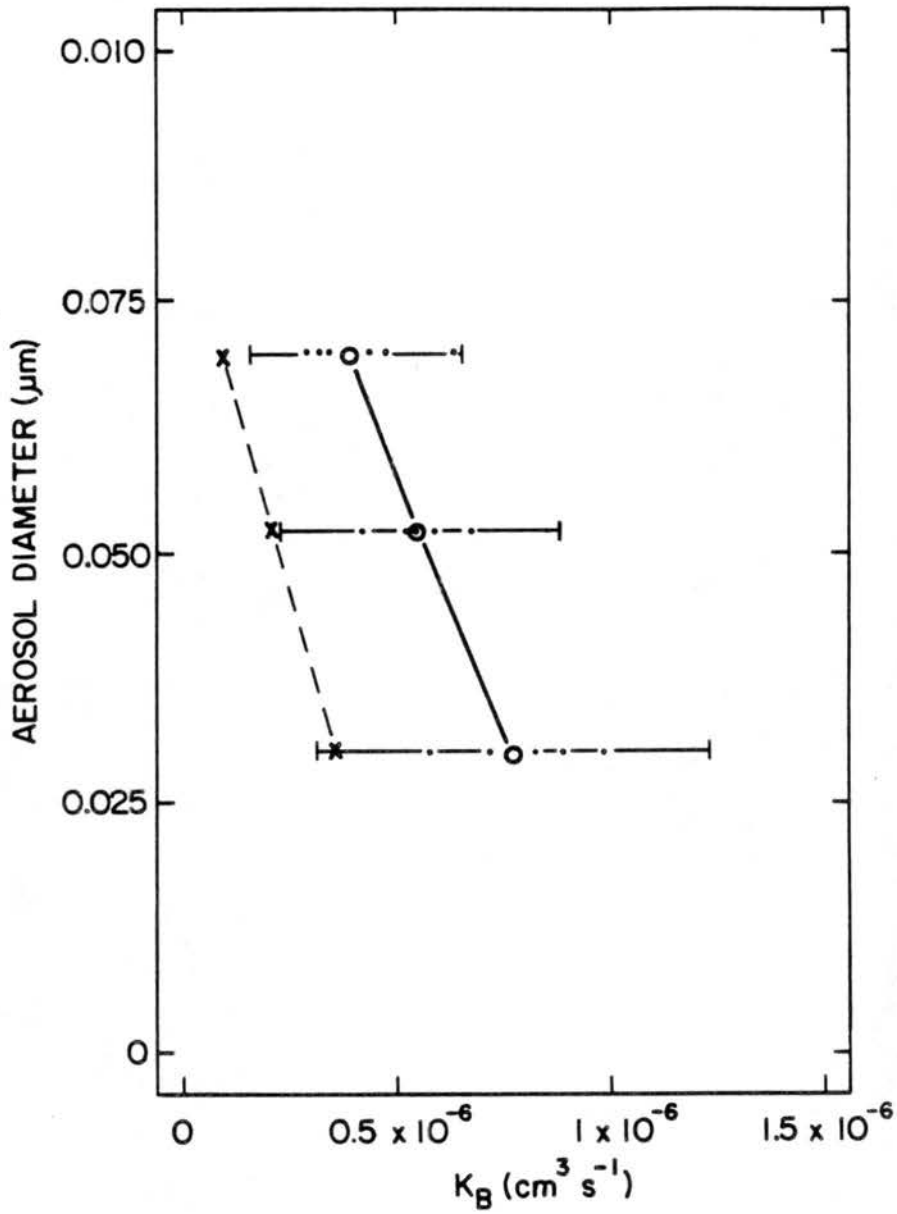

Figure 5.10 Theoretical (--x--) and experimental (dots) computations of collection kernel versus aerosol diameter, as described in the text. Average isothermal chamber experimental values (-o-) and their uncertainty based on measurement uncertainties (brackets) is also indicated.

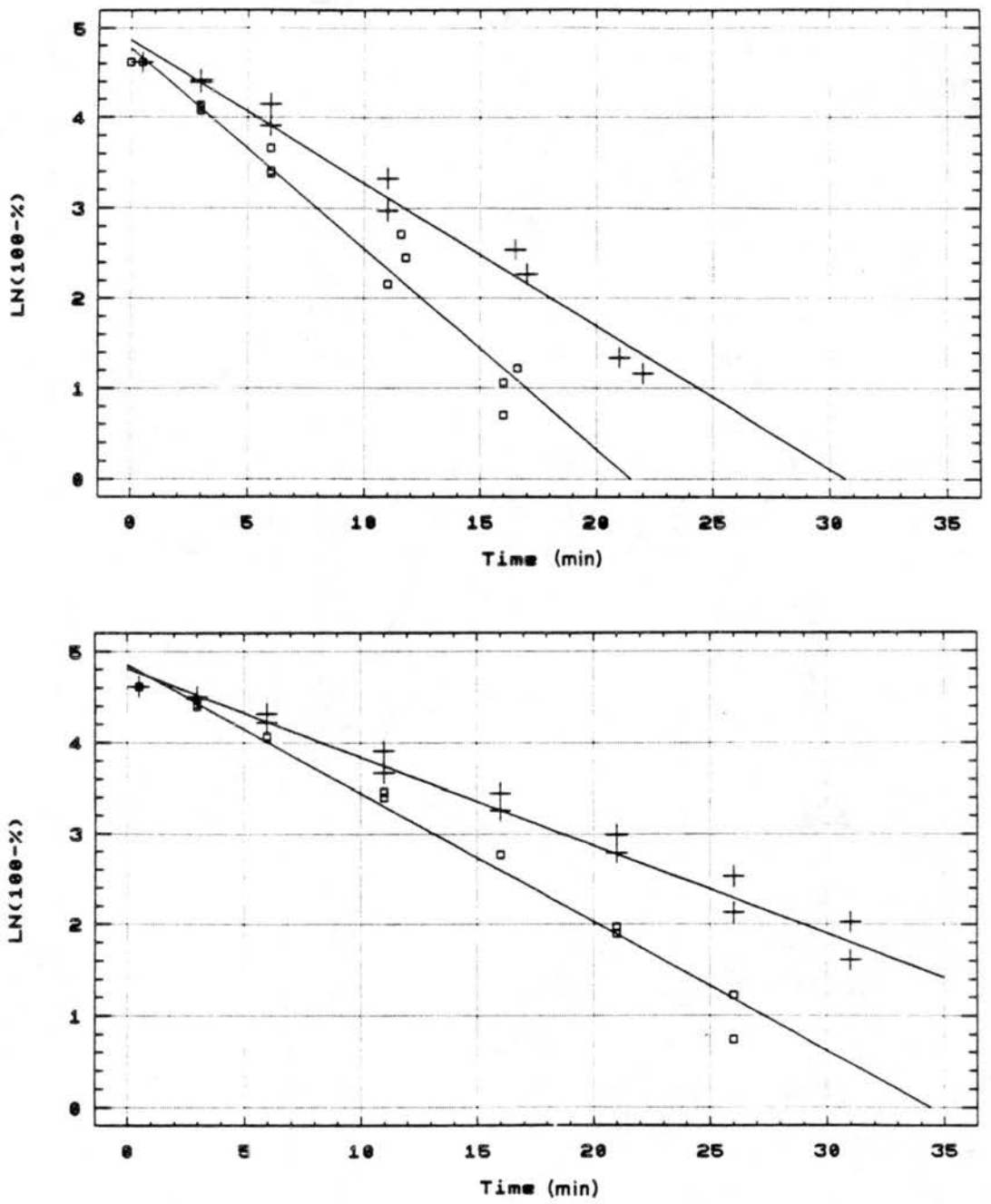

Figure 5.11 Ice crystal formation kinetics in 4300 cm^{-3} (□) versus 2100 cm^{-3} (+) clouds in the isothermal cloud chamber for 0.03 μm (a) and 0.07μm (b) AgI-AgCl aerosols at -10°C.

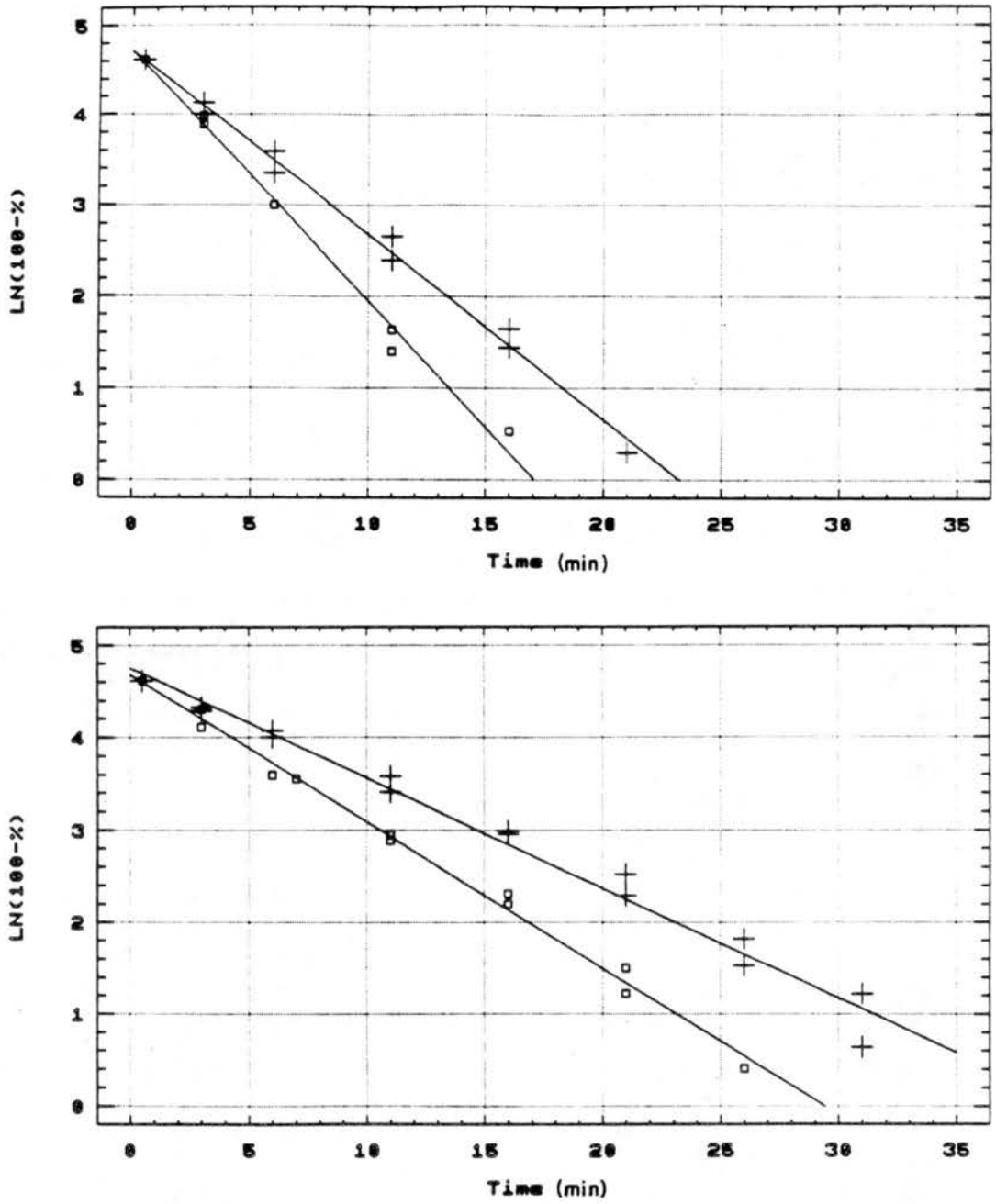

Figure 5.12 As in Figure 5.11, but at -12°C.

since the primary purposes of these experiments were to give confidence that nucleation is primarily by contact-freezing for AgI-AgCl aerosols in the ICC, and to define the potential nucleation activity (after collision) by this mechanism.

For the same aerosol, the effect of a change in droplet concentration is noted at -10 and -12°C in Figures 5.11 and 5.12. As qualitatively expected from theory for contact-freezing, higher droplet concentrations lead to faster rates of ice crystal nucleation for the same ice nucleant size. Theoretically, for Brownian collection alone, the ratio between these rates should simply be the ratio of droplet concentrations, since the droplet size distribution stays approximately the same. This ratio is 2.05. The experimental ratio is 1.53. Once again, this represents fair agreement between theory and experiment, and the difference can partly be explained by measurement uncertainties.

For every experiment, the apparent potential aerosol fraction effective as ice nuclei by contact-freezing must also be adjusted for dilution losses. This is done by multiplying the measured effective fraction by the ratio of the apparent rate constant to the true rate constant. These are the values listed in Table 5.1 and plotted versus temperature in Figure 5.13. Uncertainty is not indicated, but is 30% for all points. The particle sizes are distinguished to clearly show their relationship to potential fractional activity. Cooper (1974) has hypothesized that contact-freezing nucleation occurs because ice-like embryos already existing on the surface of aerosol particles which are not viable for deposition nucleation, but are viable for freezing nucleation, are brought into contact with a liquid droplet surface.

Thus, contact-freezing nucleation activity can be formulated, in a similar manner to deposition nucleation, as a function of ice supersaturation. Since effectiveness decreases sharply at warm temperatures, (5.1) can be modified as,

$$D_{ctf} = a(s_i - c)^b \qquad (5.4)$$

to fit the data. Water saturation is assumed to determine s_i (fractional supersaturation here) at any temperature in the ICC. This assumption is reasonable, regardless of ambient humidity, if one follows Cooper's arguments that particles will always be exposed to at least water saturation for a sufficient adjustment time as they are about to collide with droplets. A correlation coefficient of 0.95 was for obtained for (5.4) with the regression coefficients $a = 1.198 \times 10^{12}$, $b = 1.98$, and $c = 0.055$. Figure 5.14 summarizes the results for contact-freezing. The potential fraction active versus ice supersaturation as a function of particle size as predicted with the aid of (5.4) is presented, overlying the experimental values from which the predicted values were derived. This result is also be compared to the results of the original model fit to (5.4). The model formulation that was based on results of a study of pure AgI aerosols underestimates the contact-freezing activity of all sizes of AgI-AgCl aerosols by as much as 100. The reasons for the enhanced activity of AgI-AgCl aerosols are unknown, but some speculations have been made by DeMott et al. (1983). These were that the hexagonal crystalline symmetry and lattice parameters for AgI-AgCl aerosols should be closer to ice than for AgI, and that hydrophillic sites might also be created

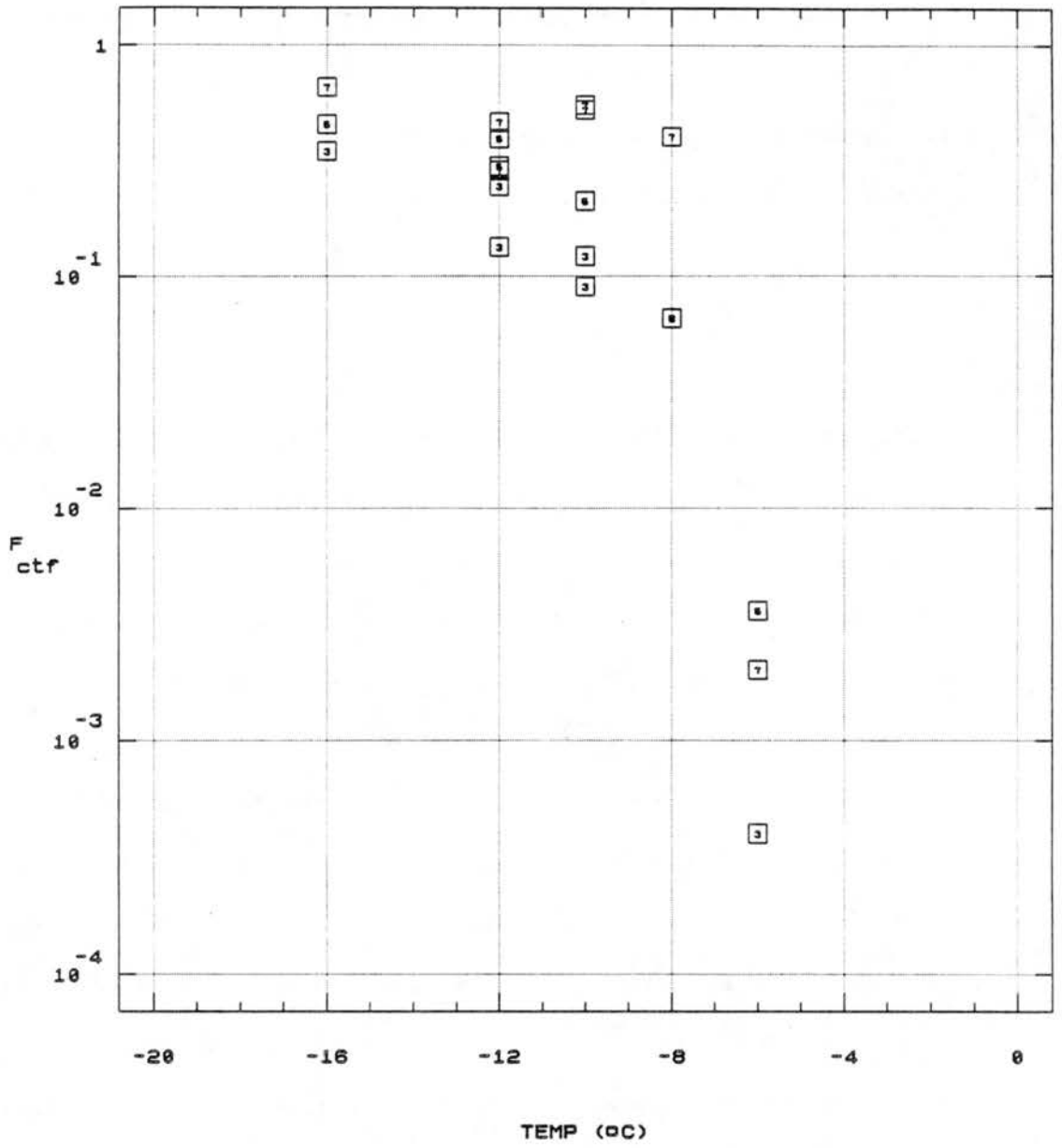

Figure 5.13 Observed fractional activities by contact-freezing versus temperature for AgI-AgCl aerosols in the isothermal chamber. Numbered symbols are 100 times the aerosol diameter in microns, and are average values for each set of temperature and droplet concentration conditions. The 5's are for the average size of the polydisperse aerosol size distribution.

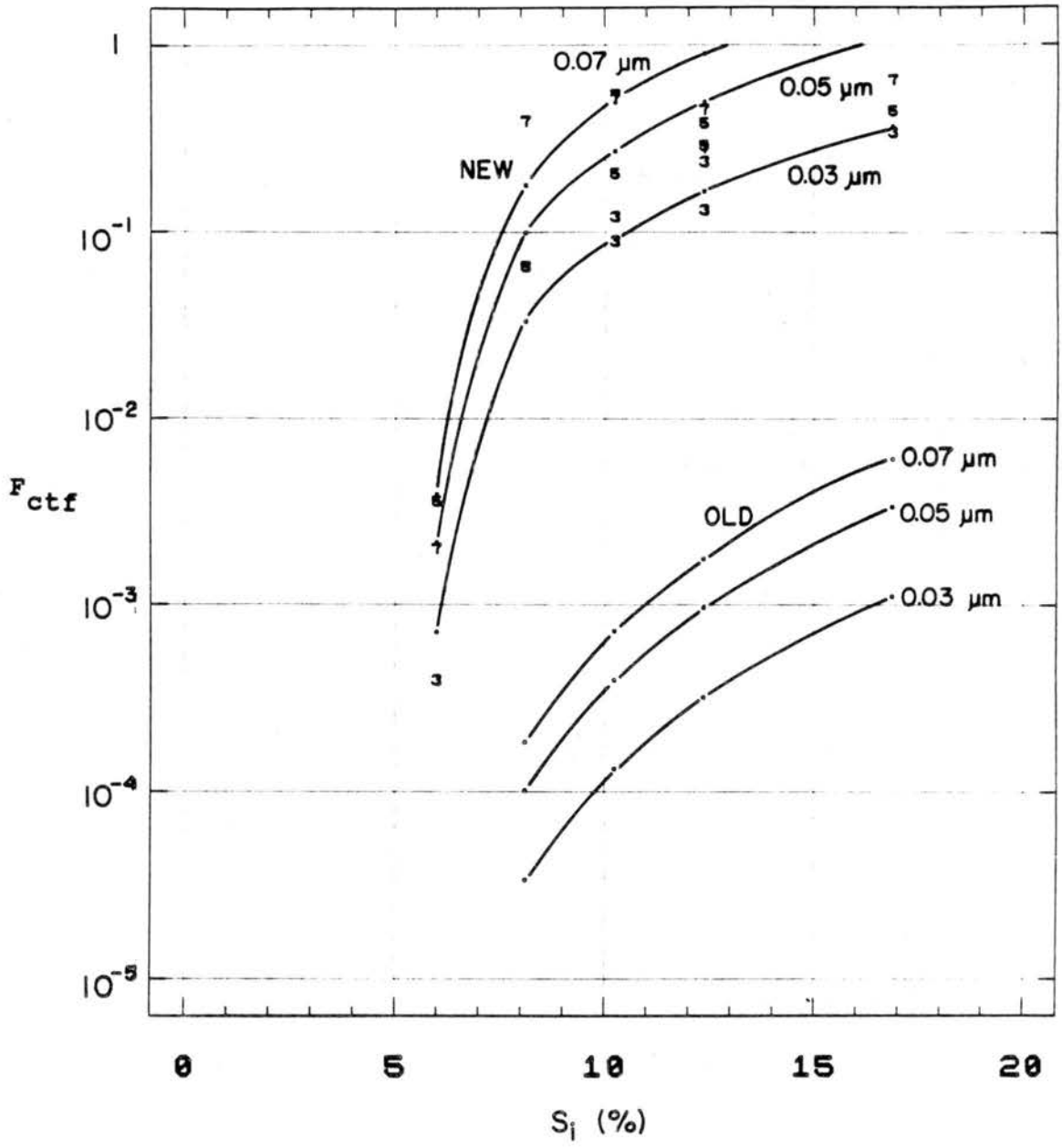

Figure 5.14 Contact-freezing activity of AgI-AgCl aerosols versus ice supersaturation as formulated in the NEW and OLD versions of the adiabatic cloud model. Average experimental data are given by symbols, as in Figure 5.13.

on the particle surface due to the substitution of impurity ions (Cl^-) in the AgI lattice. Palanisamy et al. (1986) have since reiterated these ideas and they directly correlated the closeness of match to ice of varoius lattice characteristics of AgI-AgCl solid solutions with the minimum supercooling required to freeze bulk water.

A few selected comparisons can be made between the instantaneous theoretical collection kernel and the experimental collection kernel estimated assuming all nucleation is by contact-freezing in DCC experiments using AgI-AgCl aerosols. This is done to determine whether the ICC results are relevant and transferable to the more complex clouds present in the DCC. This is vital for the differentiation of the final two nucleation modes using DCC experimental results. The experimental periods chosen for comparison were selected based on the presence of conditions where contact-freezing should be a favored nucleation mode with respect to deposition, based on results already presented, and immersion-freezing, as discussed in the next section. Contact-freezing should predominate at temperatures warmer than about -12°C when droplet concentrations, and thus collision rates, are high. The evolution of temperature, cloud characteristics, and fractional ice formation in one such experiment is depicted in Figure 5.15 (experiment 9588). Quantities are plotted versus pressure to give a one dimensional sense of a parcel rising (pressure lowering) and cooling until cloud formation. In this experiment, 0.03μm AgI-AgCl particles were injected into the DCC well before cloud formation at -8.5°C. For simplicity in this crude comparison, average cloud droplet concentrations and diameters were used for computing theoretical scavenging rates at each time step. Since clouds were only slightly supersaturated, phoretic

effects were ignored. The contribution of aerodynamic capture to collisions was also negligible. It is evident on comparing the observed and calculated contact-freezing cumulative ice amounts shown in Figure 5.15, that contact-freezing strongly contributed to ice formation, but other nucleation modes may have also operated in this particular experiment.

For experiments in which contact-freezing was expected to be dominant, it was possible to calculate an observed psuedo-collection kernel for comparison to the theoretical collection rates for monodisperse particles. In each case, the smoothed and deconvoluted cumulative ice crystal formation signal was differentiated at the same 15s intervals for which data were recorded and for which theoretical calculations were made. These ice formation rates were multiplied by the liquid water volume (cm^3) to obtain the collection kernel. Comparison of theoretical and experimental values was made to near -11°C for several experiments encompassing both monodisperse particle sizes studied. This represented 2 to 3 minutes scavenging time in cloud. The results are given in Figure 5.16. The DCC results for 0.03μm AgI-AgCl aerosols agree well on average with expectations based on the contact-freezing results found in the ICC. In fact, the equivalence between the observed and theoretical rates shows that whatever transport process was not properly accounted for in the ICC tests, was not a factor in the DCC tests. For 0.07μm aerosols, the theoretical calculations set a lower limit to the values of scavenging rate inferred from the the experimental nucleation rates. In other words, the nucleation rate does correlate reasonably well with the scavenging

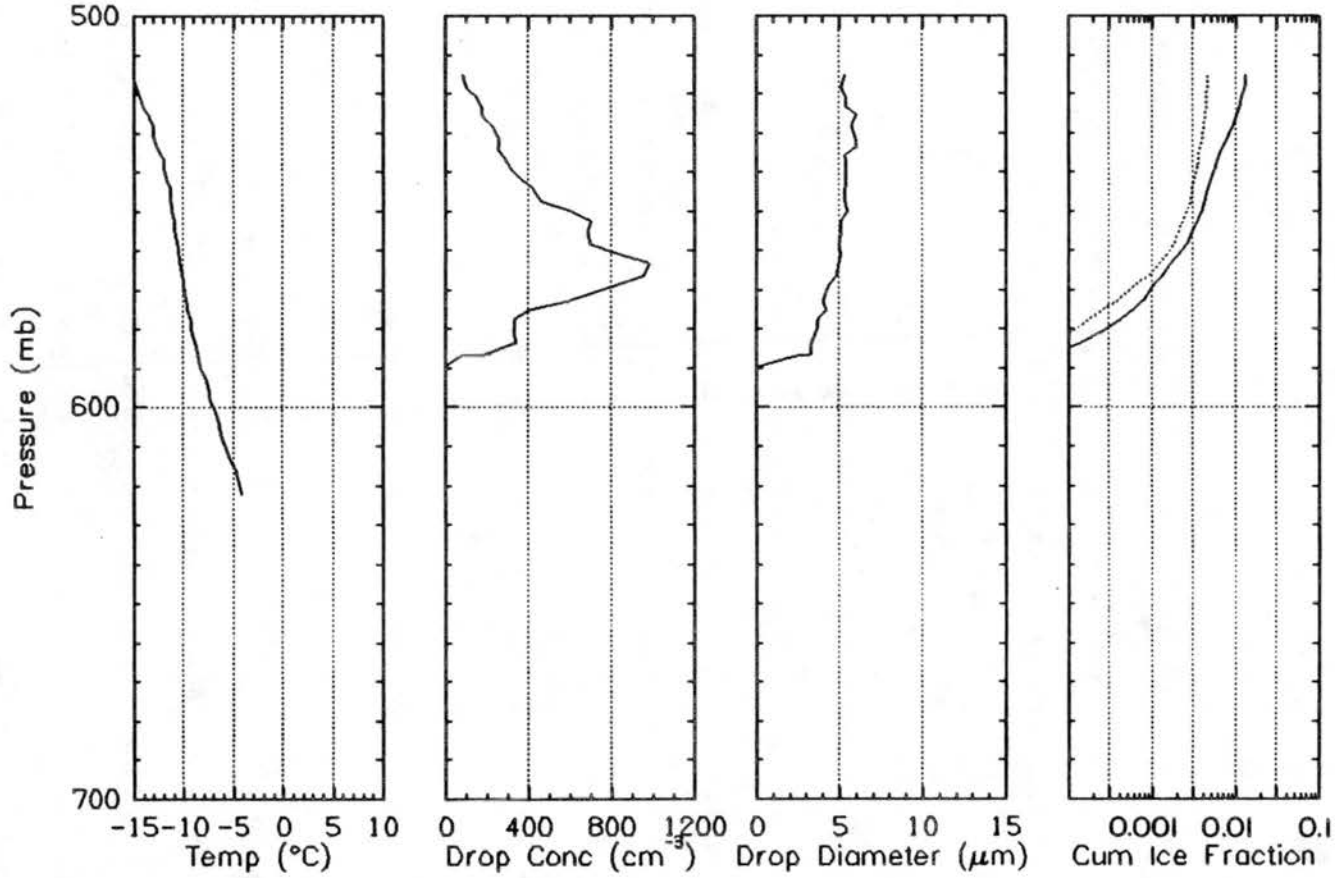

Figure 5.15 Plot of experimental quantities measured during a dynamic cloud chamber expansion in which the contact-freezing nucleation mode was anticipated to play a major role in ice formation. The cumulative (solid line) and predicted contact-freezing (dotted line) fractions nucleated by the 0.03μm AgI-AgCl aerosols injected before cloud formation are indicated in the ice panel.

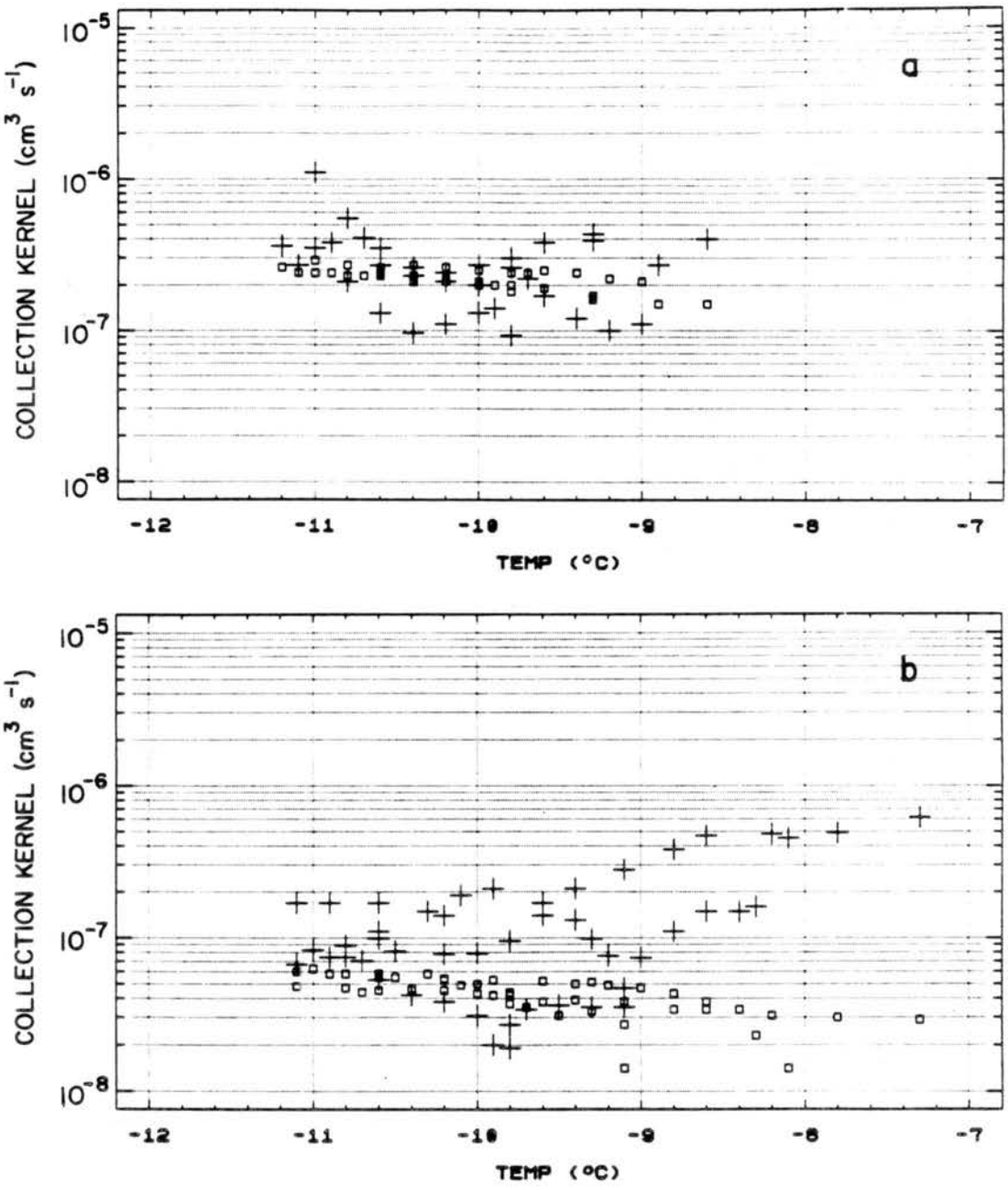

Figure 5.16 Compilation of DCC 15 s collection kernels versus T, calculated based on theory (□) and based on nucleation rates observed in experiments (+). Data are from a selection of experiments (as in Figure 5.15) in which cloud was seeded before formation with 0.03μm (a) and 0.07μm (b) AgI-AgCl aerosols.

rate, indicating the likely predominance of contact-freezing, but other nucleation mechanisms are probably acting.

5.3 Immersion-freezing Nucleation

Describing immersion-freezing required descriptions of the incorporation of ice nuclei into cloud droplets and quantification of the freezing fraction following such incorporation. Scavenging of ice nucleus aerosols by cloud droplets is controlled by the same transport processes relevant to contact-freezing nucleation. The second method of incorporation, action as CCN, has never been measured for the ice nuclei used.

5.3.1 CCN activity of ice nucleating aerosols

As described in Chapter 4, information on the CCN activity of aerosols was obtained in two different, but complimentary, ways. The parallel plate thermal gradient diffusion chamber (TGDC) technique was used to measure the fractional activity of aerosols at supersaturations that were well defined by the geometry and thermal control of the sensing chamber. The second method utilized the fact that the DCC approximates a closed thermodynamic system, so that the fractional activity at different simulated ascent rates in the DCC can be correlated with predictions of supersaturation using the adiabatic cloud model.

The TGDC was operated at a range of supersaturations from about 0.4% to as much as 3% supersaturation with respect to water. Manufacturer specified uncertainty in supersaturation ranges from 0.02% at the lowest to 0.1% at the higher supersaturation value. This is

based on an accuracy of 0.1°C in the temperature difference between the plates. Temperature is measured by thermistors. Panel meter indications of temperature difference were found to be quite consistent with thermistor resistance specifications both before and after the series of measurements were made. The concentrations of aerosols introduced into the sensing volume can also affect the supersaturation actually achieved, particularly if the aerosol is not a very good CCN. For example, a high concentration of poor CCN particles will result in the formation of large numbers of haze particles competing for vapor. To help alleviate this problem, since it could not be quantified, total aerosol concentrations introduced were typically held below 10000 cm^{-3}. Aerosols were collected in a 10L conducting plastic bag. Total bag concentration (N_p) was monitored before and after each supersaturation point, and new samples were usually collected after the bag had sat for a 10 min period at room temperature. CCN spectra were run for monodisperse sizes of the ice nucleus aerosols, and for reference, the polydisperse distribution of ammonium sulfate generated by the bubbler system. Droplets formed on particles were illuminated by a helium-neon laser beam. A 0.02 cm^3 volume was illuminated for viewing. An automated/calibrated detector system was not available, so counting was done using photography. Different supersaturation values resulted in different times for the appearance and growth of droplets, and thus differing exposure requirements. These were determined before photos were taken. An example of the results for an ascending supersaturation series are displayed in the photographs in Figure 5.17. Four to six photographss were analyzed for most supersaturation points. Results are summarized in Table 5.2. Standard deviations are reported for droplet

Table 5.2
CCN Supersaturation Spectra (Thermal Gradient Diffusion Chamber)

Aerosol Type	% SW	N_p (cm^{-3})	N_d (cm^{-3})	F_{imd}
$(NH_4)_2SO_4$	0.42	6800	3694 ± 1575	0.54 ± 0.23
	0.80	6500	6156	0.95
	0.90	6500	5130 ± 484	0.79 ± 0.07
	1.00	6500	5130 ± 484	0.79 ± 0.07
	1.10	6050	5472	0.90
	1.20	6050	4532 ± 758	0.75 ± 0.13
	1.60	5600	5643 ± 725	1.00 ± 0.13
	1.70	5600	5358 ± 197	0.96 ± 0.04
AgI-AgCl	0.42	12000	49	0.004
(r_p = 0.015μm)	0.82	10000	147	0.015
	0.86	2700	30	0.011
	0.90	10000	98	0.010
	0.96	10000	196	0.020
	1.20	9000	551 ± 123	0.061 ± 0.014
	1.80	7900	809 ± 152	0.10 ± 0.02
	1.80	2700	294 ± 69	0.11 ± 0.03
	2.70	7000	1127 ± 69	0.16 ± 0.01
	2.70	6400	930	0.15
	2.80	7000	1005 ± 35	0.15 ± 0.01
	2.80	6400	539	0.085
	2.90	6400	1127	0.18
	3.00	6400	1176	0.18
AgI-AgCl	0.63	12500	441	0.035
(r_p = 0.035μm)	0.75	12500	441	0.035
	0.75	10000	368 ± 35	0.042 ± 0.004
	0.82	12500	490 ± 277	0.039 ± 0.022
	0.86	2900	69	0.024
	1.10	10000	457 ± 150	0.046 ± 0.015
	1.20	10000	719 ± 102	0.072 ± 0.010
	1.70	9000	1068 ± 168	0.12 ± 0.02
	1.70	2900	404 ± 198	0.14 ± 0.07
	1.80	2900	270 ± 104	0.093 ± 0.036
AgI-AgCl-4NaCl	0.36	2600	110 ± 62	0.042 ± 0.024
(r_p = 0.015μm)	0.40	7700	282 ± 157	0.037 ± 0.020
	0.40	2600	49	0.019
	0.86	2600	645 ± 496	0.25 ± 0.19
	1.20	2600	1066 ± 256	0.41 ± 0.10
	1.30	7500	3038	0.41
	1.40	7800	3254	0.42
	1.70	2800	1825 ± 386	0.51 ± 0.13
AgI-AgCl-4NaCl	0.40	2600	1331 ± 394	0.51 ± 0.15
(r_p = 0.035μm)	0.86	2600	2372 ± 265	0.91 ± 0.10
	0.90	2600	2450	0.94
	1.10	2500	2205	0.88
	1.20	2500	2487 ± 323	0.99 ± 0.13
	1.20	2600	2409 ± 453	0.93 ± 0.17
	1.70	2600	2785 ± 380	1.07 ± 0.15

concentration and active fraction values where these numbers represent averages from multiple photographs.

In the combined DCC experiment and cloud model method for determining CCN spectra, known concentrations of monodisperse ice nuclei were introduced into the cloud chamber at the start of a continuous adiabatic ascent simulation. Simulated ascent rates were varied from about 1.0 m s^{-1} to 5 m s^{-1} in a series of tests in order to vary the supersaturations produced in the chamber. Peak supersaturation values in the experiments were estimated using the model power law function for droplet activation in a trial and error scheme. This function is,

$$N_d = N_0(S_w/c)^b \tag{5.4}$$

where N_d is the concentration of droplets activated (cm^{-3}), N_0 is a constant concentration parameter (cm^{-3}), S_W is water supersaturation (%), c is a slight function of temperature and supersaturation, and b is a slope constant. To apply this function to the activation of the ice nuclei injected, N_0 was redefined as the number concentration of aerosols injected, multiplied by a constant a. Then, the fraction of aerosols nucleating droplets (F_{imd}) versus peak water supersaturation for clouds forming at similar temperatures is approximately given by,

$$F_{imd} = a(S_w)^b \tag{5.5}$$

In this equation, a was constrained to be between 0 and 1 and b was constrained between 0.5 and 1.5. In a series of varied ascent rate

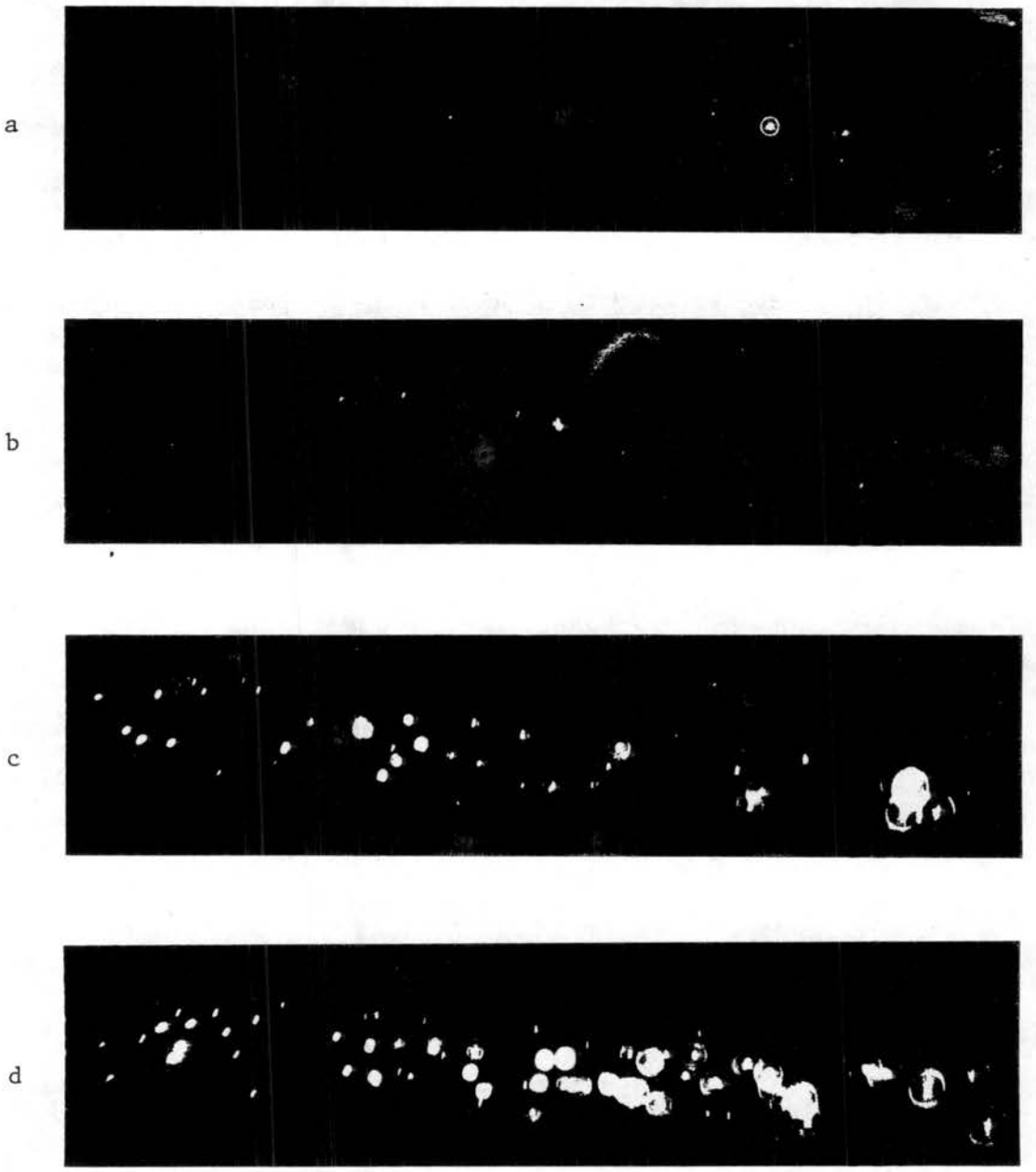

Figure 5.17 Photographs of cloud droplets formed in the thermal gradient diffusion chamber for measurement of CCN activity. Parts (a), (b), (c) and (d) are for water supersaturations of 0.5, 1.2, 1.9, and 2.7% respectively. Laser beam volume exposed is ~ 0.02 cm^3.

simulations, these quantities should be constant for the same aerosol, independent of the concentration of nucleating aerosol initially present. Therefore, the adiabatic cloud model was run for the same initial conditions and ascent rates as in the experiments and the constants **a** and **b** were varied until the differences between the resulting concentrations activated in the model runs and the measured droplet concentrations versus ascent rate were minimized. The judgment of best fit was subjective. The measured droplet concentrations used for comparison were averages of measured droplet concentrations over the first 8 to 16 records following cloud formation, the number in the average depending (inversely) on ascent rate. This introduces uncertainty, because the standard deviation of the averages is as much as 40% of the mean. This uncertainty is noted in the figures that accompany later discussion.

Results of the procedure described in the preceding paragraph are summarized in Table 5.3. Since it was only possible to generate particle concentration of about 400 cm^{-3} maximum, the technique was mostly limited to cases with supersaturation above 1%. For the AgI-AgCl-4NaCl aerosol, the method was not very useful, except to prove that the 0.07μm particles were nearly 100% efficient CCN at all supersaturations above 1%. The 0.03μm hygroscopic particles could not be generated in sufficient concentrations to be reliably measured with the FSSP after activation. Quantification of the CCN activity of the hygroscopic aerosol was thus entirely based on the TGDC tests.

The composite results of CCN active fraction versus water supersaturation measured with the TGDC (-x- symbols, each representing a photograph) and using expansion tests in the DCC (-O- symbols) for

Table 5.3

CCN Activation Experiments Using the Dynamic Cloud Chamber

"Ascent" rate ($m\ s^{-1}$)	N_a (cm^{-3})	N_d (cm^{-3})		F_{imd}		Model SW (%)
		Test	Model	Test	Model	
$(NH_4)_2SO_4$: Not modeled						
1.5	980±160	762±210	-	0.78±.21	-	-
2.5	980	711±241	-	0.73±.24	-	-
3.5	980	730±204	-	0.74±.21	-	-
5.0	980	810±243	-	0.83±.25	-	-
AgI-AgCl (r_a = 0.015μm):						
1.0	250	47±30	55	0.19±0.12	0.22	1.7±0.5
2.5	229	116±56	97	0.51±0.24	0.42	2.6±0.8
5.0	267	157±48	147	0.59±0.18	0.55	3.5±1.1
AgI-AgCl (r_a = 0.035μm):						
1.0	300	50±37	65	0.17±0.12	0.22	1.7±0.5
2.5	375	116±45	121	0.31±0.12	0.32	2.4±0.8
3.5	292	104±35	127	0.36±0.12	0.43	3.0±1.0
5.0	317	155±32	150	0.49±0.10	0.47	3.5±0.7
rapid	-	-	-	0.31	-	2.3
rapid	-	-	-	0.69	-	4.2
rapid	-	-	-	0.99	-	6.4
AgI-AgCl-4NaCl (r_a = 0.035μm): Not modeled.						
1.0	-	-		0.75	-	-
1.5	-	-		1.49	-	-
2.5	-	-		0.92	-	-
3.5	-	-		0.93	-	-
5.0	-	-		0.81	-	-

polydisperse ammonium sulfate and for the two monodisperse sizes of ice nucleus aerosols used are shown in Figures 5.18 to 5.20. Ammonium sulfate aerosols are very efficient CCN (Figure 5.18). Fitting the data to (5.5) gives a correlation coeffient r = 0.71 (a = 0.787, b = 0.384). Maximum activity is achieved for the full aerosol distribution at about 1.3%. Half of this activity is achieved at only 0.3% supersaturation.

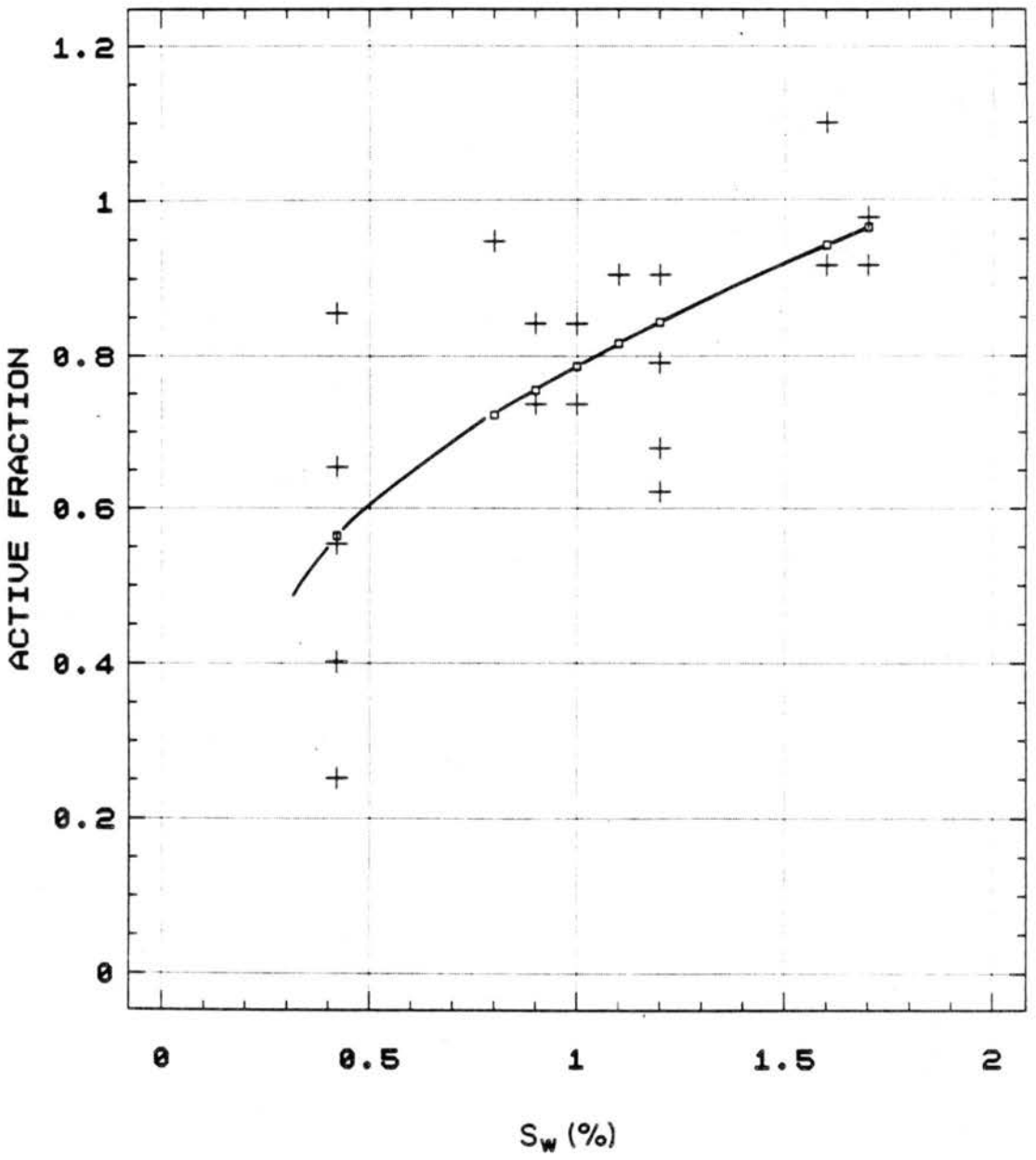

Figure 5.18 CCN supersaturation spectra for ammonium sulfate aerosols used as CCN for the dynamic cloud chamber experiments. Each data point represents a single photograph in the TGDC. A regression line using (5.5) to fit the data is also shown.

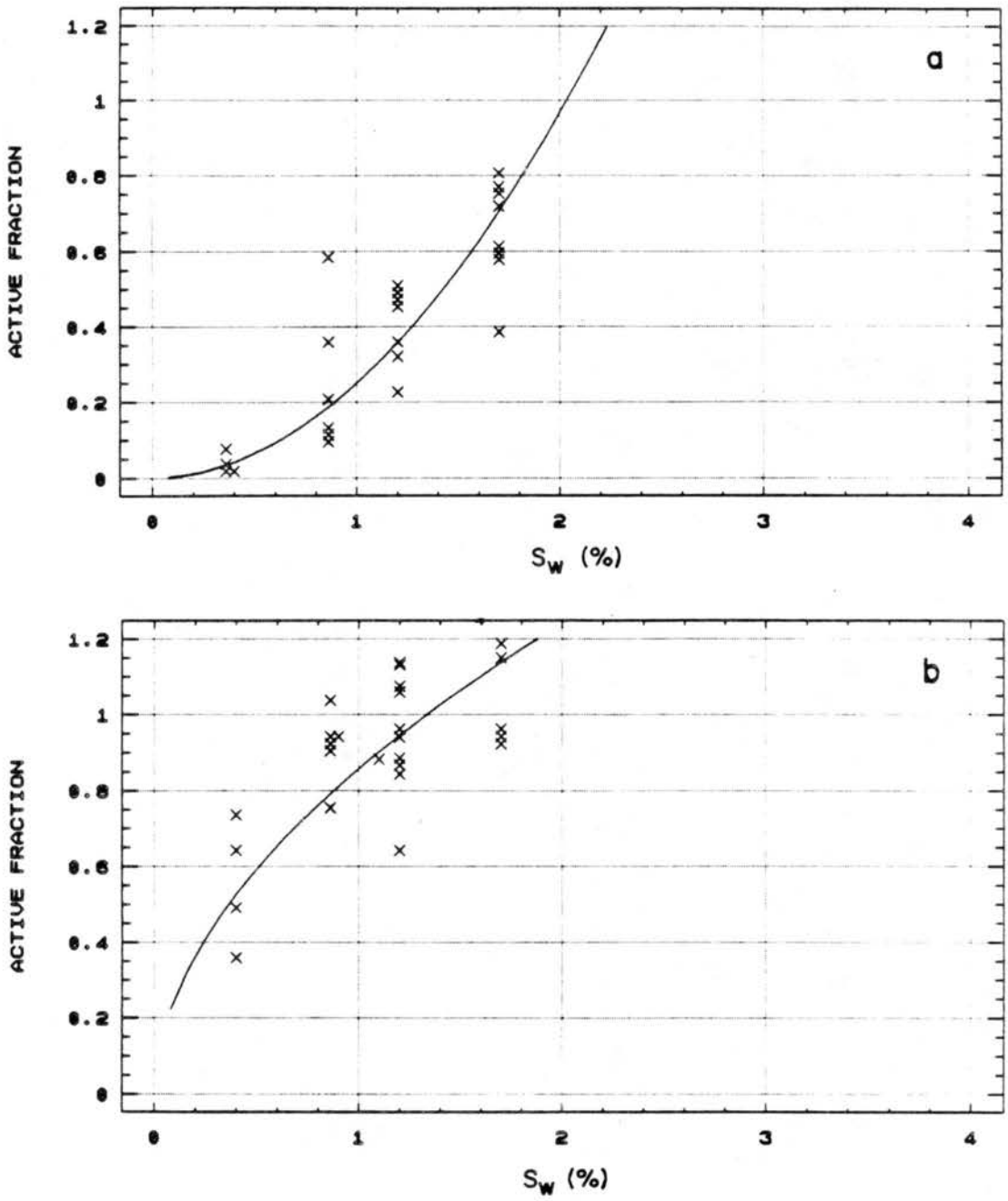

Figure 5.19 CCN supersaturation spectra measured by the TGDC method and regression fit to (5.5) for 0.03μm (a) and 0.07μm (b) AgI-AgCl-4NaCl aerosols.

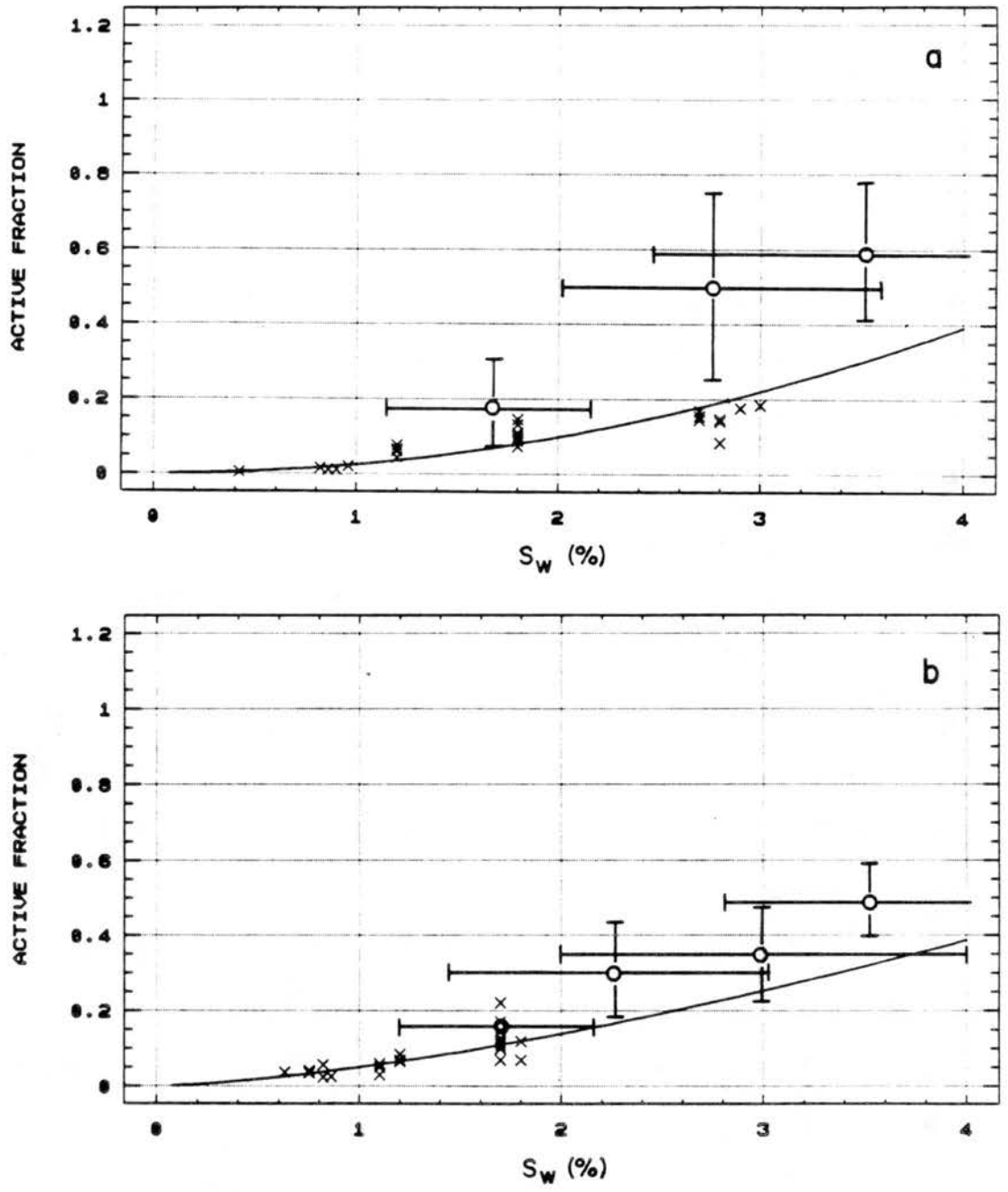

Figure 5.20 As in Figure 5.19, but for AgI-AgCl aerosols. Also included are estimates of CCN activity using dynamic cloud chamber expansions (O), in concert with numerical cloud model estimates of S_w. Uncertainty in the latter estimates, Brought about by the uncertainty in the average droplet concentration nucleated, are indicated by brackets.

The steep increase in activity with supersaturation is expected for a size distribution of soluble particles.

The ice nucleus aerosol containing a large soluble component (AgI-AgCl-4NaCl) acts in much the same manner as $(NH_4)_2SO_4$, but it does so even for monodisperse fractions (Figures 5.19a and 5.19b). The power law fit for 0.07μm aerosols is very similar to the fit for $(NH_4)_2SO_4$. In this case a correlation coefficient of 0.80 is obtained ($a = 0.874$, $b = 0.453$). This result also gives a 50% activation level at 0.3% water supersaturation. Theoretically, thermodynamic considerations predict that single sized particles should all activate at the same supersaturation (Howell, 1948). This, however, presumes that each particle contains exactly the same mass of soluble component. It appears that this is not the case for the monodisperse hygroscopic ice nucleus, and this seems reasonable considering the particles generated by combustion are mixed particles of AgI-AgCl and NaCl. A size effect is clearly noted in comparing the results for 0.03μm to the 0.07μm AgI-AgCl-4NaCl aerosols. The steep rise in activity for 0.03μm compared to 0.07μm particles is essentially offset toward higher supersaturation values. This is in agreement with theoretical expectations. Still, some droplets are formed even at low supersaturation. For 0.03μm aerosols, the correlation coefficient of the supersaturation power law is 0.87 ($a = 0.304$, $b = 1.45$).

AgI-AgCl aerosols are not good CCN, but nevertheless display some potentially important activity as such. The CCN spectra data for 0.03μm AgI-AgCl aerosols are displayed in Figure 5.20a. Considering only the TGDC data, a correlation coefficient of 0.95 is obtained for $a = 0.025$ and $b = 2.0$. The model-predicted active fractions noticeably deviate to

the high side of the TGDC, particularly at higher supersaturations. Uncertainties are large, however. For 0.07μm particles (Figure 5.20b), the correlation coefficient is 0.84, with **a** = 0.050 and **b** = 1.5. For these larger aerosols, the model-predicted fractions active in the DCC versus supersaturation are only slightly higher. A few rapid expansion tests were performed, as described in section 4.1.4, except the temperature was too warm for ice formation and no effort was made to cause droplets to evaporate after they formed. Data system update for the FSSP alone could be adjusted to as short as 2 s to give higher measured resolution of the short cloud lifetime. The ACPL cloud model, with pressure versus time option selected and the CCN spectral coefficients selected as described above, was used to define the supersaturation. These data are given in Table 5.3. Although the uncertainty may be high for this procedure (not estimated), the results are consistent with the results from the TGDC and the results from continuous expansions. This gives some confidence to the procedure used to generate high supersaturations at colder temperatures for the investigation of condensation-freezing nucleation. Nearly 100% activation of AgI-AgCl aerosols is predicted near 6% water supersaturation.

Neither size AgI-AgCl aerosol acts as one expects for soluble or insoluble CCN. There is no apparent critical supersaturation for the instant activation of all particles of one size, and comparing Figure 5.20a and Figure 5.20b, there is no significant size effect to cloud droplet nucleation by AgI-AgCl. Droplet nucleation may be related to the amount of trace insoluble material associated with these otherwise hydrophobic aerosols, and this material may not be distributed in

proportion to particle size, or uniformly at one particle size. There may be other explanations, but it is only necessary here to quantify the net effects as they relate to ice nucleation.

For the purpose of implementing the new results into the adiabatic cloud model, some assumptions and further analyses were made. First, it was assumed that CCN activation of AgI-AgCl aerosols could be described without regard to aerosol size. This is fairly well supported by the data. An adequate size-independent fit to (5.5) for these aerosols, considering TGDC and DCC results, was found setting **a** = 0.05 and **b** = 1.8. For AgI-AgCl-4NaCl aerosols, size effects to CCN activity were quantified by seeking linear size dependencies for the coefficients **a** and **b** which reproduce the results of the fits of (5.5) to the data in Figure 5.20. That is,

$$\mathbf{a} = a1 + a2\ (r_p) \tag{5.6}$$

and,

$$\mathbf{b} = b1 + b2\ (r_p) \tag{5.7}$$

with a1 = -0.123, a2 = 2.85×10^5, b1 = 2.205, and b2 = -5.0×10^5. Figure 5.21 shows a plot of **a** and **b** versus particle size for the hygroscopic aerosols, with the two experimental results indicated. When **a** is negative, no nucleation occurs. No such description was sought here for the ammonium sulfate aerosol, since it was not practical to measure the number of artificial CCN injected in each experiment, and this can vary

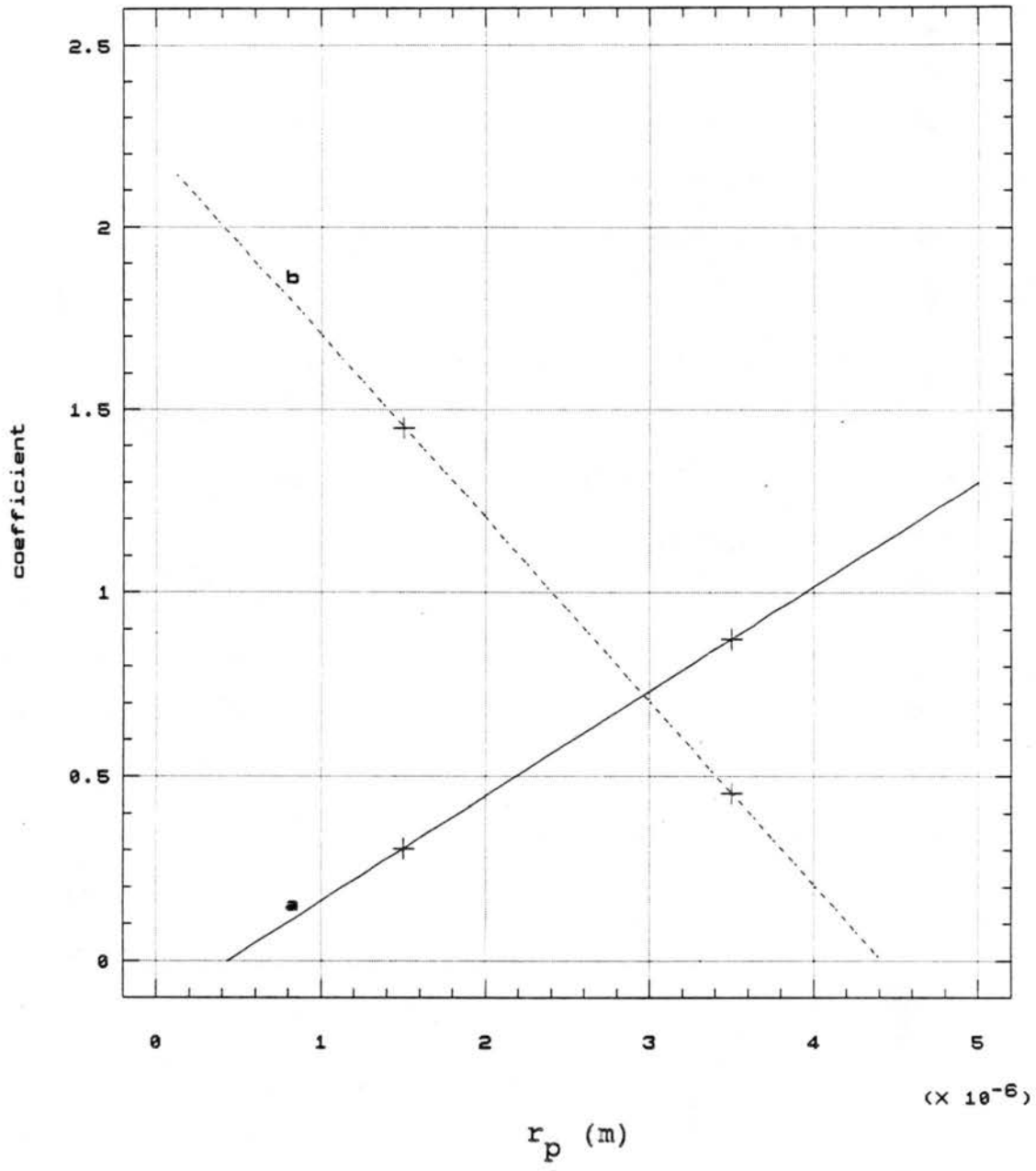

Figure 5.21 Particle size dependence formulated (from data) for CCN activity by AgI-AgCl-4NaCl aerosols.

over time as a solution remains in the CCN generator. For these experiments, it was sufficient to use the adjustable CCN spectral coefficient option already in the adiabatic cloud model to describe droplet activation in model comparisons with experiment, when CCN were present (as for other mechanistic studies described).

5.3.2 Freezing fraction of immersed aerosols

Thermodynamic, cloud, and ice quantities in a typical experiment to determine the freezing fraction of a population of ice nucleus aerosols immersed in cloud droplets is shown in Figure 5.22. In the experiment shown (experiment 3289), 215 cm^{-3} 0.07 AgI-AgCl-4NaCl aerosols were introduced at the start of expansion, with no other aerosols present to act as CCN. Expansion rate was equivalent to a 2.5 m s^{-1} updraft rate in cloud. Cloud formed at -7°C. Peak droplet concentrations nucleated were about 250 cm^{-3} and the average numbers formed were in excellent agreement with the total particle numbers injected. Thus, probably most of the aerosols acted as CCN in this experiment. The cumulative fraction of the aerosol population nucleated as ice is presented as the solid line in the ice panel of Figure 5.22. The potential contribution to nucleation of deposition on any non-immersed aerosol was computed at each time step based on the results of Section 5.1. The potential contribution from contact-freezing by non-immersed aerosols was computed using the results of Section 5.2, the scavenging routines from Young (1974b), and the temporal droplet spectral data (average diameter used). The predicted contributions from these mechanisms versus temperature in the experiment are compared to the measured ice signal minus these contributions in

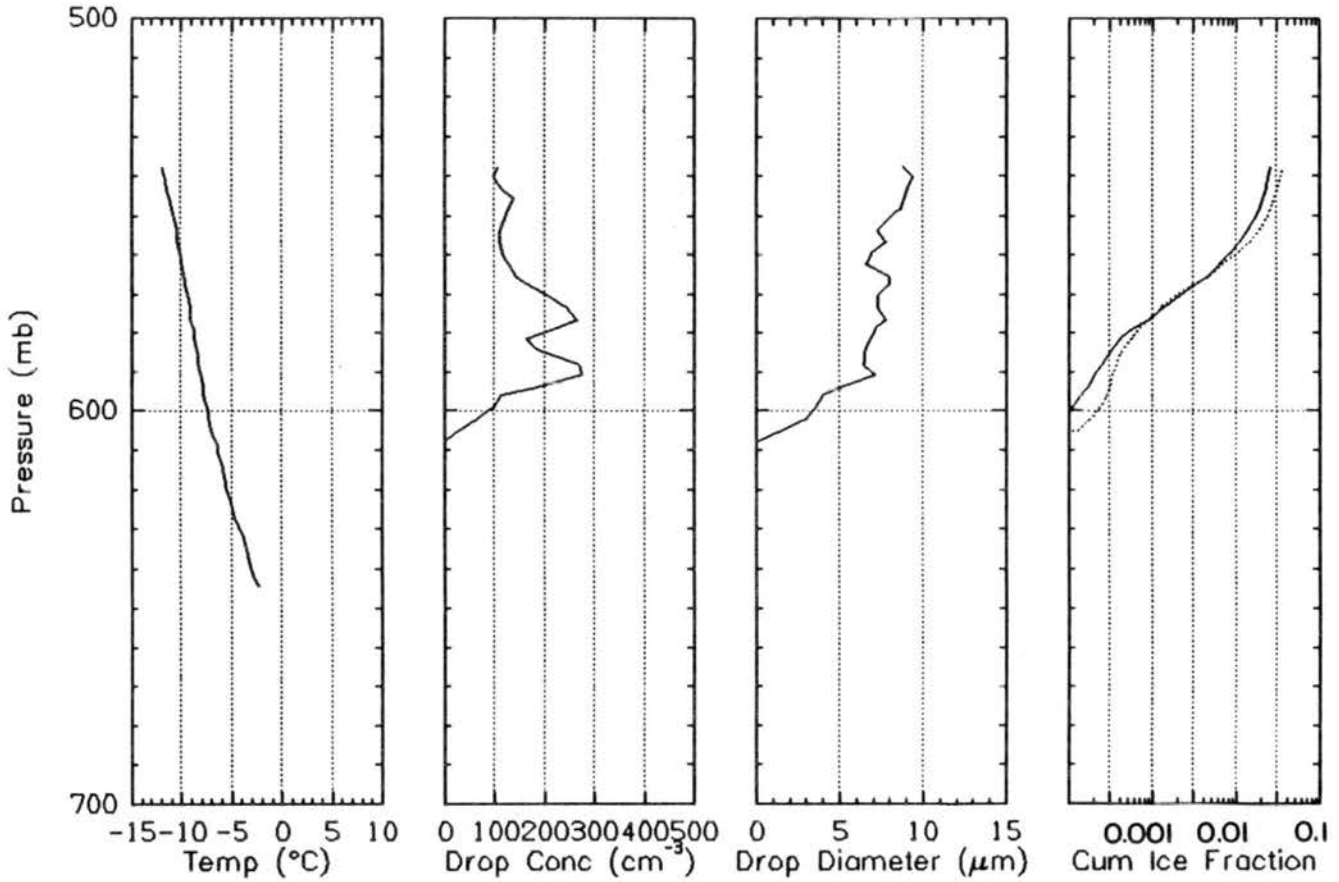

Figure 5.22 Experimental quantities measured in immersion freezing experiment for 0.07 μm AgI-AgCl-4NaCl aerosols. Ice nucleus aerosols were injected before cloud point in a concentration of 215 cm^{-3}, with no other CCN added. Cumulative ice fractions nucleated (solid line) are also presented after adjustment for the fraction of aerosols immersed at any point (dotted line) .

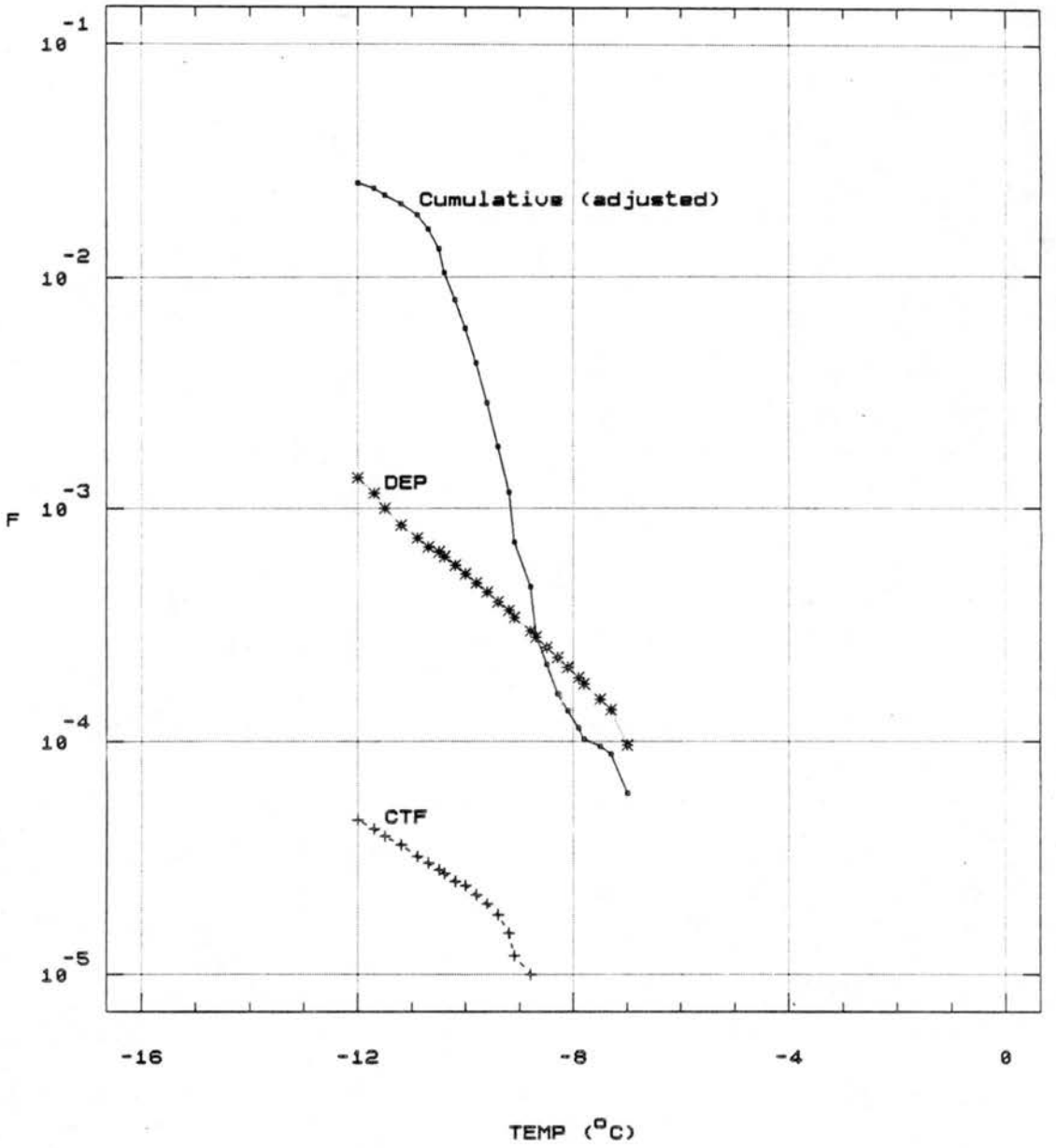

Figure 5.23 Estimated contributions to F versus cloud temperature (cooling) of contact-freezing (CTF) and deposition (DEP) nucleation, plotted with the cumulative signal adjusted for these factors. Data are for the same experiment in Figure 5.22.

Figure 5.23. It is seen that deposition is a significant contributor to ice formation in these types of experiments, but only at the warmest temperatures. The dotted line in the ice panel of Figure 5.22 is the observed fraction effective versus temperature (adjusted for the contributions of deposition and contact-freezing) converted into a fraction potentially active by immersion-freezing if all aerosols were immersed in droplets at any point. This is the true activity curve (fraction potentially effective versus temperature) for immersion freezing that must be combined with the CCN activation spectra to describe immersion-freezing under any circumstances. It assumes that the aerosols not immersed would act the same as the ones immersed do in forming ice in supercooled water droplets. It is also assumed that condensation-freezing was not an important factor in the immersion-freezing experiments. It will be shown in Section 5.4 that the potential contribution of condensation-freezing depends on water supersaturation and temperature. For the example given in Figure 5.23, condensation-freezing may have contributed between 10^{-3} and 10^{-4} times the fraction not immediately immersed in droplets. Therefore, condensation-freezing probably did contaminate the resulting active fractions attributed to immersion-freezing in colder cloud base experiments. There was no way to resolve this further. Ideally, more expansions would have been performed to form cloud at temperatures near -4°C

These same methods were used in eleven other immersion-freezing experiments, for both aerosols and for the two aerosol sizes. The results are summarized in Figures 5.24 and 5.25. For AgI-AgCl aerosols, Figures 5.24a and 5.24b show that 0.03μm particles are more efficient

as immersion-freezing nuclei than 0.07μm particles. This result seems counter intuitive based on classical theoretical considerations. I have no explanation for it. For AgI-AgCl-4NaCl aerosols (Figures 5.25a and 5.25b), the larger aerosols are slightly more efficient than the smaller sizes. This seems reasonable, although the difference is expected to be larger in magnitude, basically in accordance with the surface area of the particles. A multiplicative fit can be made to the active fraction as a function of temperature in all four figures, giving relatively high correlation coeffiecients. The fit is of the form,

$$F_{imf} = p\ (-(T+1))^{m} \qquad (5.8)$$

where T is temperature in °C and p, 1, and m are constants. Values for p, 1, m, and the correlation coefficients are given in the figure captions.

It is notable that there is really not much difference between the two aerosols as ice nuclei once they are immersed in droplets. This seems reasonable, since the soluble component of the hygroscopic aerosol would quickly become diluted to low molality in micron-sized cloud droplets, and the nucleating particles remaining should be similar. For this reason, it was desired to simplify the results for general application in the cloud model. Active fractions were therefore used to calculate active-site densities (D_{imf}) as a function of temperature after the data for all aerosols were combined together. The result is presented in Figure 5.26, with the correlation constants and correlation coefficient for (5.8) given in the figure caption. This

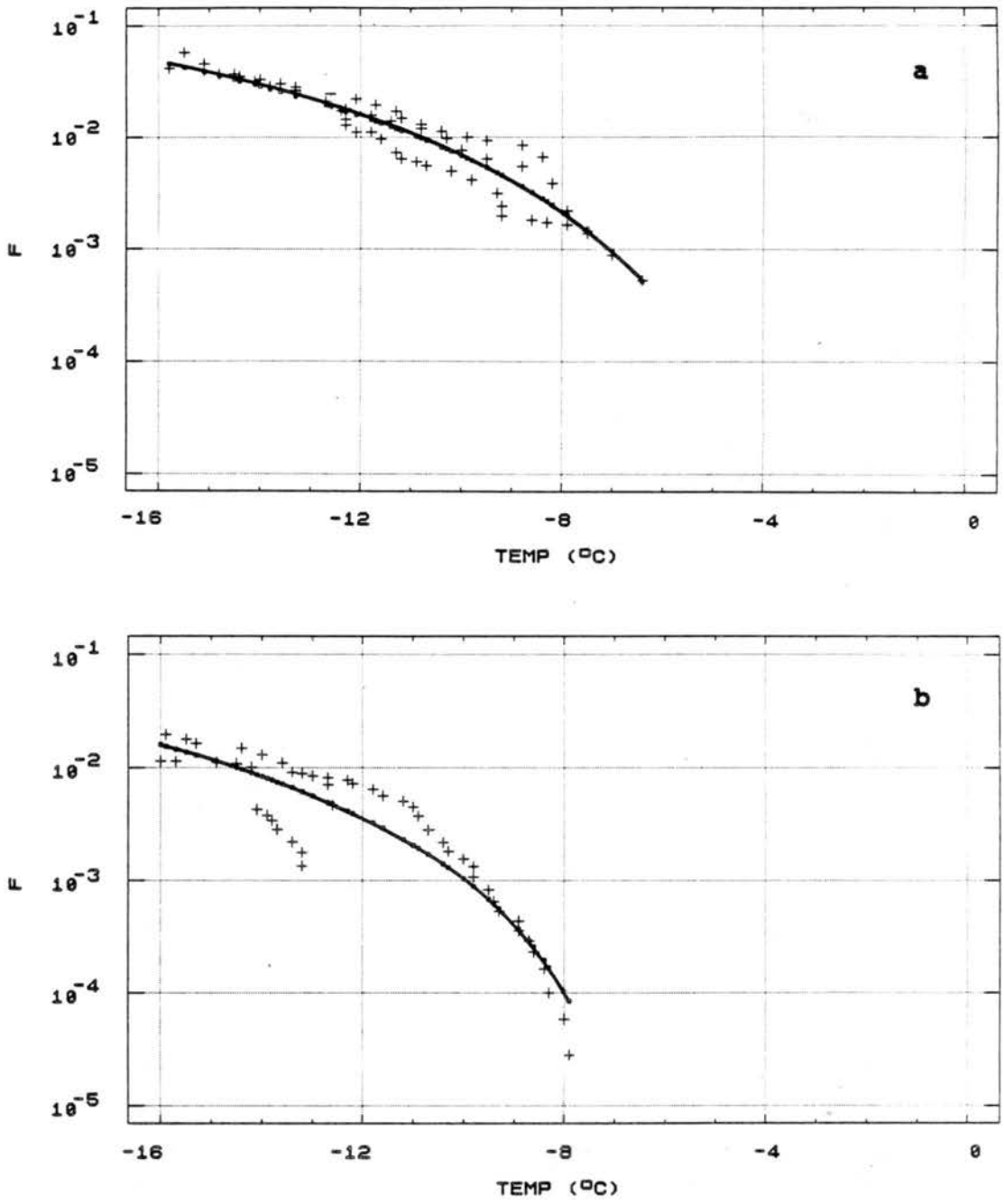

Figure 5.24 Summary of immersion-freezing fractions nucleated (F_{imf}) versus temperature in 4 experiments for 0.03μm (a) and 3 experiments for 0.07μm (b) AgI-AgCl aerosols. Regression lines for (5.8) are also presented ($p = 4.36 \times 10^{-5}$, $l = 4$, $m = 2.818$, $r^2 = 0.91$ in (a); $p = 3.36 \times 10^{-5}$, $l = 6.5$, $m = 2.737$, $r^2 = 0.89$ in (b)).

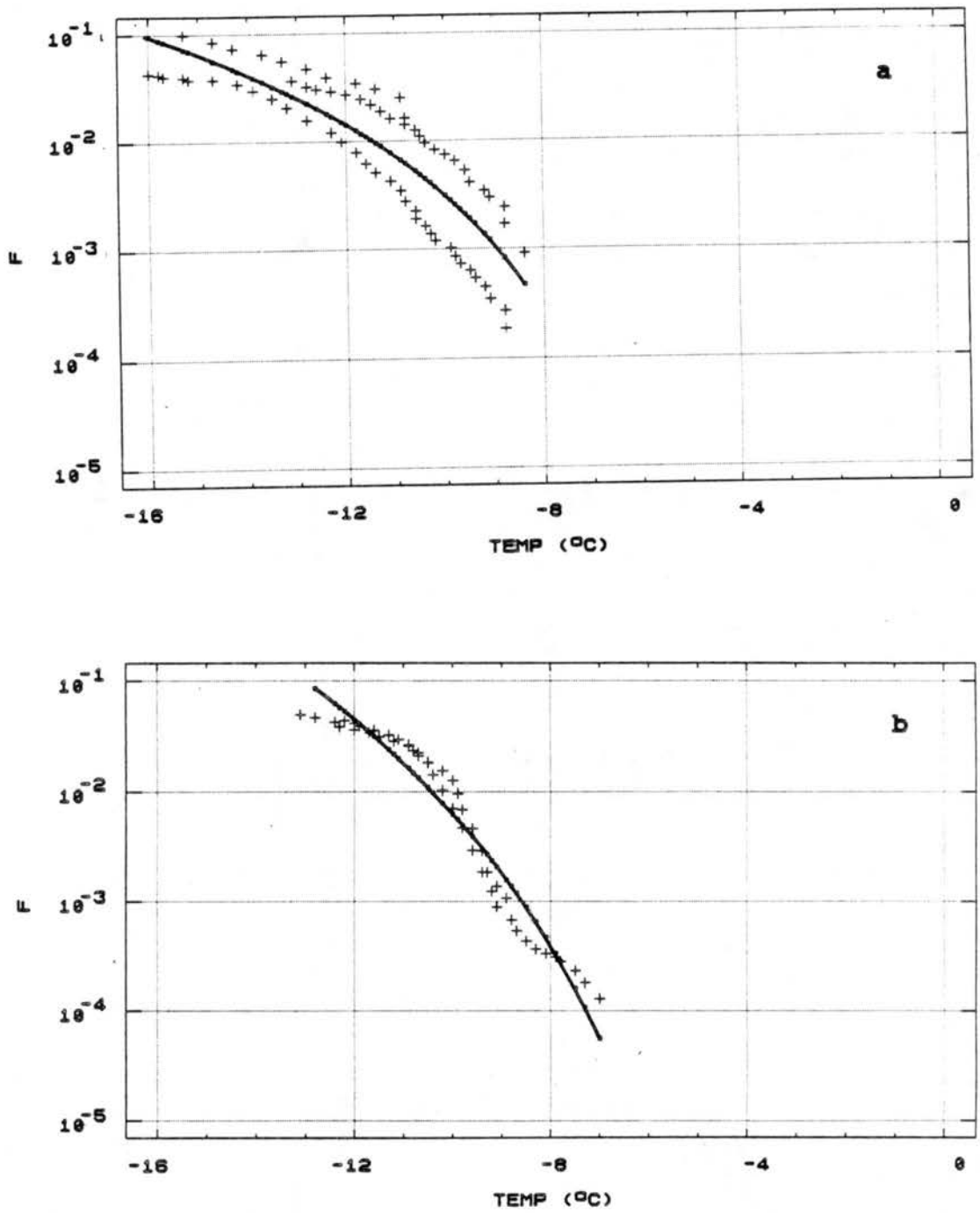

Figure 5.25 As in Figure 5.24, but for AgI-AgCl-4NaCl aerosols. For 0.03μm aerosols, (5.8) gave $p = 1.79 \times 10^{-5}$, $I = 6$, $m = 3.722$, and $r^2 = 0.80$. For 0.07μm aerosols, $p = 3.16 \times 10^{-8}$, $I = 4$, $m = 6.806$, and $r^2 = 0.94$.

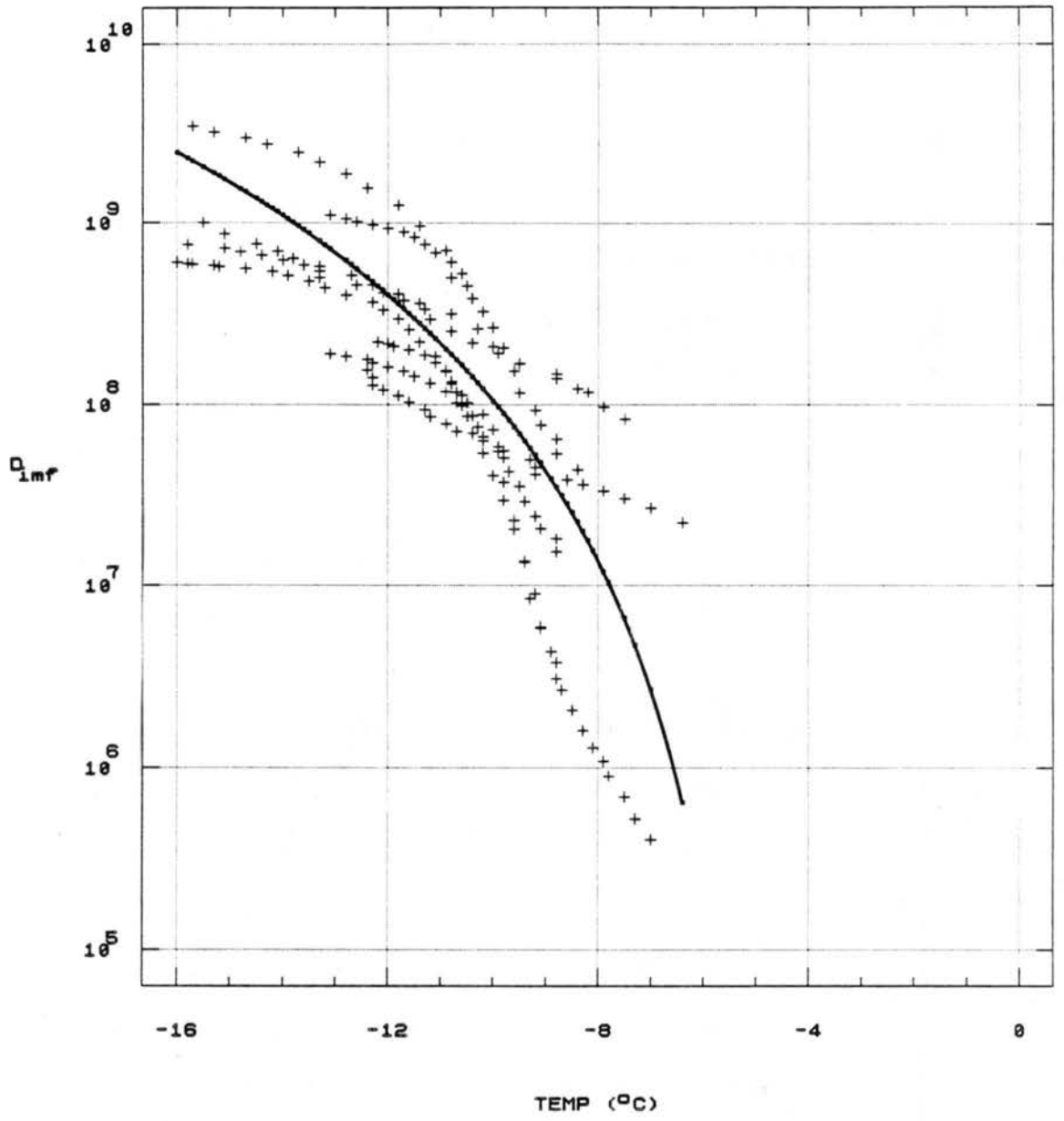

Figure 5.26 Immersion-freezing active site density versus temperature for all data (both aerosols) combined. Fitting (5.8) gives $p = 1.688 \times 10^{5}$, $l = 5$, $m = 4.0$, and $r^2 = 0.73$.

treatment appears quite adequate for generally describing immersion-freezing nucleation by either ice nucleus. The odd result for 0.07μm AgI-AgCl aerosols reduces the correlation.

The active site densities versus temperature by immersion-freezing for polydisperse hydrophobic and hygroscopic AgI aerosols are compared with the active site densities for deposition and contact-freezing modes in Figures 5.27 to 5.28. The deposition curve is computed for water saturated conditions. For now, the values for deposition and immersion-freezing must be considered minimum values because they were determined based on the presumption of temperature dependence only, not temporal dependence for nucleation. The immersion-freezing results were based on experiments at cooling rates that differed by a factor of two, but no significant difference in nucleation rates were noted. The sample size was small, however. For deposition, a different kind of experiment is needed to obtain data on any potential temporal dependence, although the earlier kinetics study by DeMott et al. (1983) suggested that deposition nucleation was a slow nucleation process even at -20°C. With this understanding, Figures 5.27 and 5.28 show that, from the standpoint of active site density immersion-freezing is less effective than contact-freezing by more than an order of magnitude. This result agrees with studies of other ice nucleants reported in the literature (see Chapter 2). Active site density for deposition is less than by the other mechanisms at all temperatures for the hydrophobic aerosols and only approaches the values for immersion-freezing at the warmest temperatures for the hygroscopic aerosols. However, deposition does not require any other special circumstances in order for the

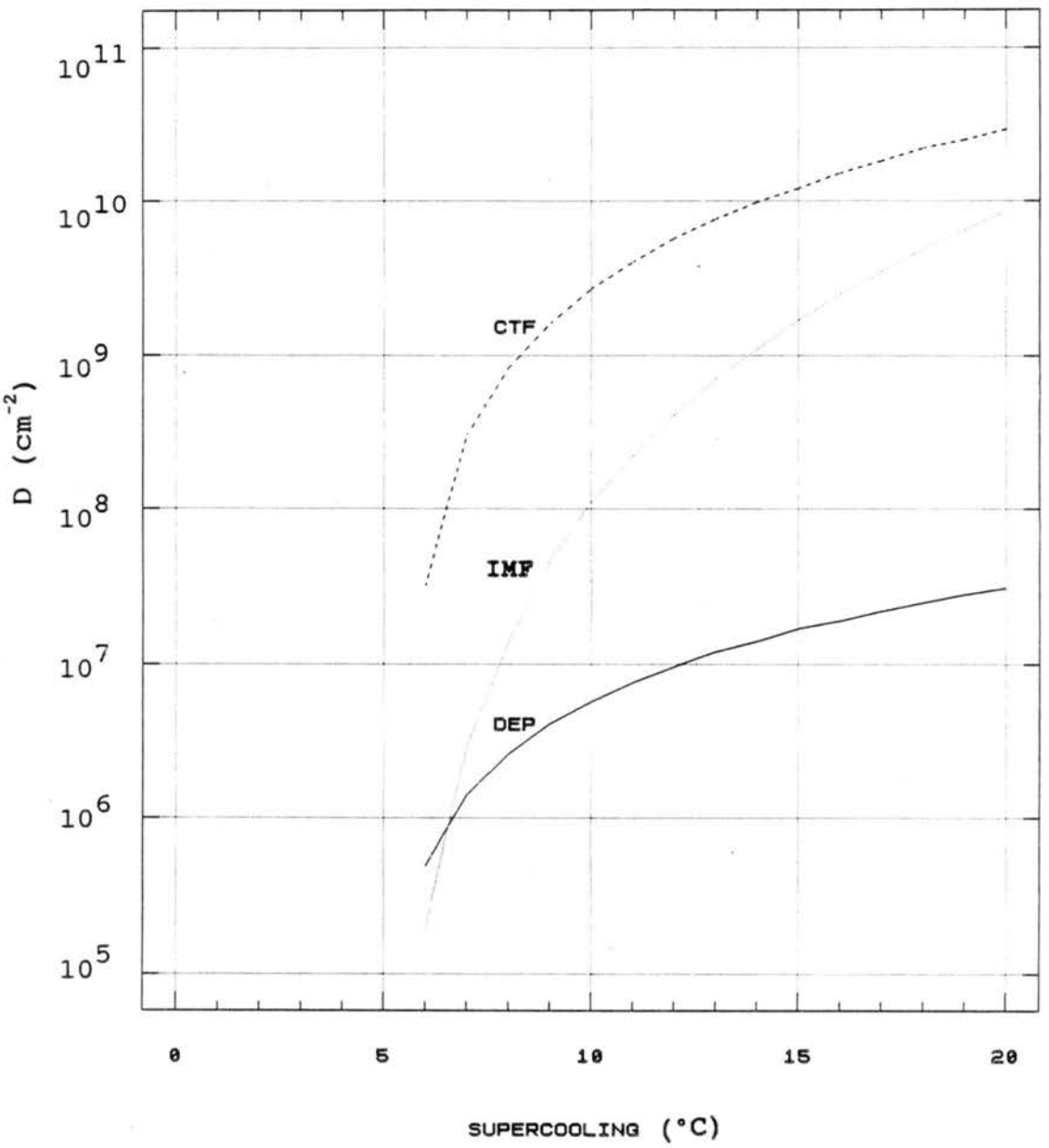

Figure 5.27 Comparison of potential active site densities by deposition (DEP), contact-freezing (CTF), and immersion-freezing (IMF) nucleation for AgI-AgCl aerosols. Computation are for a water saturated cloud.

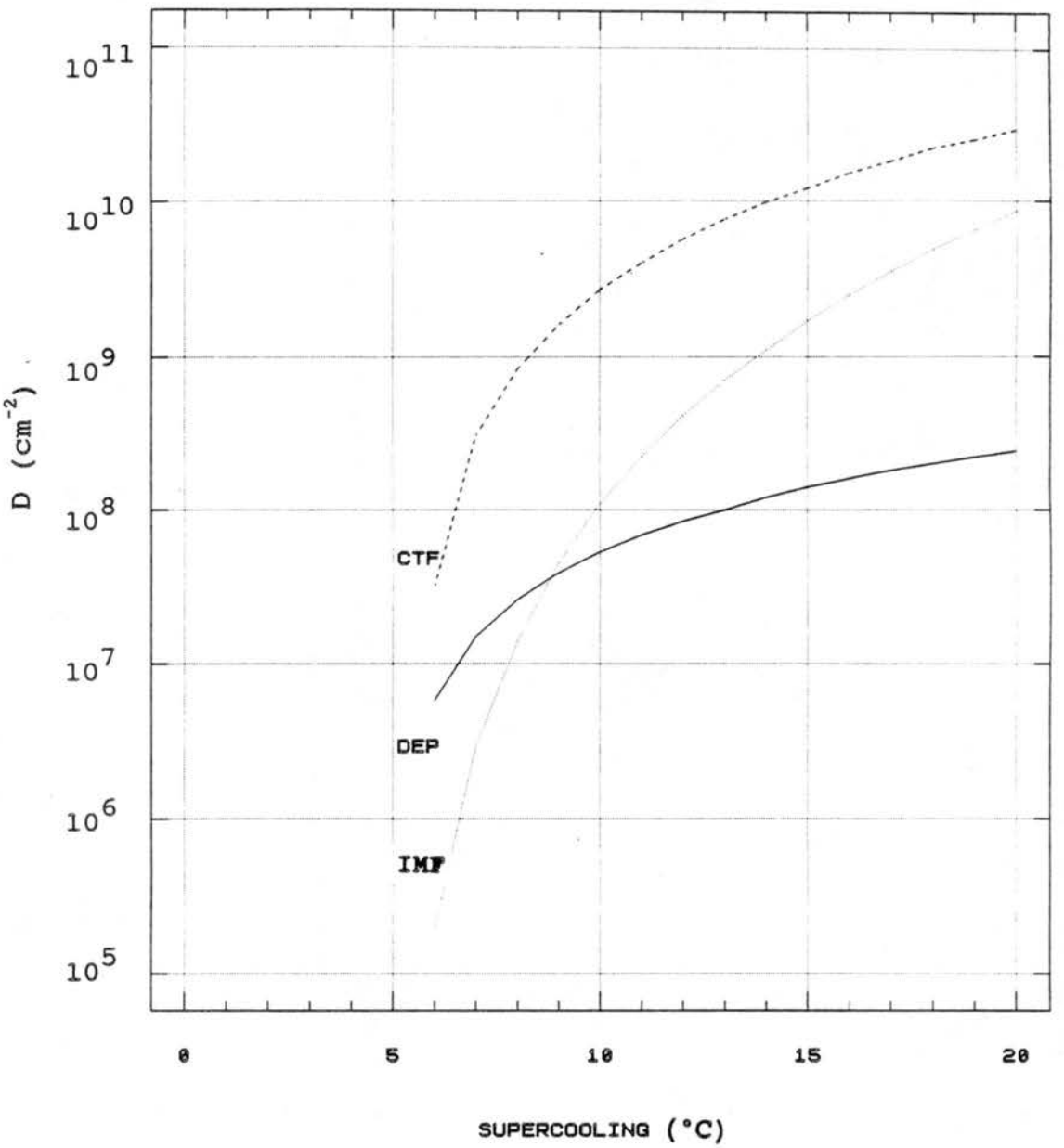

Figure 5.28 As in figure 5.27, but for AgI-AgCl-4NaCl aerosols.

active site density to be reflected in fractional activity. Contact-freezing requires collision events and immersion-freezing requires condensation or collection.

5.4 Condensation-freezing Nucleation

5.4.1 Supersaturation Profiles and Residual Computations

The continuous expansion method for the determination of condensation-freezing activity depended first on the ability to accurately numerically simulate the clouds formed, at least over short periods following the condensation point. Unless nucleation of ice was very rapid at cloud point, noticeably depleting cloud water, the exact magnitude of the ice phase present in the model was not considered to be an important factor. Thus, the original Young Model ice nucleation equations, as described in Appendix A, were used in the attempts to try to mimic the experimental clouds and predict the water supersaturation profile. The assumption that the ice phase was not a great factor in the water balance for the experimental periods simulated is examined later. An example of an experiment versus model simulation is presented in Figure 5.29 (experiment 12188). Supersaturation is clearly sustained in this experiment, as the higher ascent rate produces condensate at a rate that permits droplets to continue to grow while ice crystals grow and settle from the cloud. Problems that lead to the uncertainty in estimated supersaturation are the "perfect" nature of the model cloud and the accumulation of water and ice in the model. Model CCN spectral parameters were adjusted so that model cloud droplet concentrations were typical of the average observed values over the first several

minutes of cloud. It was not possible to control the model droplet diameters. Droplets continued to grow without "settling" from the model while they do settle in the cloud chamber. Thus, the average droplet diameter in the model soon approaches double the observed values. Dotted lines in the predicted supersaturation profile indicate adjustment of the cloud droplet concentrations nucleated by 30% in either direction. This was taken to define the maximum uncertainty in supersaturation, found to be typically of the same magnitude (ie., 0.15% at a value of 0.5% S_w).

The experimental ice signal in the same experiment is plotted along with the calculated contributions of the other nucleation modes in Figure 5.30a. The contact-freezing calculations were made as in Section 5.2, using the actual droplet measurements. Deposition was predicted using the ice supersaturation at the predicted water supersaturated value at each temperature. Both the condensation (using peak supersaturation to determine fractions immersed) and collision contributions toward immersion-freezing were calculated following cloud point. The residual cumulative ice fraction, considered to result from condensation-freezing, is plotted versus water supersaturation in Figure 5.30b. This signal is also indicated in the ice panel plot of Figure 5.29. Condensation-freezing nucleation dominates in this experiment using 0.03μm AgI-AgCl in a simulated 5 m s^{-1} updraft.

As discussed in Chapter 4, the pressure versus time option of the ACPL cloud model was utilized to predict supersaturation in the rapid expansion method for the study of condensation-freezing activity. Pressure and temperature versus time traces taken with a strip chart in one particular experiment for 0.03μm AgI-AgCl aerosols are shown in

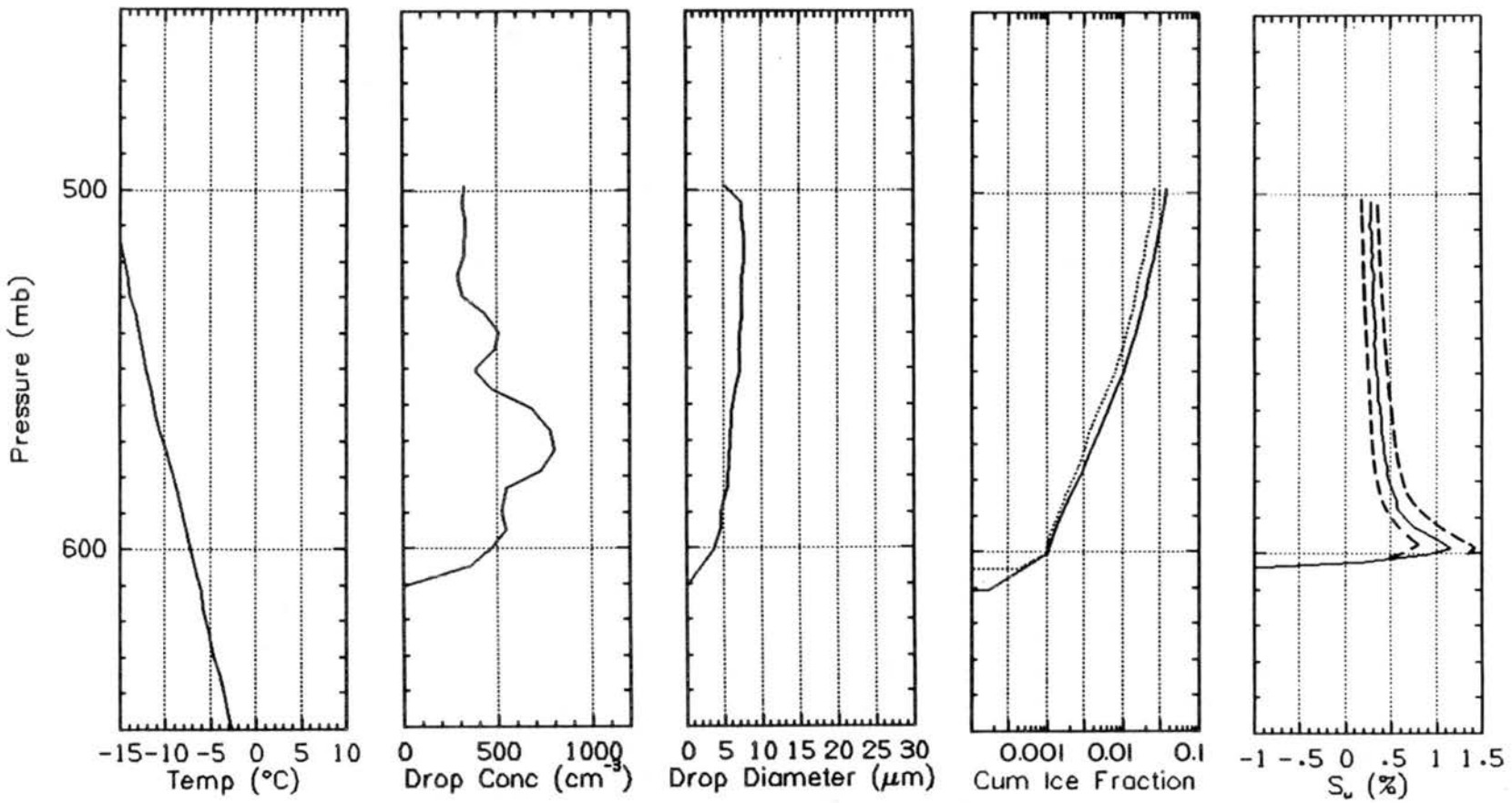

Figure 5.29 Cloud quantities measured in dominant condensation-freezing experiment using 0.03μm AgI-AgCl aerosols. Simulated ascent rate was 5 m s^{-1}. Aerosols were injected before cloud point. Ice fractions plotted are the cumulative (solid line) and the estimated residual after subtracting CTF, IMF, and DEP contributions (dotted line). Supersaturation is from the equivalent cloud model simulation (± uncertainty, given by dashes).

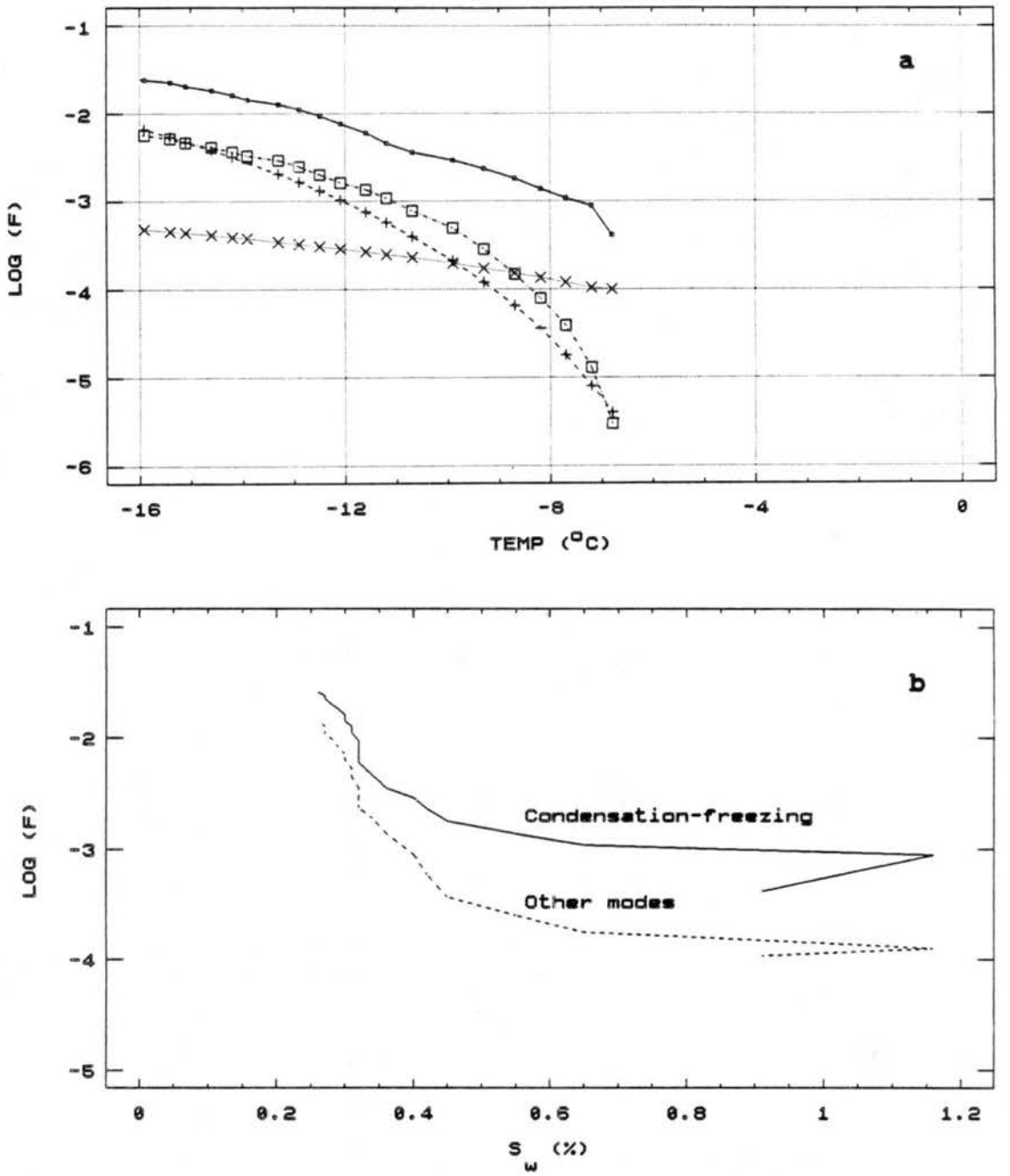

Figure 5.30 For experiment in Figure 5.29, the calculated contributions of CTF (+), DEP (x), IMF (□), and the residual (•) fractions of ice forming versus temperature in (a), and the contributions of the residual (taken as condensation-freezing fraction) and other modes combined versus S_w in (b).

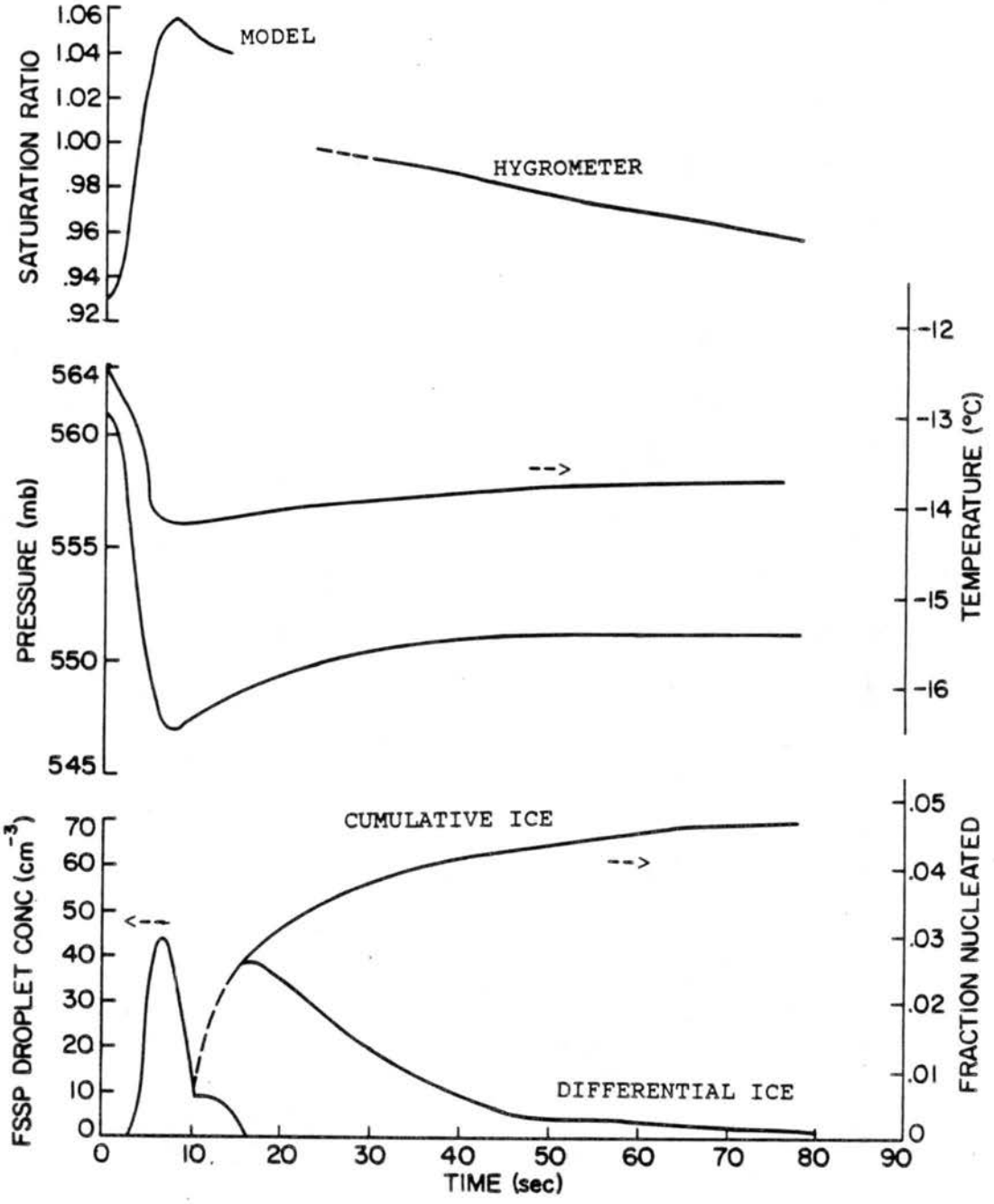

Figure 5.31 Rapid expansion method experimental data. Saturation ratio is from the ACPL model for first 10s, and from the dewpoint hygrometer at later times. Temperature and pressure traces were from a strip chart records (scales indicated by arrow). Droplet concentrations are from 2s data records. Ice values are interpolated from 15s values.

Figure 5.31. This experiment was conducted by initiating a preset 20 mb expansion using the maximum capacity of the vacuum pump system. An "overshoot" of about 4 mb is noted. Points were chosen at 1 s intervals for initialization of the ACPL cloud model. The initial humidity (93% RH) was also an input parameter. Model CCN spectral coefficients were adjusted to match the peak drop concentration value of 43 cm^{-3} observed. The predicted supersaturation profile is also shown in Figure 5.31. It is seen that cloud forms between the points where saturation ratio exceeds 1.00 and peaks at 1.057. The model experiment was terminated at 10 s after initiation of expansion, since ice processes are not included and because the humidity was below 100% as measured by the dewpoint hygrometer by 30 s after expansion initialization, without further introduction of dry air. The chamber did remain ice supersaturated while ice continued to grow and fall out. The evolution of the fraction nucleated versus time is also plotted. The deposition nucleation signal predicted from the peak saturation ratio and minimum temperature must be subracted from the total ice fraction nucleated to obtain the presumed condensation-freezing fraction active. As will be discussed, it is not clear that this procedure unambiguously isolated condensation-freezing.

5.4.2 AgI-AgCl Aerosols

The condensation-freezing cumulative fractions nucleating versus temperature and estimated supersaturation in continuous expansions are summarized for 0.03μm and 0.07μm AgI-AgCl aerosols in Figure 5.32 (14 total experiments presented). The results indicate three dimensional surfaces with increasing fractions nucleating at colder temperatures

for the same S_w, but an equally steeply rising activity at one temperature for increasing S_w. The fractions nucleated are converted to active site densities and are presented in two dimensions in Figure 5.33. Data points are coded for the estimated water supersaturation in tenths of a percent. From these data, a regression equation was sought with both temperature and S_w of the form,

$$D_{cdf} = a\,(d-T)^b\,(S_w)^c \qquad (5.9)$$

where T is in °C. For the data in Figure 5.33, $a = 3.445 \times 10^4$, $b = 4.836$, $c = 2.0$ and $d = 3$ gives a correlation coefficient of 0.79. This fit is shown with respect to the data by the solid lines in Figure 5.33. Within the uncertainty in estimated supersaturation, the agreement is reasonable, although few data are represented for supersaturations in excess of 0.5%. Rapid expansion experiment results are given in rectangles in the same figure. All were conducted with 0.03μm AgI-AgCl aerosols. Although a few of the points represent the highest activity measured warmer than -11°C, the results do not generally agree with the model for condensation-freezing that emerges from the continuous expansion data. There are two possible reasons for this result: first, supersaturation may be too transient; second, and probably more significant, the relative rates of condensation and freezing may be important in determining the results. Microscopically, the mechanism referred to in this dissertation as condensation-freezing occurs as water molecules in small numbers or in thin layers are ordered as ice on the nuclei surface. It is speculated that the nucleation rate is determined by condensation rate at smaller water

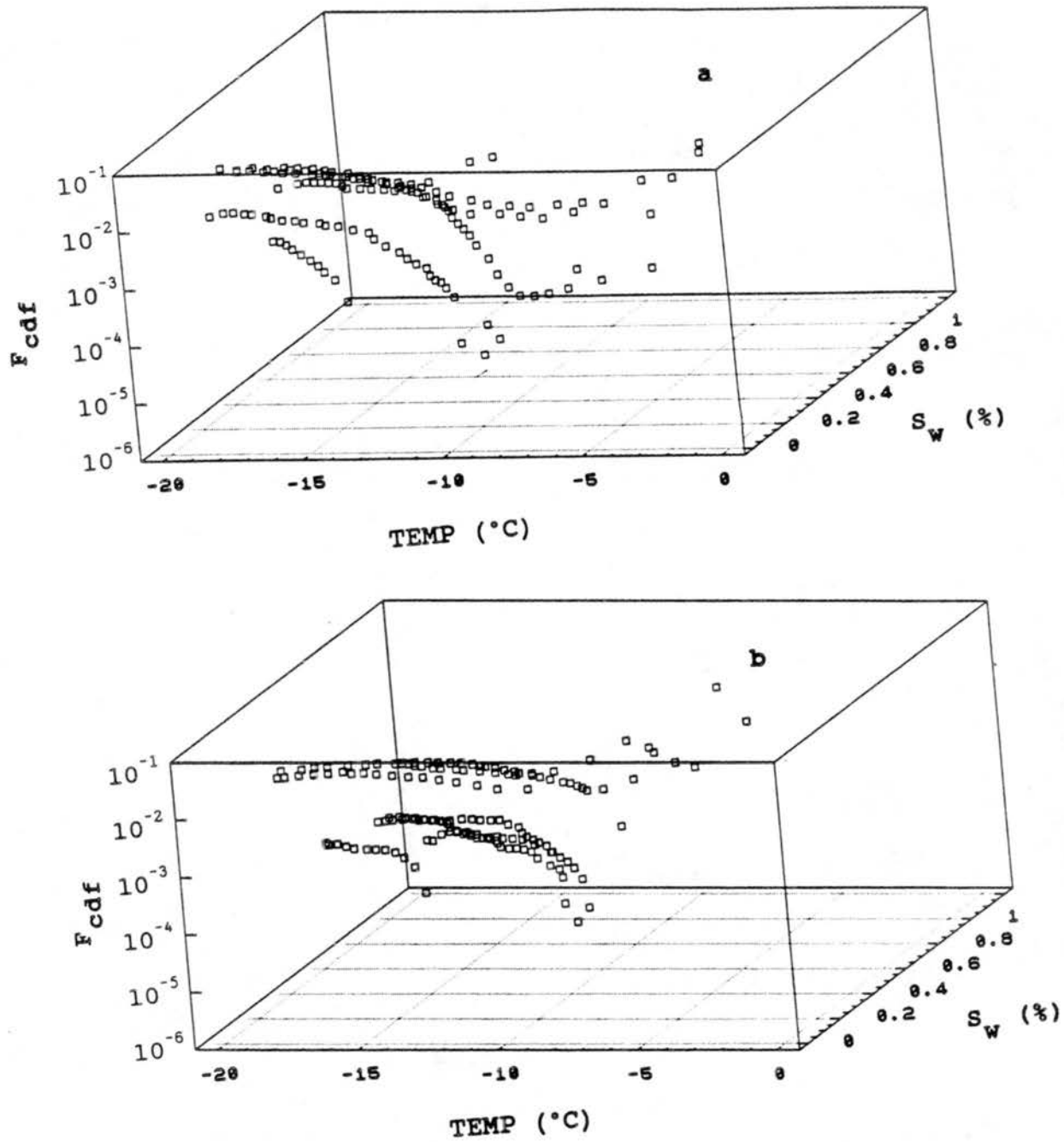

Figure 5.32 Condensation-freezing fractions for 0.03μm (a) and 0.07μm (b) aerosols as a function of both temperature and water supersaturation.

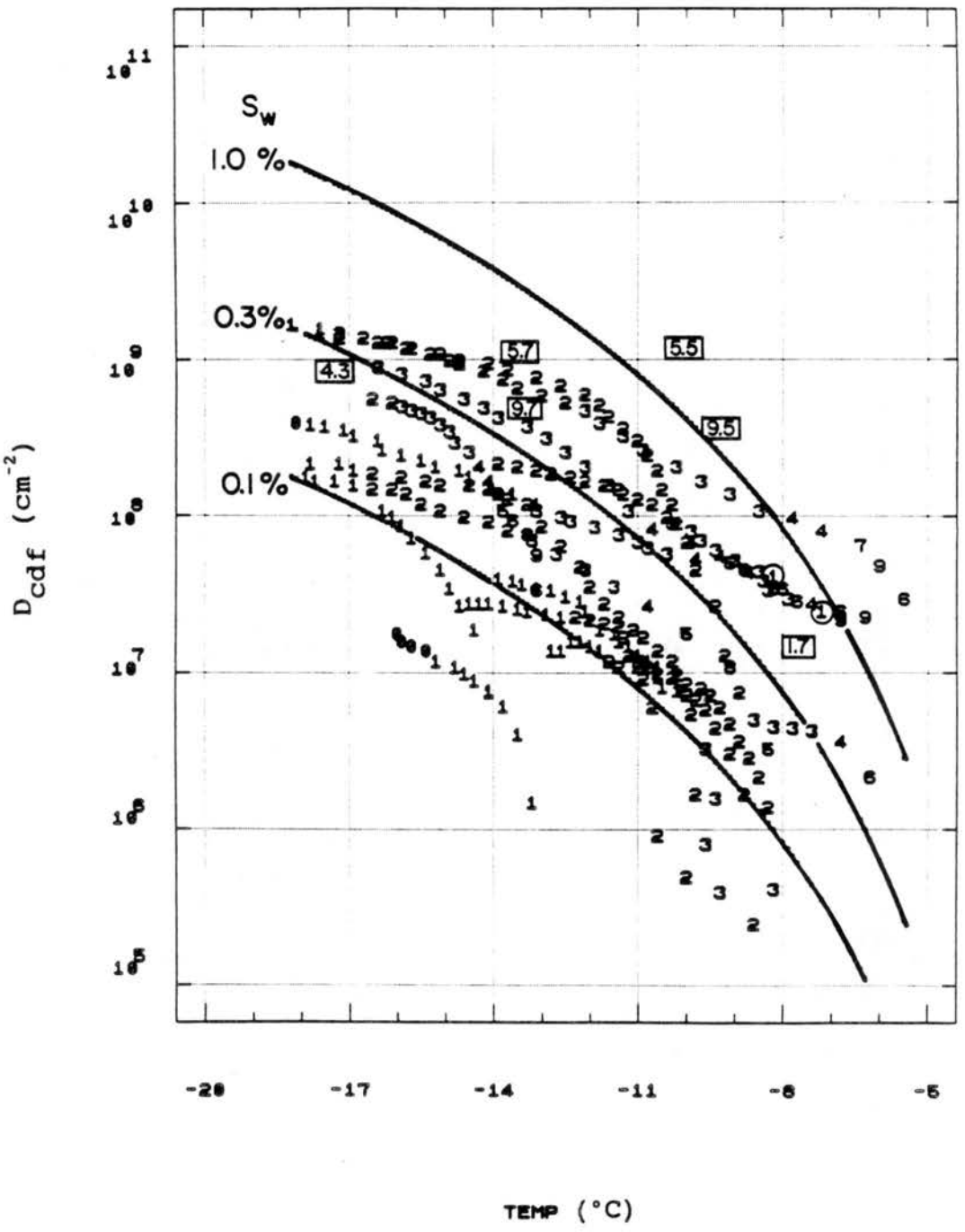

Figure 5.33 Active site density by condensation-freezing versus temperature for AgI-AgCl aerosols. Data points are coded in tenths of a percent S_w, except circled values are > 1%. Values in rectangles are from rapid expansion experiments. The solid lines are based on (5.9) for the respective S_w values given.

supersaturation, but as the rate of condensation increases with increasing S_w, freezing becomes the rate determining step. However, the freezing rate will be that of the macroscopic water droplet that will quickly form at these higher supersaturations. In fact, the rapid expansion results are in reasonable agreement with the potential immersion-freezing nucleation activity of AgI-AgCl aerosols presented in Figure 5.27. The formation of cloud droplet concentrations in near equivalence to the aerosol concentrations in the experiment shown in Figure 5.31 also supports this concept. This suggests that it is not necessary to quantify condensation-freezing at superaturations exceeding a percent or two for hydrophobic aerosols, and the rapid expansion method employed is truly just another method for examining what has been termed immersion-freezing nucleation. It is perhaps fortuitous that nucleation of cloud droplets occurs first, before condensation-freezing, in the adiabatic cloud model used for comparison of new ice nucleation formulations to experimental results in the next chapter.

The fit from (5.8) for condensation-freezing is combined with that for deposition nucleation from (5.3) to produce the two and three dimensional representations of active site density for vapor concentration-dependent nucleation in Figures 5.34 and 5.35. Based on the discussion just presented, the very steep activity rise above a few percent supersaturation, also predicted for pure AgI by Fukuta and Schaller (1982), is probably quite meaningless due to the intervention of immersion-freezing nucleation at higher S_w.

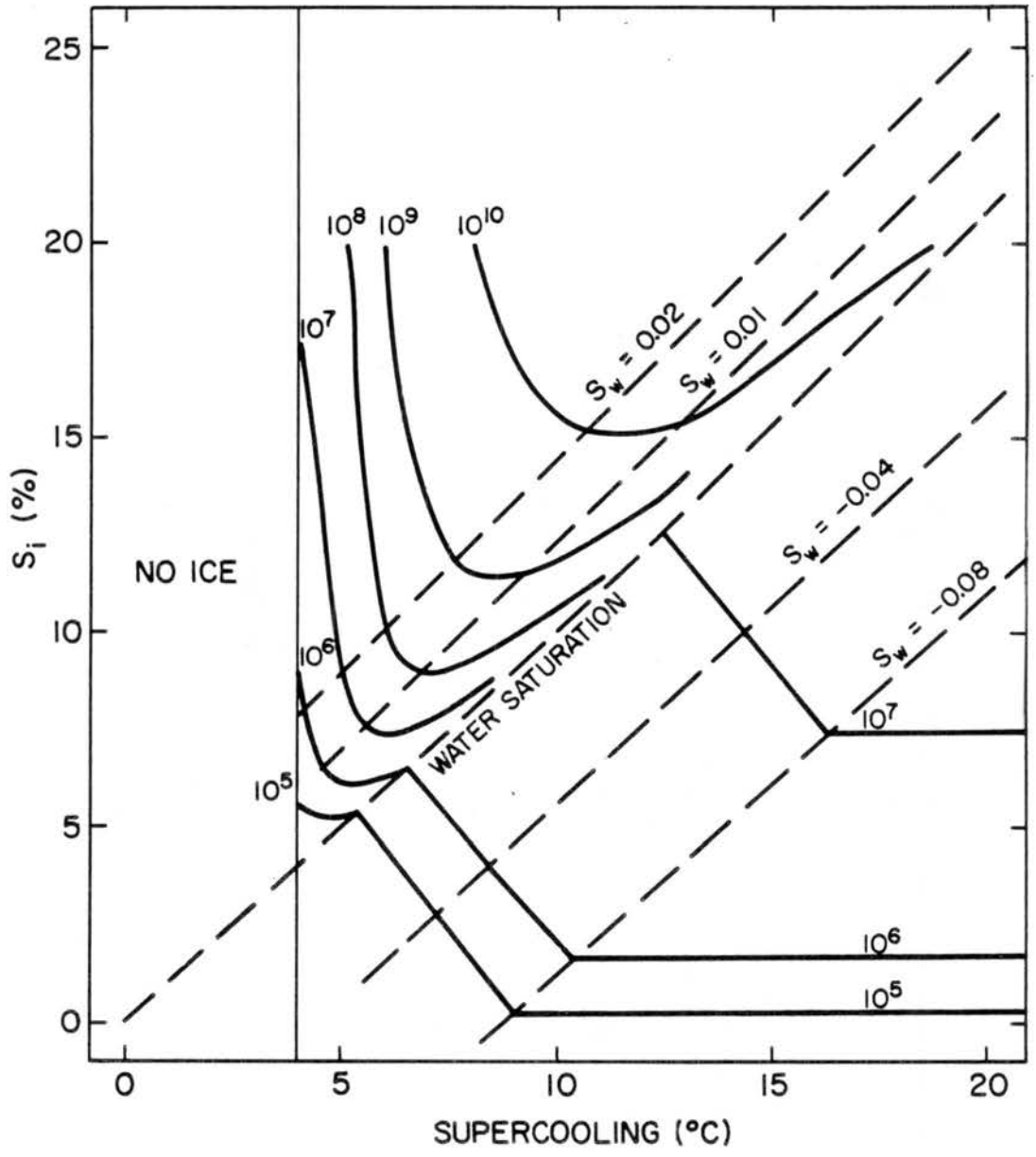

Figure 5.34 Summary of combined deposition and condensation-freezing nucleation active site densities for AgI-AgCl aerosols, quantified by (5.3) and (5.9) as a function of S_i and temperature of supercooling. Constant S_w lines (dashed) are also shown.

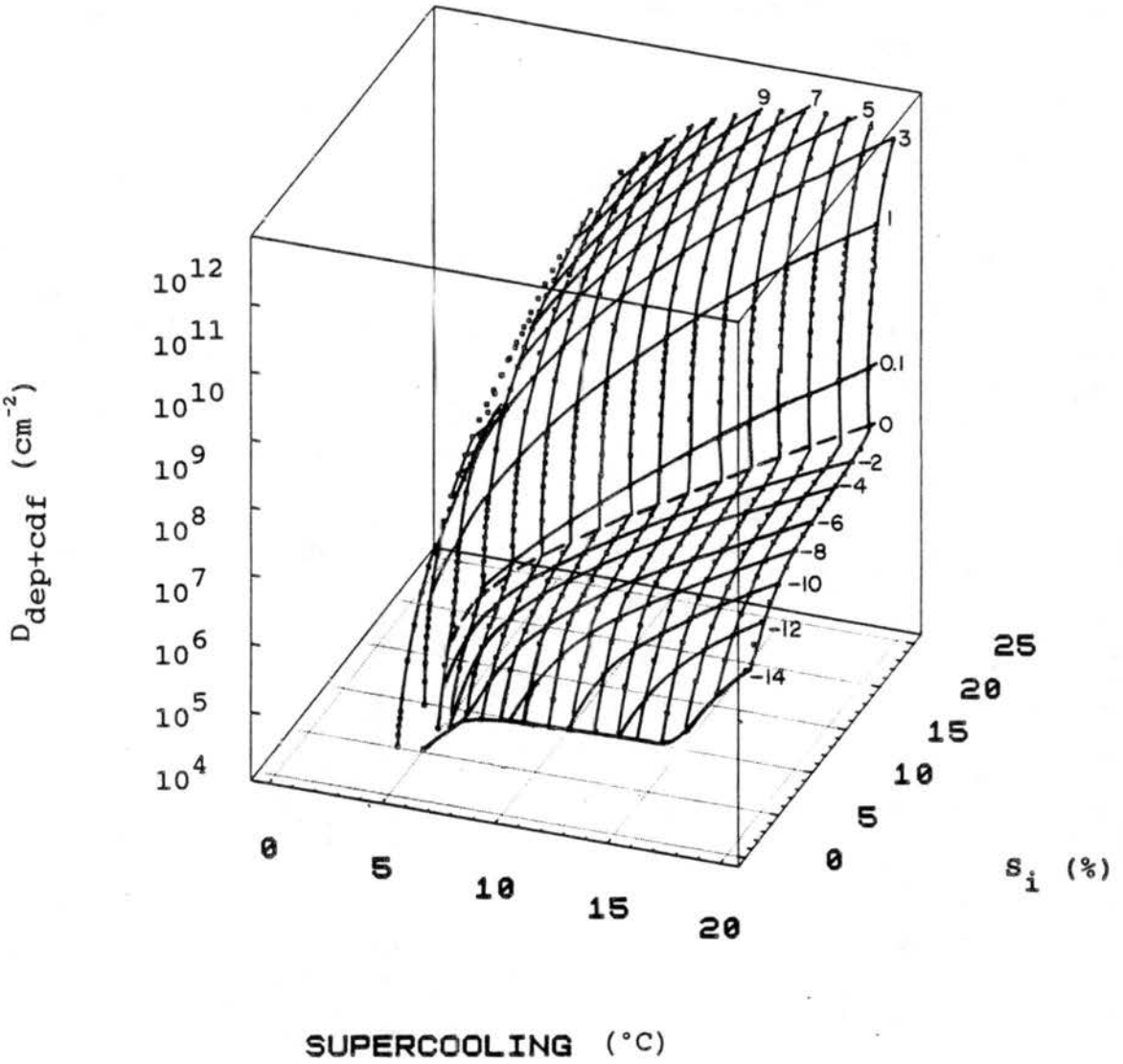

Figure 5.35 The three dimensional surface of the results shown in Figure 5.34.

5.4.3 AgI-AgCl-4NaCl Aerosols

Since condensation more readily occurs on AgI-AgCl-4NaCl aerosols at lower supersaturations than for AgI-AgCl aerosols, it might be expected that these aerosols show a higher activity as condensation-freezing nuclei. This is the case. The fractional ice formation by the different sizes of these aerosols in excess of that which can be explained by other nucleation mechanisms, and thus attributed to condensation-freezing, is shown versus temperature and estimated water supersaturation in Figure 5.36 (15 continuous expansion experiments represented). The activities are clearly higher, at least at temperatures below -8°C, than for AgI-AgCl aerosols of the same sizes. Computations of active site density and the fit to (5.8) for AgI-AgCl-4NaCl ($a = 6.583 \times 10^6$; $b = 4.73$; $c = 2.0$; $r = 0.82$) is shown in Figure 5.37. An D_{ctf} value of a little more than 10^9 at -11°C and just 0.3% S_w implies an instantaneous effectiveness of 9% of 0.05μm aerosols (average size of typical nucleus generator distribution) as ice nuclei. This is a factor of ten greater than for AgI-AgCl aerosols under the same conditions.

At first view, it is odd that AgI-AgCl aerosols actually show a more sensitive response to S_w above about -8°C than AgI-AgCl-4NaCl aerosols. This may be a consequence of the fact that supersaturations created at cloud formation at these temperatures will efficiently activate the hygroscopic aerosols as CCN before condensation-freezing can occur, so freezing proceeds at the lower activity observed in bulk water (immersion-freezing). The rapid expansion experimental results support this concept. Again, as for AgI-AgCl aerosols, the rapid expansion experiments (see values in rectangles in Figure 5.37) showed

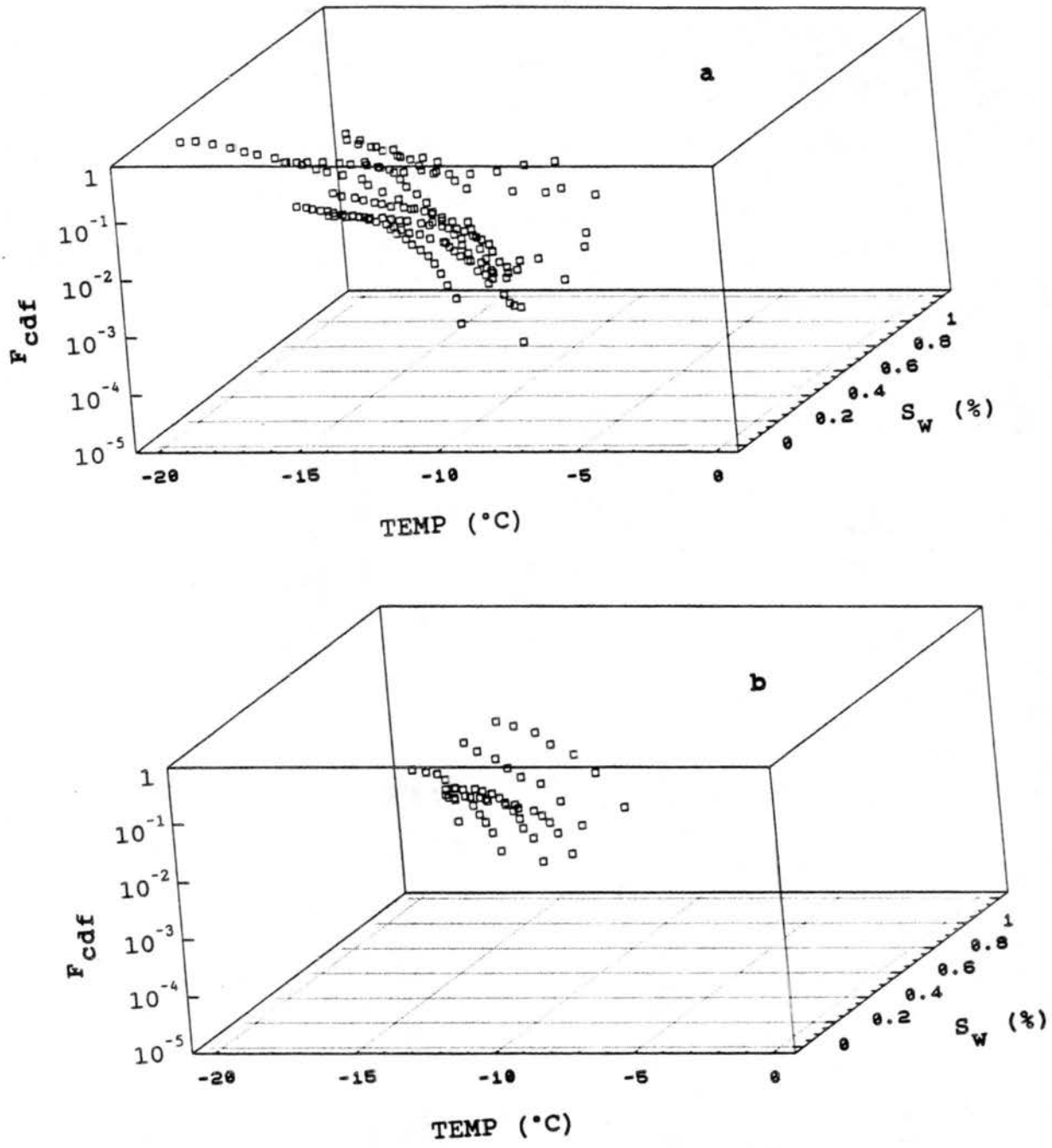

Figure 5.36 As in Figure 5.32, but for AgI-AgCl-4NaCl aerosols.

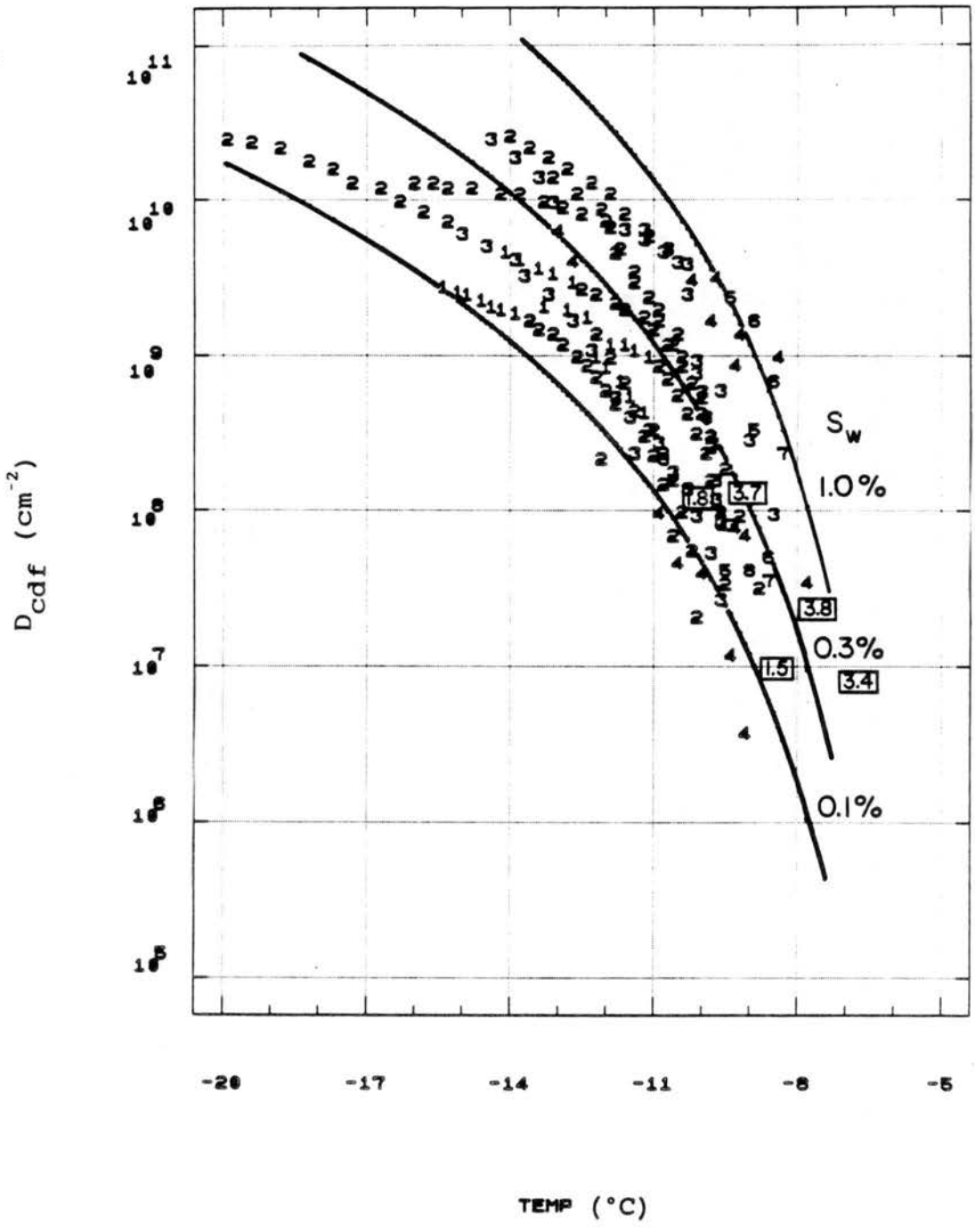

Figure 5.37 D_{cdf} versus temperature for AgI-AgCl-4NaCl aerosols. Plot formalism is the same as for Figure 5.33.

little agreement with the continuous expansion results. The same arguments made concerning the rates of condensation and freezing and the nucleation first of a water droplet in the case of the hydrophobic aerosols are even more valid for these hygroscopic aerosols. Namely, above some supersaturation, ice nucleation rate may actually decrease because aerosols enter mascroscopic cloud droplets before they can nucleate by condensation-freezing.

The two dimensional and three dimensional representation of the combined effects of deposition and condensation-freezing for AgI-AgCl are shown, repectively, in Figures 5.38 and 5.39. Based on the above discussion, the steep rise in nucleation activity predicted above 1% water supersaturation may have little relevance, and these activities will not be realized in the cloud model because cloud droplet formation would occur first. Based on these results, it is possible to put forth an explanation of the interesting related results of Feng and Finnegan (1985; 1989) for tests of AgI-AgCl-4NaCl aerosols in the isothermal cloud chamber. At water saturation in ICC, nucleation is by deposition. In reality, this may simply be an extension of condensation-freezing nucleation, since the aerosols will have deliquesced or formed haze particles. When transient high supersaturations were induced by injecting aerosols with warm saturated air, condensation-freezing activity was added, but the rapid increase in nucleation rate and activity may have resulted from the realization of the potential immersion-freezing activity.

There are obviously theoretical implications for these results. It is quite possible that the current data, some further experiments of this type, and the data of Feng and Finnegan is all the information

needed to formulate a chemical kinetic model of the essentially series first order process that describes condensation-freezing nucleation. Fukuta and Schaller (1982) attempted this with their data.

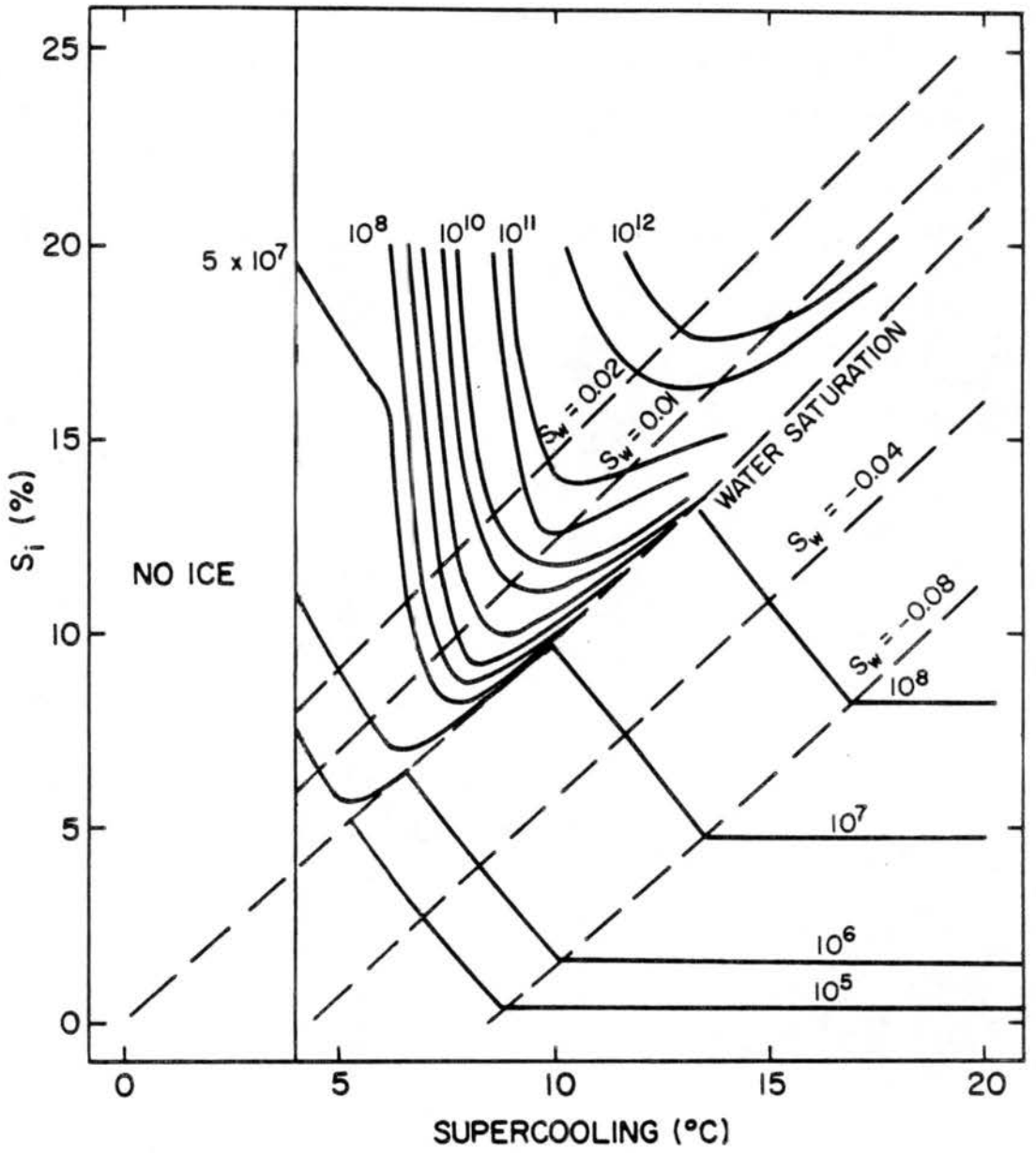

Figure 5.38 As in Figure 5.34, but for AgI-AgCl-4NaCl aerosols.

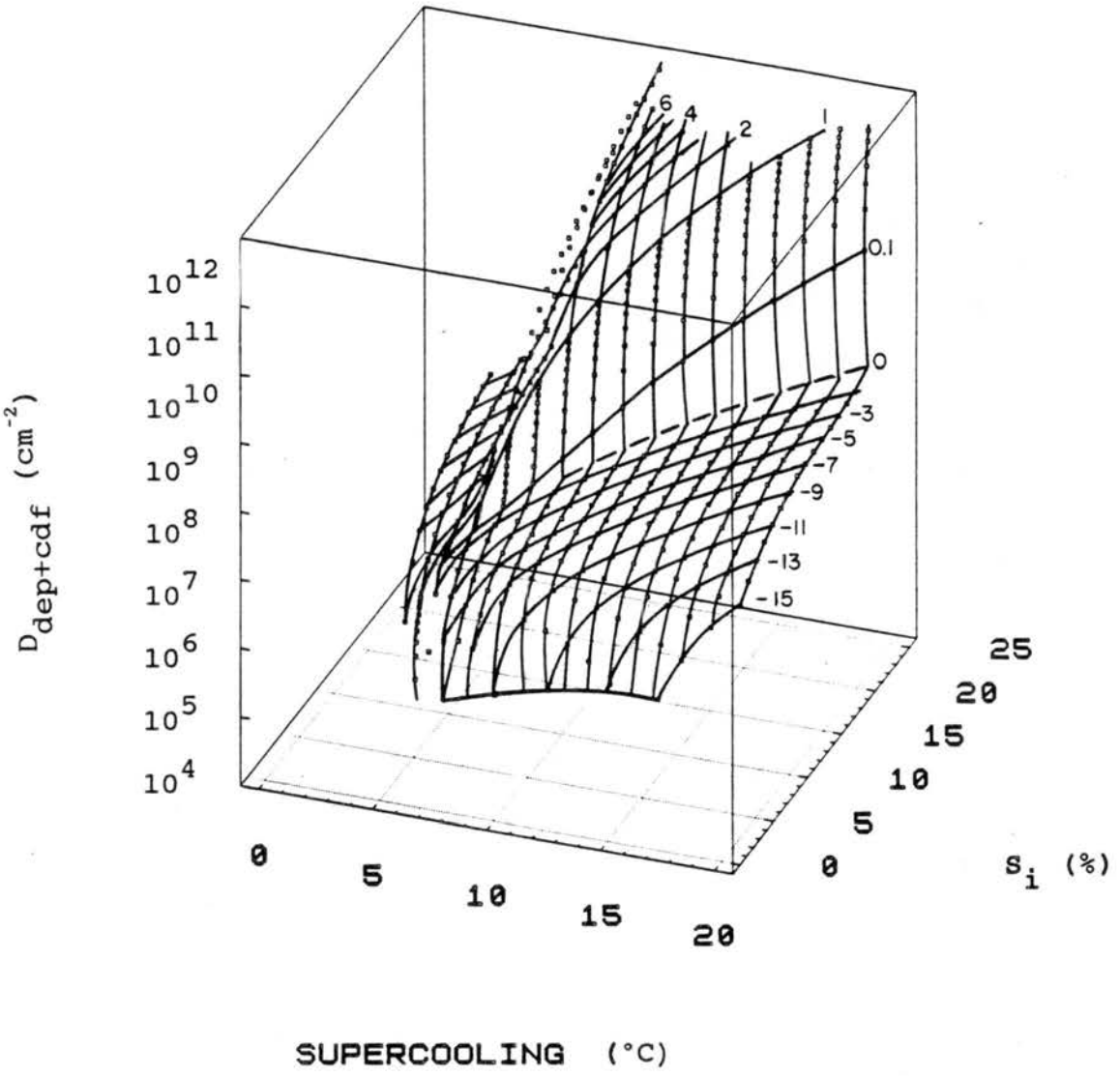

Figure 5.39 As in Figure 5.35, but for AgI-AgCl-4NaCl aerosols.

VI. NUCLEATION BY AgI-TYPE AEROSOLS: EXPERIMENT VERSUS NUMERICAL MODEL SIMULATION AND IMPLICATIONS FOR CLOUD SEEDING

Implementation of the new results from Chapter 5 into the numerical cloud model has been carried out to check the integrated effects of the new schemes versus observed nucleation in a variety of cloud chamber experiments. Some of the comparisons are blind in the sense that the experiments were performed with the full polydisperse aerosol size distributions and/or the experiments served no specific purpose in quantifying nucleation modes. These comparisons also provide the opportunity to demonstrate and understand the differing nucleation responses of the chemically different AgI aerosols to a range of conditions that might also be encountered in real clouds. Some comparison with model simulations using the old formulas for AgI nucleation are also included to demonstrate the benefit gained with the new descriptions. Finally, a few characteristic atmospheric seeding situations are considered to compare the quantitative differences to be expected using the chemically different ice nucleating aerosols. Orographic and cumulus cloud parcel simulations are included.

6.1 General considerations and new ice nucleus description implementation

Some simplifications made in the descriptions of ice nucleation by the two aerosols studied were discussed in Chapter 5. These included a unified description of immersion-freezing nucleation, independent of either aerosol chemistry, and a simple scheme to estimate haze particle size for AgI-AgCl-4NaCl aerosols before computing collection rates for contact-freezing nucleation. The immersion-freezing nucleation routine was inserted into the CONDNS subroutine (see Appendix A) of the Young cloud model. There, action of ice nuclei as cloud condensation nuclei is predicted along with the action of standard CCN, and appropriate adjustments are made to the water balance. Through the aid of global parameters, appropriate fractions of the particle numbers immersed as CCN plus numbers collected by cloud droplet scavenging processes (subroutine CONDFRZ) are frozen at each time step that immersion-freezing conditions are met. At any time step, additional ice is nucleated by contact-freezing (subroutine CONDFRZ) only when the fractions potentially effective are greater than the fraction already effective by deposition and condensation-freezing (subroutine ARTDEP). This does not affect the immersion-freezing routine. At every model time step when ice is formed, particles numbers are conserved and water mass balance is adjusted. Model time step is adjustable at any point. For these simulations, calculations were made every second and data file records were written every 5 seconds (3 times the experimental frequency).

Some assumptions that are made in performing comparative model simulations and experiments are:

1. The dilution by expansion of aerosol concentrations injected into the dynamic cloud chamber is of negligible importance when comparing to a simulation that is initialized at a later experimental time; just prior to cloud formation for example, when seeding was actually conducted 3 minutes earlier.

2. Model cloud droplet concentrations are initiated (by trial and error adjustment of CCN parameters) based on the average concentrations observed in the first few minutes after cloud forms. This is most valid over short (4 to 5 minutes) periods, as droplets settle from the cloud chamber eventually during growth.

3. Since deconvolution of the experimental ice signal accounts for growth as well as settling of ice crystals, the model ice signal total model ice signal including spherical particles ($<20\mu m$ in the model) is compared to cloud chamber experiments.

4. An inherent assumption that size effects are translatable for polydisperse particle distributions is made.

5. Accretional growth is deactivated in the model for the comparative simulations.

None of these assumptions/practices should have much impact on the results, as will be evident in the actual comparisons. Qualifications are made when comparisons become invalid; for example when cloud droplet concentrations rapidly decay experimentally, or when the

accumulating and growing ice in the model parcel begins to adversely and artificially affect the water balance. As stated, comparisons are typically made only over short time periods after cloud formation, or after ice nuclei are injected.

6.2 Nucleation by AgI-AgCl and AgI-AgCl-4NaCl aerosols : Cloud model predictions versus cloud chamber experiments

The comparisons made here can be broken down into three categories, each with its own primary purpose. These categories are injection of AgI-type aerosol to simulate its passing through cold cloud base (below -4°C), injection directly into cold cloud, and injection to simulate seeding through warm cloud base (warmer than 0°C). The cold cloud base seeding tests have some direct relevance to seeding experiments which might be conducted in the atmosphere. Winter orographic cloud seeding of cold-based storms in the Intermountain West using ground generators below cloud base, or aircraft upwind of the upstream cloud edge are a few relevant examples. However, the simulated updraft rates employed in the cloud chamber experiments are much higher than typically encountered in these wintertime situations. The primary utility of these pre-cold cloud comparisons is to test the integrity of the new formulations and to demonstrate effects of nucleus physical and chemical characteristics, and cloud conditions, on ice formation by the various nucleation modes. The comparisons made for direct injection into cloud have more direct implication to atmospheric cloud seeding with the aerosols studied. An example which is comparable is direct (aircraft) single cloud seeding experiments in the summertime using acetone solution burning generators. An example of one such field

experiment and a comparison with model results is given in the next chapter. Another method sometimes employed in the seeding summertime cumulus clouds is releasing ice nucleus aerosols below warm cloud base. The final comparisons address the utility of this method, simply from a nucleation standpoint, for the AgI aerosols studied. In the discussion of specific experimental results, experiments are referred to by their number (first 2-3 digits) and year (last 2 digits). A list of all experiments and their characteristics is included in Appendix B.

6.2.1 Cold Cloud Base Seeding

In similar experiments for the respective AgI aerosols, monodisperse particles were injected into the cloud chamber prior to the formation of cold cloud (other CCN present). Figures 6.1 and 6.2 show some quantities of interest in equivalent experiment (experiment 12188) and model simulations of a cloud seeded through its base near -7°C with 0.03μm AgI-AgCl aerosols. The updraft simulated by this expansion was 5 m s^{-1}. The model simulation of cloud formation excellently mimics experimental cloud formation in this case. The only difference is the evolution of the cloud droplet sizes. Figure 6.3 compares the cloud droplet size spectra experimentally and in the model simulation. It is seen that droplets grow slower, the size distribution is more dispersive, and concentrations deplete faster in the cloud chamber experiments versus the numerical model simulation. The last factor is due to the lack of a removal mechanism for cloud droplets in the cloud model to simulate the sedimentation that occurs for the fixed cloud parcel in the chamber. This will be the subject of future model modification as an option for simulating chamber experiments. It is not

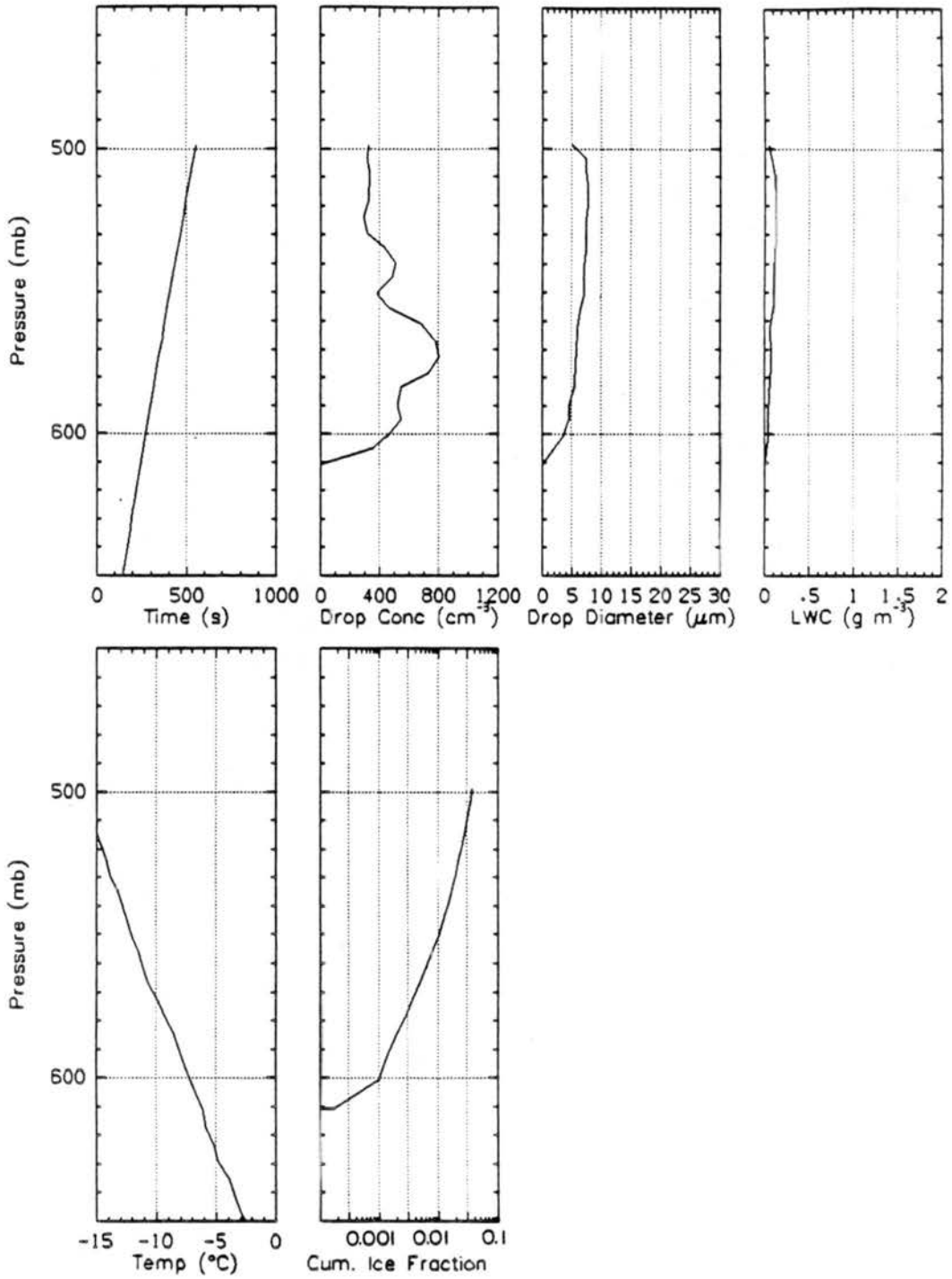

Figure 6.1 Time, droplet concentration, average droplet diameter, liquid water content, temperature, and ice nucleating as a fraction (F) of the aerosol injected versus pressure in experiment 12188. AgI-AgCl aerosols (0.03μm) were introduced before cloud formation at -7°C in this experiment. Equivalent updraft by expansion was 5 m s^{-1}.

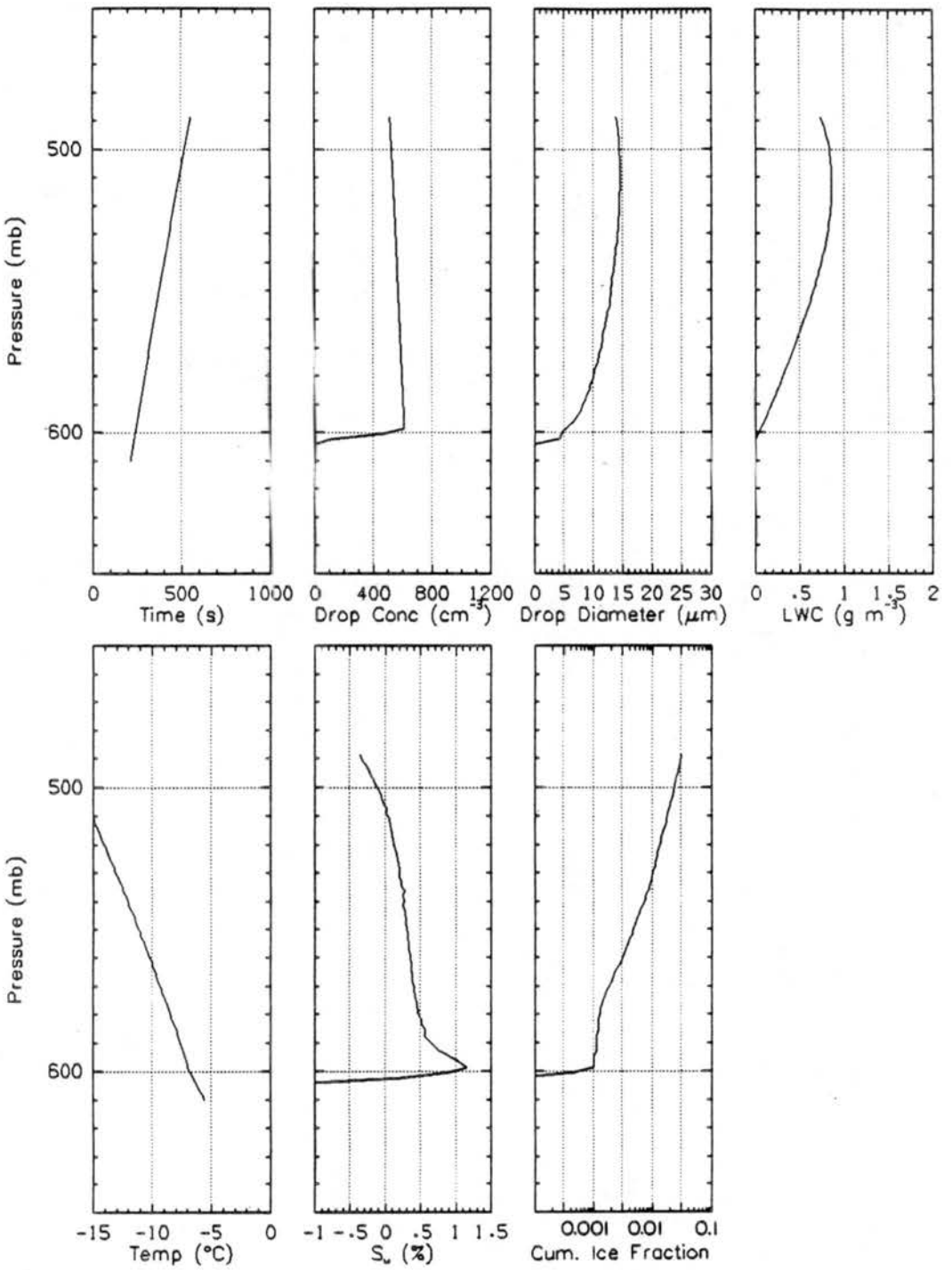

Figure 6.2 Numerical cloud model simulation (Young model) of experiment 12188 using the new ice nucleus formulations from Chapter 5.

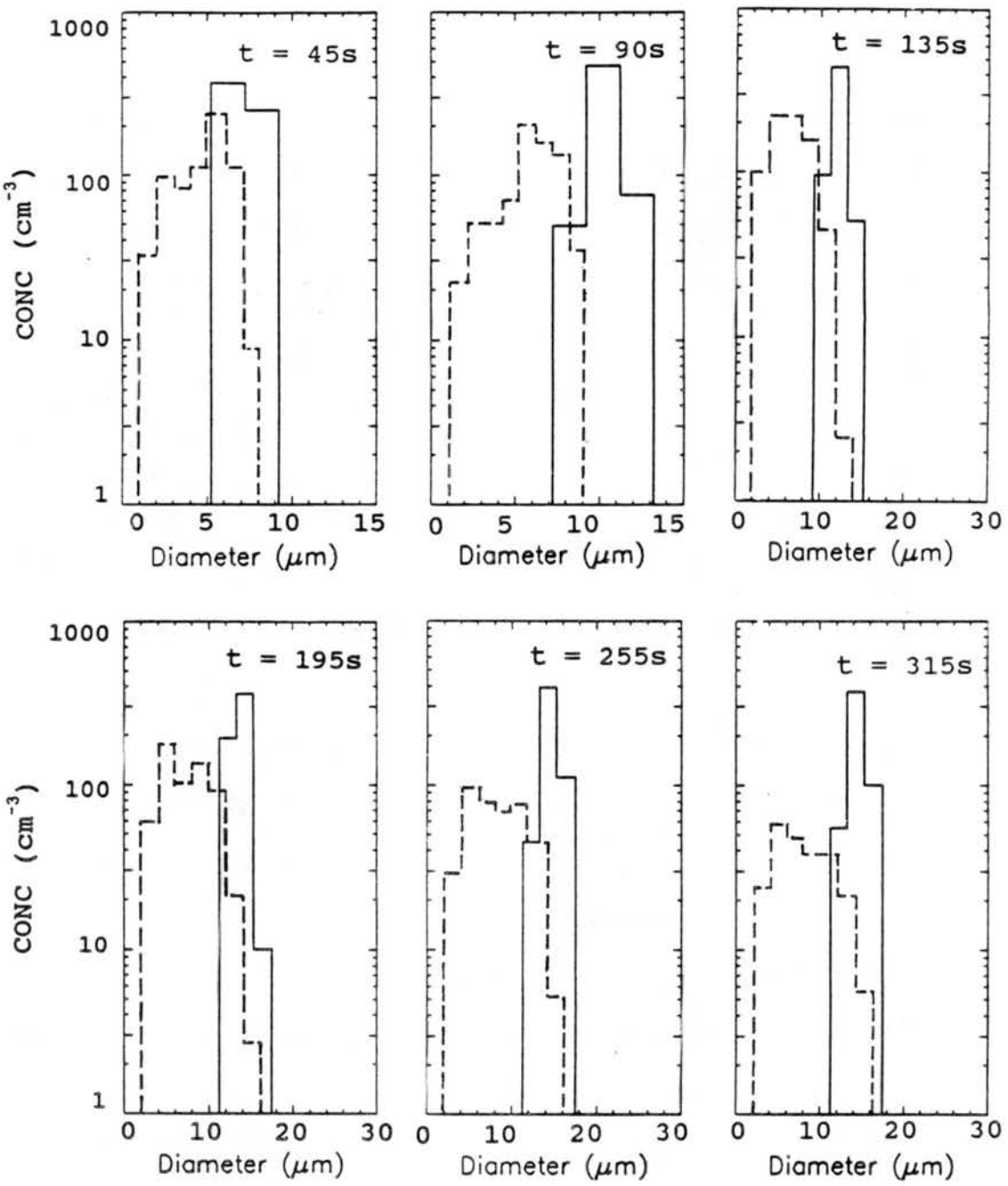

Figure 6.3 Measured versus model cloud droplet spectra at various times after cloud forms in experiment 12188.

known at this time if the first two factors are artifacts created by the deviation from ideal, homogeneous adiabatic conditions in the chamber, or they indicate inherent deficiencies in the theoretical treatment of cloud formation and growth. Except for a study by Hindman (1989) using this same cloud chamber, no one has measured the evolution of droplet size distributions in attempted laboratory simulations of early cloud growth. This will be the subject of future investigations.

Figures 6.4 (experiment 9588) and 6.5 (equivalent model simulation) show another example of cold cloud formation and ice nucleation by 0.03μm AgI-AgCl aerosols, this time for a 2.5 m s^{-1} equivalent updraft by expansion. Again, the model cloud is an acceptable reproduction of the experiment excepting droplet diameter, and thus also LWC. The 2:1 difference noted in predicted peak S_w between experiment 12188 (Figure 6.2) and experiment 9588 (Figure 6.5) is characteristic of that achieved by the 2:1 change in simulated vertical motion. The degree to which cloud formation and growth could be reproduced successfully with the cloud model could have some influence on the degree of agreement between model and experiment ice formation in some cases. Cooling rate was sometimes not the ideal value in cloud chamber experiments, and adjustments to temperature "overshooting" affected cloud formation and growth in ways that could not be reproduced with the model. Also, as previously discussed, the degree of success of the deconvolution procedure for experimental data and the overdepletion of water supersaturation due to ice accumulation and growth in the model simulations also affected the comparisons.

Nucleation differences due to particle size, updraft rate (and thereby supersaturation), and particle chemistry are demonstrated in

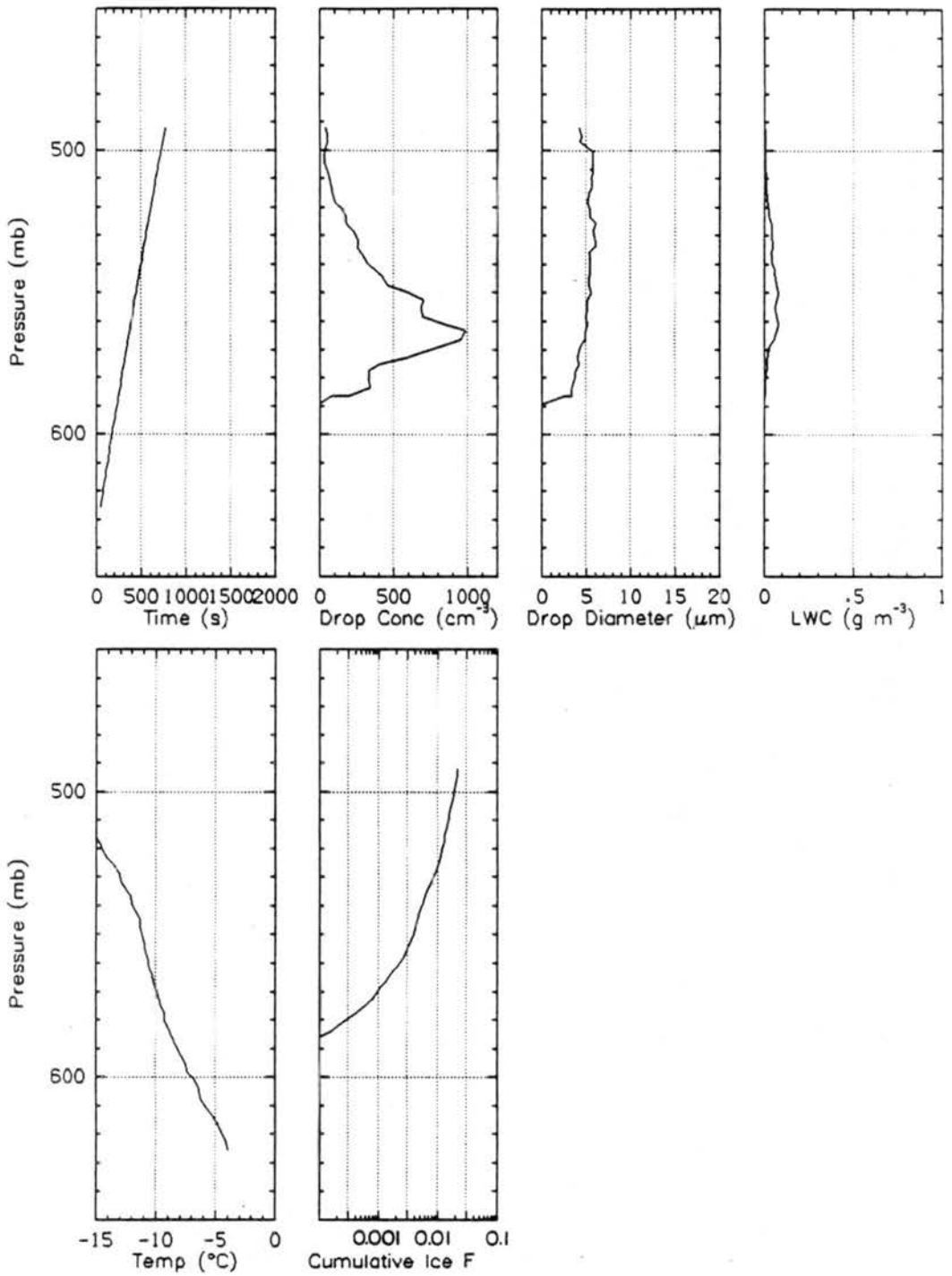

Figure 6.4 As in Figure 6.1, but for a 2.5 m s^{-1} equivalent updraft expansion with cloud forming at -8.5°C (experiment 9588).

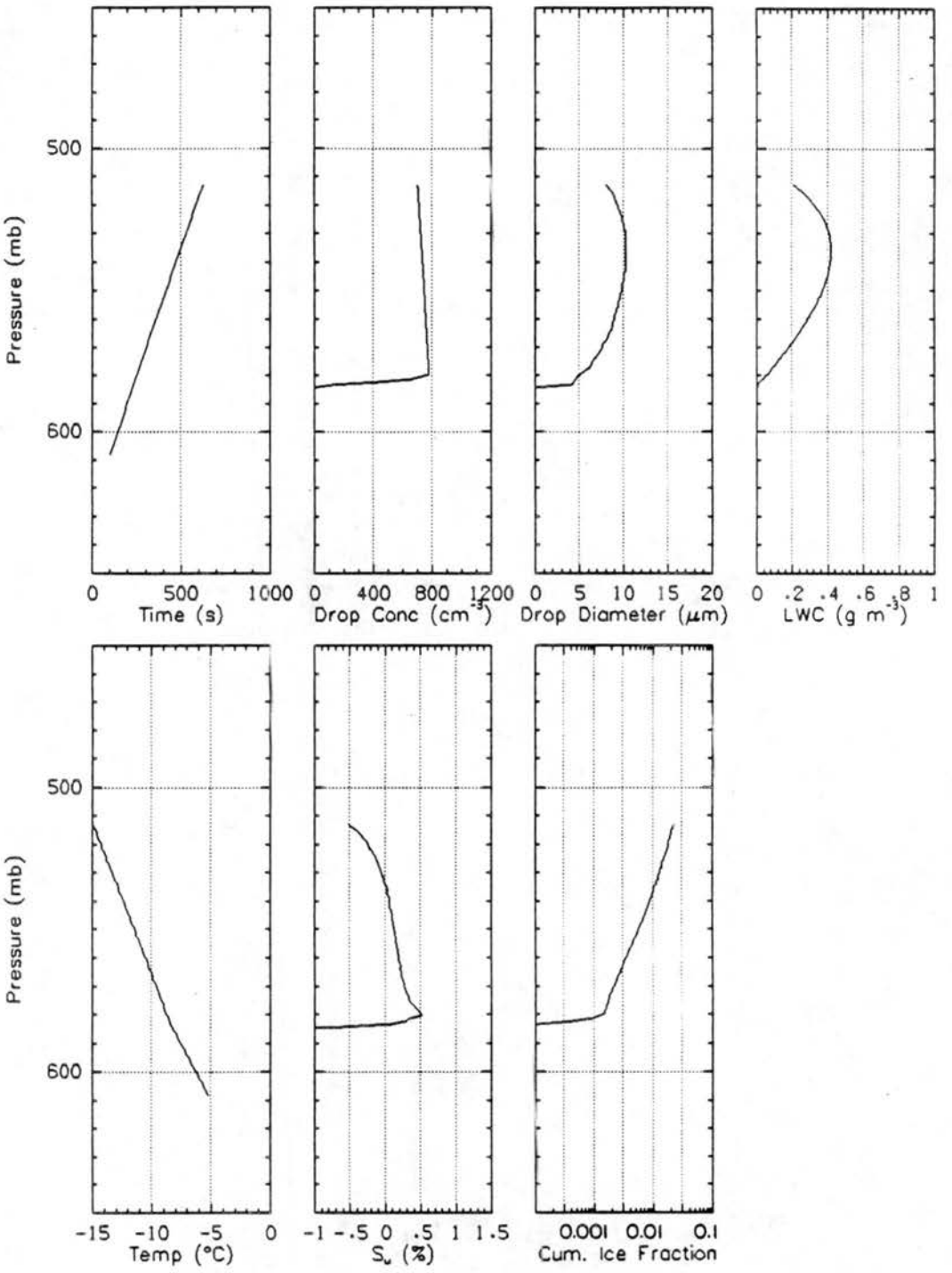

Figure 6.5 **Model simulation of experiment 9588.**

the cloud chamber experiment versus numerical model ice formation comparisons which follow. Figure 6.6 (experiment 9588) and Figure 6.7 (experiment 9188) show the differential and cumulative amounts of ice formed versus temperature in similar experiments in which cloud formed between -8 and -9°C for a simulated 2.5 m s^{-1} updraft. Both experiments were seeded before cloud formation point, as indicated by arrows; experiment 9588 with 0.03μm and experiment 9188 with 0.07μm AgI-AgCl aerosols. Both the cloud chamber experiments and the model results indicate higher activity for 0.07μm aerosols at temperatures warmer than about -12°C. There is an indication that the model overpredicts ice nucleation at cloud formation point in both cases, though more so for experiment 9588 (Figure 6.6). This effect is clearly related to the supersaturation generated at cloud point. This is emphasized when the mechanistic contributions to ice formation are delineated, as shown in Figures 6.8 and 6.9. The two sized aerosols have similar activity as contact-freezing and immersion-freezing nuclei, but the 0.07μm aerosols are more efficient as deposition and condensation-freezing nuclei. This is particularly true near the supercooled cloud point, where condensation-freezing and deposition dominate ice formation. This is observed in the cloud chamber experiments, although not to the degree predicted. Contact-freezing nucleation is seen to be particularly dominant below -10°C for the 0.03μm aerosols. This differs from the situation portrayed by using the original model formulations for nucleation by AgI aerosols. Figures 6.10 and 6.11 show that the old model formulations predicted that deposition/sorption (includes condensation-freezing) should dominate nucleation by either sized aerosol, because contact-freezing is a minor player. Clearly, the

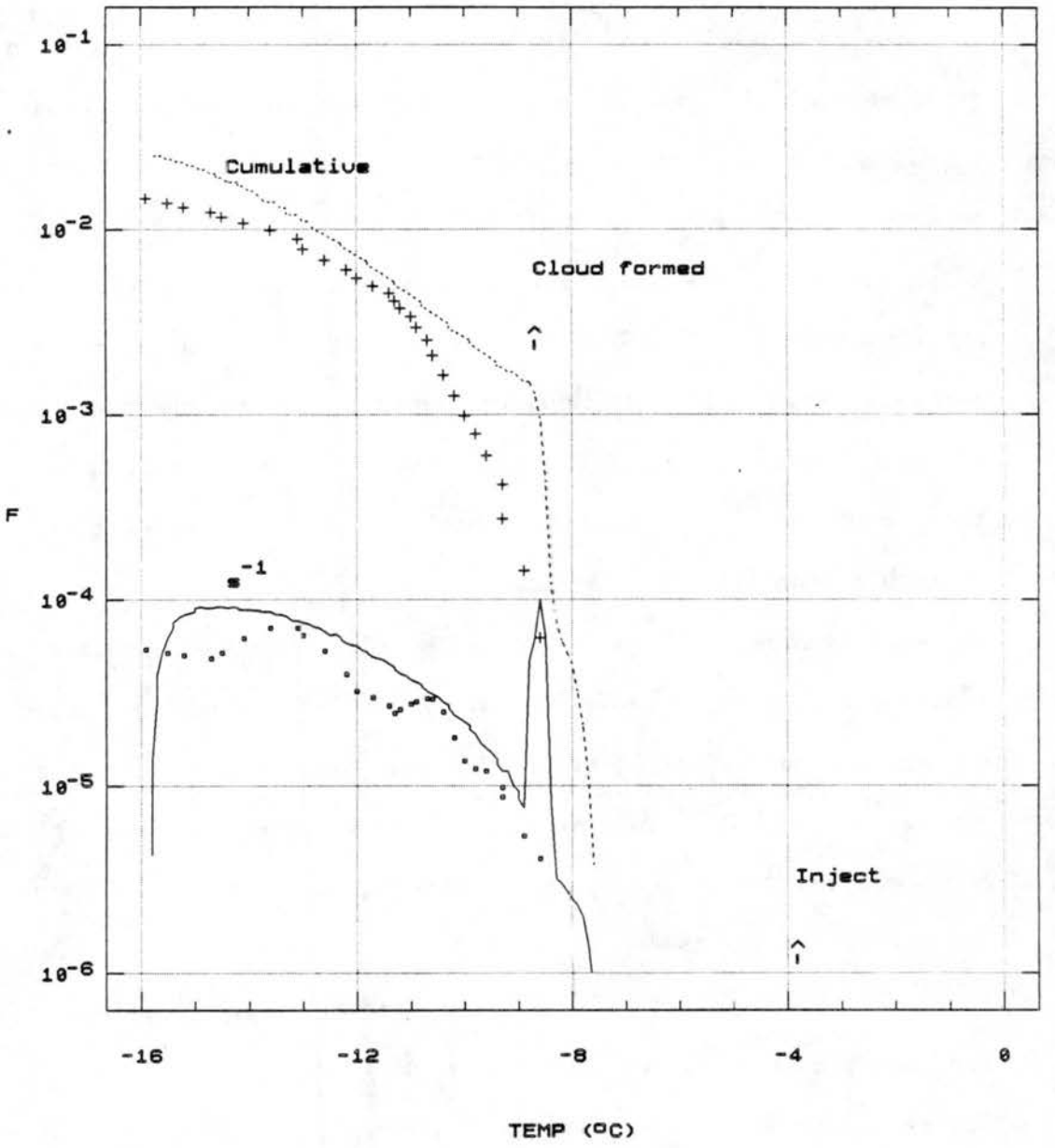

Figure 6.6 Cumulative (+) and differential (□) fractions of ice forming versus temperature in experiment 9588. Aerosol injection point and cloud formation point are indicatedby arrows.

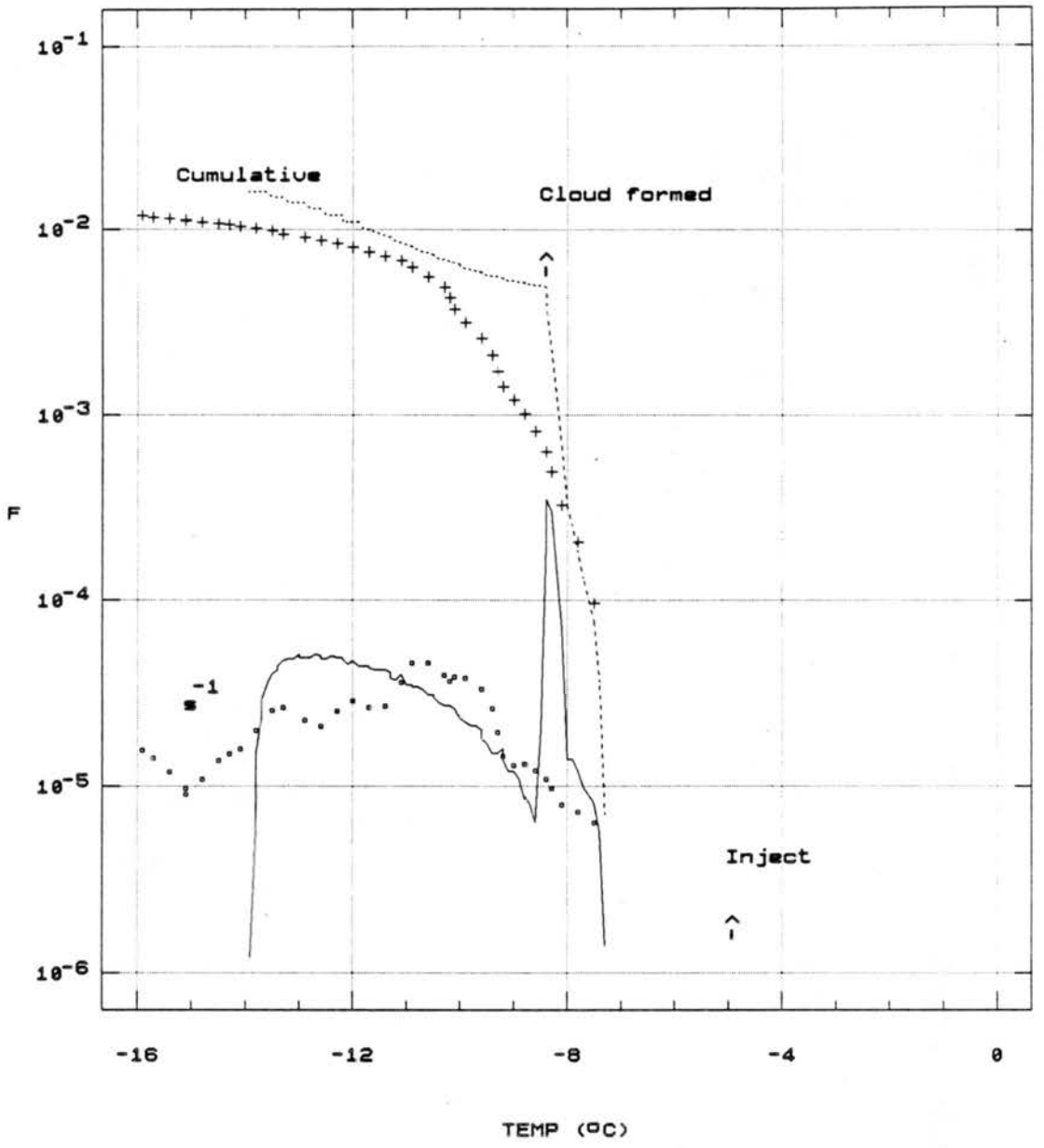

Figure 6.7 As in Figure 6.6, but for experiment 9188 (0.07μm AgI-AgCl).

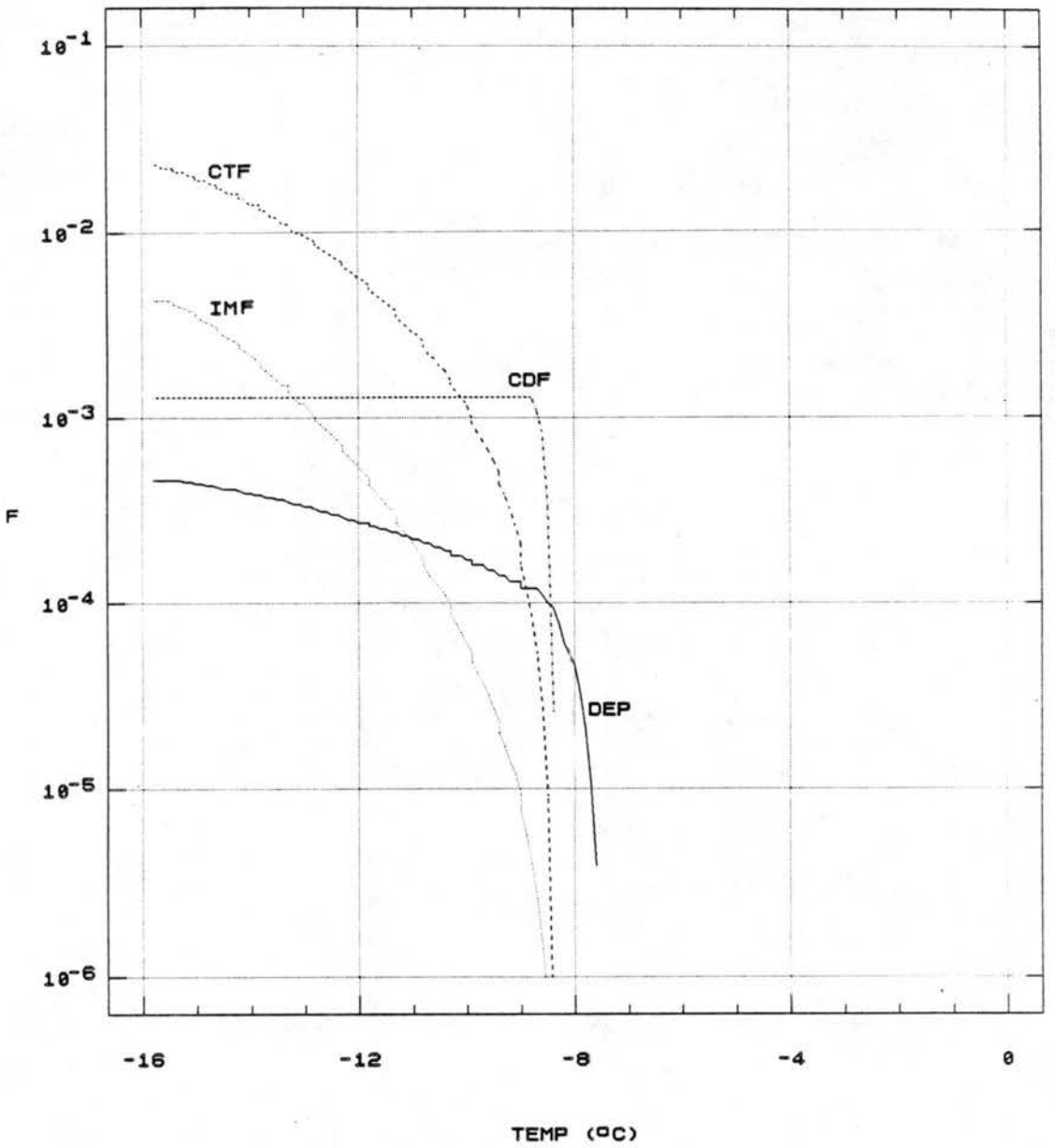

Figure 6.8 Contributions to F of contact-freezing (CTF), immersion-freezing (IMF), deposition (DEP), and condensation-freezing (CDF) nucleation in experiment 9588, as predicted by the model simulation using the new ice nucleus formulations.

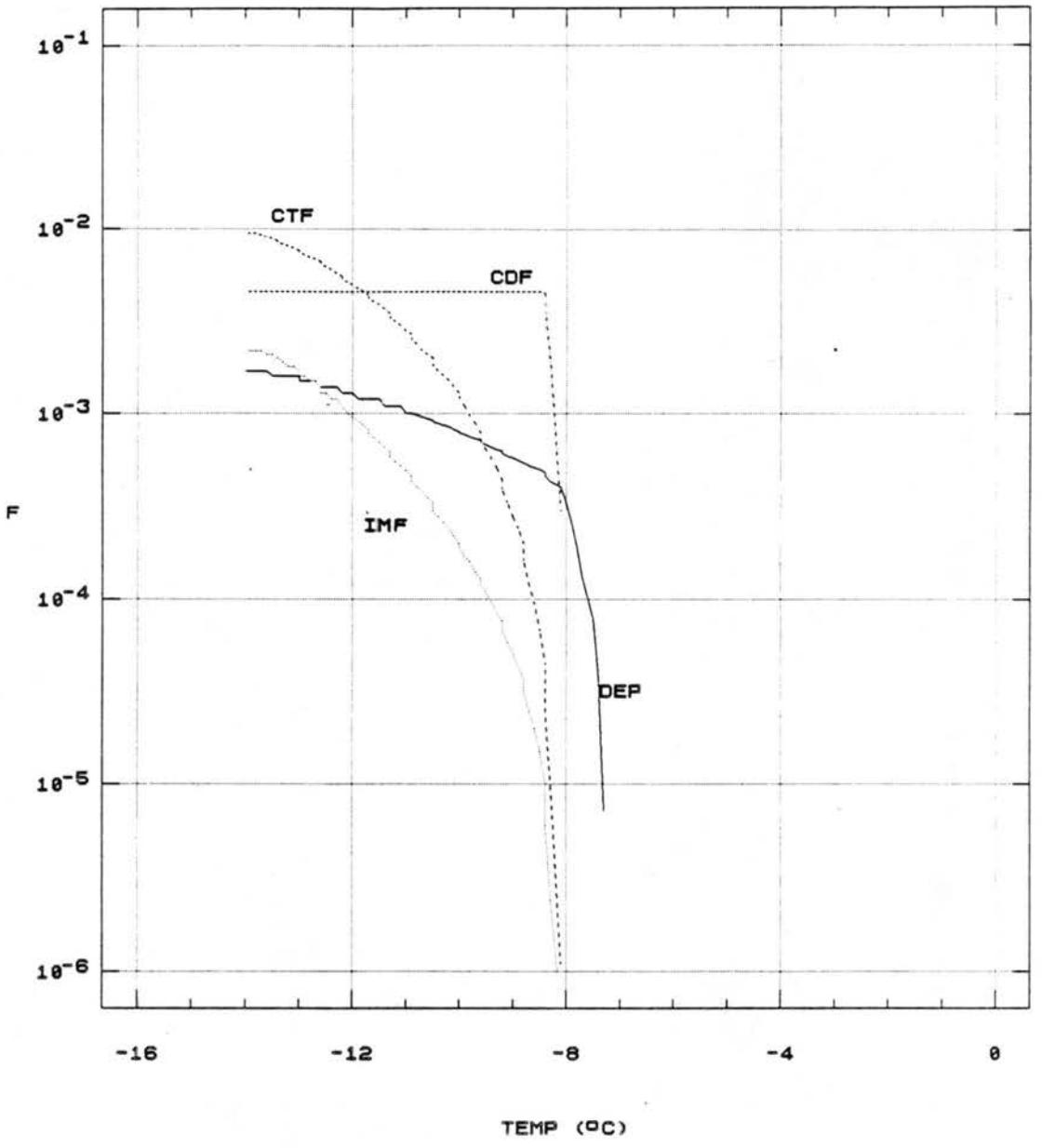

Figure 6.9 As in Figure 6.8, but for experiment 9188.

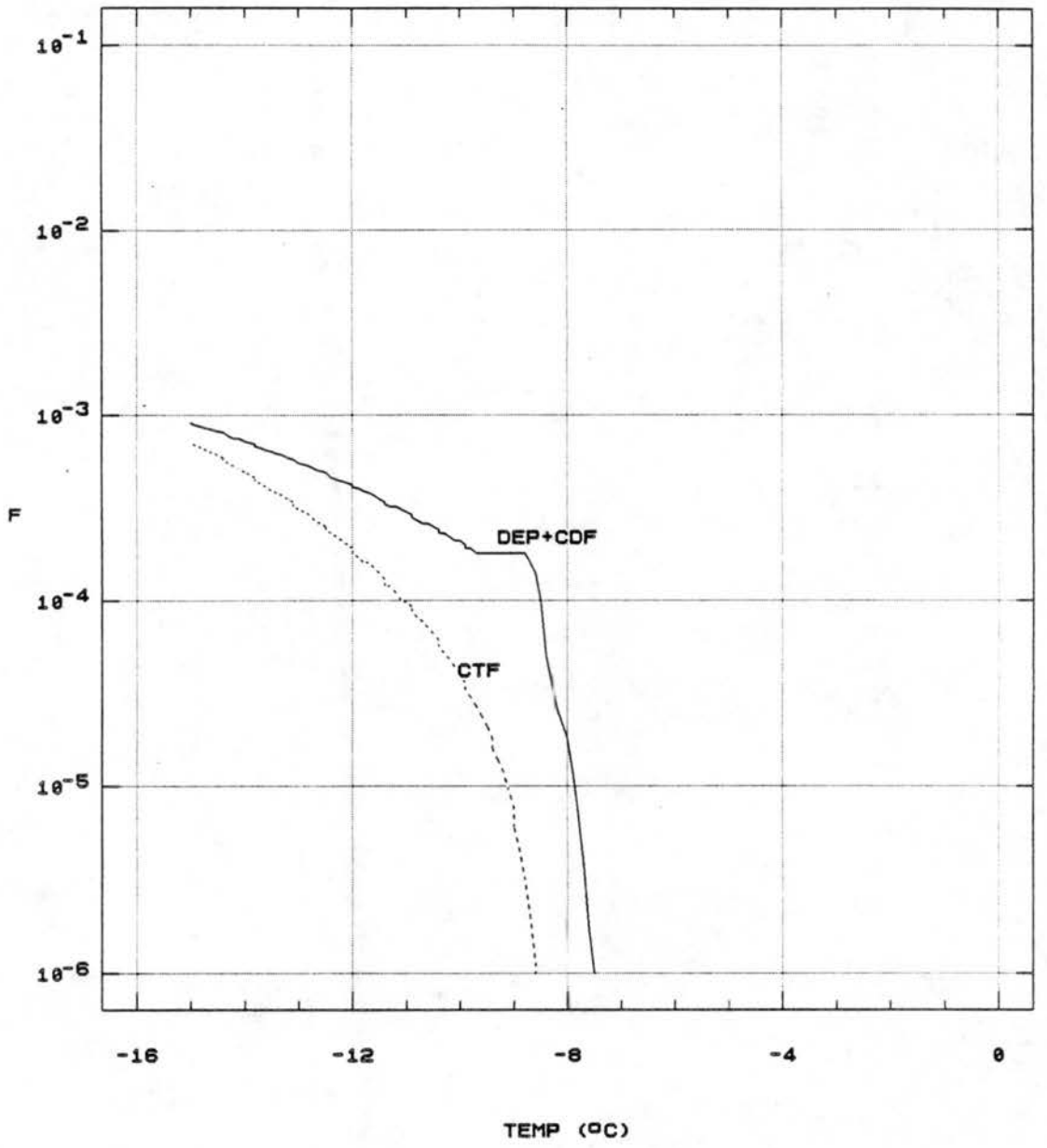

Figure 6.10 Contribution of nucleation mechanisms as formulated for pure AgI in the original version of the cloud model. Simulation is of experiment 9588. Immersion-freezing was not formulated in the original model.

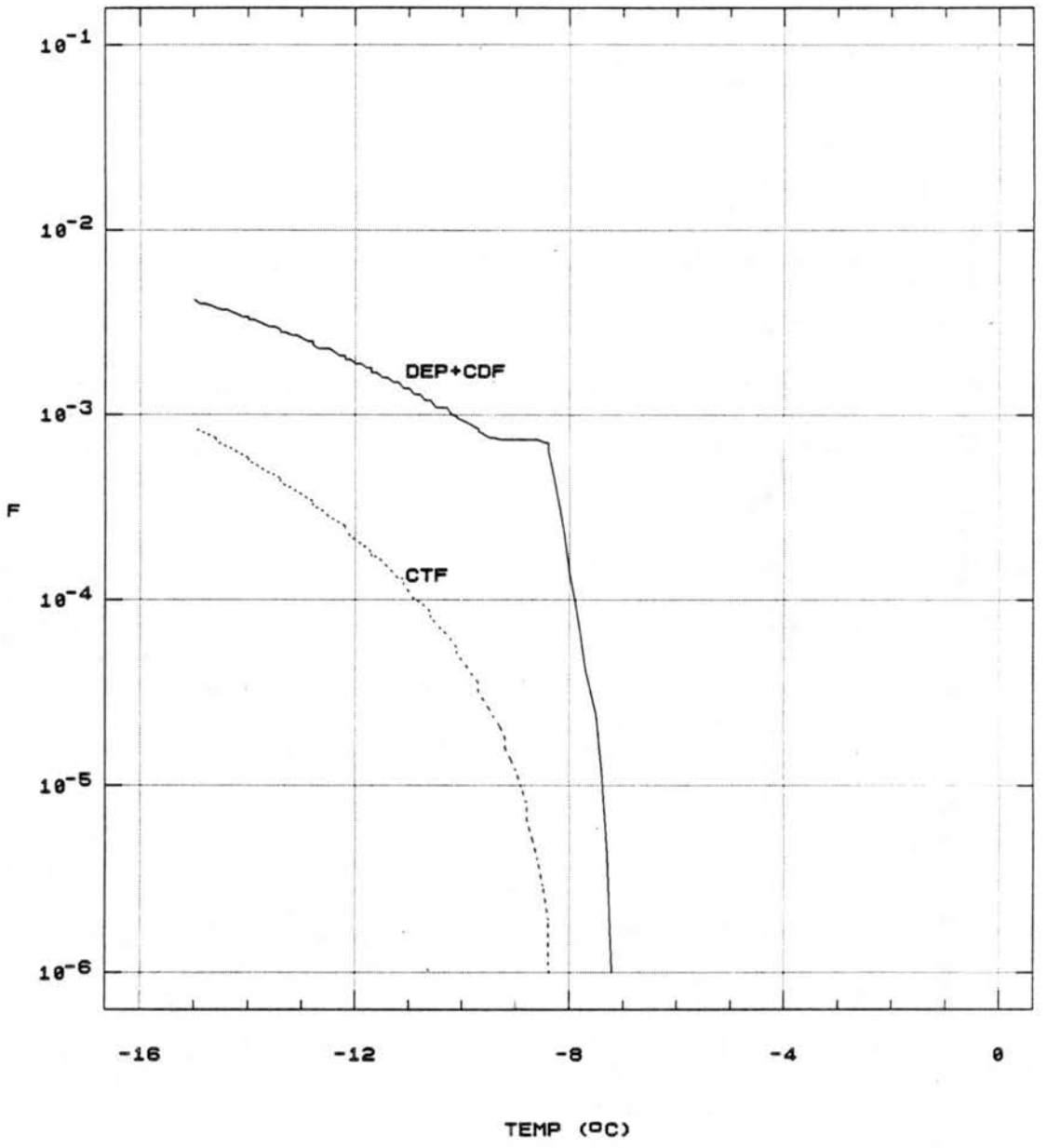

Figure 6.11 As in Figure 6.10, but for experiment 9188.

greatest improvement made in these cases is the redefinition of the active site density for contact-freezing and the addition of a description of immersion-freezing nucleation. The new description of condensation-freezing nucleation appears to merit further improvement.

Nucleation is enhanced for both sized AgI-AgCl aerosols when the peak and steady state supersaturations are increased. In cloud chamber experiments, this was accomplished by increasing the cloud expansion cooling rate. The effect is most evident at the cloud formation point. This is demonstrated by comparing Figures 6.6 (experiment 9588) and 6.7 (experiment 9188), 2.5 m s^{-1} equivalent updraft expansions, with Figures 6.12 (experiment 12188) and 6.13 (experiment 9788), which are 5 m s^{-1} equivalent updraft expansions. The peak supersaturations predicted in each case are noted in the figure captions. The profile of S_w in experiment 12188 is included in Figure 6.2. Figures 6.14 and 6.15 show the cumulative ice formation versus temperature as a function of peak supersaturation in some other experiments and equivalent model simulations for both aerosol sizes. Reasonably good consistency among chamber experimental results and between chamber results and model simulations is shown. Mechanistically, nucleation increases primarily due to the enhanced condensation-freezing nucleation reponse at cloud formation point. At the same time, the decrease in contact-freezing nucleation due to a collection time decrease is compensated for by increased immersion-freezing nucleation. This comes about as a result of increased activation of the AgI-AgCl aerosols as CCN. The model immersion-freezing contributions from condensation and collision events are separated for experiments 9588 and 12188 in Figure 6.16 to make this point clear. At the higher S_w peak in experiment 12188,

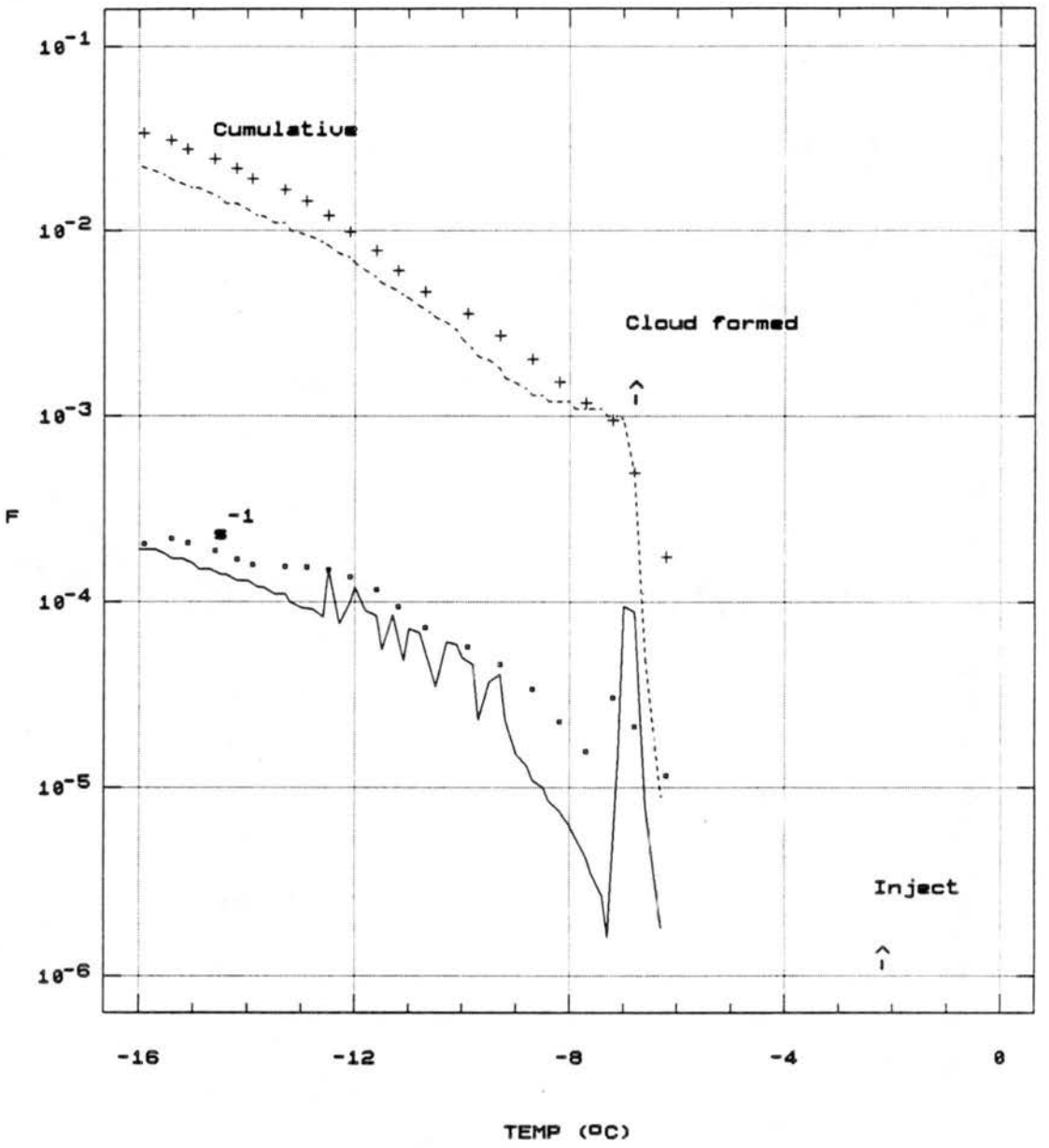

Figure 6.12 Observed cumulative (+) and differential (□) fractions of ice forming versus temperature in experiment 12188 (5 m s^{-1} expansion), and in the equivalent model simulation (lines).

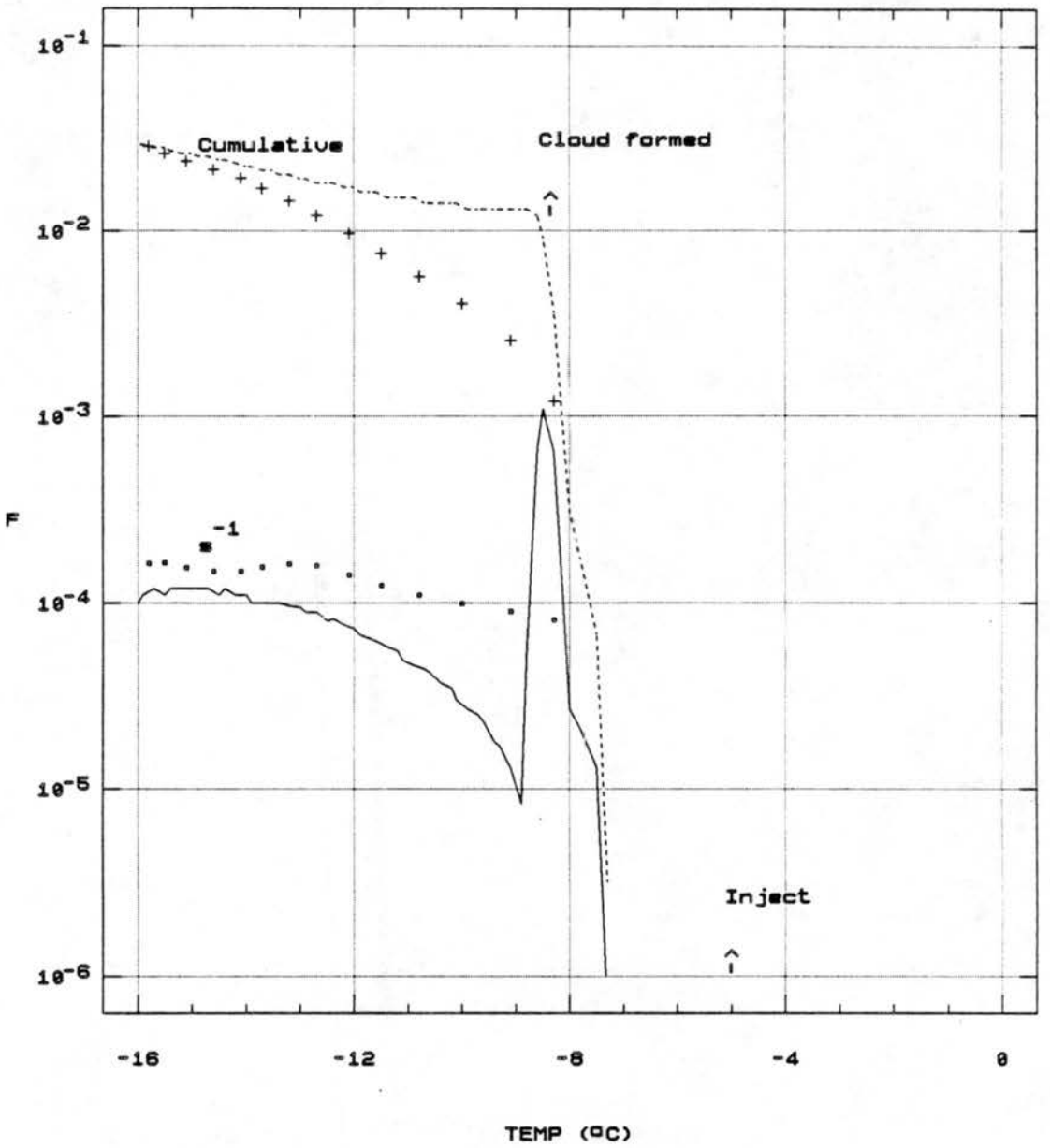

Figure 6.13 As in Figure 6.12, but for experiment 9788, a 5 m s^{-1} expansion seeded pre-cloud with 0.07μm AgI-AgCl aerosols.

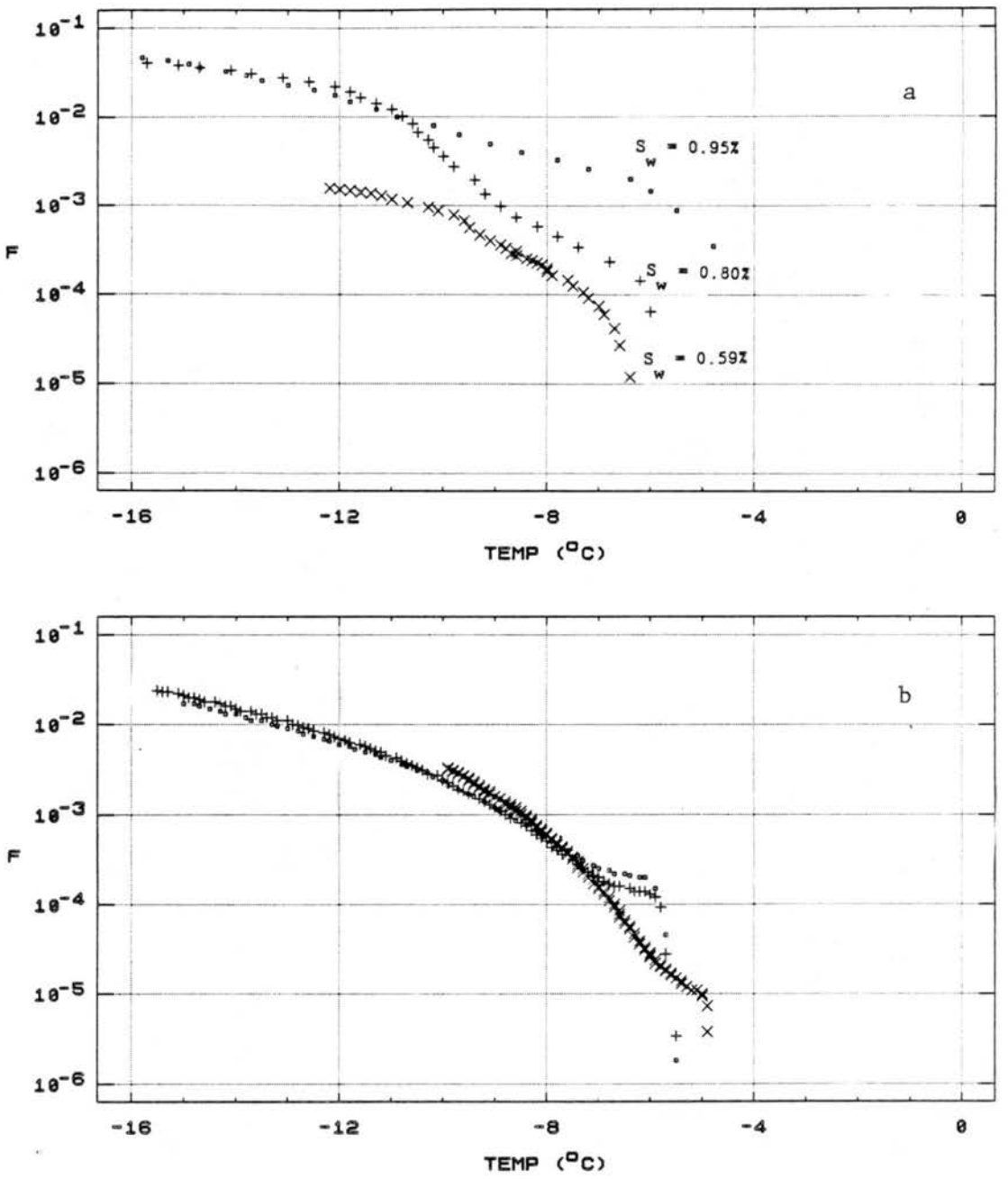

Figure 6.14 The effect of peak supersaturation at thermodynamic cloud point on cumulative ice formation by 0.03μm AgI-AgCl aerosols. Observations are given in (a) and model results in (b). Simulated ascent rates of 1.5 (x), 3.5 (+), and 5 m s^{-1} (·) are represented (experiments 11688, 11588, 11788).

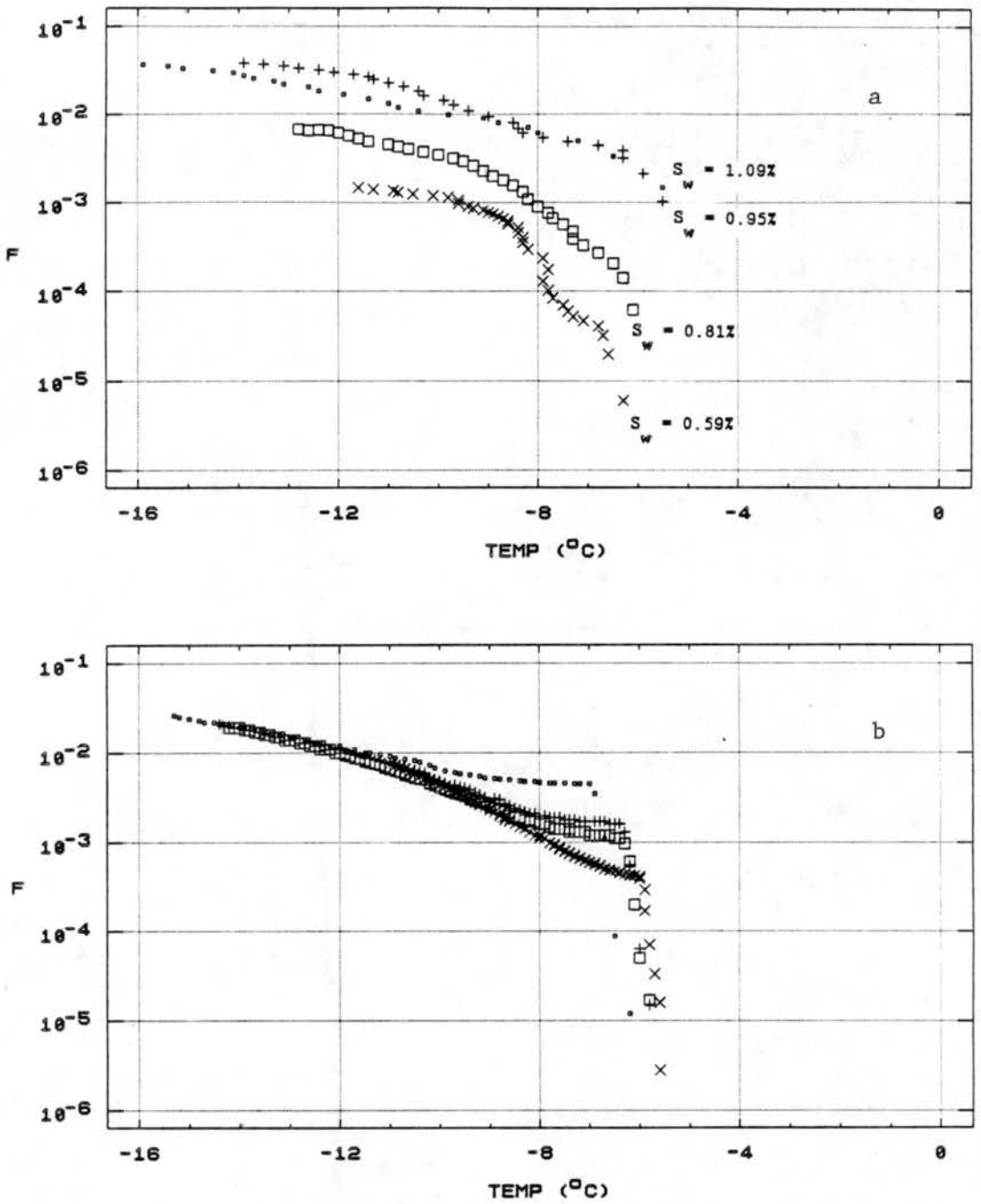

Figure 6.15 As in Figure 6.14, but for 0.07μm AgI-AgCl aerosols. Simulated ascent rates of 1.5 (x), 2.5 (□), 3.5 (+), and 5 m s^{-1} (•) are represented (experiments 11288, 9388, 11188, 11388).

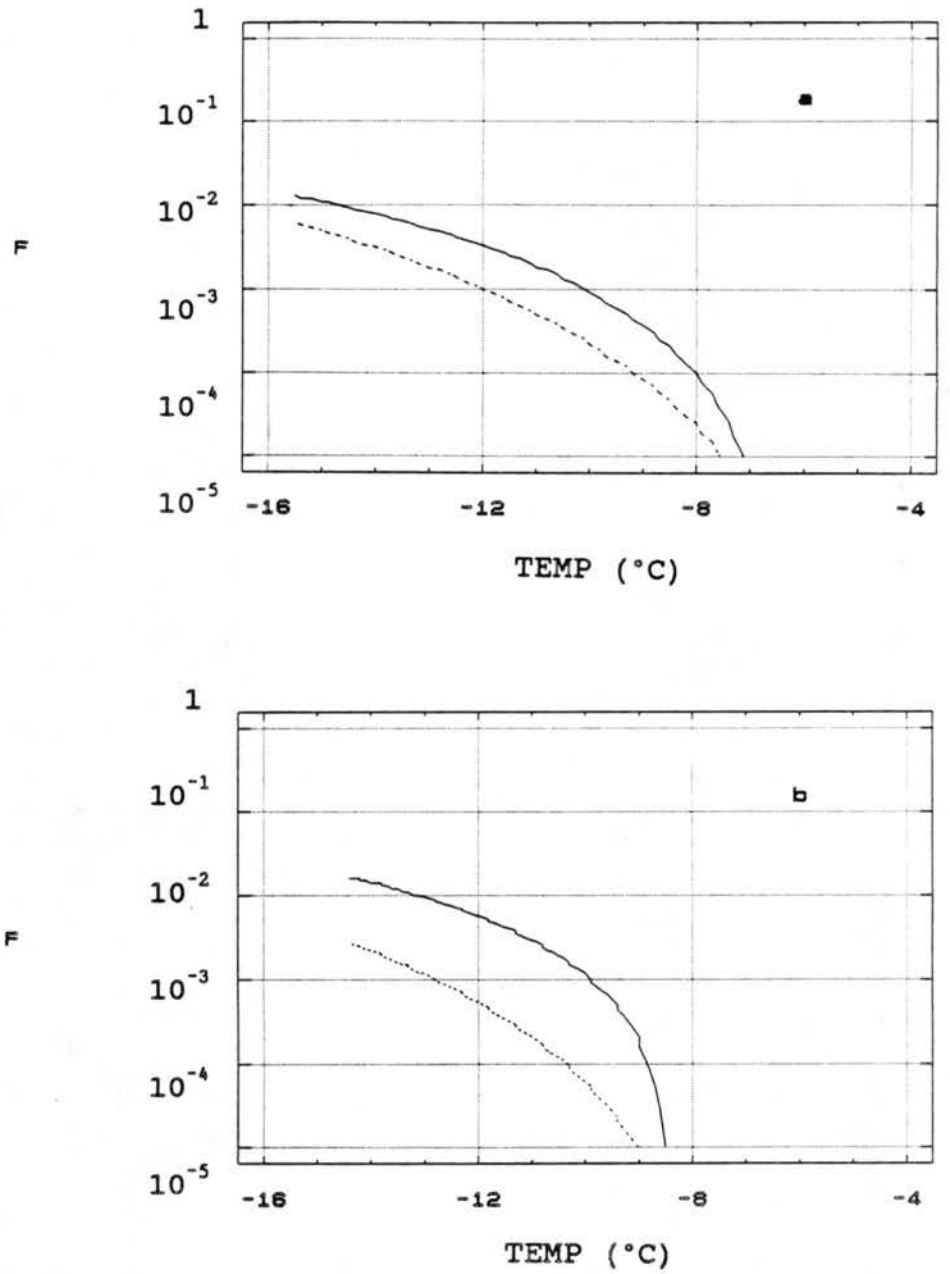

Figure 6.16 Separation of immersion-freezing nucleation into its component sources from particles collected by cloud droplets (solid line) and those acting as CCN at cloud formation point (dashed lines) in experiments 12188 (a) and 9588 (b).

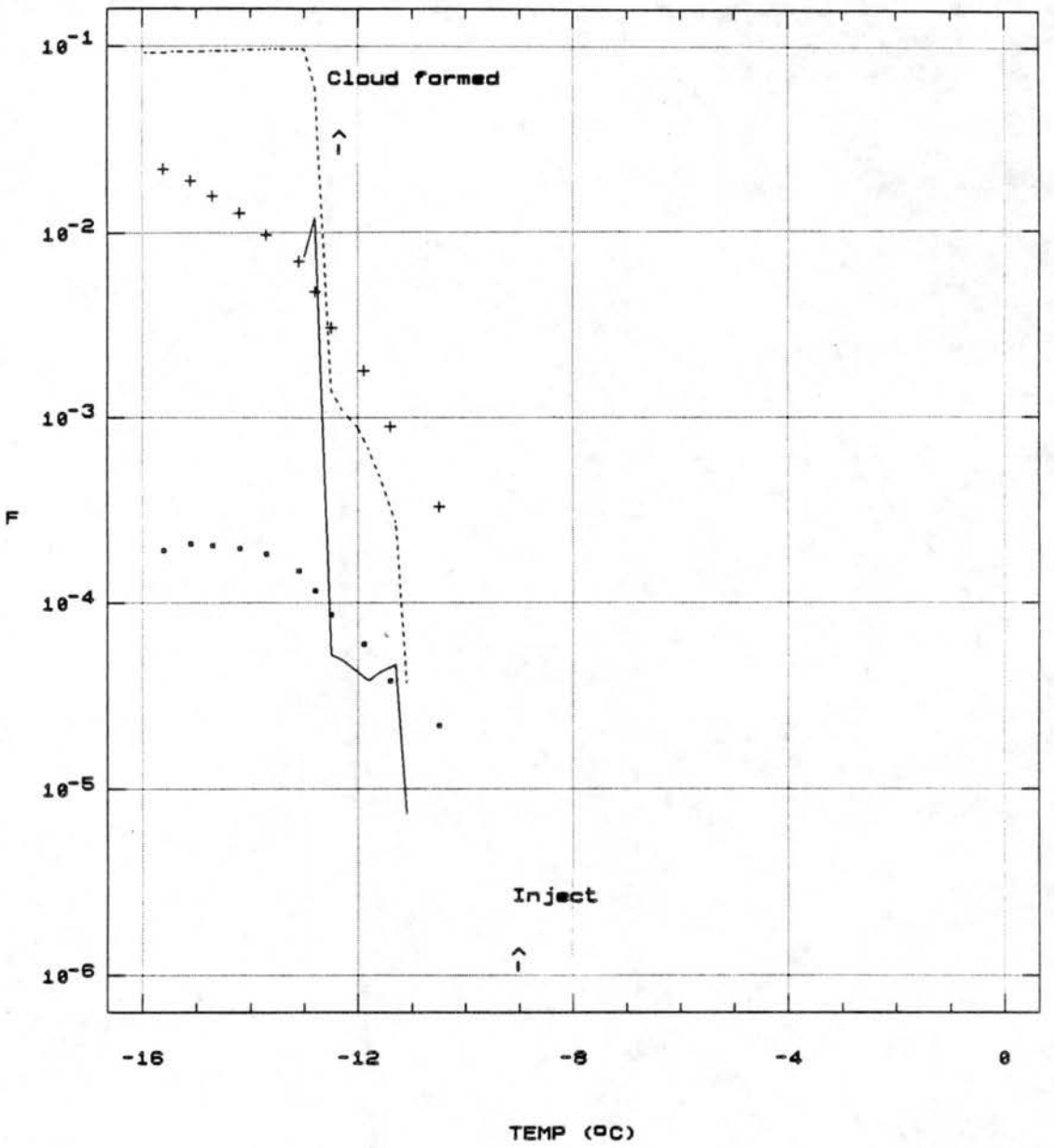

Figure 6.17 Exactly as in Figure 6.13, but for cloud forming at -12.5°C.

condensation events increased the immersion-freezing nucleation signal. At colder cloud point temperatures, as shown in Figure 6.17 (experiment 1789), condensation-freezing is completely dominant, even for this hydrophobic aerosol. The excellent prediction of deposition nucleation is notable in this experiment, while the reason for the overprediction of condensation-freezing is not clear. The overnucleation and lack of sink for nucleated crystals led to glaciation (complete conversion to ice) of the model cloud, something which did not occur in the experiment until -20°C.

The hygroscopic AgI-AgCl-4NaCl aerosols also display nucleation sensitivities to particle size and supersaturation when they are present as cloud forms at some cold temperature. The relationship between cumulative amounts of ice nucleated in a given parcel ascent and particle size is more complex for AgI-AgCl-4NaCl aerosols than for AgI-AgCl aerosols. As shown in Chapter 5, the CCN activity of these aerosols varies greatly as a function of particle size and supersaturation. For the same ascent conditions, the larges sizes in the generator particle size distribution (PSD) will act more efficiently as CCN than the smaller ones. This effectively limits the action of that fraction of the PSD as ice nuclei to the immersion-freezing mechanism. The particles that do not act as CCN are free to form ice, primarily by condensation-freezing nucleation, at colder temperatures during expansion. The net effect can sometimes be that the cumulative ice nucleated by different monodisperse AgI-AgCl-4NaCl aerosols for the same cloud conditions is very similar, while masking a difference in source modes. The strong sensitivities of condensation and condensation-freezing nucleation to supersaturation also makes the

model simulation of cloud characteristics (thermodynamic cloud point, droplet concentration nucleated initially) rather critical to the agreement between cloud chamber and model results for ice nucleation.

Figures 6.18 and 6.19 compare the evolution of ice crystals nucleated in equivalent 2.5 m s^{-1} ascent rate simulations seeded before cloud formation in the vicinity of -9°C with 0.03 (experiment 5788) and 0.07μm (experiment 8488) AgI-AgCl-4NaCl aerosols, respectively. Cloud forms about 0.5°C warmer for 0.03μm aerosols, so the initial ice signal is higher for these particles, but the net observed cumulative ice signal is not much different for the two sizes. The cloud model predicts somewhat higher nucleation rates initially for the 0.07μm particles. The mechanistically differentiated cumulative ice fractions plotted in Figures 6.20 and 6.21 show that this initial signal difference comes from differences in deposition and condensation-freezing nucleation. Fortunately, such a large discrepancy for 0.07μm AgI-AgCl-4NaCl experiment versus model results was not a general occurrence. Also, it will be shown that this is not such an important factor when the full polydisperse particle distribution is modeled.

Two additional factors should be noted in Figures 6.18 through 6.21. First, the model tends to underpredict at colder temperatures. This clearly occurs due to the rapid reduction in saturation ratio, an artifact of the growth of the large numbers of ice crystals nucleated and not removed from the model parcel, combined with the sensitivity of these aerosols to saturation ratio. The second factor of note is the difference in the magnitude of the immersion freezing fractions nucleated. For these same ascent conditions, immersion-freezing becomes an increasingly more important mechanism for 0.07μm aerosols as the

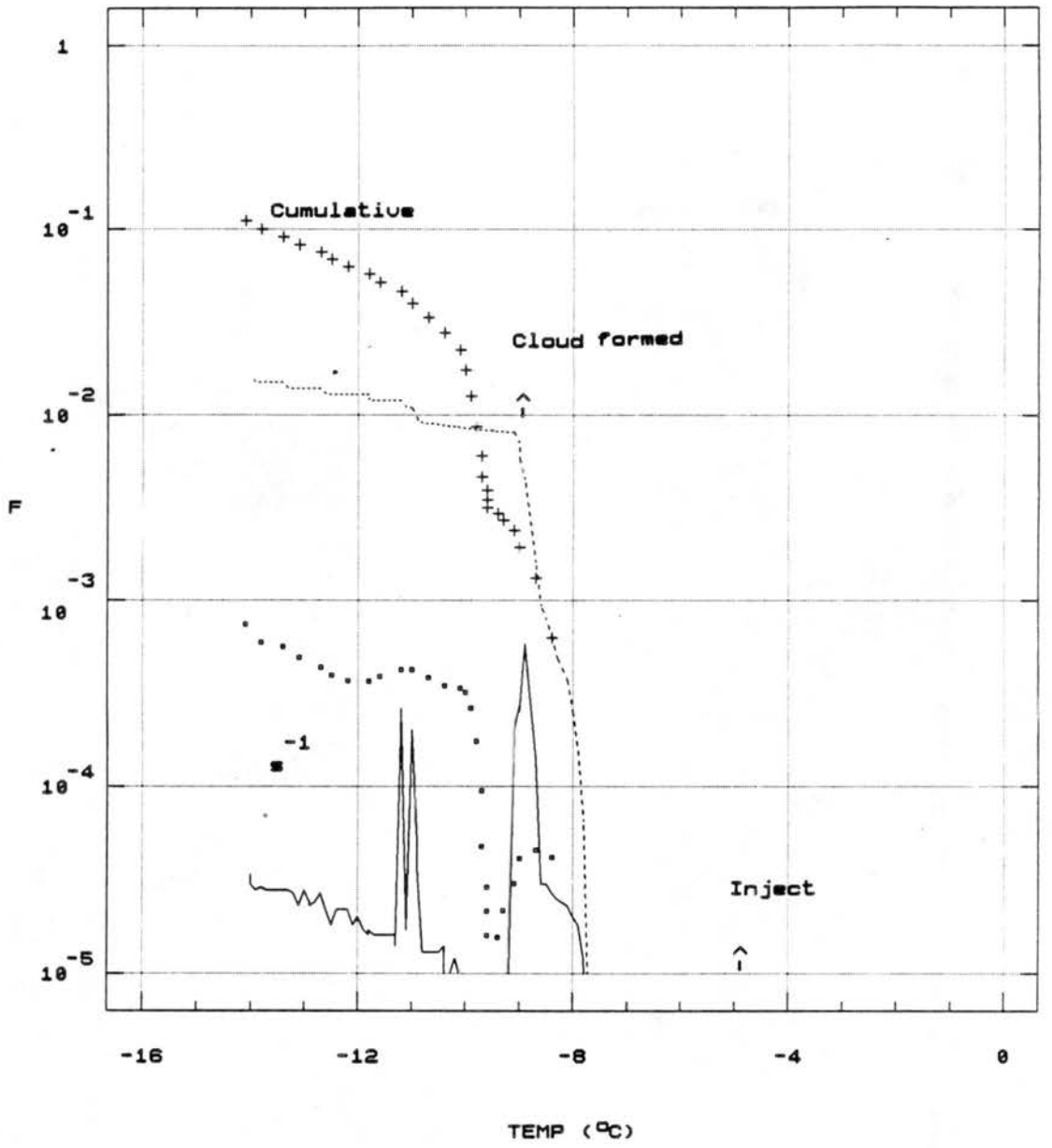

Figure 6.18 Observed (symbols) and model (lines) cumulative and differential F values versus temperature in pre-cloud seeding experiment with 0.03μm AgI-AgCl-4NaCl aerosols (experiment 5788). Equivalent expansion updraft rate is 2.5 m s^{-1}.

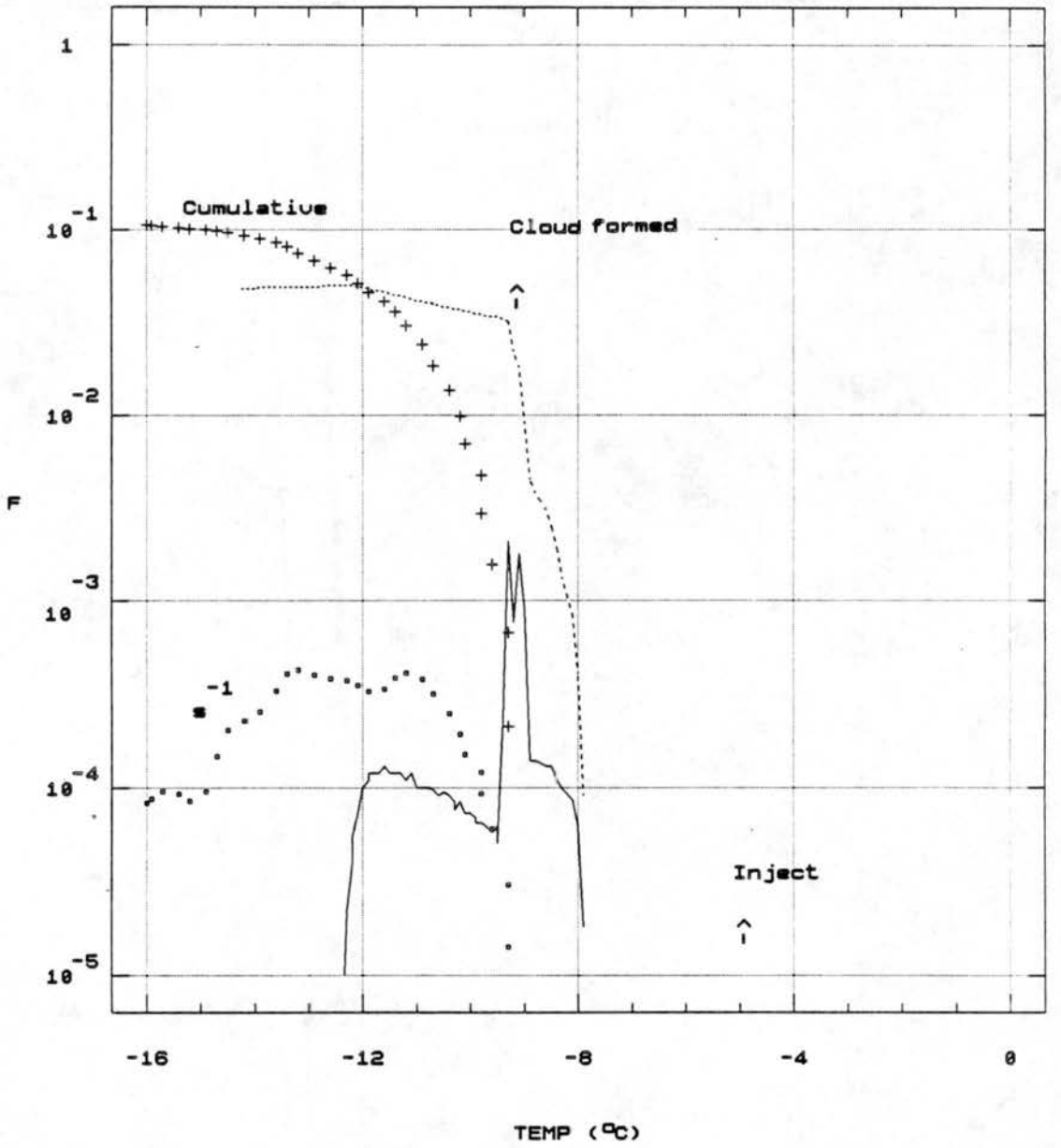

Figure 6.19 As in Figure 6.18, but for 0.07μm aerosols (experiment 8488).

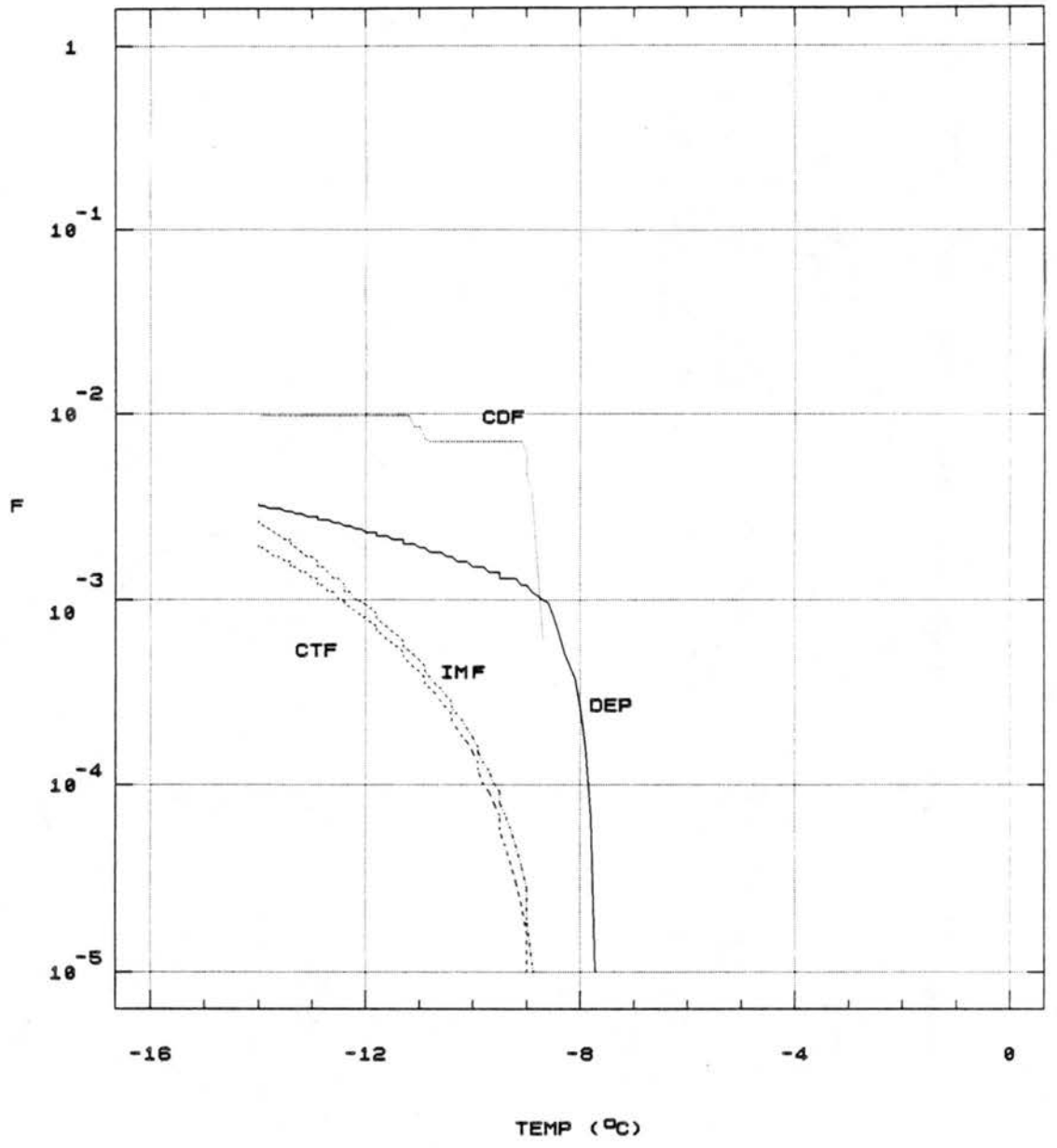

Figure 6.20 Model-predicted contributions of the various ice nucleation modes in experiment 5788. Symbols are as used in previous figures.

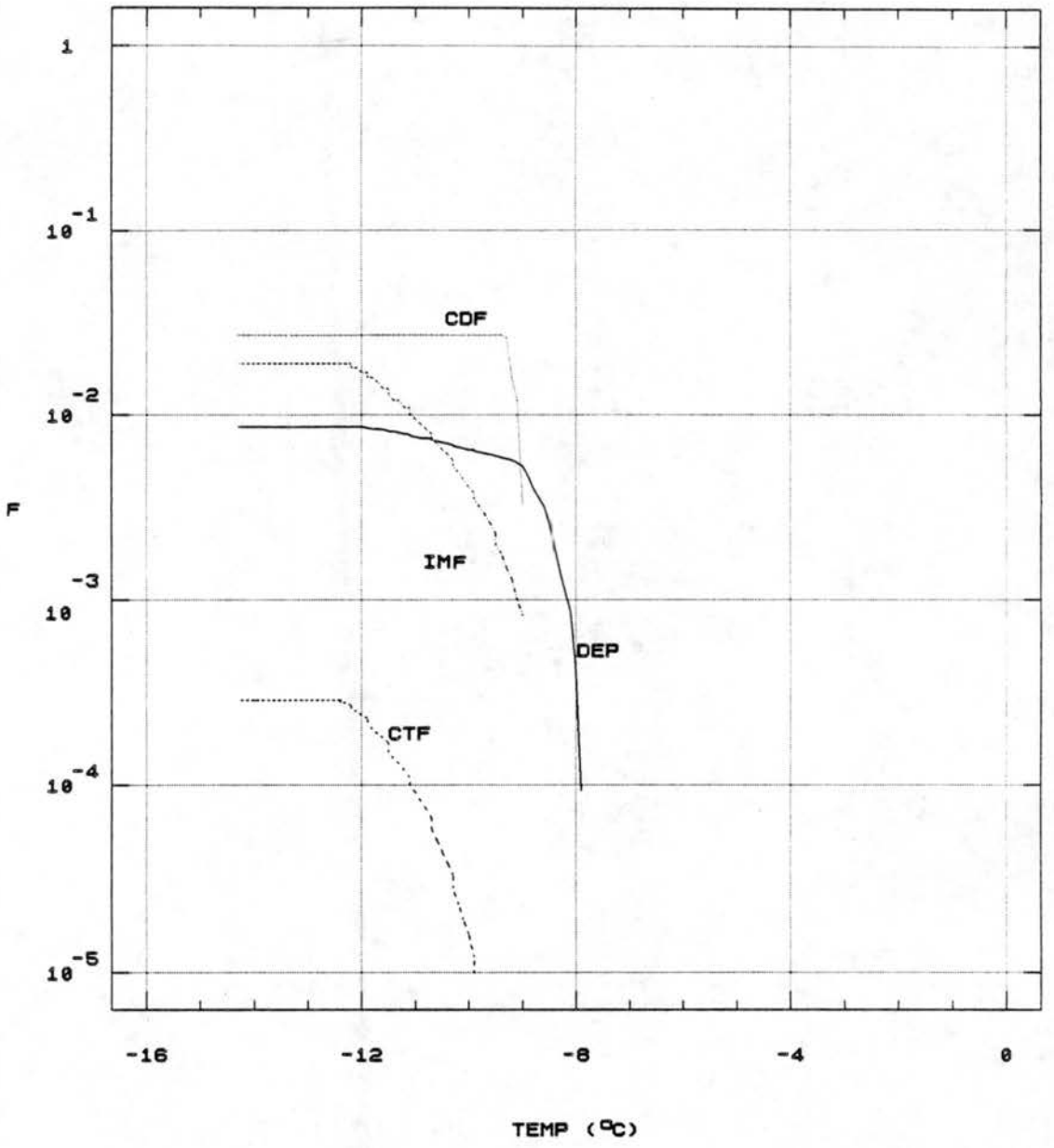

Figure 6.21 Model-predicted contributions of the various ice nucleation modes in experiment 8488.

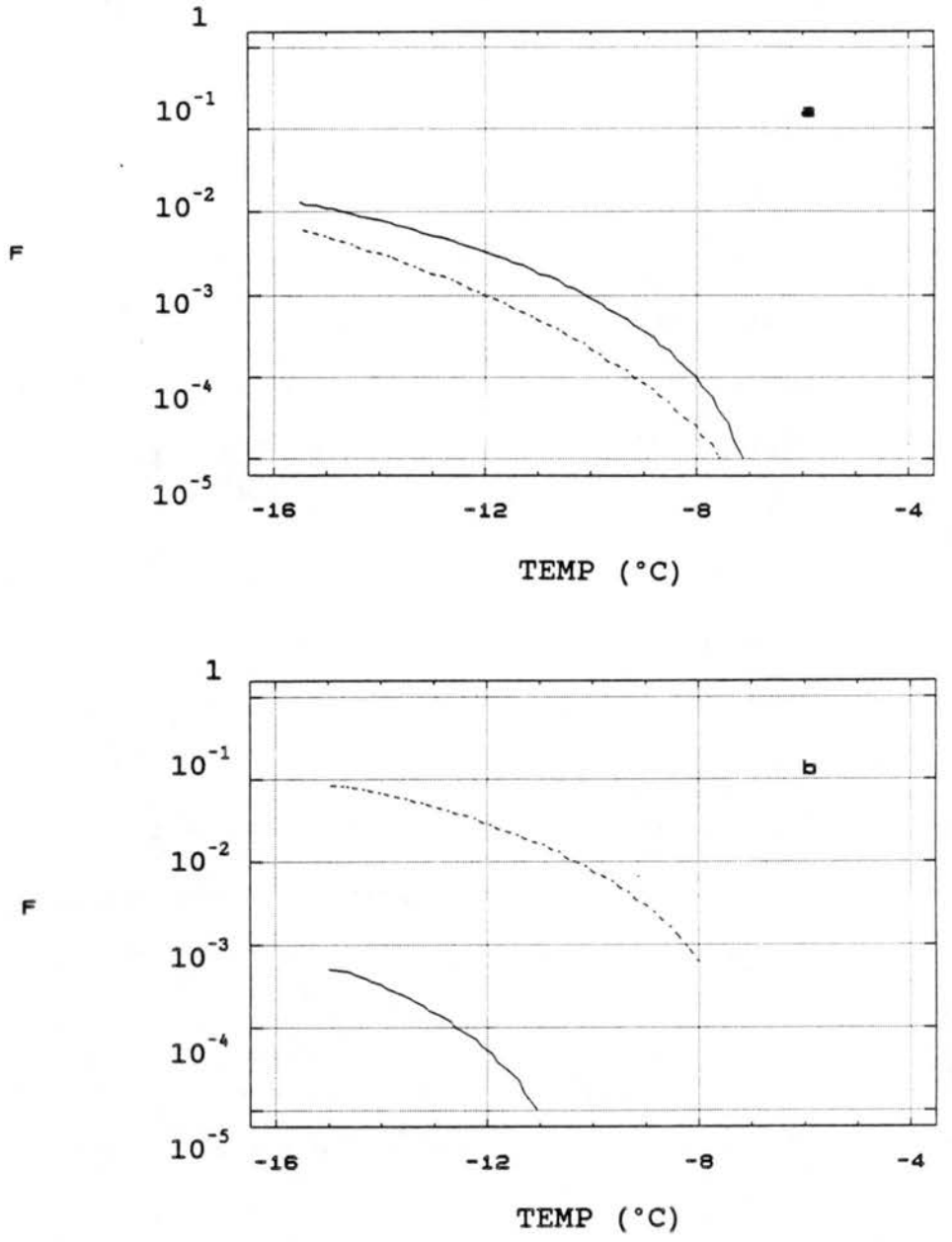

Figure 6.22 Separation of immersion-freezing nucleation into its component sources (solid lines for collision scavenging, dashed for condensation nucleation for chemically different particles. Part (a) is for 0.03μm AgI-AgCl aerosols (experiment 12188) and part (b)is for 0.07μm AgI-AgCl-4NaCl aerosols (experiment 8288).

cloud cools than for 0.03μm aerosols. As pointed out previously, this is a result of the greater CCN activity of the larger aerosols. The source of the immersion-freezing events via condensation versus collision events is a major difference between the two chemically different aerosols. This is shown clearly in Figure 6.22 (experiment 12188 for AgI-AgCl; experiment 8288 for AgI-AgCl-4NaCl aerosols).

The vapor concentration sensitivity of AgI-AgCl-4NaCl aerosols is seen by comparing Figure 6.23 (experiment 8288), a cold cloud experiment simulating 5 m s^{-1} ascent seeded before formation with 0.07μm aerosols, to Figures 6.20 and 6.21 (experiment 8488). In this case, the reason for the higher activity in the higher ascent rate simulation is due to the greater response of immersion-freezing, not an increase in condensation-freezing. Peak supersaturation in the 5 m s^{-1} ascent was predicted as 0.90% at -8°C, versus 0.42% at -9°C in the 2.5 m s^{-1} ascent. The higher supersaturation at a warmer temperature makes immersion-freezing a more important nucleation mode. The absence of a description of this mechanism, combined with the underestimated role of deposition plus condensation-freezing, explains the very poor simulation of nucleation by this aerosol using the original model formulation for AgI (Figure 6.24). When a moderate supersaturation is slowly generated at a colder cloud point, condensation-freezing can completely overwhelm immersion-freezing as cloud starts to form. This is demonstrated in experiment 14388 (Figures 6.25a and b), a 5 m s^{-1} ascent through -12.2°C cloud base (0.52% peak supersaturation predicted) seeded with the same 0.07μm aerosols. It is interesting to note the similarity in behavior of the chemically different aerosols (see Figure 6.17, experiment 1789) in this seeding situation. The

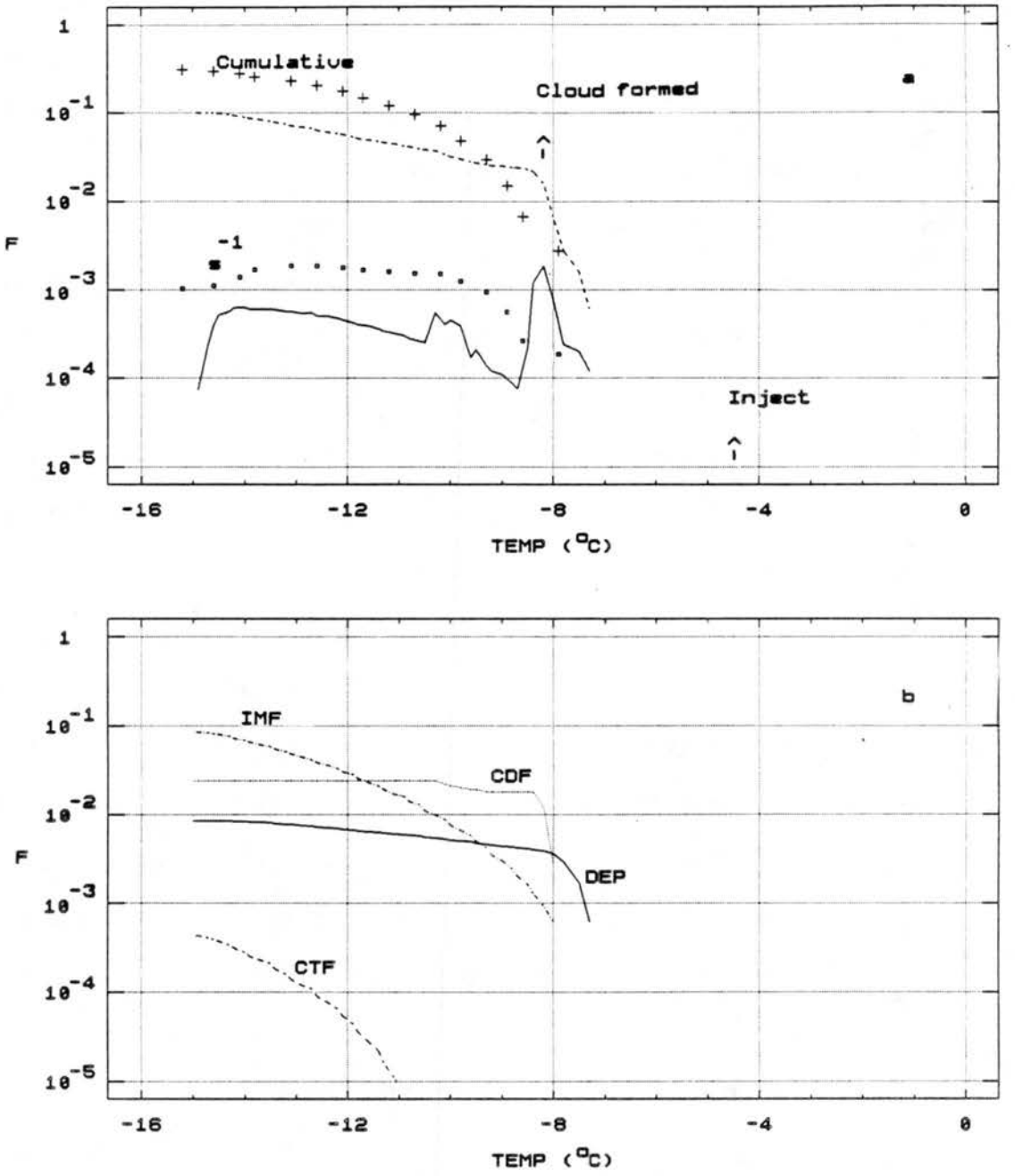

Figure 6.23 Observed (symbols) and model (lines) cumulative and differential F values versus temperature in pre-cloud seeding experiment with 0.07μm AgI-AgCl-4NaCl aerosols (experiment 8288) are shown in (a). Model predicted mechanistic contributions to ice formation are delineated in (b). Simulated ascent rate was 5 m s^{-1}.

differing responses of AgI-AgCl-4NaCl aerosols, dependent on both temperature and supersaturation, have implications for seeding cumulus clouds where supersaturation profiles may vary with temperature due to varying (often increasing) updraft rates as the updraft core cools. An example of this is given in the next chapter.

The true test of the integrity of the new formulations for nucleation by the chemically different artificial ice nucleus aerosols is the ability to simulate experiments seeded with the actual polydisperse aerosol size distributions obtained directly from the seeding generator. The polydisperse percentage size distributions for each nucleant chemistry, shown in Section 4.4, were multiplied by the total aerosol number injected in each experiment to obtain the number distribution for use in the model. The few cloud chamber experiments that were done injecting polydisperse aerosols prior to cold cloud formation show excellent agreement compared to numerical model results. Figure 6.26 (experiment 9088) compares the experimental and model cumulative and differential (s^{-1}) curves for ice crystal formation in a 2.5 m s^{-1} simulated ascent with cloud forming at -8.2°C. This cloud was seeded with AgI-AgCl aerosols. Both the cloud point ice nucleation peak, due to condensation-freezing and deposition nucleation, and the slow increase in nucleation rate resulting from contact-freezing and immersion-freezing nucleation are well represented by the model simulation. A comparable experiment (excepting the 5 m s^{-1} ascent rate in this case) seeded with polydisperse AgI-AgCl-4NaCl aerosols is shown in Figure 6.27 (experiment 13088). Again, the agreement between the model and actual experimental nucleation signals is quite good. Deviation occurs at temperatures below -10°C. This is understandable

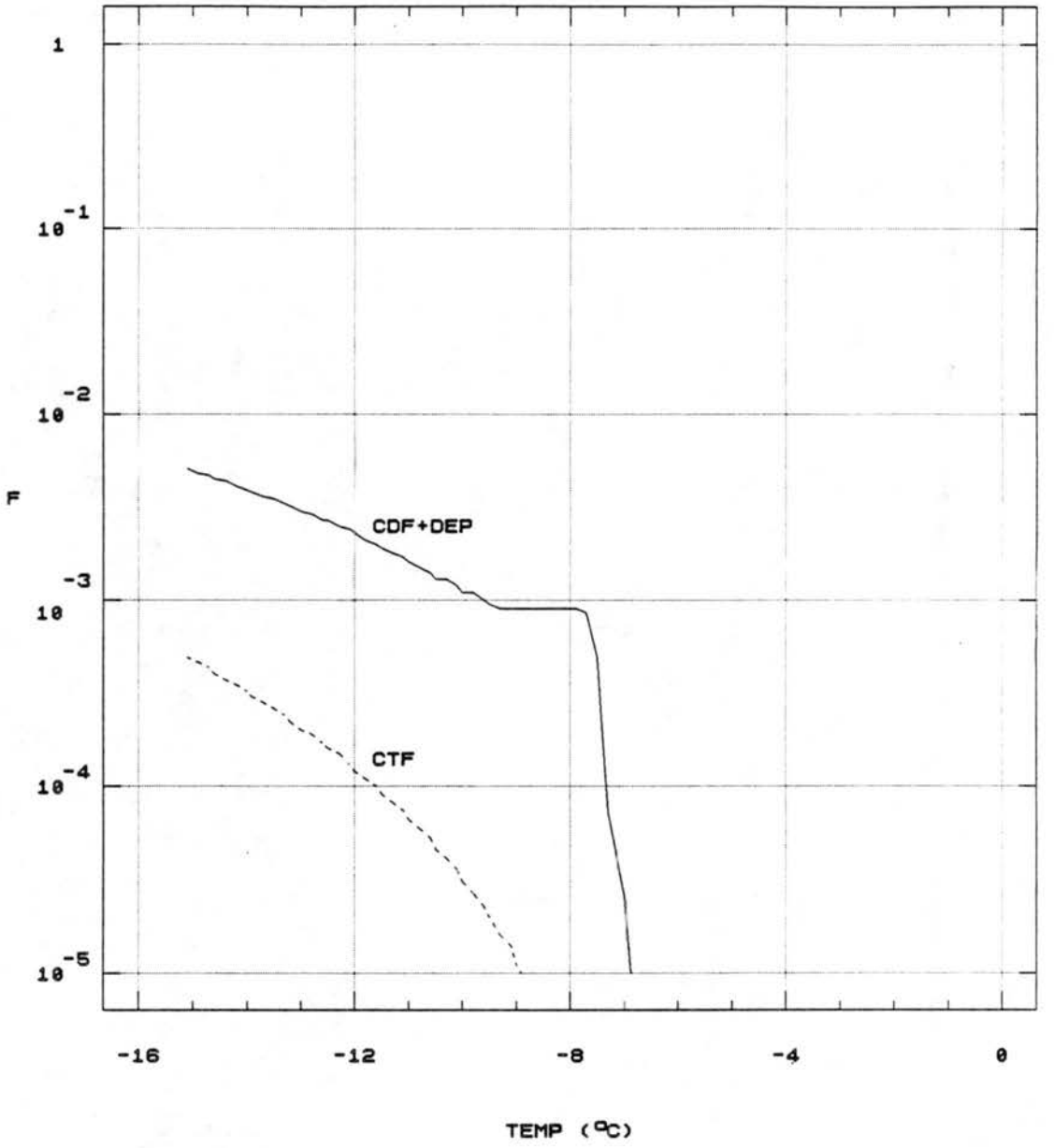

Figure 6.24 Model-predicted contributions of various nucleation modes in experiment 8288, using the original model ice nucleation formulations.

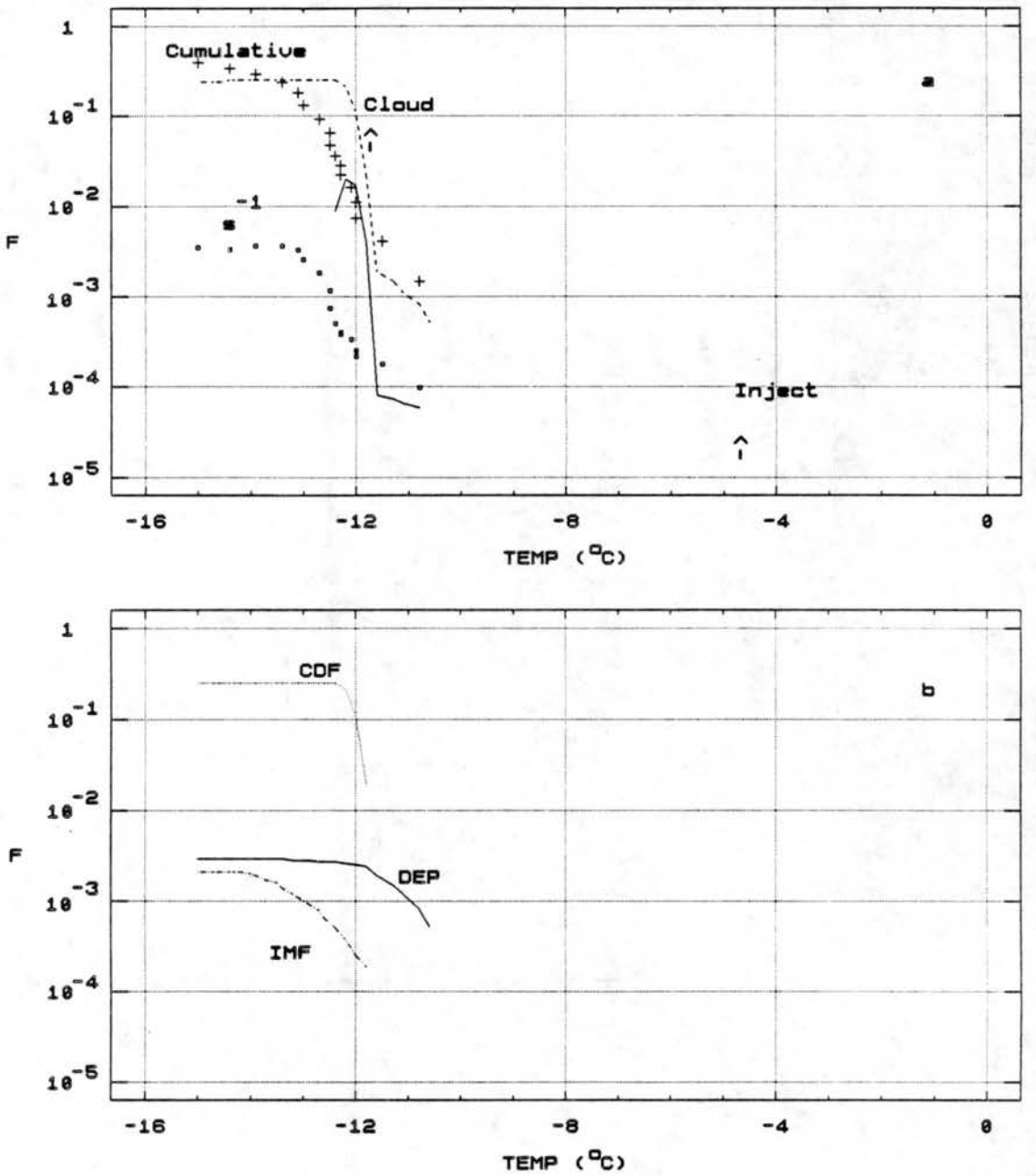

Figure 6.25 Exactly as in Figure 6.23, but for cloud forming at -11.8°C.

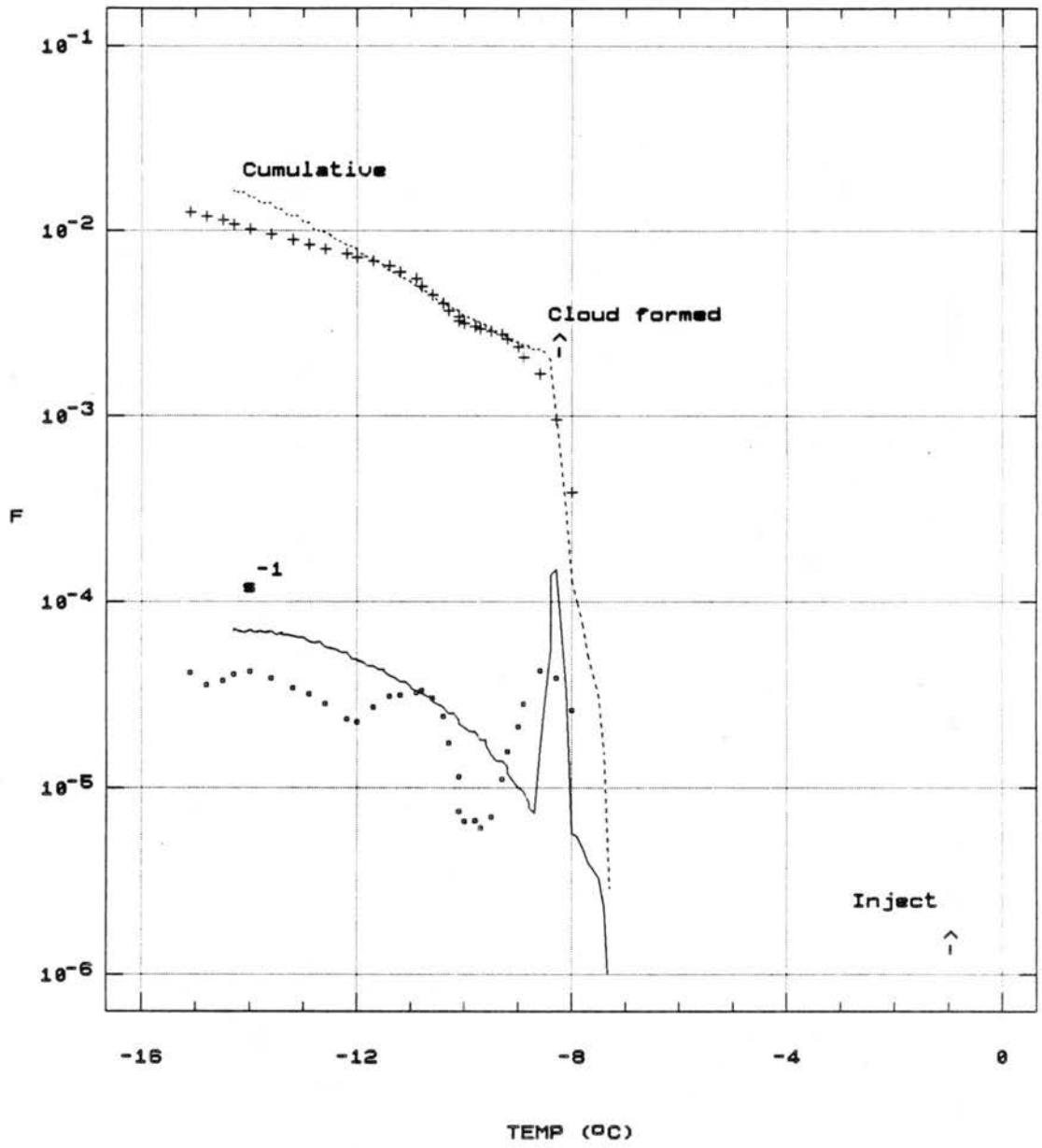

Figure 6.26 Cumulative and differential F values (experiment and model, following conventions from previous figures) for polydisperse AgI-AgCl aerosols present during cloud formation at -9°C in a 2.5 m s^{-1} equivalent updraft expansion (experiment 9088).

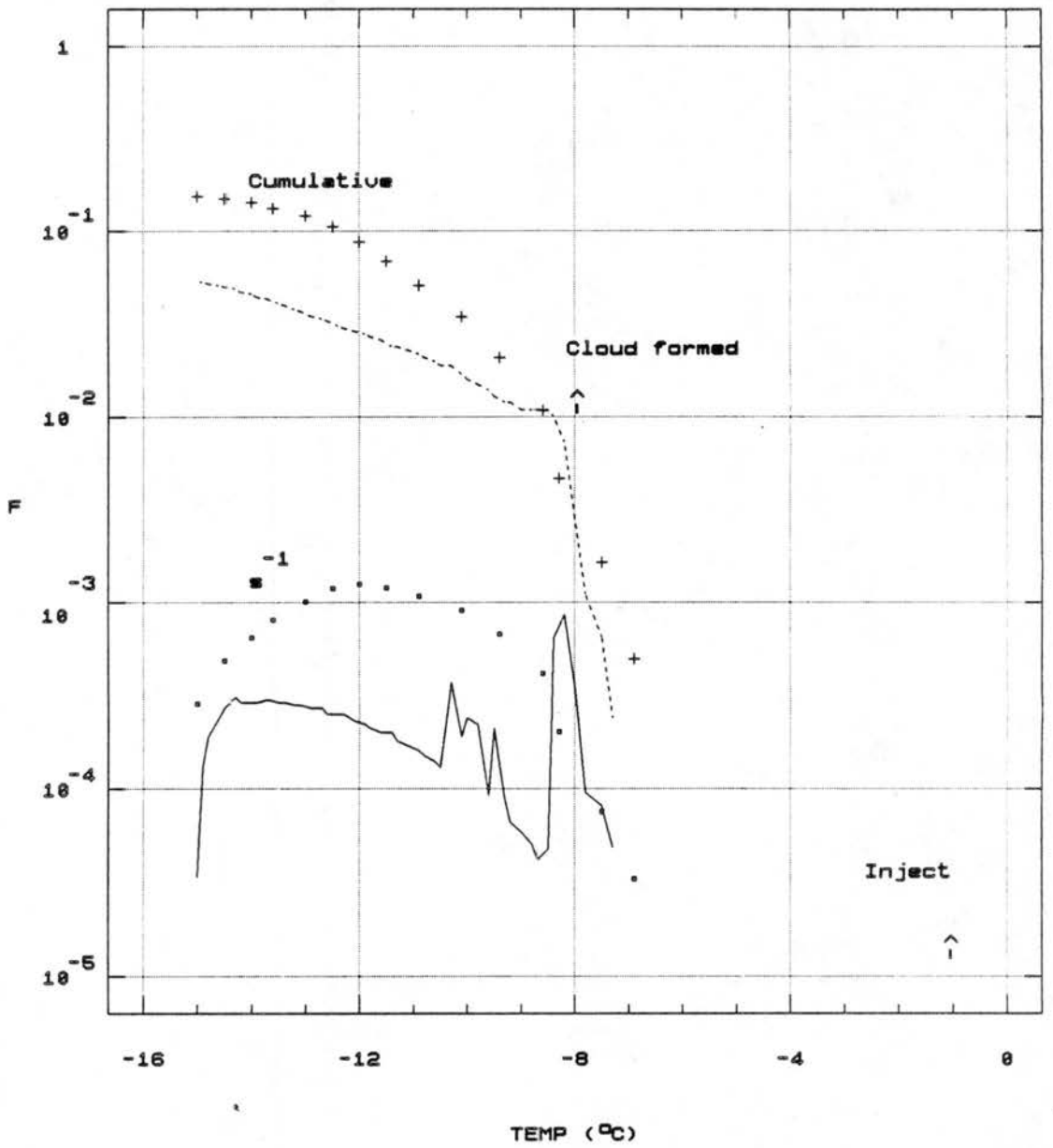

Figure 6.27 As in Figure 6.26, but for polydisperse AgI-AgCl-4NaCl aerosols in a 5 m s^{-1} equivalent updraft expansion (experiment 13088).

considering that the saturation ratio falls below water saturation at -12°C in the model simulation. Water supersaturation is probably maintained in the cloud chamber since ice crystals settle out within about 2 minutes after initial formation.

6.2.2 In-Cloud Seeding

As mentioned, introductions of the ice nucleating aerosols into supercooled clouds in the dynamic chamber, during expansion, were done primarily as blind-type experiments to characterize the response of the chemically different nuclei in this situation and to test the prediction of the new ice nucleus formulations. This also provided a comparison to the below-cloud seeding experiments. It can be expected, based on the results of mode-specific experiments and the comparisons shown in Section 6.1, that the dominant nucleation modes may vary depending on which methodology of seeding is used. These experiments were to document the in-cloud seeding methodology. The difference compared to the real atmospheric situation is that the solution combustion to form aerosols is not done directly in the cloud here. In atmospheric clouds this adds both heat and water vapor with the particles. There is some debate as to what happens to the added heat and water vapor in this situation. As discussed in Chapter 2, it is clear that the simple addition of some ice nucleus aerosols with warm and saturated air to a supercooled cloud can induce rapid ice nucleation. However, for generators burning in real clouds, the flame is very hot and the relative rates of water vapor and thermal diffusion will determine whether condensation occurs on the particles. Finnegan and Pitter (1988) have purported that water vapor remains to induce a

transient high water supersaturation after the particles cool to ambient temperature. This would induce both condensation (and thus enhanced immersion-freezing) and condensation-freezing nucleation. These same authors showed evidence of a ground seeding generator producing copious amounts of ice in subfreezing conditions even well below 100% relative humidity (no cloud present). However, it is not known if the amounts of ice nucleated could be explained by deposition nucleation. They noted a cloud produced above the flame, but this may not occur for the airflow conditions existing with aircraft seeding. This problem is an important one relevant to the nucleation activity of aerosols released in-cloud, and can probably best be addressed by atmospheric study. In the laboratory, the particles are introduced warm and dry. This should limit the artificial generation of supersaturation. Simple calculation also shows that the cooling by expansion of the room temperature sample air was not sufficient in these experiments to generate supersaturation. Thus, these experiments are relevant to the hypothesis that particles introduced into cloud adjust and respond only to the ambient humidity conditions. This serves as a baseline for comparison to any actual measurements made in real seeded clouds.

Model simulations of these experiments entailed more uncertainty than those presented in Section 6.2.1. It has already been shown that over long cloud periods, the model droplet diameters grow to exceed the observed droplet diameters by a factor of two or more. Also, model concentrations are not subject to the effects of gravitational sedimentation. This problem was exacerbated when simulating clouds forming near 0°C, but not seeded until -8°C or colder. Therefore, most

experiments of these types were conducted to form cloud a few degrees prior to seeding. For clouds that formed near 0°C (4 experiments), a model option to input the cloud particle distribution was utilized. An expansion was initialized to form a cloud about 2°C prior to the temperature at which seeding material was to be injected. An approximation to the observed droplet distribution at this point in the cloud chamber experiment was input into the model, a few time steps prior to cloud point. In this way, supersaturation was limited at cloud point and droplet sizes were nearer the observed sizes at the point where seeding material was injected. There was no way to know how appropriate the supersaturation profile was. This is probably most critical for simulations of AgI-AgCl-4NaCl nucleation.

The in-cloud seeded tests showed particle size, temperature, supersaturation, and nucleant chemistry effects, much the same as in the cold cloud formation tests. A comparison of various experimental and model quantities in a cloud seeded at -8°C with 0.07μm AgI-AgCl is shown in Figure 6.28 (experiment 7188). Equivalent ascent rate by expansion was 2.5 m s^{-1}, as it was in all in-cloud seeding tests. The model versus experiment cumulative fractional ice plot (Figure 6.29a) shows that the agreement was quite good in this case. The initial ice after injection is dominated by deposition and condensation-freezing nucleation events, which then give way to contact-freezing (Figure 6.29b). This is similar to the situation of cloud forming at -8°C, but condensation-freezing is not as dominant due to the lower supersaturations. Results for an equivalent experiment using 0.07μm AgI-AgCl-4NaCl aerosols is shown in Figure 6.30a and b (experiment 8188). Although the agreement between model and experiment is not as

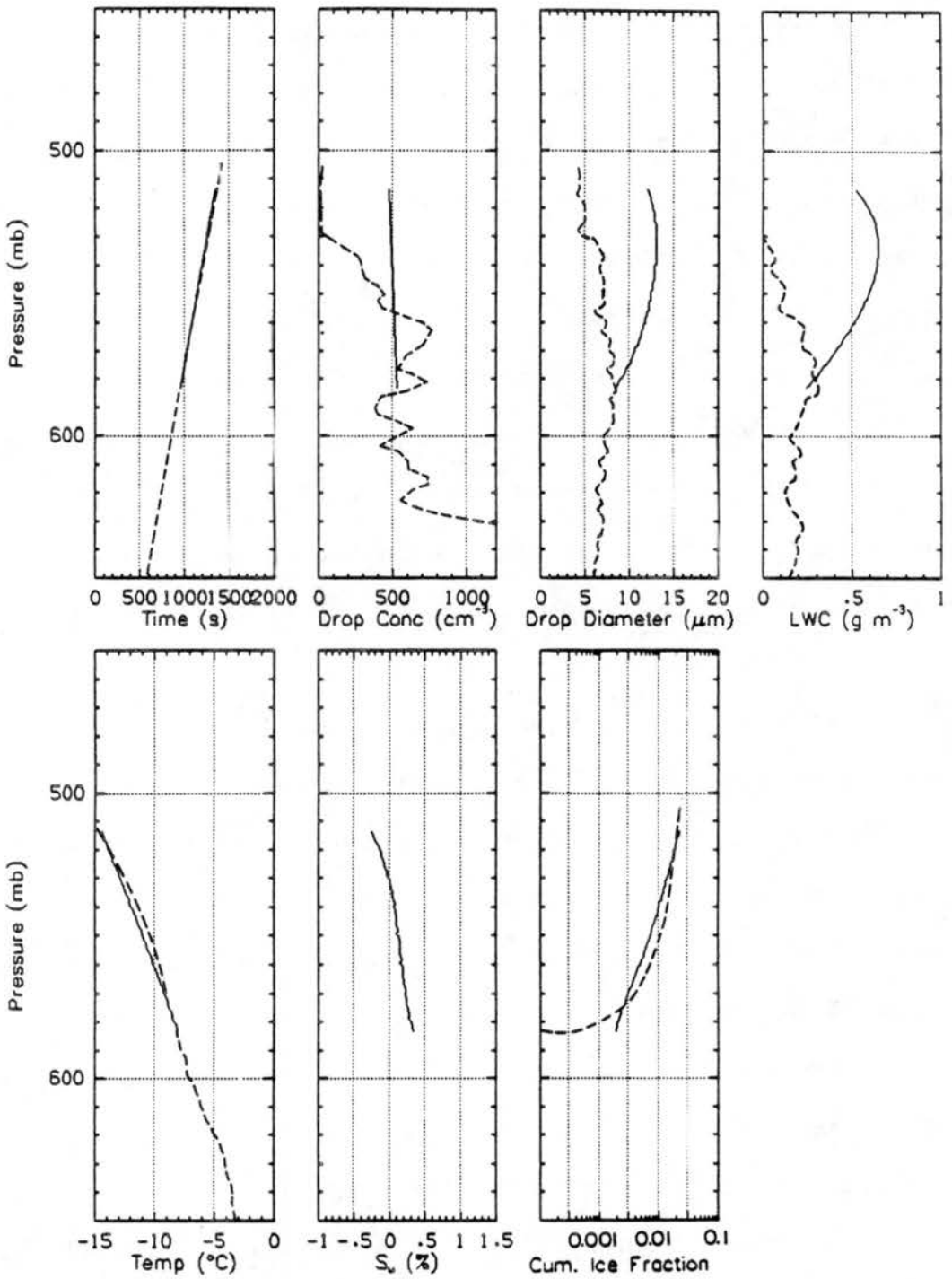

Figure 6.28 Model (solid lines) versus experimental (dashed lines) thermodynamic and cloud quantities in in-cloud seeding experiment using 0.07μm AgI-AgCl aerosols (experiment 7188). Aerosols were introduced into cloud at -8°C (see arrow). The model simulation was initiated with the observed cloud droplet characteristics at a point preceding aerosol injection.

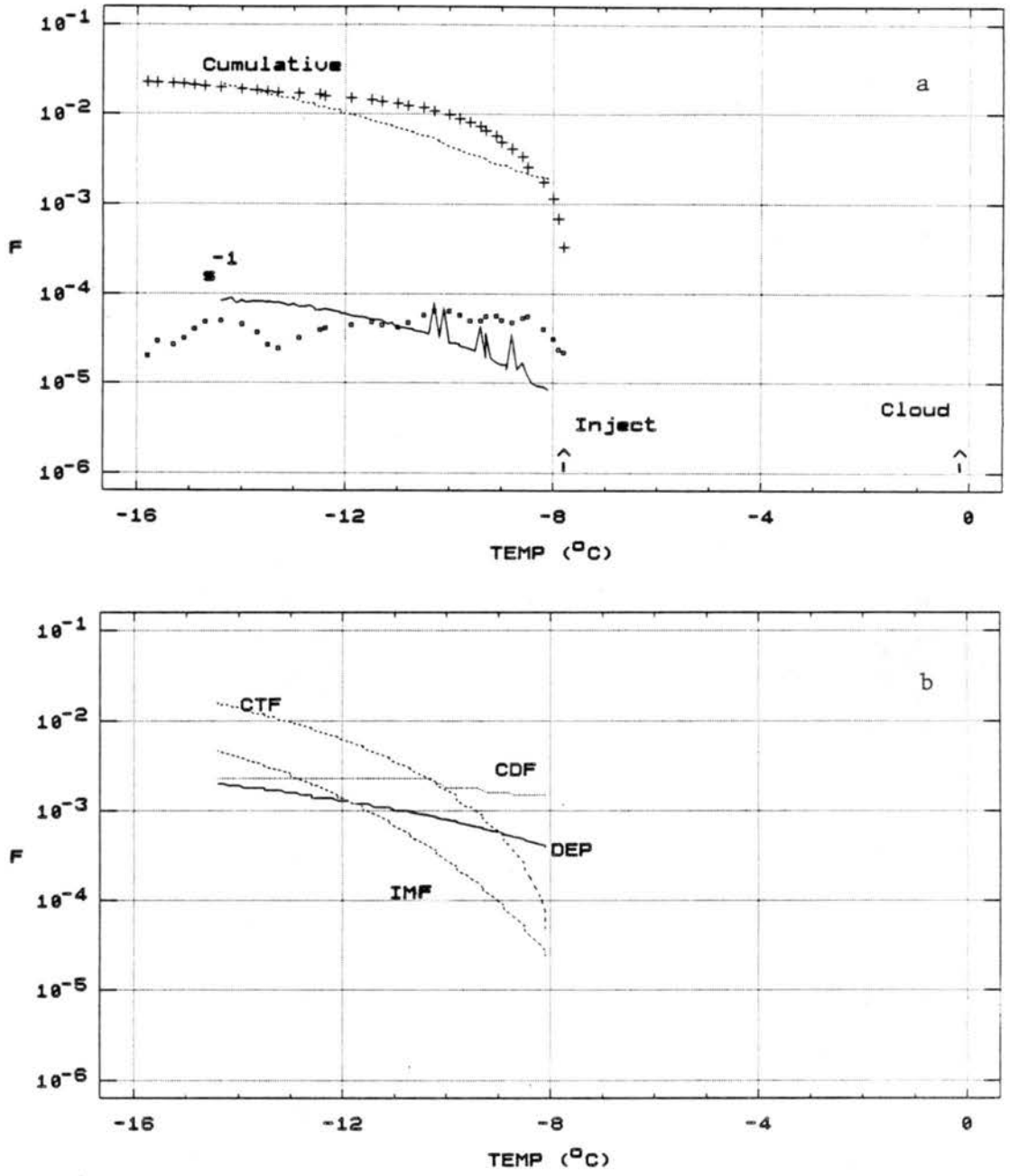

Figure 6.29 Model-predicted and observed ice formation versus temperature (a), and predicted contributions of various nucleation modes in experiment 7188.

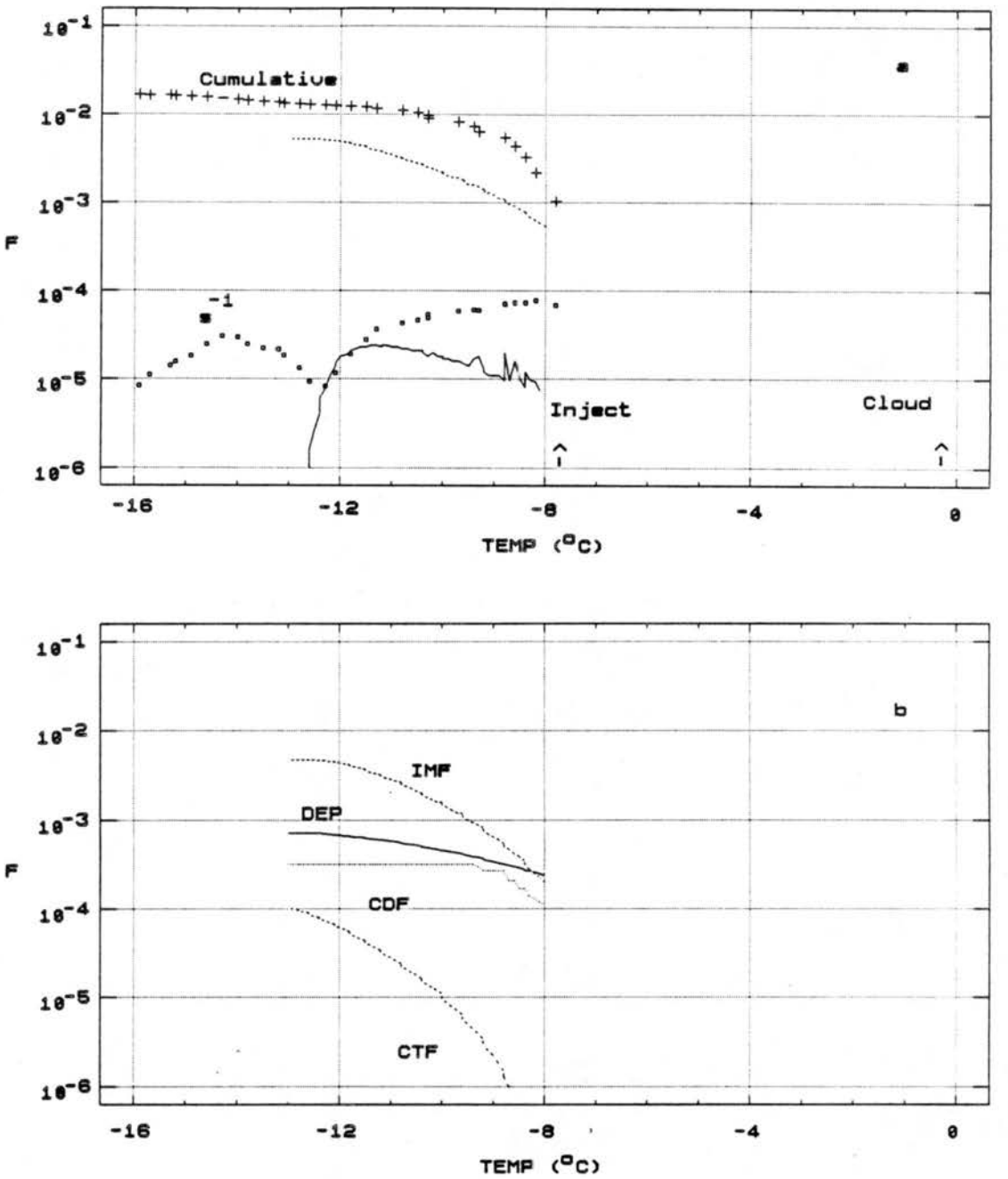

Figure 6.30 As in Figure 6.29, but for 0.07μm AgI-AgCl-4NaCl aerosols (experiment 8188).

good for this particular experiment, it is notable that the cumulative fractions nucleated are higher than for AgI-AgCl.

Figures 6.31(AgI-AgCl aerosols) and 6.32(AgI-AgCl-4NaCl aerosols) show cumulative ice formation versus temperature results for a number of the in-cloud seeded experiments and the equivalent model formulations performed for these. Injection tempuratures betweeen -8 and -12°C are represented. Several points can be made. For AgI-AgCl aerosols, a slight (mostly < factor of 2) size effect favoring 0.07μm aerosols is predicted by the model at any injection temperature. This was not observed in the cloud chamber experiments. The difference between the cumulative F values of the two different sized aerosols was not expected to be great, based on the experiments discussed in Section 6.2.1, because the smaller aerosols are scavenged more efficiently, making up for their lower activity versus the larger aerosols. Also, the droplet concentration could have a significant effect on the ice formed in each experiment. Of final note for AgI-AgCl aerosols is the apparent tendency for an increase in the ultimate ice formed with warmer seeding temperature. For equivalent cloud conditions, this is expected because the warmer cloud temperature increases the number of aerosols available for immersion-freezing at colder temperatures without significantly depleting the numbers available for contact-freezing. This result certainly suggests that there are no significant nucleus deactivation mechanisms operating that need to be quantified (at least in the absence of sunlight).

For AgI-AgCl-4NaCl aerosols, cumulative ice increases are noted to directly depend on the particle size in both cloud chamber experiments and in the cloud model at all injection temperatures. The magnitude of

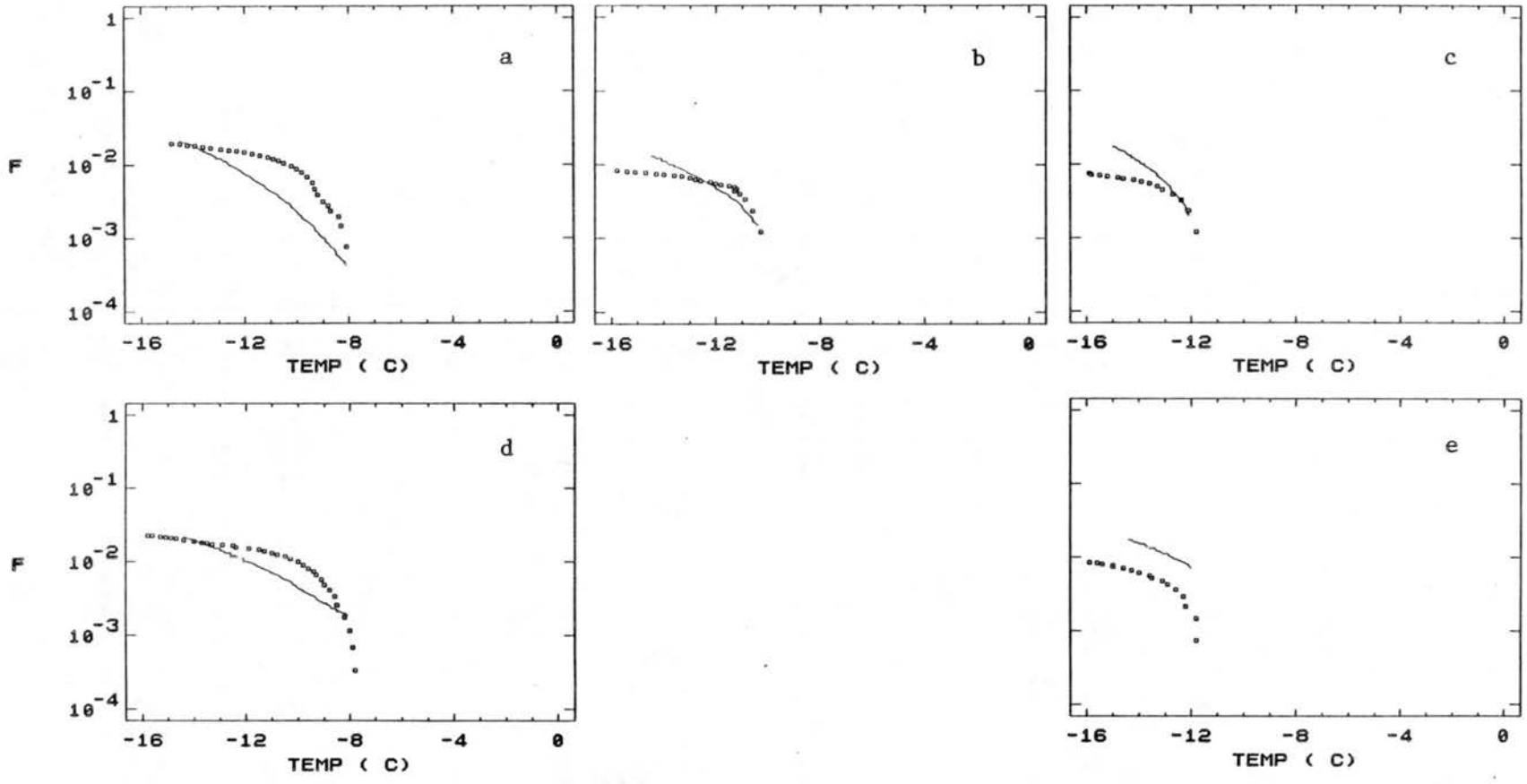

Figure 6.31 Experiment (symbols) and equivalent model simulation (lines) cumulative ice formation versus temperature for several in-cloud seeding experiments with AgI-AgCl aerosols. Injections of 0.03μm aerosols (experiments 7288, 5787, 2589) are shown in plots (a) to (c), while 0.07μm aerosol injections (experiments 7188, 2689) are shown in plots (d) and (e). Equivalent expansion updraft is 2.5 m s^{-1}.

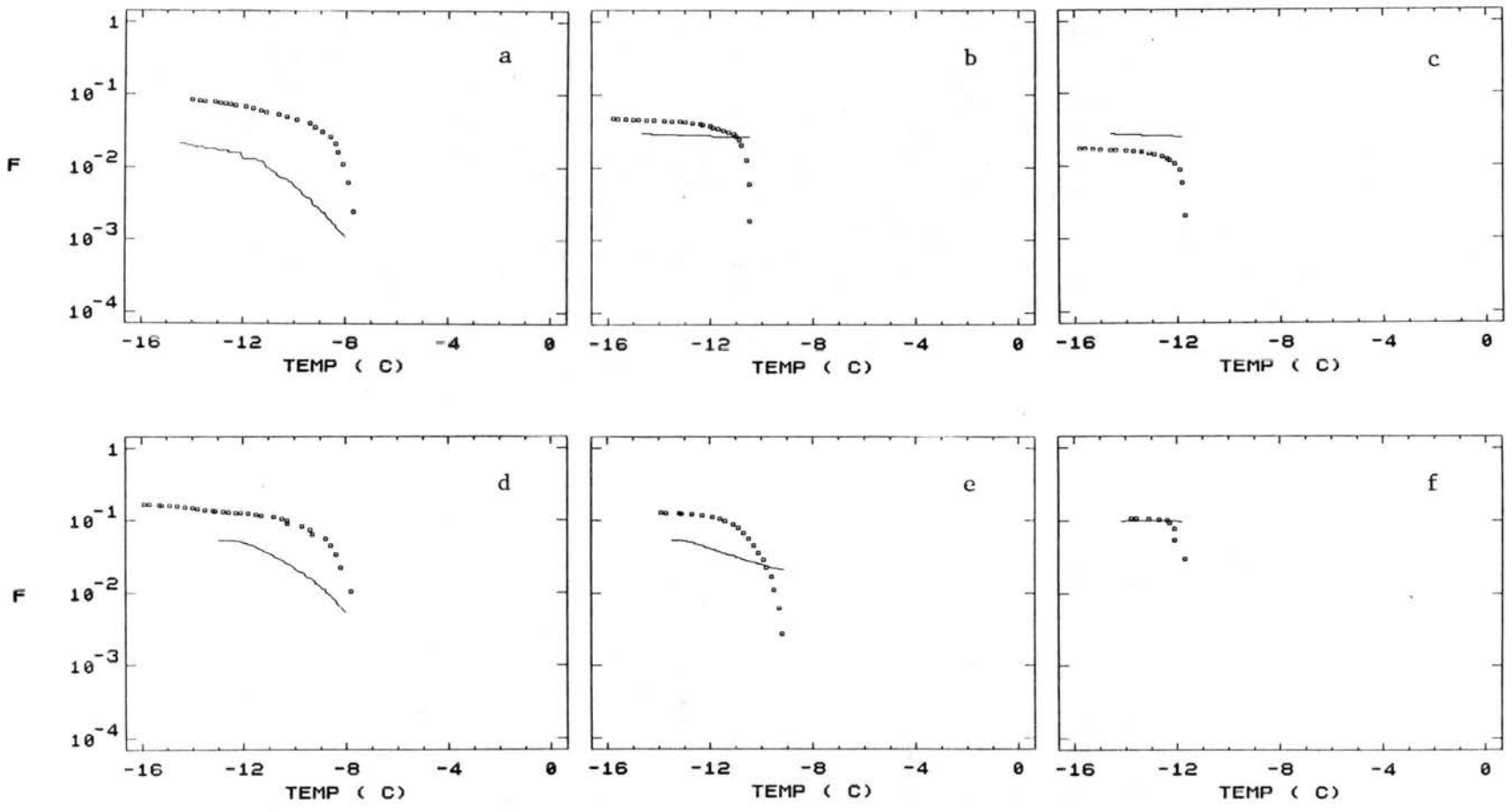

Figure 6.32 As in Figure 6.31, but for AgI-AgCl-4NaCl aerosols. Panels (a) to (c) are for 0.03μm aerosol injections (experiments 8088, 3689, 3489), and panels (d) to (f) are for 0.07μm aerosol injections (experiments 8188, 6188, 3589).

the effect is approximately equivalent to a ratio somewhere between the ratio of the particle sizes and the ratio of the particle areas. This clear size effect in contrast to the cold cloud base tests of Section 6.2.1 results because of the dominance of a single nucleation mechanism, condensation-freezing, in all but the -8°C inject tests. In the latter tests, nucleation is a combination of immersion-freezing, condensation-freezing, and deposition. Condensation-freezing becomes dominant at colder temperatures. For condensation-freezing alone, the fraction of particles nucleating should follow the particle area for the same cloud conditions, based on the results presented in Chapter 5. The experimental cloud conditions for each particle size were quite identical for the AgI-AgCl-4NaCl experimental series presented in Figure 6.32. A slight increase in the fractional activity observed in the cloud chamber is noted with increasing temperature only for 0.03μm aerosols, and this may be an artifact of the cloud depletion that occurred due to overseeding. No such effect is found for 0.07μm aerosols, nor is it evident in the model simulations. Certainly, lower seeded concentrations would have been desireable for these tests. For all of the AgI-AgCl-4NaCl in-cloud seeded tests taken together, the fractional activities are significantly higher than for the AgI-AgCl seeded cases. For the 0.07μm sized aerosols, the factor approaches 10. This suggests a clear benefit for seeding with the hygroscopic nucleus in-cloud versus the hydrophobic one. A steady state supersaturation must be present for this to be so, however.

6.2.3 Warm Cloud Base Seeding

There has always been some concern in the weather modification community about the ability of artificial ice nucleus aerosols to survive the transit through warm cloud (non-ice nucleating temperatures) and act efficiently to produce ice at cold temperatures. Nevertheless, below cloud base seeding is still actively practiced. Therefore it is important to characterize the nucleating ability of the AgI-type aerosols for this situation. This is also a further test of the new nucleation formulations versus real experiments of a very different variety than those already discussed. With cloud forming at least 5°C prior to nucleating temperatures, added time is available for aerosol scavenging by condensation nucleation and transport processes which force collisions with cloud droplets. In simulating these experiments with the numerical cloud model it is expected that the amount of ice formed in the model simulation will exceed the amount of ice observed in the cloud chamber over longer time periods due to the unrealistic conservation of cloud droplets in the model parcel. Only reduction in concentration due to parcel expansion occurs. In the dynamic chamber experiment, droplet concentrations reduce from sedimentation, taking with them ice nuclei immersed by scavenging or condensation. No corrections are made for this factor. Typically, clouds for these experiments were formed in higher concentrations (more CCN added at expansion start) to limit droplet growth and sedimentation.

A comparison of chamber cloud and thermodynamic quantities and those in an equivalent model simulation of a cloud forming at about 0°C (2.5 m s^{-1} equivalent updraft by expansion) and seeded with 0.03μm AgI-

AgCl is shown in Figure 6.33 (experiment 7488). The cloud concentrations compare reasonably well until about -10°C. Observed concentrations peak as much as 30% higher. This suggests that the model will underestimate collection rates of particles for contact-freezing nucleation. However, average model drop diameters exceed those observed by about 1.5. This implies a potential overestimate of collection rates by as much as 2. Given these limitations, prediction of ice by the model is in excellent agreement with the observations. This gives good support to the quantification made of both contact-freezing and immersion-freezing processes which are primarily responsible for nucleation by the smaller AgI-AgCl aerosols in this situation.

The cumulative and differential fractions of particles nucleating ice (F) in the warm cloud base seeding tests of the two aerosols are shown in Figures 6.34(a,b,c) and 6.35(a,b,c). Tests of both monodisperse sized aerosols and the polydisperse smoke are presented for each type nucleant. The model predicted quantities are shown for comparison. These results strongly support the validity of the model formulations for describing ice formation in this seeding situation and they support the expectation that ice might be underpredicted at the coldest temperatures.

The only apparent differences between the observed (cloud chamber) activities of the two chemically different aerosols for below-warm cloud seeding are the higher initial activity (at warmest temperatures of nucleation) of AgI-AgCl aerosols, and the higher activity of AgI-AgCl-4NaCl aerosols below about -8°C. Certainly more data is desired to give more confidence in these results. The difference at warmer temperatures is not predicted by the model. The model clearly shows a

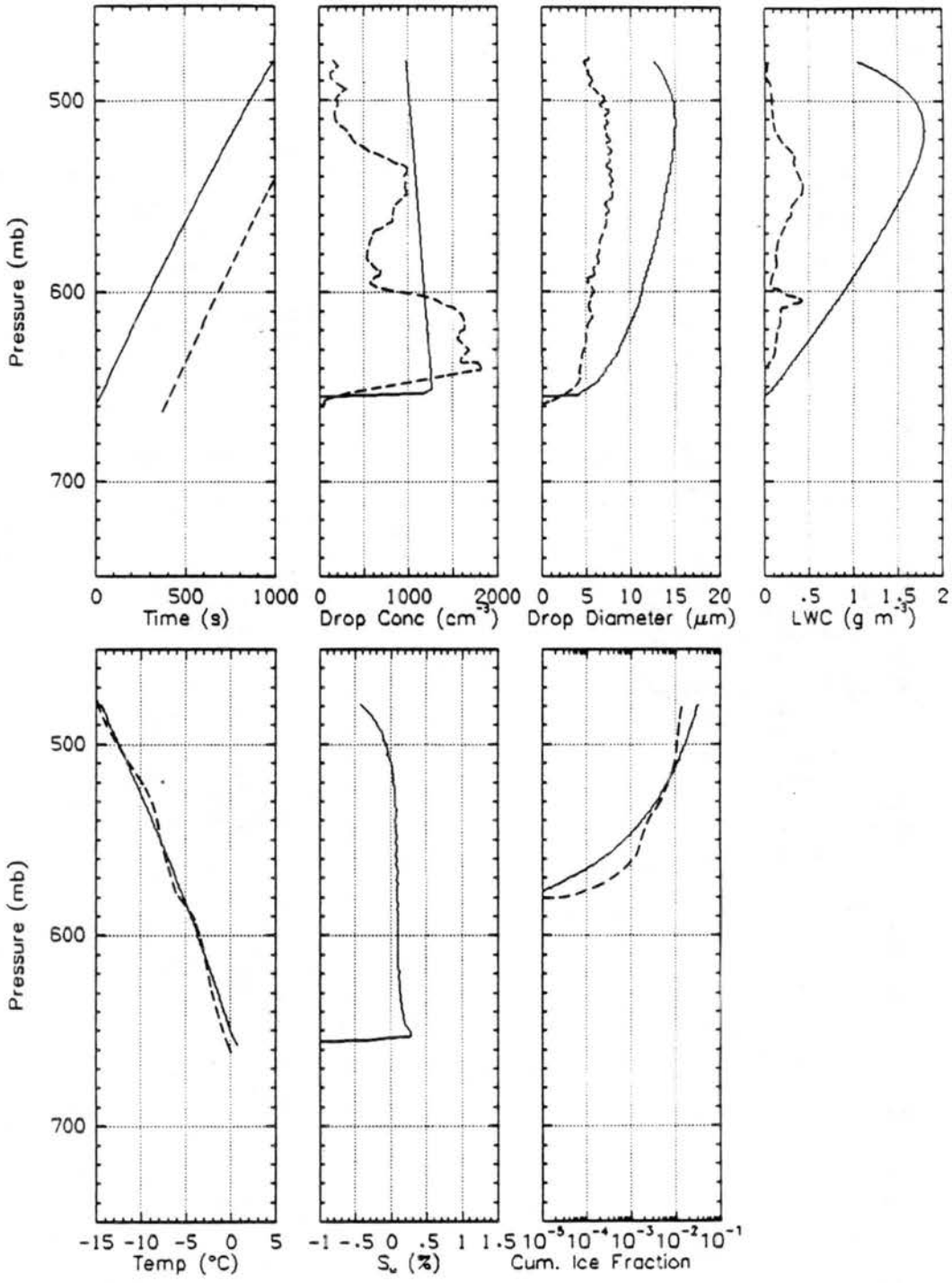

Figure 6.33 Model (solid lines) versus experimental (dashed lines) thermodynamic and cloud quantities in warm cloud base seeding experiment using polydisperse AgI-AgCl aerosols (experiment 7488). Equivalent expansion updraft is 2.5 m s^{-1}.

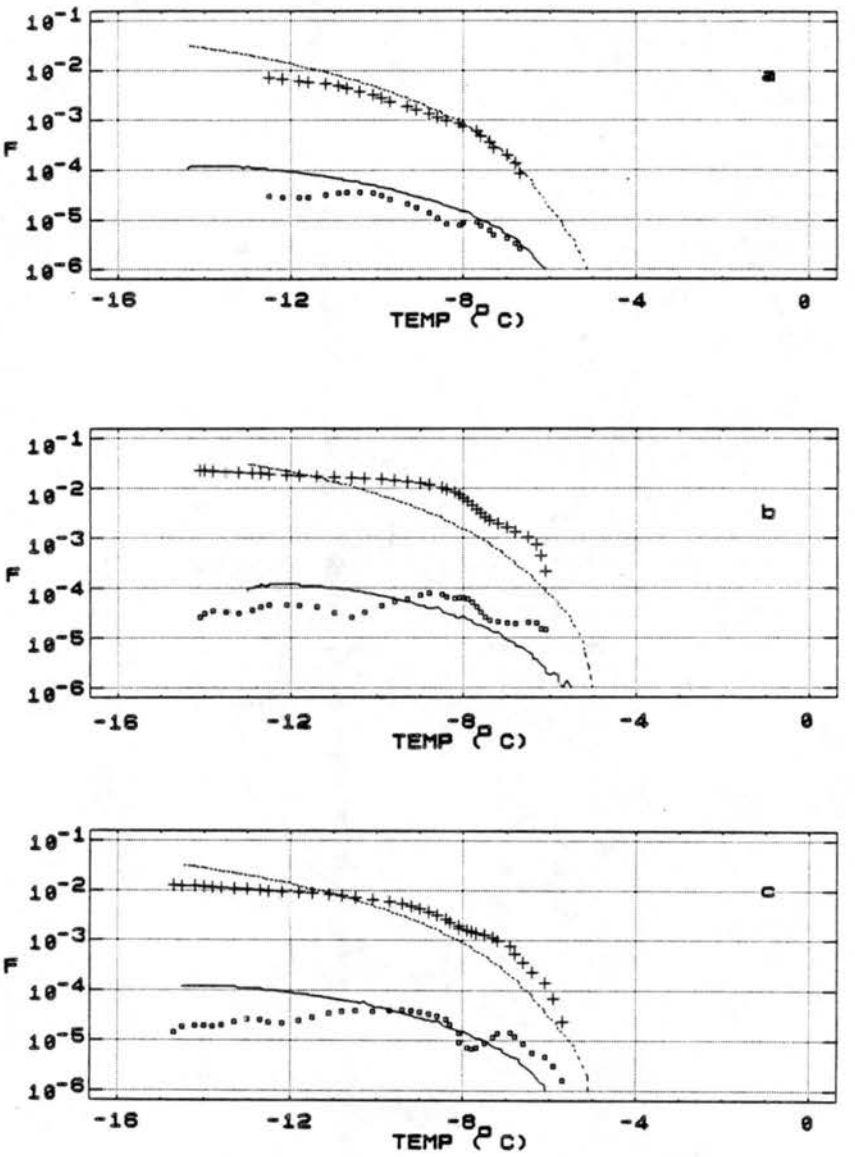

Figure 6.34 Cumulative (+) and differential (□) F values observed and those predicted by new model formulations (lines) in clouds seeded before formation near 0°C with 0.03μm (a), 0.07μm (b), and polydisperse (c) AgI-AgCl aerosols. Cooling rate is approximately 1°C min^{-1} for these 2.5 m s^{-1} ascent simulations (experiments 7688, 7588, 7488).

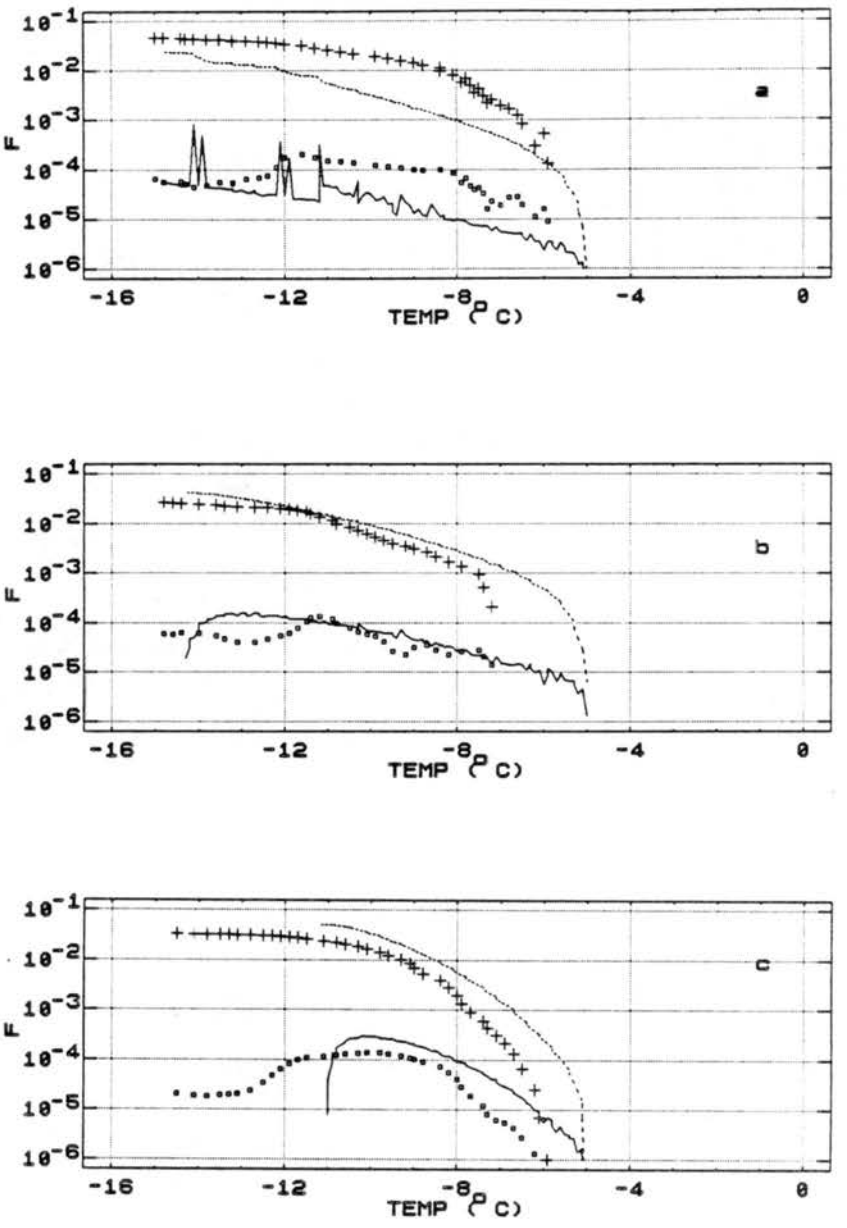

Figure 6.35 As in Figure 6.34, but for 0.03μm (a), 0.7μm (b), and polydisperse (c) AgI-AgCl-4NaCl aerosols (experiments 7988, 6488, 6688).

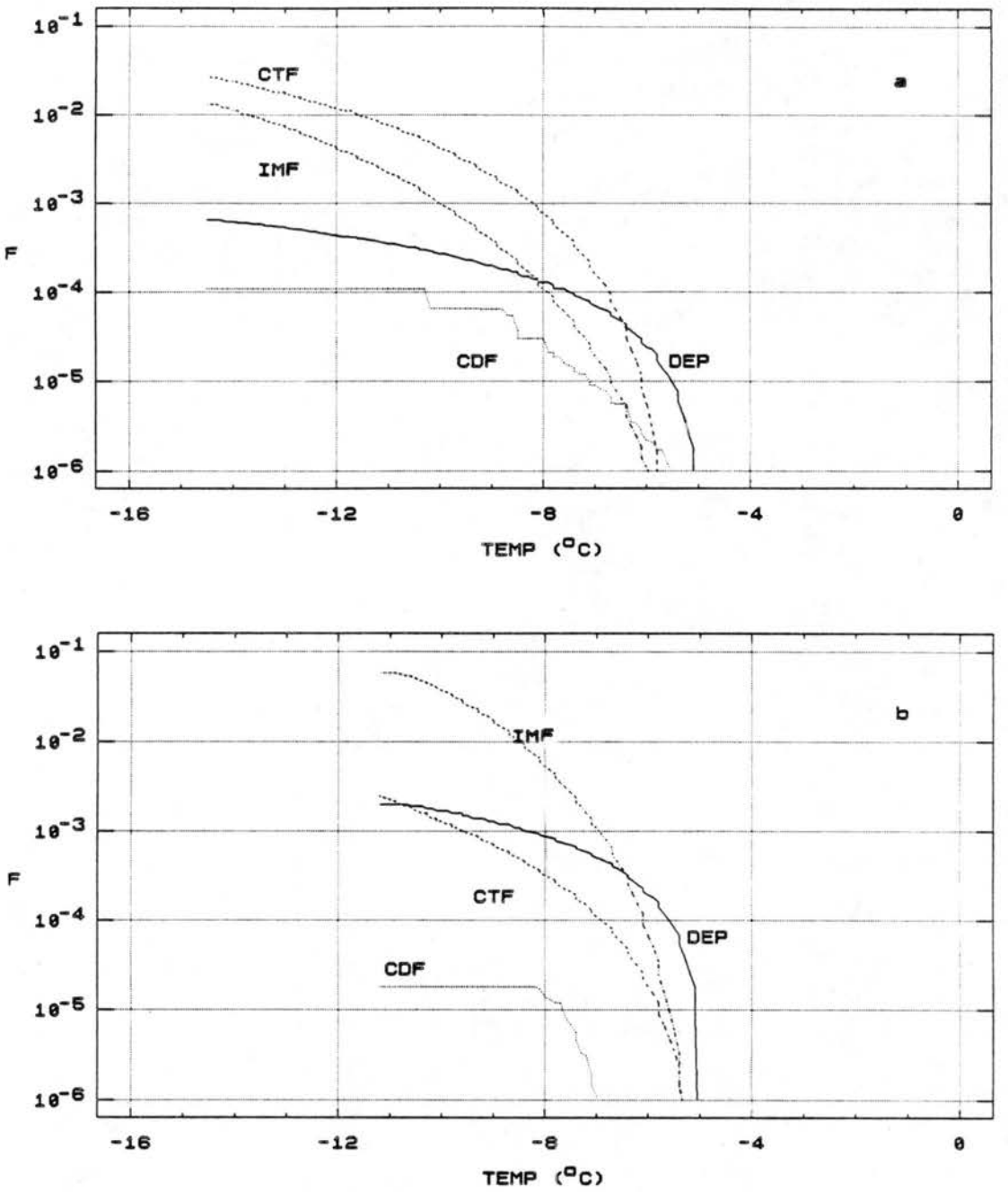

Figure 6.36 Comparison of contributions of various nucleation modes to ice formation by polydisperse AgI-AgCl (a) and AgI-AgCl-4NaCl (b) aerosols seeded before the formation of cloud at 0°C.

tendency to predict more ice formation than actually observed at the warmest temperatures for AgI-AgCl-4NaCl aerosols. This may relate to the lack of quantification of potential temporal (rate) nucleation effects at warm temperatures, as noted in isothermal cloud chamber experiments by Feng and Finnegan (1985; 1989). This also may result from aerosols activated as CCN subsequently settling from the chamber. The different activities for the different nucleating aerosols noted at colder temperatures is predicted by the cloud model. This difference is consistent with the findings of the in-cloud seeding tests, but occurs here for different mechanistic reasons than in those experiments. Figure 6.36(AgI-AgCl aerosols in (a); AgI-AgCl-4NaCl aerosols in (b)) shows the modal breakdown of ice formation in the model simulations of the polydisperse seeding before warm cloud formation. This shows that immersion-freezing nucleation thoroughly dominates ice formation by AgI-AgCl-4NaCl aerosols below -7°C. Large fractions of these aerosols are immersed in cloud by condensation at warm temperatures where ice nucleation does not occur. Others are collected over time by the cloud droplets present. The result is that few aerosols remain free to form ice by other mechanisms, such as condensation-freezing, which dominates for in-cloud seeding at cold temperatures. For AgI-AgCl aerosols, Figure 6.36a confirms the expectation that contact-freezing dominates nucleation, with immersion-freezing becoming an increasingly important contributor toward colder cloud temperatures. The difference between seeding into cloud or below cloud with either aerosol does not appear significant from the standpoint of ice crystal concentrations produced, although it may be from dispersion and targeting standpoints.

6.3 Generalized Model Simulations of Seeding with AgI-AgCl and AgI-AgCl-4NaCl Aerosols

The previous sections of this chapter have shown that the cloud model with the new formulations for ice nucleation has the sensitivity to pick up differences in ice formation between the two ice nucleating aerosols studied, for a variety of seeding situations. It is useful to run a few simulations with the one dimensional microphysical model that more directly relate to cloud seeding situations in the atmosphere in order to make some general statements of their potential or preferential utility based on the laboratory results. In Chapter 7 the validity of making such conclusions will be tested by comparing model predictions versus actual data from an atmospheric cloud seeding test using one of the methodologies examined.

For the relevant examples, a seeded parcel is considered entering a continental orographic cloud with a base temperature of -5°C, and a continental cumulus cloud with a 5°C base temperature and a constant vertical velocity of 8 m s^{-1} seeded from below or at the -5°C level. Vertical motion in the orographic simulation is initialized to be 25 cm s^{-1}, as might be found upstream of a mountain barrier where seeding would occur, accelerating (0.08 cm^2 s^{-1}) to 1.2 m s^{-1} at -10°C, characteristic of vertical motions at a position near the barrier in vigorous orographic flow.. Droplet concentrations are about 150 cm^{-3} in the orographic simulation, and 700 cm^{-3} peak in the cumulus cloud. These simulations provide the opportunity to examine the potential effects of the ground generator or warm temperature release method in wintertime, and both the cloud base and in-cloud seeding (with wing-tip acetone burning generators) methodologies in the summer. The

comparisons made here are simply of the cumulative ice formed in these situations by either ice nucleus.

Figure 6.37 shows the evolution of the parcel thermodynamics and cloud characteristics for the orographic simulation seeded with polydisperse AgI-AgCl aerosols. These cloud characterisitics did not vary much with the seeding material used. Figure 6.38 shows a comparison of the fractions of aerosol nucleating ice for the two nucleants. Nucleating aerosol concentrations entering cloud in these simulations, as well as in the summertime ones, were 10000 L^{-1}. Ice crystal numbers per liter can thus be obtained by multiplying the fractions by 10000. The results show a consistent factor of 2 to 3 increase in ice nucleated using the hygroscopic AgI-AgCl-4NaCl aerosols versus seeding with AgI-AgCl aerosols. Although the mechanisms responsible for ice formation will not be discussed in detail, deposition, condensation-freezing and immersion-freezing all contribute in similar magnitude to nucleation for the hygroscopic aerosols, while contact-freezing largely dominates for the AgI-AgCl aerosols. The "standard" activity of the polydisperse aerosols, which one would infer from isothermal cloud chamber "calibrations" is very similar to the 0.05μm curve in Figure 5.13 (for either aerosol). Using the standard activity curve to describe potential ice formation without knowledge of the physical and temporal response of the various nucleation modes to cloud conditions would greatly overestimate ice formation (by a 10 to 15 factor) for the simulations whose results are presented in Figure 6.37. This demonstrates the magnitude of predictive accuracy gained with the new formulations.

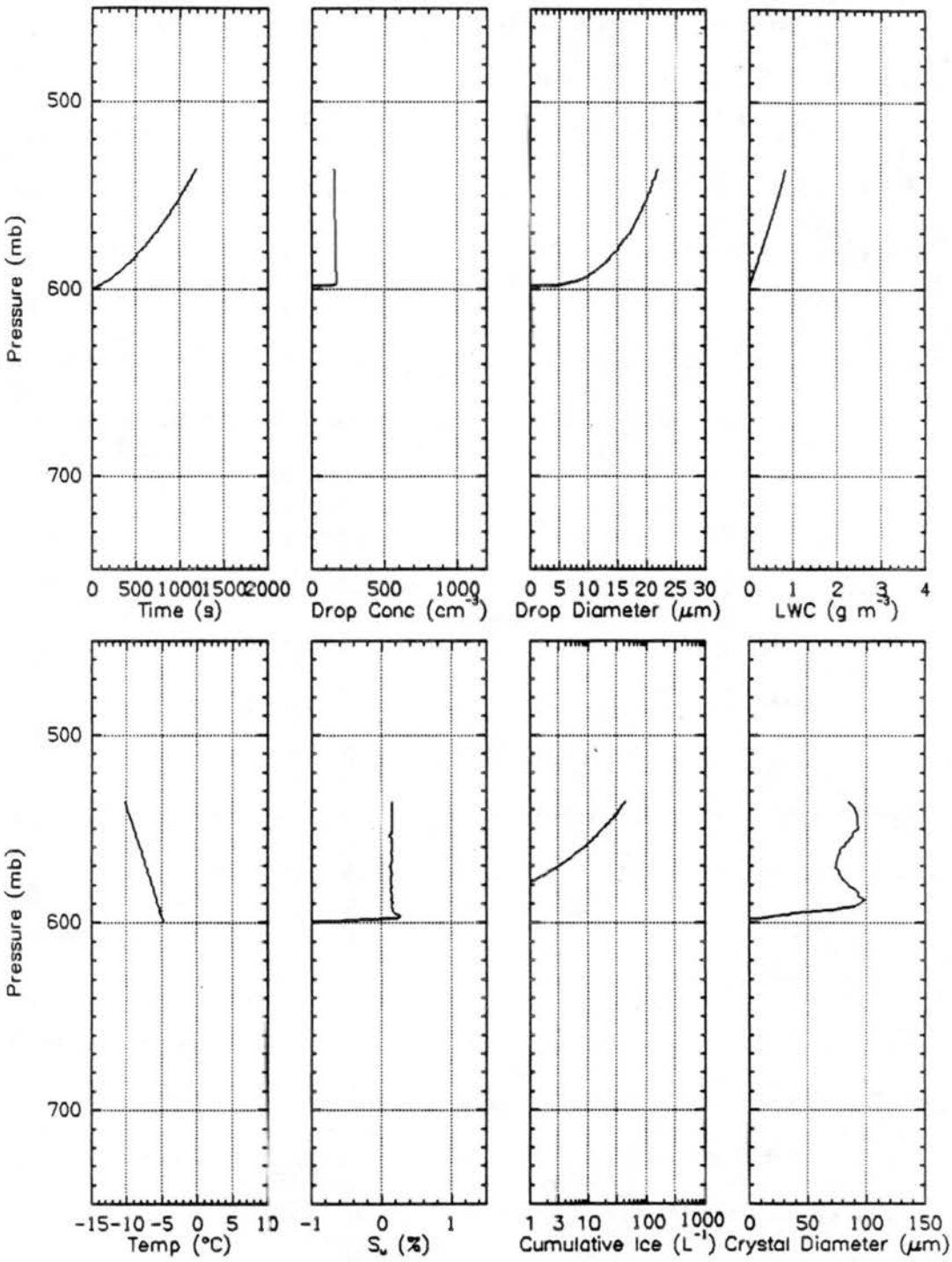

Figure 6.37 Model thermodynamic and cloud quantities for simulation of below-cloud seeding of an orographic cloud with AgI-AgCl aerosols. The ice signal is given L^{-1}. The initial parcel concentrations were 10^4 L^{-1}. A panel for average maximum crystal dimension is included with the quantities previously displayed for cloud chamber simulations.

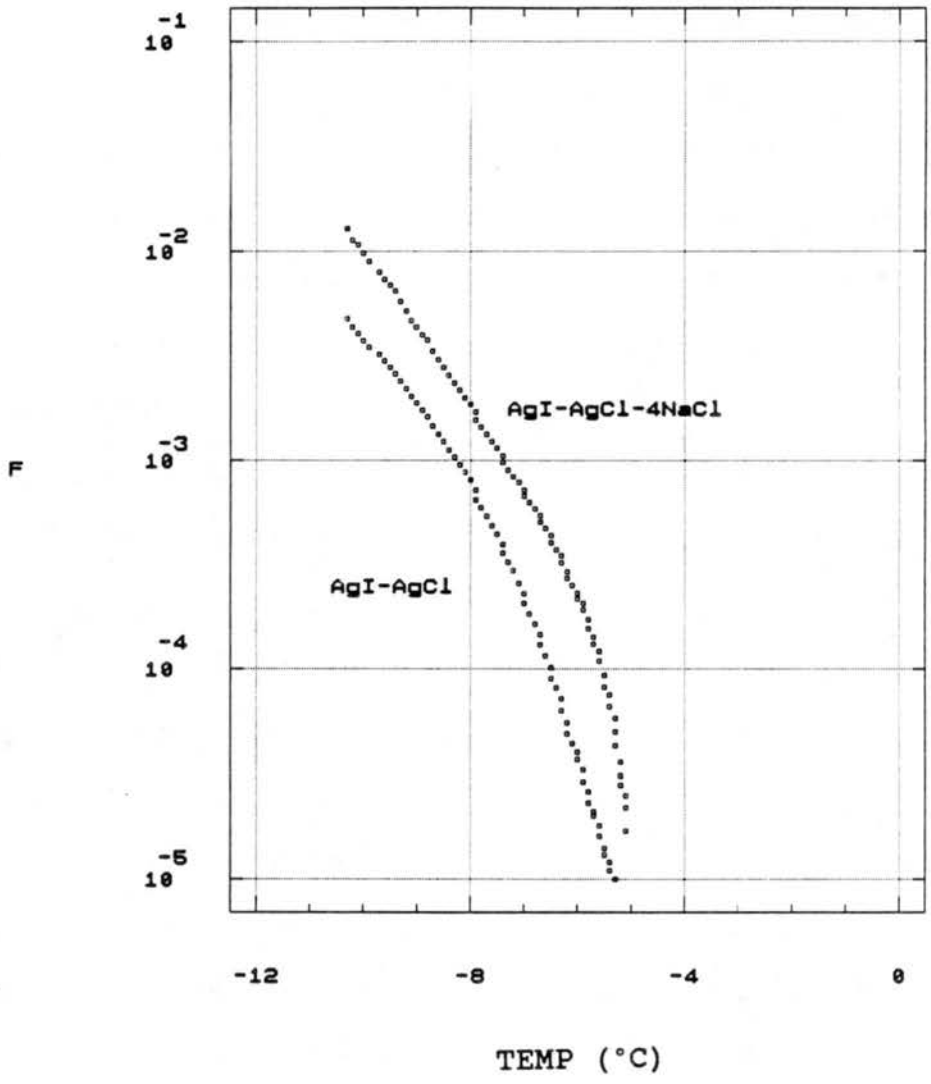

Figure 6.38 Comparison of cumulative ice fractions formed versus temperature in orographic seeding simulation using AgI-AgCl aerosols or AgI-AgCl-4NaCl aerosols.

It is also evident from the results shown in Figure 6.37 that the use of the hygroscopic nuclei, frequently slangly referred to a "fast" nuclei, does not preclude the continued nucleation of ice as a parcel slowly rises on approach to a mountain barrier in this idealized situation. As Figure 6.37 indicates, the supersaturations are low, but are sustained to colder temperatures along the parcel trajectory due to the increase in vertical motion and thereby condensate supply rate. To a large extent, the improvement noted for the hygroscopic ice nuclei is manifested due to this parcel thermodynamic profile chosen. If a constant 25 cm s^{-1} ascent is assumed, water supersaturations are smaller at any temperature, and AgI-AgCl aerosols show an advantage. Factors not considered in this general comparison are the dispersion characteristics of the two aerosol types and the potential accretional scavenging of aerosols collected by cloud droplets that are presumed here to survive to act as immersion-freezing nuclei. Also, strong fluctuations in supersaturation can exist in cumulus clouds, shich could greatly affect nucleation by either aerosol.

The thermodynamic and cloud characteristics of the cumulus cloud parcel is shown in Figure 6.39. These parcel characteristics did not vary much with seeding method. The parcel was followed to -15°C. The cumulative ice formed by the two nucleating aerosols for seeding the parcel below cloud versus seeding into cloud are shown in Figure 6.40(a and b), respectively. These results again show a distinct advantage, increasing to nearly an order of magnitude at coldest temperatures, using the AgI-AgCl-4NaCl aerosols for seeding below cloud base. In contrasting the two methods of seeding, the in-cloud method shows no distinct advantage or disadvantage for AgI-AgCl aerosols and only a

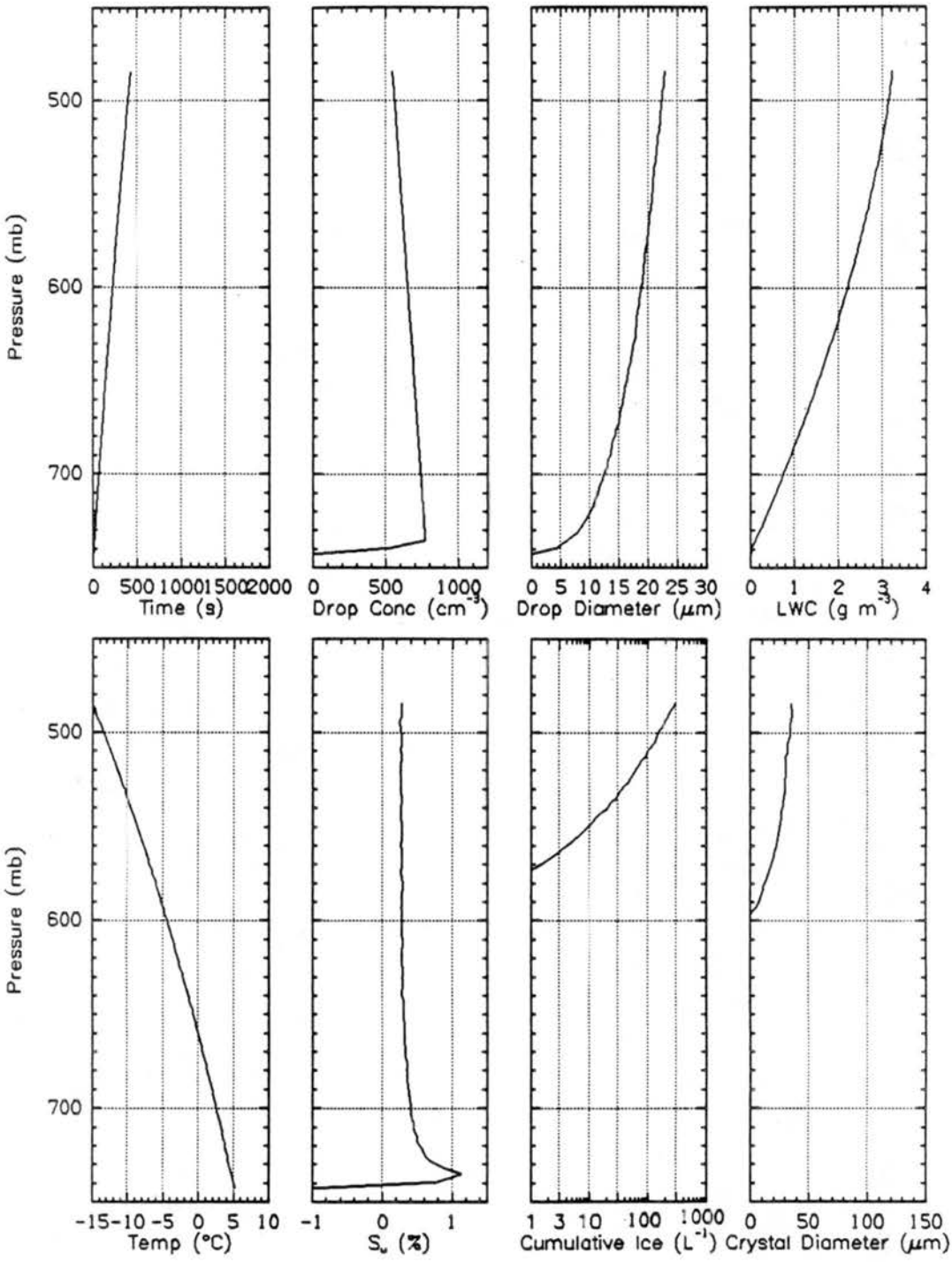

Figure 6.39 Model thermodynamic and cloud quantities for simulation of below cloud seeding of a summertime cumulus cloud with AgI-AgCl aerosols. Parcel initial conditions and updraft characteristics are described in the text.

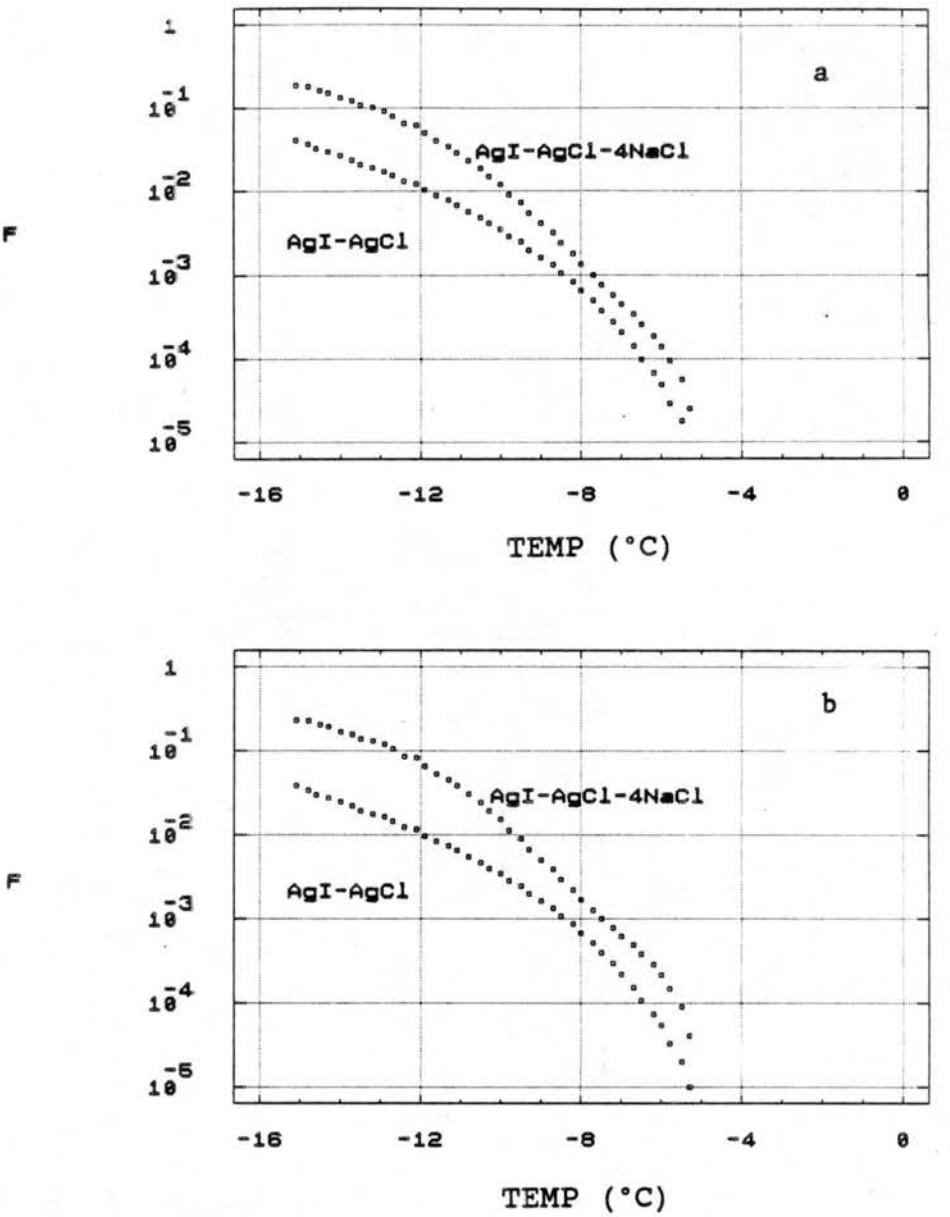

Figure 6.40 Comparison of cumulative ice fractions nucleated in cumulus seeding simulations with AgI-AgCl versus AgI-AgCl-4NaCl aerosols. Cases of seeding below 5°C cloud base (a) and into cloud at -5°C (b) are shown.

slight advantage for AgI-AgCl-4NaCl aerosols. This result for AgI-AgCl probably differs from results of experiments presented by DeMott (1988), which predicted larger differences, because the simulated updraft was much lower and the droplet concentrations much higher in those experiments. This greatly enhanced collection rates, limiting contact-freezing when aerosols were introduced before warm cloud, and enhancing it when aerosols were introduced directly into cloud. Results for AgI-AgCl-4NaCl aerosols given by DeMott (1988) agree with the results of the model simulations presented here. Namely, the hygroscopic aerosols are largely insensitive to seeding methodology.

The logical extension of these types of analyses in the future is to implement the nucleation models into 2-D and 3-D simulations which include both microphysical and dynamic interactions.

VII. COMPARISON OF MODEL SIMULATIONS TO FIELD SEEDING EXPERIMENTS

7.1 Experiment Background

It was desired to make some comparisons between data obtained in cloud seeding experiments and model predicted quantities. For the most straightforward comparison using the same one dimensional cloud model used in the laboratory studies, this requires special circumstances regarding cloud types, the types of data collected, and the ways that data are collected. Ice crystal concentration, preferably as a fraction of initial nucleus concentrations released, cloud droplet size and concentration, and the temporal variation of these quantities are the data of greatest interest.

Three types of atmospheric situations were sought for initial comparisons. In the wintertime, an ideal situation relevant to orographic cloud modification was an ice nuclei release upwind of a steady-state cloud layer near a mountain barrier. With low updrafts and minimal vertical mixing processes expected, it should be possible to follow intact seeded parcels into and through the cloud layer with a cloud physics aircraft and an appropriate navigation system. Experiments of this type were planned and conducted as part of the Fourth Colorado Orographic Seeding Experiment (COSE), over the Park Range of Northern Colorado (Rauber, 1987). Procedures were specified with the intent of filling the exact data needs of this dissertation.

Separate 10 minute releases of both of the aerosols studied in the cloud chamber experiments were made upwind of cloud edge. Following each release a cloud physics aircraft measured ice crystal concentration in the targeted plume along a line with the wind through cloud. After passing through the leading edge of the plume, based on mean horizontal wind estimates, unseeded cloud was sampled on a parallel path to the plume, back to cloud edge. Unfortunately, the occurrence of satisfactory events was limited to just two and on the best day the seeding generators malfunctioned at some point during a flight that included duplicate releases of both aerosols. It could not be ascertained when malfunction occurred, so all of the data were rejected. One of those cases targeted the plume over a 1.8 cm radar, which detected an apparent microphysical response of large magnitude timed exactly with respect to the expected arrival and duration times of the seeded cloud volume. A fifth case in a different day will require special filtering of ice crystal concentrations measured (by a Particle Measuring Systems 2-DC probe) to remove the smallest optical images recorded, because they appear to be large cloud droplets present throughout the natural cloud. In addition, cloud dissipation was occurring during the flight. In the future, similar data will be sought from other experimental wintertime programs. It would also be desirable to include an ice nucleus measurement system on the aircraft to monitor at least relative changes in aerosols concentrations and assure that the seeded plume is being sampled.

At least two summer cumulus cloud situations present reasonably good cases for comparisons to the explicit predictions made with the adiabatic/microphysical model. Both involve the seeding of an

identifiable single cumulus cloud or "feeder" cloud adjacent to a larger cumulonimbus. The first situation is an ice nucleus aerosol release into the top of a vertically limited or slowly growing cumulus with cloud top temperature warmer than -15°C (to minimize the effect of natural nucleation processes). The updraft rate is thus well defined, it should be possible to find the seeded parcel, and aerosols spend a lot of time in a narrow temperature range. Another cumulus cloud situation sought for comparison was a release into cloud or below-cloud, directly into the updraft region, which could be targeted by navigation "pointer" techniques and intercepted at various points at colder temperatures.

Summertime cumulus experiments of the type described have been underway in North Dakota (Stith et al., 1986; Stith and Benner, 1987; Stith et al., 1990). These experiments are part of the North Dakota/NOAA Federal/State Cooperative Program in weather modification research (Reinking, 1985). The experiments have the added benefit of the use of inert gas (SF_6) tracer techniques in coincidence with AgI aerosol releases. Measured tracer concentrations are used to quantify parcel dilution following release, thereby quantifying seeding agent concentration. In concert with ice crystal measurements, this permits an estimate in some cases of fractional activation versus time.

Examples of two of the summer cumuli situations desired for comparison were the subject of detailed discussion in Stith et al. (1990). The first occurred on 22 June 1987. AgI-AgCl aerosols were released with SF_6 at -11.5°C into a cloud described as "not very active". Cloud top temperature was near -14°C. Sampling was conducted by a fully instrumented cloud physics aircraft at -13.5°C, 300 m above

the seeding altitude. Measurements made included ice crystal concentrations and sizes, droplet concentrations and sizes, temperature, pressure, and x-y-z winds. No ice was detectable at the time of seeding. Based on the first detection of ice, well correlated with tracer, at the sampling altitude 4 minutes later, the average vertical motion in the seeded cloud region was around 1 m s^{-1}. Sampling continued at -13.5°C, with little change in cloud top, for two more passes covering several more minutes. The measurement of average tracer concentrations and a knowledge of its release rate, ice concentrations were normalized to be fractions of the AgI-AgCl concentrations initially injected. The resulting fractions nucleating in time were directly comparable to this quantity as predicted by the Young model.

The second seeding test of relevance, from Stith et al. (1990), for comparison to model prediction of ice formation occurred on 28 June 1987. This experiment was a cloud base release of AgI-AgCl aerosols near +6°C. Ice and gaseous tracer were measured coincidentally for several minutes (16 to 20 minutes after release) at supercooled cloud temperatures between -5 and -13°C. Adequate data were presented by Stith et al. to estimate average vertical motions in the cloud. Natural ice was present in regions of this cloud, but not at warmer temperatures in the "fresh" updraft region seeded. In these upshear regions of the updraft, only small ice crystals were found in coincidence with tracer. A fractional activation analysis was not performed in this case due to the uncertainties involved in transit of aerosols through the deep cloud layer. Rather than attempt such an analysis, the expected ice concentrations versus those observed were compared using the first case study to define initial parcel AgI

concentrations at cloud base. Since entrainment is not modeled, it was expected that the comparison might only be valid for peak ice crystal concentrations.

7.2 Simulation Methodology

Several things were done to make the simulations as equivalent as possible to the actual seeded cases. Also, some reasonable assumptions were made.

1. The assumption is made that the AgI-AgCl aerosols generated using the aircraft generator are only potentially different from the AgI-AgCl aerosols studied (from the CSU laboratory ground generator) in their size distribution, not in the behavior of particularly sized particles. Therefore, one needs only to describe the size distribution of aerosols from the airborne generator. This has never been measured, but the difference between the airborne and ground generator particle sizes can be estimated from the differences in peak effectiveness values (at say -20°C) determined for each aerosol in the isothermal cloud chamber. Peak values from the airborne generator (on file for AgI-AgCl aerosols at the Cloud Simulation and Aerosol Laboratory) are slightly higher, so the size distribution of the ground generator aerosol was slightly shifted and peaked more toward smaller sizes.

2. Natural nucleation in the model was not activated. Based on some trial simulations, it would not have made a difference.

3. Initial mixed parcel seeding agent concentrations were an unknown. I chose a value of 10000 L^{-1} for two reasons. First, the studies by Holdroyd et al. (1988) and Super and Heimbach (1988) mentioned in Chapter 2 reported peak AgI ice nucleus concentrations (effective at -20°C) measured with an NCAR counter (Langer, 1973) shortly after generation on the order of 1000 L^{-1}. These numbers assumed the counter used measured only 10% of the total nuclei present, based on Langer's calculations of ice particle losses due to the physical design of the instrument. Using the estimates of Sackiw et al. (1984) that the true fraction measured is only 1% compared to numbers nucleated at -20°C in the CSU isothermal cloud chamber for some aerosols, the initial mixed aerosol concentrations released from a typical seeding generator may be closer to 10000 L^{-1}. Secondly, the ice crystal concentrations nucleated in the first simulations of the in-cloud seeded case (22 June 1987), where observations were very near the seeding level, agreed well with the observed crystal concentrations using the 10000 L^{-1} initial value. This same value was thus used at cloud base level in the simulation of the 28 June case.

4. An updraft profile was composed to crudely approximate an average profile for the cloud on 28 June 1987. This was based on information given in Stith et al. (1990); namely, observed vertical velocities at different levels and cloud depth versus temperature. Cloud base vertical motion was 2.5 m s^{-1}, vertical acceleration was 0.002 m s^{-1} until near -5°C, followed by decelleration of 0.004 m s^{-1} to the coldest sample temperature. Seeding was initiated at the same temperature as in the field experiments. Humidity was adjusted such

that cloud base temperature was just colder than the temperature indicated at seeding level (5.7°C) on 28 June. The same cloud base temperature and updraft profile was used for the 22 June cloud, except the updraft was tapered to 10 cm s^{-1} at -13.4°C, where field observations continued for several minutes in this stable cloud region.

5. The model CCN spectra was adjusted to cause the nucleation of a maximum droplet concentration near 700 cm^{-3}. This value was based on data presented by Stith et al. and further detailed data provided to me by the lead author.

6. Collision and coalescence was not activated in the simulations, due to a current problem in this routine. This omission may have affected the evolution of liquid water content somewhat, but the absence of entrainment and turbulence-induced supersaturation fluctuations in the model are far greater sources of potential differences between the observations and the adiabatic simulation.

7. Although seeding was done only with AgI-AgCl aerosols in the field test, model simulations are done for both of the chemistries tested in the laboratory studies, just for comparison.

7.3 22 June 1987 Case

Figure 7.1 includes eight model quantities plotted versus pressure for the simulation of the 22 June seeding test. Included are time, droplet concentration and diameter, liquid water content, vertical

motion profile, ice concentration and maximum average crystal dimension. The inital observed cloud characteristics at the time of seeding are indicated by ⊗ symbols. These data indicate that the most unrealistic aspect of the simulation is probably the liquid water content. This is a result of the unmixed adiabatic nature of the model. Droplet concentrations and diameter are reasonably estimated. Therefore, the simulation performed is probably adequate. However, steady depletion of LWC with time and rapid growth evolution of the ice phase were observed in the real cloud, but not in the model simulation. At 7 minutes after seeding, the average crystal size is about 100μm in the model compared to about 500μm in the real cloud.

Figure 7.2 shows the model parcel histories of temperature and ice crystal concentration as a function of time after seeding. The ice data is also presented as a fraction of the total initial ice nucleus aerosol concentration. This latter quantity may be compared to observed active fractions estimated by Stith et al. (1990). These authors estimated the fraction of aerosol nucleating and growing to detectable sizes at any temperature using the equation,

$$F(T) = \frac{Q_t \, C_i(T)}{Q_a \, E(T) \, C_t(T)} \qquad (7.1)$$

where Q_t and Q_a are tracer and aerosol release rates, respectively, C_t and C_i are measured concentrations of tracer and ice crystals,

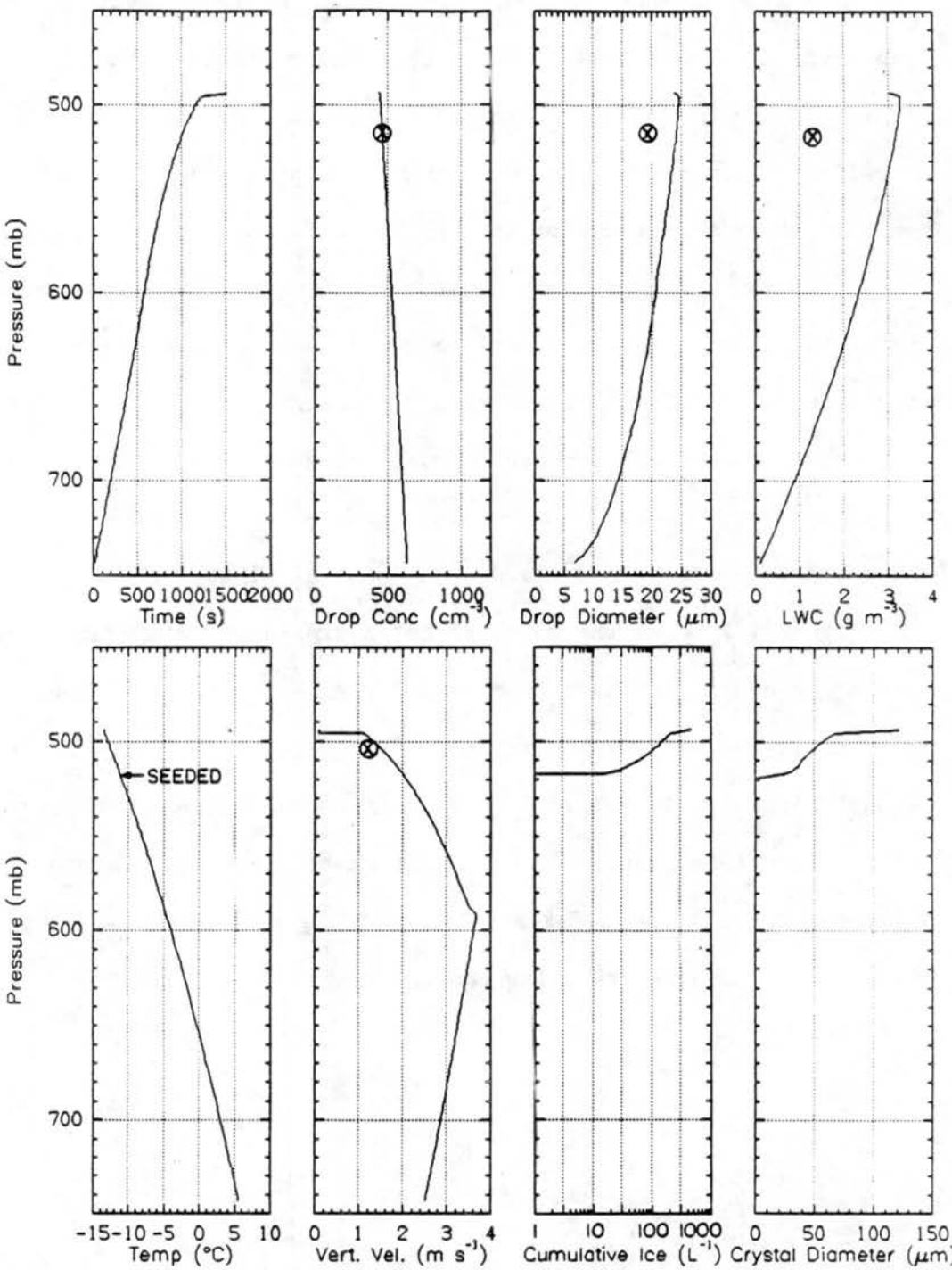

Figure 7.1 **Adiabatic cloud model profiles of cloud and thermodynamic quantities in the simulation of the 22 June case. Vertical velocity replaces the supersaturation profile shown in previous figures of this type. A few observations from the real cloud are overlain in repective plots (⊗).**

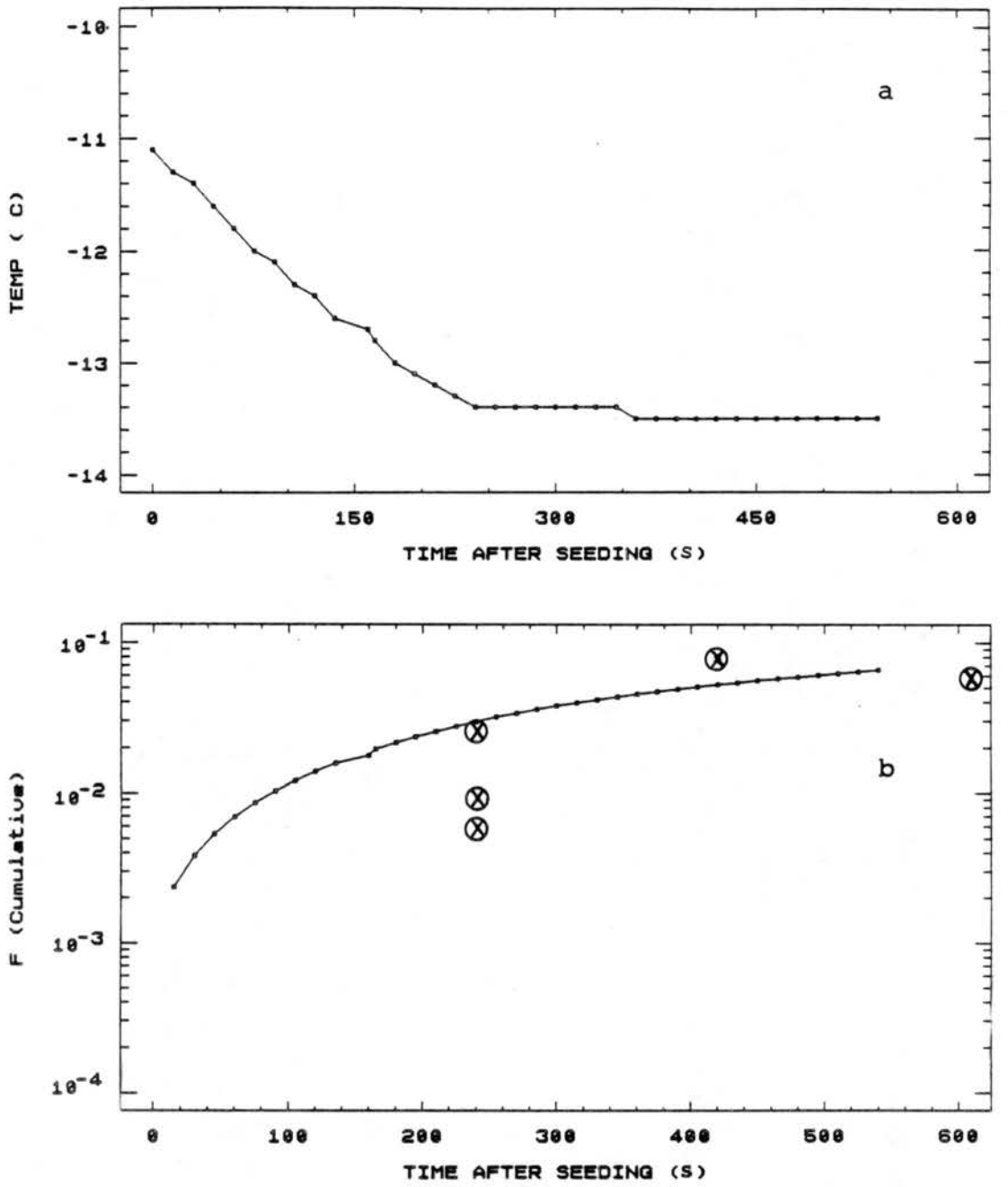

Figure 7.2 Time histories of temperature (a) and ice formation (b). Ice is given both as the concentration L^{-1} and as a fraction of initial aerosol concentrations injected. In (b), observed data are shown (⊗), from Stith et al. (1989).

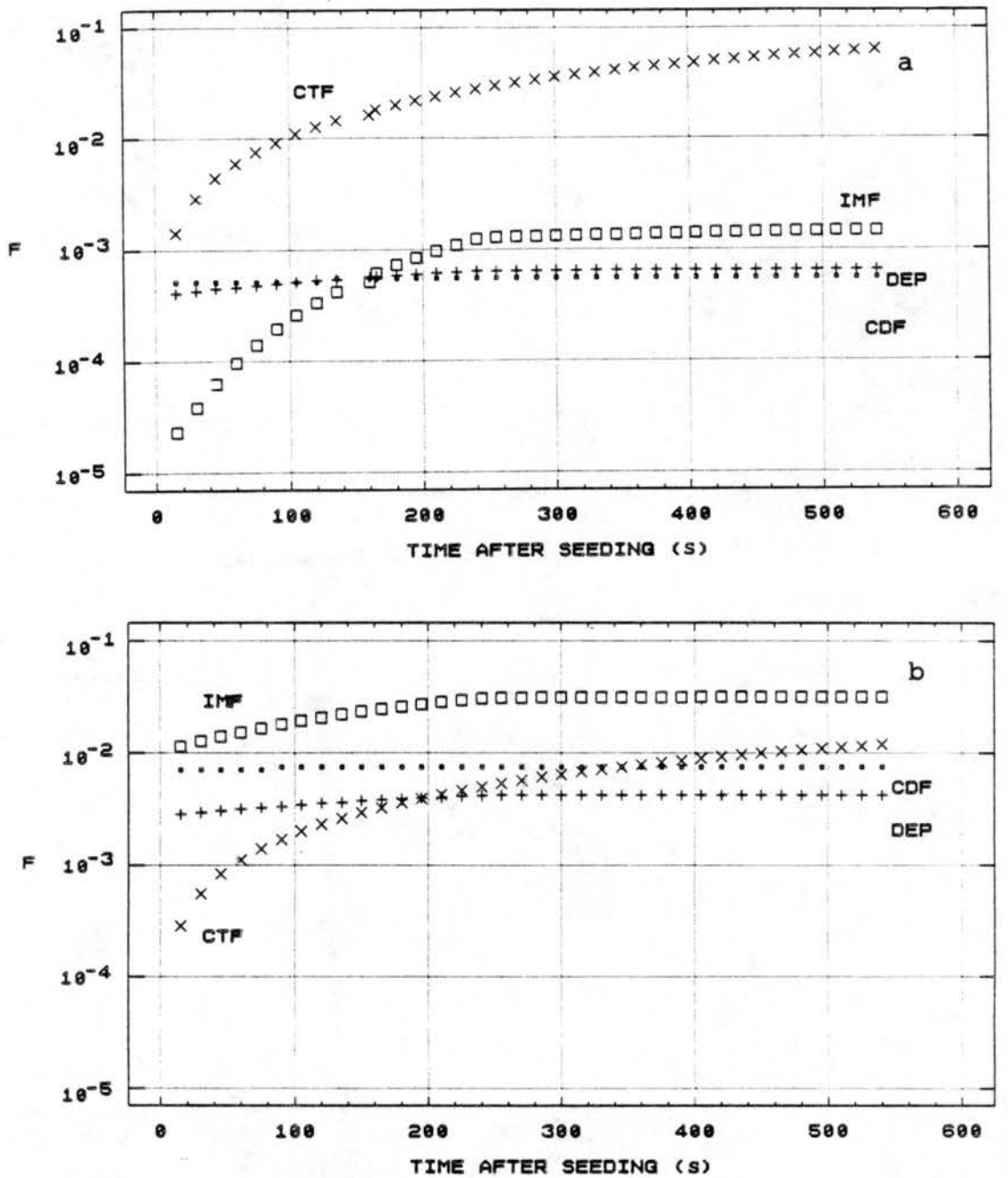

Figure 7.3 Model-predicted nucleation mode contributions to ice formation in the simulation of the 22 June case (a), and those predicted if seeding had been done with AgI-AgCl-4NaCl aerosols (b).

Table 7.1

Observed and Model Fraction Effective : 22 June 1987 Cumulus

(T = -13.5°C)

Time after seeding (s)	$F(T)_{obs}$	F_{obs}	F_{model}
240	0.022	0.008	0.029
240	0.063	0.022	0.029
240	0.014	0.005	0.029
420	0.240	0.069	0.054
630	0.150	0.053	0.072

respectively. The factor E(T) is the effectivenes (g^{-1} AgI) from isothermal cloud chamber tests. Table 1 in Stith et al (1990) presents these F(T) values. If these are multiplied by $E_{-13.5}/E_{max}$ (~0.35 for based on isothermal cloud chamber data for AgI-AgCl aerosols produced by the Lohse airborne generator used in the program), where E_{max} is the maximum potential activity, at say -20°C, the fractions will be in terms of the total aerosol numbers initially injected. These are the values (⊗ symbols) plotted in Figure 7.2b (arrows indicate the vertical scale to use) and listed in Table 7.1. The model results compare well to the experimental results. One implication is that one does not have to invoke the concept of high rates of nucleation induced by burning the aerosol generator right inside the cloud, in order to explain the observed ice concentrations. If high supersaturations were produced during the combustion process in cloud, it is expected that immersion-freezing nucleation would dominate for both aerosols, based on discussion in Chapters 5 and 6. It is interesting therefore, that the predicted fractions nucleating assuming 100% immersion in cloud

droplets (using Figure 5.26 and the aerosol sizes involved) are approximately 0.10 to 0.20.

For seeding with AgI-AgCl aerosols, the dominant model nucleation mode was contact-freezing nucleation. This is shown in Figure 7.3a. Because of this, the model overestimates the active aerosol fraction, since the model did not mimic the changes in cloud droplet concentration in time. If the cloud had been seeded with AgI-AgCl-4NaCl aerosols, the cloud model predicts much greater ice formation initially after seeding (in -11 to -12°C temperature range), although ice amounts are similar to AgI-AgCl seeding after about 4 minutes (Figure 7.3b). Also, after 200s (in the nearly isothermal cloud region), the only additional ice being formed is from the contact-freezing mechanism. This mechanism is very inefficient for AgI-AgCl-4NaCl aerosols compared to AgI-AgCl aerosols. The higher ice formation initially for AgI-AgCl-4NaCl, by nearly a factor of ten compared to AgI-AgCl is the result of strong contributions by condensation-freezing and immersion-freezing nucleation.

7.4 28 June 1987 Case

Figure 7.4 shows the various model quantities for this simulation, overlain wherever possible with values observed in the real cloud. Again, with the exception of the prediction of adiabatic liquid water content, the simulation is a good representation of the observed cloud characteristics. LWC was fairly well sustained in this cloud, so the simulation should be reasonably accurate for the purposes of comparing nucleation effects.

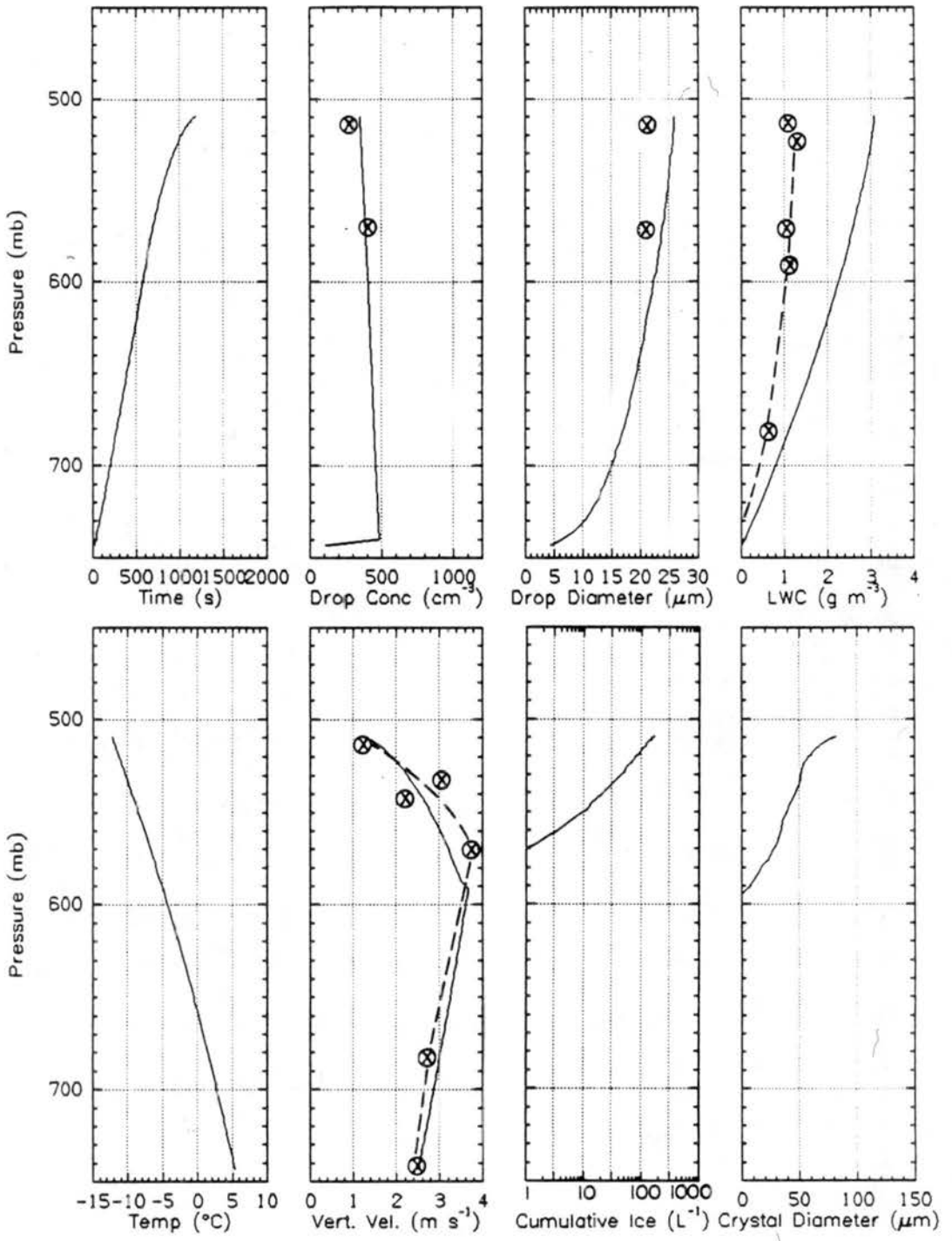

Figure 7.4 As in Figure 7.1, for the 28 June case.

The temporal history of predicted ice crystal crystal concentrations for this simulation are presented in Figure 7.5. The range of observed ice crystal concentrations in the upshear (updraft) portion of the cloud are indicated for comparison. The observed values group to the lower side of the model values, but the agreement is good. Concentrations predicted at temperatures near cloud top are similar to peak values observed in downshear regions of this particular cloud (100 to 200 L^{-1}).

The nucleation modes operative for this below-cloud base seeding simulation with AgI-AgCl aerosols are differentiated in Figure 7.6a. Compared to the in-cloud seeded simulation, much more ice is nucleated by way of immersion-freezing, and this contribution increases as the cloud cools. These nucleation events are primarily from particles that were collected by cloud droplets lower in the cloud where the temperature was too warm and/or the efficiency too low for contact-freezing. By comparison, the use of AgI-AgCl-4NaCl aerosols in this situation (Figure 7.6b) is predicted to form more ice at the warmest temperatures, due to the more efficient deposition nucleation mechanism, but similar amounts of ice in mid and upper cloud layers (later times). The dominant mechanism for ice formation for AgI-AgCl-4NaCl aerosols would be immersion-freezing.

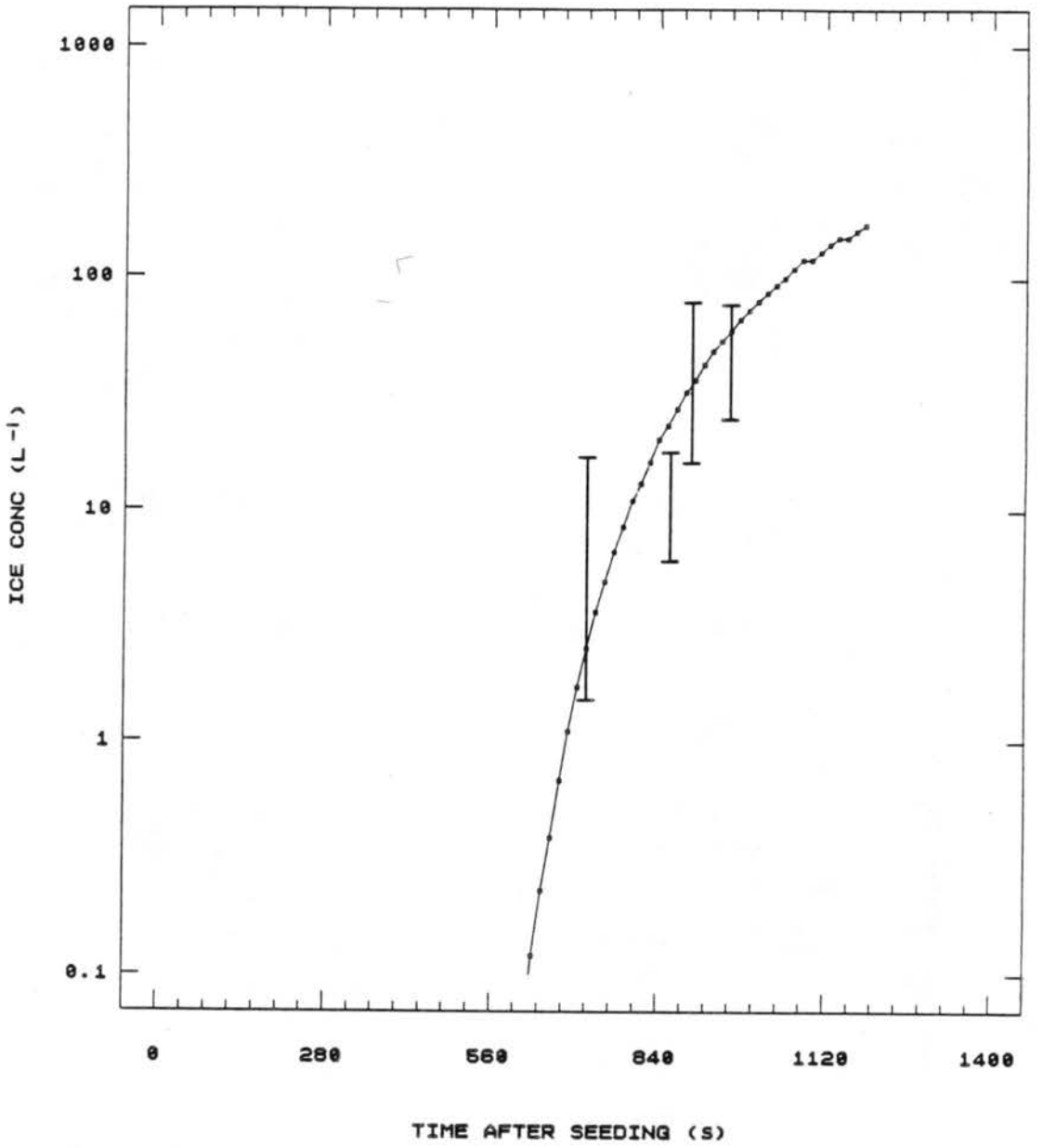

Figure 7.5 Predicted ice concentration versus time (temperature) for 28 June cloud. The range of concentrations observed in the upshear cloud region is shown by brackets.

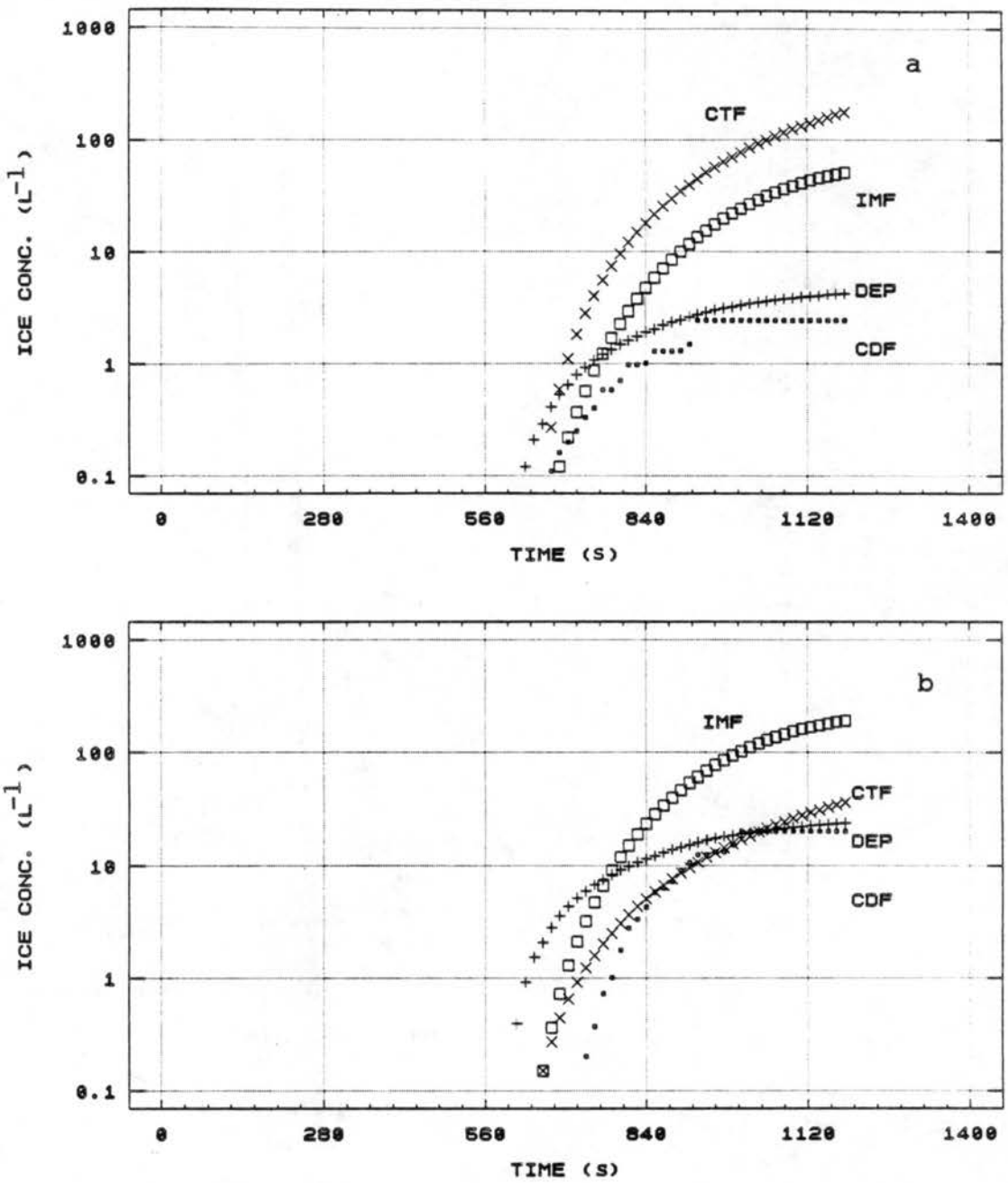

Figure 7.6 As in Figure 7.3, but for the 28 June cloud seeded from below cloud base.

VIII. SUMMARY AND CONCLUSIONS

8.1 Summary of Results

This dissertation research addressed the controls that affect the nucleation of artificial ice nuclei in differing cloud environments. The experiments reported herein utilized a unique and specialized cloud chamber (DCC) to attempt to reproduce the varied environments that particles can encounter in clouds. Special experimental methodologies were developed to try to isolate the different ice nucleation modes operative using this cloud chamber. Implementation of the new quantitative information in "equivalent" experimental simulations using an existing adiabatic parcel/cloud model (Young, 1977) are shown to successfully reproduce most of the observed ice nucleating behavior of the aerosols in the cloud chamber. This is so whether aerosols are introduced before cloud forms or directly into clouds of varied temperatures. In addition, excellent agreement was found between simulations based on the new ice nucleus formulations and oservations made in summertime cumuli.

Specific results, not necessarily listed in order of significance, are:

1. The use of a controlled expansion cloud chamber to successfully simulate adiabatic expansion of a cloud parcel (with mixed water phases present) was demonstrated. Equivalent numerical simulation

was used to quantify supersaturation with respect to water (with 30% uncertainty), supplementing the array of measurement systems already in place.

2. A mathematical technique was developed to retrieve the initial ice formation signal (as a function of time and temperature) from the measured fallout of ice crystals in the cloud chamber. This should be of general benefit to laboratory cloud physics research using large cloud chambers.

3. Specific methods were developed to isolate and quantify the potential contributions of different nucleation modes for the aerosols studied. These met with varied degrees of success. Deposition nucleation was analyzed as an instantaneous event which depends primarily on temperature and supersaturation with respect to ice. Ice was measured for two aerosols, preceding cloud formation at a variety of temperatures. Contact-freezing nucleation experiments conducted in the CSU isothermal cloud chamber defined nucleation activity as a function of temperature, time, and particle size. Measured collection rates were compared to theoretical values, and showed that some aerosol transport mechanisms are still not well defined in this chamber. Immersion-freezing nucleation was analyzed by using ice nucleus aerosols as CCN in the dynamic cloud chamber. The results for immersion-freezing were made generally relevant to any atmospheric conditions by defining the CCN supersaturation spectra for the ice nucleus aerosols, primarily using a thermal

gradient diffusion chamber. Condensation-freezing nucleation proved most difficult to quantify. These experiments had the greatest associated uncertainty because the condensation-freezing activity is taken as the residual of the ice signal after adjustment for the contributions of the other nucleation mechanisms. In addition, the uncertainty in supersaturation alone was enough to give a factor of 3 to 5 uncertainty to any fit of the results. Still, highly enhanced nucleation rates at even moderate estimated supersaturations marked this as a clearly distinct mechanism from the others.

4. AgI-AgCl aerosols possess the greatest potential efficiency to nucleate ice by contact-freezing nucleation (approaching 1 at -20°C) and size effects are in nearly exact relation to the particle surface area. The nucleation activities are nearly two orders of magnitude higher than those indicated for pure AgI in other studies. Immersion-freezing is the next most potentially efficient nucleation mode for AgI-AgCl aerosols, but is at least one order of magnitude less efficient than contact-freezing and requires time or high S_w for its realization in clouds. Collection by brownian diffusion and other transport processes is the primary means by which the association with a cloud droplet occurs for AgI-AgCl because condensation nucleation activities are low (< 10% active at 1% S_w). Thus, immersion-freezing is an important contributor to ice nucleation when cloud bases are warm, but never dominates contact-freezing. Deposition nucleation is not particularly efficient for AgI-AgCl aerosols (~1%

efficiency at -20°C) and size effects were best related directly to particle size, rather than to particle surface area. Condensation-freezing can be a predominant nucleation mode for AgI-AgCl, but only as water supersaturations approach 1% or more in cloud. At 0.3% supersaturation, condensation freezing active site density is of the same magnitude as for immersion-freezing, but at 0.1% S_w it is one order of magnitude less. For very high supersaturations (in excess of 2 to 3%) produced in rapid expansion simulations, the high predicted activities by condensation-freezing were not realized. Instead, ice formation appeared to be governed by the immersion-freezing limit. This implies a complex interaction of condensation and freezing rates at higher supersaturations.

5. Vapor-dependent mechanisms dominate ice formation by AgI-AgCl-4NaCl aerosols, as might be expected for a hygroscopic aerosol. Under various circumstances, condensation-freezing or immersion-freezing may predominate. More often they contribute in similar amounts to ice formation. The contributions primarily depend on where aerosols are introduced with respect to the cloud S_w profile. This occurs since AgI-AgCl-4NaCl aerosols are excellent CCN (30 to 90% activation at 1% S_w, depending on particle size). Consequently, immersion-freezing dominates if aerosols are introduce at warm cloud temperatures. The nucleation activity realized by immersion-freezing is an order of magnitude or more higher than for AgI-AgCl aerosols under the same circumstances, not because of higher freezing activity, but

because of the more efficient immersion process. Condensation-freezing activities are 1 to 2 orders of magnitude higher than for AgI-AgCl aerosols as a function of S_w at temperatures below -8°C. Condensation-freezing at specific temperatures is also an order or more of magnitude more efficient than immersion-freezing. When AgI-AgCl-4NaCl aerosols are introduced directly to supercooled cloud, condensation-freezing predominates over immersion because less particles become completely immersed in could droplets. As with AgI-AgCl aerosols, the situation appears to reverse at high superaturations. Deposition nucleation is an order of magnitude more efficient for AgI-AgCl-4NaCl aerosols than for AgI-AgCl aerosols. Activities approach 5% at -20°C. This mechanism only predominates at temperatures warmer than -9°C, where the freezing mechanisms are both very inefficient. Contact-freezing plays little role for AgI-AgCl-4NaCl aerosols, in agreement with the presumption that their mobility is limited by their water activity.

6. Adiabatic cloud model simulations of particular experiments using the new ice nucleus formulations, reproduced many of the features of dependencies on particle chemistry, particle size, saturation ratio, and seeding method (thermodynamic and cloud history) that are observed. These dependencies reflect the relative importance of different nucleation modes in different situations.
Model versus experiment comparisons for experiments seeded with polydisperse aerosols, representing blind comparisons, showed particularly good agreement. This was true for clouds with warm

or cold formation temperatures. No deactivation or limitation to ice formation was detected. It was also predicted and found, under most conditions, that AgI-AgCl-4NaCl aerosols possess greater utility (from an ice nucleus activity standpoint) than AgI-AgCl aerosols. Both aerosols have greater utility than AgI alone.

7. Simulations of generalized atmospheric situations showed that a simple temperature dependent description of nucleation by AgI-AgCl aerosols in clouds is very inadequate, but nucleation by AgI-AgCl-4NaCl aerosols may be readily described this way for use in dynamical/microphysical cloud models.

8. The excellent agreement found between model predictions of ice formation and observations made in actual atmospheric seeding tests of two seeding methodologies gives some initial confidence to the transferability of the laboratory results to atmopheric situations.

8.2 Utility of Results and Future Research

The results of this study should be useful in the planning, conduct and numerical simulation of cloud modification experiments which use the ice nucleus aerosols examined. To a large extent, these applications indicate potential future research directions. The following are areas of further research that should be undertaken.

1. Refine and improve the experimental and numerical methods employed in this study. Model modifications should be made to remove cloud particles as occurs in the cloud chamber. This should improve estimates made of water supersaturations over extended time periods. Secondly, experimental methods for the investigation of temporal nucleation effects should be developed. This is mainly an engineering problem. Finally, a more sensitive ice crystal detection system would be useful, and the deconvolution procedure for this signal should be refined to be as valid as possible for the appropriated temperature and cloud conditions.

2. Standardize methods for the detailed study of any artificial ice nucleus. For these types of studies to be financially feasible, an effort must be defined that takes no more than 4 or 5 weeks for any particular aerosol. This would require careful planning to include a minimal, but sufficient number of each type of required experiment. Implementation in the cloud model should amount to the simple redefinition of equation coefficients.

3. Further verify the results obtained in this study using field experiments. The ideal situation is an aircraft seeding program that includes the use of both of the aerosols studied in the laboratory, an ice nucleus detector to verify aerosol plume interception during cloud penetrations, gaseous tracer techniques to estimate the dilution of initial aerosol concentrations, and a navigational "pointer" system to help study the development of

ice crystal concentrations in time. Available data that fill most of these criteria should be sought.

4. Attempt to include experimentally developed ice nucleus formulations in model simulations which include cloud dynamics and the ability to predict quantitative precipitation effects in seeded and non-seeded clouds (for example, two and three dimensional numerical simulations). Although this research has proven that different ice nucleating aerosols can cause different quantities of ice to form in clouds under various circumstances, and this behavior can be quantified, the extended effects on precipitation are uncertain.

5. Apply the general experimental and numerical procedures towards the study of the action of natural ice nuclei. This would fill the need to more accurately define the potential importance of primary nucleation to ice formation in the atmosphere. Such studies would require a more sensitive method for sensing ice crystal concentrations An added complication is the unknown character and concentration of potential ice nucleus aerosols. Presumably, naximum concentrations should be indicated by the most potentially effective mechanism, probably condensation-freezing nucleation. Supporting measurements with other experimental devices (for example, a continuous flow ice-thermal diffusion chamber) should also be made.

6. Relate current results to theories of ice nucleation.

7. Continue investigations of cloud droplet nucleation and initial growth in the dynamic cloud chamber. Preferably, such studies would use nearly monodisperse CCN particles.

REFERENCES

American Metorological Society, 1985: Planned and inadvertent weather modification. *Bull. Am. Met. Soc.*, **66**, 447-449.

Anderson, B.J. and J. Hallett, 1976: Nucleation from the vapor on single crystal substrates. *J. Atmos. Sci.*, 33, 822-832.

Baumgardner, D., W. Strapp and J.E. Dye, 1985: Evaluation of the Forward Scattering Spectrometer Probe. Part II: Corrections for coincidence and dead-time losses. *J. Atmos. Oceanic Tech.*, 2, 636-643.

Baumgardner D., J.E. Dye and W.A. Cooper, 1986: The effects of measurement uncertainties on the analysis of cloud particle data. Preprints, Joint Sessions, 23rd Conf. on Radar Met. and Conf. on Cloud Physics, 22-26 Sept., Snowmass, CO, Vol. 3, 313-316.

Blumenstein, R.R., R.M. Rauber, L.O.Grant, and W.G. Finnegan, 1987: Application of ice nucleation kinetics in orographic clouds. *J. Clim. Appl. Meteor.*, **26**, 1363-1376.

Braham, R.R., Jr., 1985: Summary of the Workshop on Precipitation Enhancement, 23-24 May, 1984, Park City, Utah. *Bull. Am. Met. Soc.*, **66**, 304-306.

Cerni, T.A., 1983: Determination of the size and concentration of cloud drops with an FSSP. *J. Clim. Appl. Meteor.*, **22**, 1346-1355.

Cooper, W.A., 1974: A possible mechanism for contact nucleation. *J. Atmos. Sci.*, **31**, 1832-1837.

Cooper, W.A., 1988: Effects of coincidence on measurements with a Forward Scattering Spectrometer Probe. *J. Atmos.Oceanic Tech.*, 5, 823-832.

Cotton. W.R., G.J. Tripoli, R.M. Rauber, and E.A. Mulvehill, 1986: Numerical simulation of variying ice crystal nucleation rates and aggregation processes on orographic snowfall. *J. Clim. Appl. Meteor.*, **25**, 1658-1680.

Davis, C.I., 1974: The ice-nucleating characteristics of various AgI aerosols. PhD. Dissertation, Dept. Mech. Eng., Univ. Wyo., Laramie, Wyo., 267 pp.

DeMott, P.J., W.G. Finnegan and L.O. Grant, 1983: An application of chemical kinetic theory and methodology to characterize the ice nucleating properties of aerosols used in weather modification. *J. Clim. Appl. Meteor.*, 22, 1190-1203.

DeMott, P.J., R.D. Horn, W.G. Finnegan, R.R. Blumenstein and L.O. Grant, 1984a: Comparison of pre-cloud versus in-cloud seeding using mechanistically different ice nuclei in a dynamic cloud chamber. Extended abstracts, 9th Conf. Weather Modification, 21-23 May, Park City, UT, 4-5.

DeMott, P.J., W.G. Finnegan, R.D. Horn and L.O. Grant, 1984b: Experimental Studies of the kinetics of deposition nucleation on an ice nucleant used in weather modification. Ppnts. 11th Intnl. Conf. on Atmos. Aerosols, Cond. and Ice Nuclei, 2-7 Sept., Budapest, Hungary, Vol. 2, 10-14.

DeMott, P.J., W.G. Finnegan and L.O. Grant, 1985: On the effectiveness of artificial seeding from below cumulus cloud base. 4th WMO Scientific Conference on Weather Modification, 12-14 Aug., 1985, Honolulu, Hawaii.

DeMott, 1982: A laboratory characterization of mixed silver iodide silver chloride ice nuclei. M.S. Thesis, Department of Atmos. Sci., Colorado State University, Fort Collins, 124 pp.

DeMott, P.J., 1988: Comparisons of the behavior of AgI-type ice nucleating aerosols in laboratory-simulated clouds. *J. Wea. Mod.*, **20**, 44-50.

DeMott, P.J. and D.C. Rogers, 1989: Humidity measurements during simulated adiabatic expansion and cloud formation using infrared hugrometry. Submitted to *J. Atmos. Oceanic Tech.*.

DeMott, P.J. and D.C. Rogers, 1990: Apparent homogeneous-freezing nucleation of aqueous solution droplets measured in laboratory simulations of natural clouds. *J. Atmos Sci.* , **47**, 1056-1064.

Detwiler, A.G. and B. Vonnegut, 1981: Humidity required for ice nucleation from the vapor onto silver iodide and lead iodide aerosols over the temperature range -6 to -67°C. *J. Appl. Meteor.*, **20**, 1006-1012.

Dye, J.E. and D. Baumgardner, 1985: Evaluation of the Forward Scattering Spectrometer Probe. Part I: Electronic and optical studies. *J. Atmos. Oceanic Tech.*, 1, 329-344.

Edwards, G.R. and L.F. Evans, 1960: Ice nucleation by silver iodide: I. Freezing vs sublimation. *J. Meteor.*, **17**,627-634.

Edwards, G.R. and L.F. Evans, 1971: The mechanism of activation of ice nuclei. *J. Atmos. Sci.*, **28**, 1445-1447.

English, M. and J.D. Marwitz, 1981: Comparison of AgI and CO^2 seeding effects in Alberta cumulus clouds. *J. Appl. Meteor.*, **20**, 483-495.

English, M., B. Kochtubadja and D.C. Rogers, 1984: A comparison of effects of seeding cumulus clouds with AgI and CO^2. Invited paper presented at Precipitation Enhancement Workshop, 23-24 May, Park City, Utah.

Feng, D. and W.G. Finnegan, 1985: An efficient, fast functioning nucleating agent - Composite AgI-AgCl-NaCl ice nuclei. In, *Collected Papers on Met. Sci. and Tech.*, Selection of cooperative papers by Chinese and American authors, Chang Shu Ping, ed., Meteorological Press, 37-42.

Feng, D. and W.G. Finnegan, 1989a: An efficient, fast functioning nucleating agent -- AgI•AgCl-4NaCl. *J. Wea. Mod., 21*, 41-45.

Feng, D., C. Rhuzen, J. Genwang and H. Gen, 1989: A laboratory study of ice nucleation under water sub-saturation. Papers submitted to 5th WMO Scientific Conf. on Wea. Mod. and Appl. Cloud Phys., Beijing, China, *WMO Tech. Doc. No. 269*, 137-140.

Finnegan, W.G., D. Feng and L.O. Grant, 1984: Composite AgI-AgCl-NaCl ice nuclei: Efficient, fast functioning aerosols for weather modification experimentation. Ext. Abs. 9th Conf. on Wea. Mod., 21-23 May, Park City, Utah, 3.

Finnegan, W.G. and R.L. Pitter, 1988: Rapid ice nucleation by acetone-silver iodide generator aerosols. *J. Wea. Mod.*, **20**, 51-53.

Fitzgerald, J.W., 1975 Approximation formulas for the equilibriun size of an aerosol particle as a function of its dry size and composition and the ambient relative humidity. *J. Appl. Meteor.*, **14**, 1044-1049.

Fukuta, N. and R.C. Schaller, 1976: Ice nucleation by aerosol particles. *Proc. Intnl. Conf Cloud Physics*, 26-30 July, Boulder, CO, 47-52.

Fukuta, N. and R.C. Schaller, 1982: Ice nucleation by aerosol particles: Theory of condensation-freezing nucleation. *J. Atmos. Sci.*, **39**, 648-655.

Gagin, A., 1972: The effect of supersaturation on the ice crystal production by natural aerosols. *J. Rech. Atmos.*, **6**, 175-185.

Garvey, D.M., 1975: Testing of cloud seeding materials at the cloud simulation and aerosol laboratory, 1971-1973. *J. Appl. Meteor.*, **14**, 883-890.

Gerber, H.E., 1976: Relationship of size and activity for AgI smoke particles. *J. Atmos. Sci.*, **33**, 667-677.

Grant, L.O., ed., 1971: The Second Inteernational Workshop on Condensation and Ice Nuclei. Dept. of Atmos. Sci., Colo. St. Univ., Ft. Collins, CO, 149 pp.

Grant, L.O. and R.L. Steele, 1966: The calibration of silver iodide generators. *Bull. Amer. Meteor. Soc.*, **47**, 713-717.

Hallett, J. and S.C. Mossop, 1974: The production of secondary ice particles during the riming process. *Nature*, **249**, 26-28.

Hindman, E., ed., 1985: Ninth Conference on Planned and Inadvertent Weather Modification, 21-23 May, 1984, Park City, Utah, *Bull. Am. Met. Soc.*, **66**, 302-303.

Hindman, E.E., 1989: Formation and optical properties of a warm cloud in a slow-expansion cloud chamber. *J. Atmos. Sci.*, **46**(24), 3653-3663.

Holdroyd, E.W. III, J.T. McPartland, and A.B. Super, 1988: Observations of silver iodide plumes over the Grand Mesa of Colorado. *J. Appl. Meteor.*, **27**, 1125-1144.

Howell, W.E., 1949: The growth of cloud droplets in uniformly cooled air. *J. Meteor.*, **6**, 134-149.

Hsie, E.Y., R.D. Farley and H.D. Orville, 1980: Numerical simulation of ice phase convective cloud seeding. *J. Appl. Meteor.*, **19**, 950-977.

Huffman, P.J., 1973: Supersaturation spectra of AgI and natural nuclei. *J. Appl. Meteor.*, **12**, 1080-1082.

Kahan, A., 1989: Infrared hygrometer. *Measurements and Control*, Feb. 1989, 134-138.

Kochtubadja, B. and D.C. Rogers, 1984: Seeding effects on liquid water and ice crystal concentrations. Ext. Abs. of 9th Conf. on Wea. Mod., 21-23 May, Park City, Utah, 102-103.

Lamb, D., J. Hallett and R.I. Sax, 1981: Mechanistic limitations to the release of latent heat during the natural and artificial glaciation of deep convective clouds. *Quart. J. Roy. Met. Soc.*, **107**, 935-954.

Langer, G, 1973: Evaluation of NCAR ice nucleus counter. Part I. Basic operation. *J. Appl. Meteor.*, **12**, 1000-1011.

Langer, G., G. Cooper, C.T. Nagamoto, and J. Rosinski, 1978: Ice nucleation mechanisms of submicron monodispersed silver iodide, 1,5-Dihydroxynaphthalene and phloroglucinol aerosol particles. *J. Appl. Meteor.*, **17**, 1039-1048.

Lawson, R.P. and R.A. Stewart, 1983: An improved optical ice particle counter. 5th Symp. Meteor. Obs. and Instr., 11-15 April, Toronto, Ont., Canada, 46-53.

Mage, D.T. and J. Noghrey, 1972: True atmospheric pollutant levels by use of transfer function for an analyzer system, *J. Air Poll. Control Assoc.*, **22**, 115-118.

Marwitz, J.D. and R. Stewart, 1982: Microphysical effects of seeding wintertime stratiform clouds near the Sierra Nevada mountains. *J. Appl. Meteor.*, **21**, 874-880.

Matthews, L.A., D.W. Reed, P. St. Amand and R.J. Stirton, 1972: Rate of solution of ice nuclei in water drops and its effect on nucleation. *J. Appl. Meteor.*, **11**, 813-817.

Morrison, B.M., 1989: A characterization of dry ice as a glaciogenic seeding agent. Colorado Sate Univ., Dept. of Atmos. Sci., Atmos. Sci. Paper No. 441, 109.

Mossop, S.C. and K.O.L.F.Jayaweera, 1969: AgI-NaI aerosols as ice nuclei. *J. Appl. Meteor.*, **8**, 241-248.

Nelson, L.D., 1982: Non-contact sensing of atmospheric temperature, humidity and supersaturation. Preprints, AMS Conf. Cloud Physics, 1982, Chicago, Ill., 293-296.

Nimitz K.S. and M. Plooster, 1980: Atmospheric Cloud Physics Laboratory (ACPL) Simulation System Mathematical Description. General Electric Co., Huntsville Operations, Huntsville, Alabama, 89 pp.

Orville, H.D., R.D. Farley and J.H. Hirsch, 1984: Some surprising results from simulated seeding of stratiform-type clouds. *J. Clim. Appl. Meteor.*, **23**, 1585-1600.

Palanisamy, M., K. Thangaraj, R. Gobimathan and P. Ramasamy, 1986: X-ray diffraction and ice nucleation studies of AgI-AgCl solid solutions. *J. Crystal Growth*, **79**, 1005-1009.

Pinnick, R.G., and H.J. Auvermann, 1979: Response characteristics of Knollenberg light-scattering aerosol counters. *J. Aerosol Sci.*, **10**, 55-74 .

Plooster, M.N. and N. Fukuta, 1975: A numerical model of precipitation from seeded and unseeded cold orographic clouds. *J. Appl. Meteor.*, 14, 859-867.

Plooster, M.N., 1985: Computer models for simulation of experiments in the Atmospheric Cloud Physics Laboratory (ACPL). Report 5-31701, Denver Research Institute, Univ. Denver, Denver, CO, 78pp.

Pruppacher, H.R. and J.D. Klett, 1978: *Microphysics of Clouds and Precipitation*. D. Reidel, Boston, 714 pp.

Rauber, R.M., 1981: Microphysical processes in two stably stratified orographic cloud systems. Atmos. Sci. Paper #337, Colo. St. Univ., Ft. Collins, CO., 151 pp.

Rauber, R.M., 1987: Characteristics of cloud ice and precipitation during wintertime storms over the mountains of Northern Colorado. *J. Clim. Appl. Meteor.*, **26**, 488-524.

Reinking, R.F., 1985: An overview of the NOAA Federal-State Cooperative Program in weather modification research, Fourth WMO Sci. Conf. on Wea. Mod., WMO/IAMAP Symposium, Honolulu, WMO /TD-No. 33, Geneva, II: 643-648.

Rogers, D.C., 1982: Field and laboratory studies of ice nucleation in winter orographic clouds. PhD. Dissertation, Dept. of Atmos. Sci., Univ. of Wyoming, 160 pp.

Roger, D.C., 1988: Development of a continuous flow thermal gradient diffusion chamber for ice nucleation studies. *Atmos. Res.*, **22**, 149-181.

Rogers, D.C. and G. Vali, 1987: Ice crystal production by mountain surfaces. *J. Clim. Appl. Meteor.*, **26**, 1152-1168.

Rogers, D.C. and P.J. DeMott, 1990: Measuring nucleation rates in a cloud chamber - Correcting for delays in crystal detection. Preprints of AMS Cloud Physics Conf., San Francisco, CA.

Sackiw, C.M., F.E. Robataille, J.W. Mason, F.D. Barlow, W.G. Finnegan, R.D. Horn, and J.A. Heimbach, Jr., 1984: Comparison test of NCAR ice nucleus counters. Extended abstracts from 9th Conf. on Wea. Mod., Park City, UT, Amer. Meteor. Soc., 12-15.

Saunders, C.P.R. and S. Al-Juboory, 1988: A dynamic processing chamber for ice nuclei filter samples. In *Lecture Notes in Physics: Atmospheric Aerosols and Nucleation Proc. 12th Intnl. Conf. on Atmos. Aer. and Nucl.*, P.E Wagner and G. Vali, eds., Springer-Verlag, 697-700.

Sax, R.I. and P. Goldsmith, 1972: Nucleation of water drops by brownian contact with AgI and other aerosols. *Quart J. Roy. Met. Soc.*, **98**, 60-72.

Schaller, R.C. and N. Fukuta, 1979: Ice nucleation by aerosol particles: Experimental studies using a wedge-shaped ice thermal diffusion chamber. *J. Atmos. Sci.*, **36**, 1788-1802.

Squires, P. and C.A. Gillespie, 1952: A cloud droplet sampler for use on aircraft. *Quart. J. Roy. Meteor. Soc.*, **78**, 387-393.

St. Amand, P., W.G. Finnegan and L. Burkhardt, 1971: Understanding of the use of simple and complex ice nuclei generated from pyrotechnics and acetone burners. *J. Wea. Mod.*, **3**, no. 1, 31-48.

Stith, J.L., D.A. Griffith, R. Lynn Rose, J.A. Flueck, J.R. Miller, Jr., and P.L. Smith, 1986: Aircraft observations of transport and diffusion in cumulus clouds. *J. Clim. Appl. Meteor.*, **25**, 1959-1970.

Stith, J.L. and R.L. Benner, 1987: Applications of fast response continuous SF_6 analyzers to in situ cloud studies. *J. Atmos. Ocean. Tech.*, 4, 599-612.

Stith, J.L., A.G. Detwiler, R.F. Reinking, and P.L. Smith, 1990: Investigating mixing and the activation of ice in cumuli with gaseous tracer techniques. *J. Atmos. Res.*, **25** 195-216.

Super, A.B. and J.A. Heimbach, Jr., 1983: Evaluation of the Bridger Range winter cloud seedng experiment using control guages. *J. Clim. Appl. Meteor.*, **22**, 1989-2011.

Super, A.B. and J.A. Heimbach, Jr., 1988: Microphysical effects of wintertime cloud seeding with silver iodide over the Rocky Mountains. Part II: Observations over the Bridger Range, Montana. *J. Appl. Meteor.*, **27**, 1152-1165.

Super, A.B. and B.A. Boe, 1988: Microphysical effects of wintertime cloud seeding with silver iodide over the Rocky Mountains. Part III: Observations over the Grand Mesa, Colorado. *J. Appl. Meteor.*, **27**, 1166-1182.

Super A.B., B.S. Boe, and E.W. Holdroyd, III, 1988: Microphysical effects of wintertime cloud seeding with silver iodide over the Rocky Mountains, Part I. Experimental design and instrumentation. *J. Appl. Meteor.*, **27**, 1145-1165.

Tomlinson, E.M., 1980: A new horizontal gradient, continuous flow ice thermal diffusion chamber and detailed observations of condensation-freezing and deposition nucleation. PhD. Dissertation, Dept. of Meteor., Univ. of Utah, 108 pp.

Vali, G., 1971: Quantitative evaluation of experimental results on the heterogeneous freezing nucleation of supercooled liquids. *J. Atmos. Sci.*, **28**, 402-409.

Vali, G., 1975: Ice Nucleation Workshop, 1975. *Bull. Am. Met. Soc.*, **56**, 1180-1184.

Vali, G., ed., 1976: Third International Workshop on Ice Nucleus Measurements. Univ. of Wyoming, Laramie, WY, 187 pp.

Vali, G., 1985: Nucleation terminology. *J. Aerosol Sci.*, **16**, 575-576.

Young, K.C., 1974a: A numerical simulation of wintertime orographic precipitation: Part I. Description of model microphysics and numerical techniques. *J. Atmos. Sci.*, 31, 1735-1748.

Young, K.C., 1974b: The role of contact nucleation in ice phase initiation in clouds. *J. Atmos. Sci.*, 31, 768-776.

Young, K.C., 1974c: A numerical simulation of wintertime orographic precipitation. Part II. Comparison of natural and AgI-seeded conditions. *J. Atmos. Sci.*, 31, 1749-1767.

Young, K.C., 1975: The evolution of drop spectra due to codensation, coalescence and breakup. *J. Atmos. Sci.*, 32, 965-973.

Young, K.C., 1977: A microphysical parcel model. 1974 - Revised 20 January 1977. Univ. Arizona, Tuscon, 67pp.

APPENDIX A. ADIABATIC MICROPHYSICAL (PARCEL) CLOUD MODEL OF YOUNG (1974;1977)

A.1 General Description

In broad terms, the model simulates the three major processes of nucleation, diffusion and collection, that are key to precipitation formation. In regard to ice nucleation, the model calculates the contact-freezing nucleation rate and the deposition/sorption nucleation rate as a function of particle size for both natural and one of three potential types of artificial ice nucleating aerosols. Natural ice formation processes are turned off for comparison to cloud chamber experiments and only the model descriptions for nucleation by silver iodide aerosols are used. Further description of the physical and empirical nature of these nucleation routines and cloud droplet formation are given in section A.2. Iterative techniques are used to calculate values of ambient vapor density and temperture based on the difussion equations for heat and water vapor. The trial values are then used to calculate particle temperatures explicitly, including the effect of latent heat release due to accretion. Coalescence and accretion are treated quasi-stochastically (Young, 1975). Collection of cloud droplets by ice particles distinguishes between ice spheres, columns and disks. Coalescence and accretion processes were turned off for the cloud chamber experiment simulations, since the short times

involved precluded their importance. This also allowed the model to run much faster on the MicroVAX workstation.

Four classes of water and ice particles are considered in the model. These are liquid water, freezing water (frozen raindrops or melting particles), spherical ice water (ice crystals < 20 μm diameter or graupel), and ice crystals. The model uses a continuous bin scheme for accounting particles. A separate array of bins exists for each particle type. Spherical particles can occupy any of 48 bins, while ice crystals occupy a 20x20 array sized according to a-axis and c-axis length. Growth and evaporation are permitted. Particle size distributions were specified for the various simulations. For the cloud chamber experiment simulations, the monodisperse or polydisperse AgI-type aerosol sizes used in the particular experiment were input. The natural ice nuclei size distribution was taken from Young (1974b).

No cloud dynamics other than a prescribed updraft are considered. Also, particles remain within the parcel. Thus some care was necessary in the interpretation of results in comparison to longer duration cloud chamber experiments.

A.2 Nucleation in the Cloud Model

Nucleation within the cloud model bears further elucidation, since this is the primary focus for the comparison of experiment versus model results.

A.2.1 Deposition/Sorption Nucleation Mode

This model describes nucleation from the vapor state below and above water saturation. Thus, both depostion and the sorption form of

condensation-freezing are treated. It mimics the semi-quantitative data of Schaller and Fukuta (1979). These authors used a small wedge-shaped ice-thermal gradient diffusion chamber to produce a variety of known temperatures and saturation ratios at which the nucleation rates of various artificial ice nucleating aerosols could be estimated. Nucleation rates were determined as the fraction or percent of the total aerosol population that nucleated in one minute. Young used these experimental fractions (F_{dep}) values and an estimate of the mean surface area of the particles generated for Schaller and Fukuta's tests (~0.13 μm radius AgI aerosols, for example) to compute an areal active site density or coverage (D_{dep}) for deposition/sorption as a function of temperature and ice saturation ratio. Assuming that D_{dep} is independent of particle size and that nucleation occurs stochastically, Young's model calculates the fraction of a given size class j of aerosol particles ($r_p(j)$) instantaneously active under given conditions as,

$$F_{dep} = 1 - \exp\left(- 4\pi\, r_p(j)^2\, D_{dep}\right) \qquad \text{(A1)}$$

If F_{dep} is greater than the percent of artificial aerosol particles of class I already activated, then new ice crystals are formed. An ice nucleus spectrum is thus inherent with the choice of the size distribution and concentration of aerosols input.

Table A1 describes the conditions for which D_{dep} is estimated by various empirical formulations for AgI (Subroutine ARTDEP). Fractional supersaturations with respect to water and ice are abbreviated as s_w and s_i respectively in the table. Figure A1 is the resulting plot of

Table A1. Active Site Coverage for Deposition/Sorption by AgI Aerosols (Original Model)

$s_w \leq 0$:

$s_i \leq 0$	$s_w < -.0658$	$0 > s_w \geq -.0658$
No Ice	$s_i = s_i$	$s_i = s_i - .76(s_w) - .05$
	$D_{dep} = 10^{10} (s_i)^{2.6}$	$D_{dep} = 10^{10} (s_i)^{2.6}$

$s_w > 0$:

$s_w > .0147\ (268.7-T)$		$s_w \leq .0147\ (268.7-T)$	
$T = T - 6.6\ (s_w)$		$P = 2.25 - 5(s_w)$	
$T_x = 266.96 + 300\ (s_w)$			
$T \geq 268.7$	$T < 268.7$	$T \geq T_x$	$T < T_x$
No Ice	$D_{dep} = 3.9 \times 10^6\ (268.7-T)^{2.55}$	No ice	$C = 5.364 - .145\ (s_w)/(.01 + s_w) - 700\ (s_w)^3$
			$D_{dep} = 10^C\ (T_x-T)^P$

D_{dep} as a function of temperature and supersaturation with respect to ice and water.

The model formulation appears to be seriously in error for water supersaturations greater than a few percent, particularly at cold temperatures, where D_{dep} can take on the same value for two different values of s_w below $s_w = .0147\ (268.7-T)$. Admittedly, the supersaturations (shown in Figure A1) at which this erroneous behavior occurs are greater than can typically be achieved naturally. However,

due to the same error, the formulation begins to underestimate D_{dep} at temperatures as warm as -12°C for s_w in the atmospheric range. A discontinuity also occurs at $s_w \sim .03$ to .05 and as warm as -7°C, along the line $s_w = .0147\ (268.7 - T)$, because of the error in the mathematical description.

New ice formed by deposition/sorption enters the ice mass as 1.6 μm radius spherical ice particles. The ice remains and grows spherical until it is 20 μm along both the a and c-axes. At this point it enters the ice water category.

A similar routine also exists in the model for deposition/sorption by natural aerosols (Subroutine NATDEP). This appears to be based on data from Fukuta and Schaller (1976) for "local soil" and kaolinite. A few model experiments were performed to test the influence of natural ice in experiments with artificial ice nucleus aerosols. However, since the amounts of ice formed were small at temperatures warmer than -20°C and since natural aerosols are effectively eliminated by filtering air for cloud chamber experiments, natural deposition/sorption nucleation was turned off in the model for experimental comparison. Separate new formulations for deposition and sorption (termed condensation-freezing here) are used in the modified version of the model.

A2.2 Condensation and Natural Droplet Freezing Nucleation

In this portion of the model (CONDNS), the number of CCN activated is calculated for each time step during which the effective s_w is calculated to exceed its previous maximum value. New droplets enter as 2.1 μm radius particles. The effective s_w is calculated for a reference temperature of 20°C, using the theoretical temperature dependence of

Table A2: Condensation Nucleation, Natural Condensation-Freezing and Natural Immersion-Freezing Nucleation (Original Model)

CCN routine:

$\underline{T \geq 273.16}$

$K = 3.667 - .00893(T)$

$\underline{T < 273.16}$

$\underline{T \geq 253.16}$

$K = 4.765 - .01295(T)$

$\underline{T < 253.16}$

$K = 5.625 - .01635(TAM)$

$$N_d = N_0 \, (100(s_w)/K)^B$$

Natural Condensation-Freezing and Immersion-Freezing Routine:

$\underline{268.16 \geq T > 263.16}$

$F_{imfn} = 0.006 \, (10^{((T-263.16)\ RM2 + 26\ (RM1))})$

$\underline{263.16 \geq T > 237.16}$

$F_{imfn} = (0.006) \, 10^{((T-237.16)\ RM1)}$

F_{imfn} : fraction of natural droplet population frozen

RM1, RM2 : (-.126, -.506) standard values.

the critical s_w. The number activated as cloud droplets is determined by adjustable N_o and B parameters in a power law of the form $N_d = N_0(s_w)^B$ (see Table A2). No literature reference is given for the natural condensation nucleus spectrum used in the model. For simulation of cloud chamber experiments, N_o and B were chosen based on experimental versus model comparison of cloud droplet formation on a known concentration of the CCN aerosols used. Potential weaknesses of this description are that no time step reduction occurs (unless specified in the input file) to accurately predict initial cloud

formation (probably wouldn't help since drops begin as 2.1 μm radius drops) and CCN spectrum parameters is the only input option.

After 1977, a natural condensation and immersion-freezing routine was added to our version of the model based on Vali (1971) (personal communication with Dr. Robert Kelly, University of Wyoming Department of Atmospheric Sciences). This was not activated in this study. The fractions of the droplet population that will freeze at a given temperature are determined by adjustable coefficients in the equations shown in Table A2. Weaknesses of this routine are that ambient temperature, not droplet temperature, is used as the freezing temperature, and droplet volume effects are not explicitly treated. Still, this method was useful as a guide for parameterization of artificial immersion-freezing nucleation.

A.2.3 Homogeneous-Freezing, Scavenging and Contact-Freezing

A single model routine (Subroutine CONDFRZ) performs procedures for homogeneous condensation-freezing nucleation, scavenging of ice nucleus aerosols of various types by both liquid and ice particles, and contact-freezing nucleation resulting from nucleus-droplet collisions. The homogeneous-freezing scheme was not referenced as to its source. Therefore, it was altered to represent that of Pruppacher and Klett (1978), as discussed by DeMott and Rogers (1990). This was done by fitting an empirical formulation to the results of computations given in tabular form in Pruppacher and Klett. Homogeneous-freezing was of no importance to the research reported in this dissertation, since it occurs mostly below -30°C.

The primary procedure performed is computation of the removal (scavenging) of ice nucleus aerosols by all the categories of water present (ice water (IW), spherical ice water (SIW), and liquid water (LW) in this study). Contact-freezing nucleation results from the segment where particles are scavenged by liquid water. The combined (additive) effects of Brownian collection, thermophoresis, diffusiophoresis and aerodynamic capture are considered. Calculations of collection rates and kernels closely follow the equations from Young (1974). The routine considers first the collection of particles of one size by cloud droplets of all sizes present, then increments particle size and repeats the process. Ice nucleation occurs only when the particles collected are "active" (areal active site coverage based on Fukuta and Schaller (1976)) at the drop temperature and then only when the active fraction of a given size is greater than the fraction already activated by deposition/sorption. Provisions were made in the code to keep track of these particles after scavenging. Ice nucleated in this routine grows initially as spherical ice, starting at frozen droplet size.

The maximum fractional activity of various aerosol sizes for contact-freezing nucleation by AgI is determined from the equations,

$$D_{ctf} = 1x10^{10} \ (s_i - .05)^{2.6} \qquad \text{(A3)}$$

$$F_{ctf} = 1 - \exp(-\ 4\pi\ r_p(j)^2\ D_{ctf}) \qquad \text{(A4)}$$

The quantity D_{ctf} is just the areal coverage (density) of active sites for contact-freezing , again estimated from Fukuta and Schaller(1976).

Table A3: Scavenging Relevant to Contact-Freezing Nucleation

Thermophoresis:

$$Y = 4\pi r_d(k)\ kcon\ (1 + .3RELW(J)^{.5}\ (PR)^{.33})\ (T - TLW(k))$$

$$TH = 4.185x10^7\ (f_{th}(x))\ (Y)/P \qquad \text{[Eq. 1 Young,1974b]}$$

$$f_{th}(x) = \frac{.4\ (1 + x(1.45 + .4\ \exp(-1/x)))\ (kcon + .175x)}{(1 + 3x)\ (2\ kcon + .007 + .035x)}$$

$$X = (\text{Knudsen \#}) = \gamma_a/r_p(j)$$

$$PR = (\text{Prandtl \#}) = 0.71280174$$

Diffusiophoresis:

$$Z = \frac{4\pi\ r_d(k)^2\ D\ (\rho_v - \rho_{vx})\ (1 + BRCY\ (RELW(k)^{.5}))\ (1.1409/\rho_a)}{(r_d(k) + 25\ d\ (2\pi/R_a\ T)^{.5})} \qquad \text{[Eq. 2 Young,1974b]}$$

$$BRCY = .3\ (\eta/(D_p\rho_a))^{.33}$$

Brownian Collection:

$$BR = 4\pi D_p\ r_d(k)\ (1 + BRCY\ (RELW(k)^{.5})) \qquad \text{[p.771 Young, 1974b]}$$

Aerodynamic Capture:

$$AC = \pi\ r_d(k)^2\ CE\ |VT_d(k) - VT_p|$$

Net Collection Kernel:

$$PCHG = (\Delta t/V)\ (BR + TH + ZZ + AC)$$

where,

D_p: diffusivity of aerosol particles in air

D: diffusivity of water vapor

T: ambient temperature

ρ_a: density of air

P: pressure

TLW(k): droplet temperature

ρ_v: ambient absolute vapor density

ρ_{vx}: vapor density at droplet surface

$r_d(k)$: radius of drop class k

RELW(k): Reynold's # for drop class k
$r_p(j)$: radius of particle class j

kcon: thermal conductivity of air
$VT_d(k)$: terminal velocity of water droplets

VT_p: terminal velocity of aerosol particles

R_a: gas constant of dry air
γ_a: mean free path of air molecules
ρ_a: air density
Δt: time step
V: parcel volume
CE: collision-collection efficiency

Then,

PCHG = PCHG(XNLW(k))

PCHG = 1 - exp(-PCHG)

PCHG = PCHG(YN(j))

$N_p(j) = N_p(j)$ - PCHG

XNLW(k): number concentration of droplets of class k

$N_p(j)$: concentration of aerosols in class j

No ice is permitted for $s_i \leq .05$ for AgI and .12 for natural aerosols. The fractional percent active (PCT = F_{ctf}) is plotted as a function of particle radius and s_i for AgI-type aerosols in Figure A2. Considering standard results at water saturation in the CSU isothermal cloud chamber (see, for example, DeMott et al., 1983), the AgI curves used in the model appear greatly underestimated for most AgI aerosols produced for cloud seeding. However, any desired experimental results can be accomodated by the model (through D_{ctf}) if activity as a function of particle size is known.

New ice is formed only if F_{ctf} is greater than the percent already activated as deposition nuclei. Then, only a fraction of F_{ctf} is realized in a given time step, based on the fraction of class j particles scavenged. Table A3 summarizes the equations governing the scavenging of aerosols. Thermo- and difusiophoretic, brownian, and aerodynamic transport processes are considered.

The calculations presented in Table A3 are repeated for all droplet classes, then particle class I is incremented and the whole series repeated until all sizes of particles are covered. These same collection type calculations are also made for freezing water, spherical ice water, and ice water categories. These are done for natural and/or AgI-type aerosols.

A.2.4 Mechanistically Differentiated Results

Modifications were made to Young's original code to keep track of nucleation by the various modes and the elimination of potential nucleation aerosols by scavenging processes. Examples of mechanistically differentiated results are given in the body of this dissertation.

A.3 New Nucleation Routines

The derivation and presentation of new nucleation routines is given in the main body of this dissertation. For comparison purposes, the form of the modified routines is given here.

Table A4

Summary of Nucleation Activity Descriptions (New Versions)

Mechanism	AgI-AgCl	AgI-AgCl-4NaCl
Deposition:		
$T < 269.2°K$		$T \geq 269.2°K$
$S_w > -8\%$		No Ice
$D_{dep} = a\,(S_i - .65S_w - 5)^b$	$a = 5.018 \times 10^5$ $b = 1.493$	$a = 5.8655 \times 10^6$ $b = 1.3462$
$S_w \leq -8\%$		
$D_{dep} = a\,(S_i)^b$		
Contact-freezing:		
$s_i > 0.055$		$s_i \leq 0.05$
$D_{ctf} = a(s_i - 0.055)^b$	$a = 1.198 \times 10^{12}$ $b = 1.98$	No Ice
Immersion-freezing:		
$F_{imd} = a(S_w)^b$	$a = 0.05$ $b = 1.8$	$a = 0.123 - 2.85 \times 10^5 r_p$ $b = 2.205 - 5.0 \times 10^5 r_p$
$T < 268.2°K$		$T \geq 268.2°K$
$D_{imf} = a(268.2 - T)^b$	$a = 1.688 \times 10^5$ $b = 4.0$	$a = 1.688 \times 10^5$ $b = 4.0$	No Ice
Condensation-freezing:		
$D = a(270.2 - T)^b (S_w)^c$	$a = 3.445 \times 10^4$ $b = 4.83558$ $c = 2$	$a = 6.583 \times 10^6$ $b = 4.7295$ $c = 2$

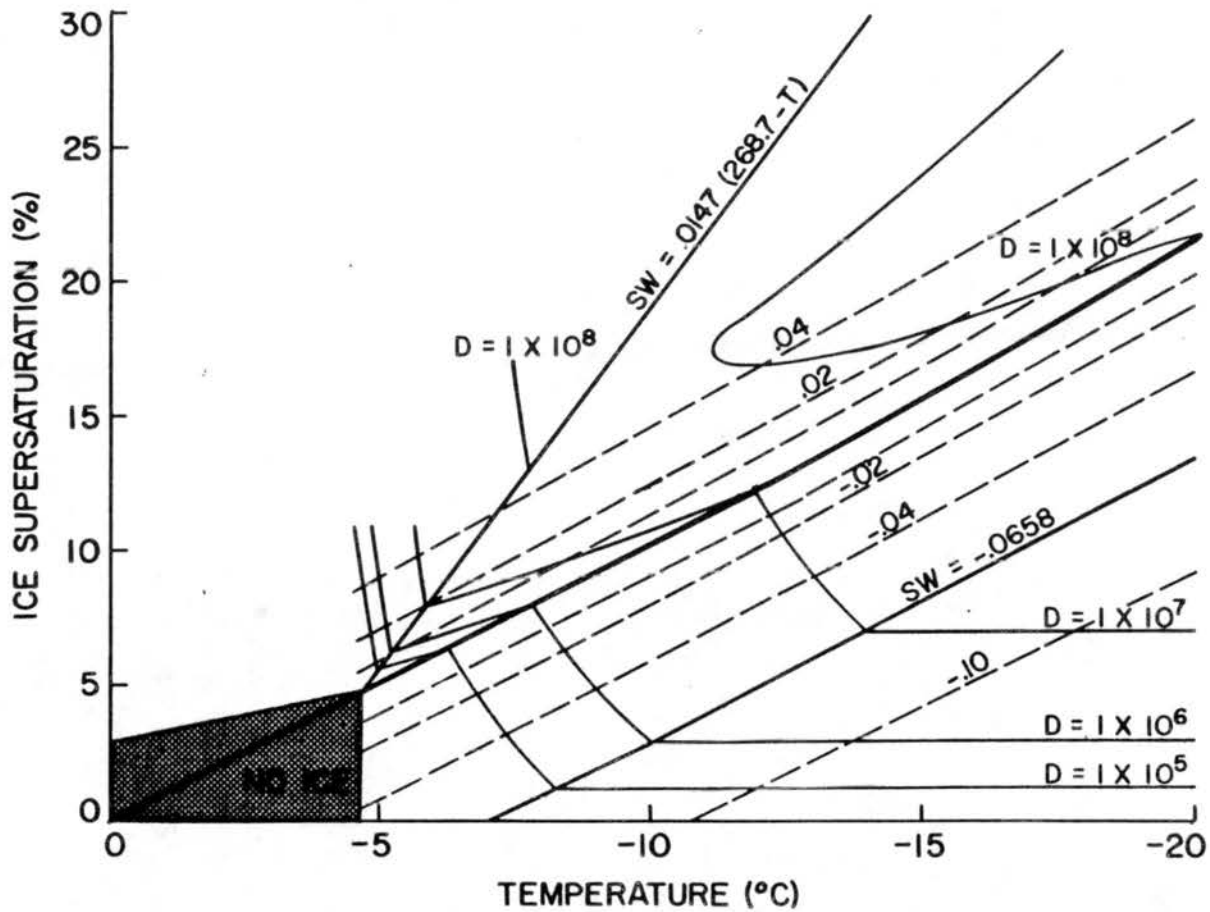

Figure A1 Deposition/sorption nucleation active site density (D_{dep}) on an ice supersaturation-temperature plane, as parameterized in the original model version.

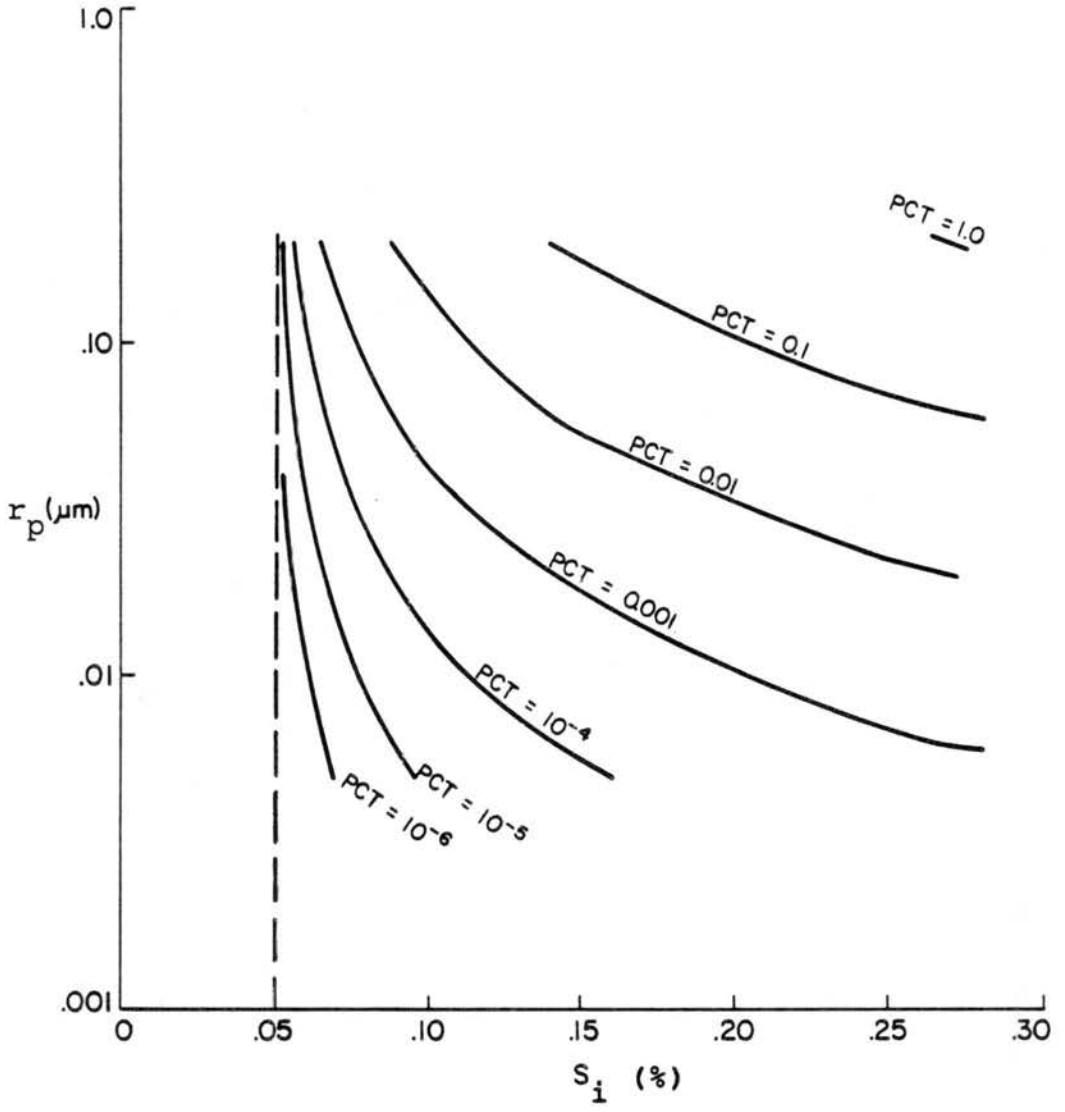

Figure A2 Fractional percentage activity (PCT = F_{ctf}) by contact-freezing nucleation as a function of aerosol size and ice supersaturation.

APPENDIX B: LISTS OF EXPERIMENTS

This appendix contains two tables. The first table lists pertinent information concerning all of the dynamic cloud chamber experiments for which data were reduced and analyzed for this dissertation. This table gives the number of the experiment (###year), the type of experiment (chemical type, CCN added or not, simulated updraft rate), the particle size used, the temperature at which cloud formed, the temperature at which aerosols were injected (pre- means before cloud formed), and the number of aerosols injected into the chamber. In Table B1, AAN and AA refer to AgI-AgCl-4NaCl and AgI-AgCl aerosols, respectively. Polydisperse aerosols are indicated by the abbreviation "poly". The second table summarizes initialization data for the numerical model experiments performed for comparison to cloud chamber experiments. All data are accessible through the staff of the Colorado State University Cloud Simulation and Aerosol Laboratory.

TABLE B1
LIST OF DCC CONTINUOUS EXPANSION TESTS

Expt. No.	Type	Size (μm)	Tcloud (^{o}C)	Tinj (^{o}C)	N_p
7988	AAN,2.5m/s	.03	0	pre-	3.10×10^{7}
6588	AAN,2.5m/s	.03	0	pre-	4.50×10^{7}
6488	AAN,2.5m/s	.07	0	pre-	1.55×10^{8}
6688	AAN,2.5m/s	poly	0	pre-	2.50×10^{8}
14788	AAN,no CCN,2.5m/s	.07	-6	pre-	1.60×10^{8}
14188	AAN,2.5m/s	.03	-6	pre-	4.20×10^{7}
14088	AAN,3.5m/s	.03	-7	pre-	7.20×10^{7}
13888	AAN,5.0m/s	.03	-6	pre-	6.70×10^{7}
13988	AAN,5.0m/s	.03	-6	pre-	6.50×10^{7}
13788	AAN,2.5m/s	.07	-6	pre-	1.30×10^{8}
3289	AAN,no CCN,2.5m/s	.07	-7	pre-	2.15×10^{8}
13288	AAN,3.5m/s	.07	-6	pre-	1.55×10^{8}
13488	AAN,5.0m/s	.07	-6	pre-	1.10×10^{8}
13388	AAN,2.5m/s	poly	-6	pre-	1.55×10^{8}
13188	AAN,5.0m/s	poly	-6	pre-	9.00×10^{7}
14288	AAN,2.5m/s	.03	-8.5	pre-	4.10×10^{7}
5788	AAN,2.5m/s	.03	-9	pre-	6.00×10^{7}
2789	AAN,no CCN,2.5m/s	.03	-7.5	pre-	1.00×10^{8}
3389	AAN,no CCN,2.5m/s	.03	-8.3	pre-	1.80×10^{8}
6388	AAN,no CCN,2.5m/s	.03	-8	pre-	1.00×10^{8}
12988	AAN,5.0m/s	.03	-8	pre-	3.60×10^{7}
3189	AAN,5.0m/s	.03	-8	pre-	1.00×10^{8}
2989	AAN,no CCN,5.0m/s	.03	-9	pre-	1.45×10^{8}
8488	AAN,2.5m/s	.07	-8.8	pre-	5.50×10^{7}
2889	AAN,no CCN,2.5m/s	.07	-8.3	pre-	3.25×10^{8}
6288	AAN,no CCN,2.5m/s	.07	-8	pre-	3.90×10^{8}
8288	AAN,5.0m/s	.07	-8	pre-	8.40×10^{7}
13688	AAN,5.0m/s	.07	-8	pre-	1.80×10^{8}
3089	AAN,no CCN,5.0m/s	.07	-9.3	pre-	2.80×10^{8}
3789	AAN,no CCN,5.0m/s	.07	-9	pre-	2.20×10^{8}
6788	AAN,2.5m/s	poly	-9	pre-	1.80×10^{8}
13088	AAN,5.0m/s	poly	-8	pre-	2.10×10^{8}
3088	AAN,5.0m/s	.07	-10	pre-	2.50×10^{7}
3188	AAN,5.0m/s	.07	-10	pre-	2.90×10^{7}
6088	AAN,2.5m/s	.03	-13	pre-	4.30×10^{7}
14388	AAN,5.0m/s	.03	-11.7	pre-	3.10×10^{7}
5988	AAN,2.5m/s	.07	-14	pre-	5.30×10^{7}
3488	AAN,2.5m/s	.07	-13.5	pre-	4.40×10^{7}
5888	AAN,2.5m/s	.07	-13.5	pre-	2.00×10^{8}
14488	AAN,5.0m/s	.07	-14	pre-	1.25×10^{8}
6888	AAN,2.5m/s	poly	-13.5	pre-	1.25×10^{8}
14688	AAN,5.0m/s	poly	-13.5	pre-	2.20×10^{7}
8088	AAN,2.5m/s	.03	0	-8	5.10×10^{7}
8188	AAN,2.5m/s	.07	0	-8	8.80×10^{7}
6188	AAN,2.5m/s	.07	-8	-9	6.10×10^{7}
3689	AAN,2.5m/s	.03	-10	-10.5	5.20×10^{7}
3489	AAN,2.5m/s	.03	-8	-12	8.60×10^{7}
3589	AAN,2.5m/s	.07	-8	-12	1.00×10^{8}
7488	AA,2.5m/s	poly	0	pre-	3.20×10^{8}

Table B1 (Continued)

Expt. No.	Type	Size (μm)	Tcloud (^{o}C)	Tinj (^{o}C)	N_p
7588	AA,2.5m/s	.07	0	pre-	2.80×10^{8}
7688	AA,2.5m/s	.03	0	pre-	1.80×10^{8}
11488	AA,no CCN,5m/s	.07	-4	pre-	1.60×10^{8}
11688	AA,1.5m/s	.03	-4.5	pre-	1.70×10^{8}
7987	AA,2.5m/s	.03	-6	pre-	1.70×10^{7}
1289	AA,2.5m/s	.03	-6	pre-	2.00×10^{8}
11588	AA,3.5m/s	.03	-5.5	pre-	1.40×10^{8}
11788	AA,5.0m/s	.03	-5.5	pre-	3.00×10^{8}
11888	AA,no CCN,5m/s	.03	-5.5	pre	2.20×10^{8}
11288	AA,1.5m/s	.07	-6	pre-	2.00×10^{8}
9388	AA,2.5m/s	.07	-6	pre-	1.62×10^{8}
11188	AA,3.5m/s	.07	-6	pre-	1.60×10^{8}
11388	AA,5.0m/s	.07	-6	pre-	1.90×10^{8}
6087	AA,2.5m/s	.03	-8.2	pre-	1.40×10^{8}
0689	AA,2.5m/s	.03	-8	pre-	1.90×10^{8}
8988	AA,2.5m/s	.03	-9	pre-	1.38×10^{8}
9588	AA,2.5m/s	.03	-8.5	pre-	1.38×10^{8}
0789	AA,no CCN,2.5m/s	.03	-8	pre-	2.20×10^{8}
12188	AA,5.0m/s	.03	-6.5	pre-	1.50×10^{8}
12088	AA,no CCN,5.0m/s	.03	-8	pre-	2.20×10^{8}
1489	AA,no CCN,5.0m/s	.03	-8.5	pre-	3.00×10^{8}
9288	AA,2.5m/s	.05	-8	pre-	1.98×10^{8}
9688	AA,2.5m/s	.07	-7	pre-	1.74×10^{8}
7088	AA,2.5m/s	.07	-9	pre-	1.00×10^{8}
9188	AA,2.5m/s	.07	-7.8	pre-	1.72×10^{8}
1389	AA,no CCN,2.5m/s	.07	-8	pre-	2.40×10^{8}
9788	AA,5.0m/s	.07	-8.3	pre-	1.68×10^{8}
1889	AA,no CCN,5.0m/s	.07	-8	pre-	2.60×10^{8}
9088	AA,2.5m/s	poly	-8	pre-	1.54×10^{8}
11988	AA,1.5m/s	.07	-10	pre-	3.60×10^{8}
7788	AA,2.5m/s	.03	-12.9	pre-	1.50×10^{8}
1989	AA,2.5m/s	.03	-11.5	pre-	2.70×10^{8}
2189	AA,no CCN,2.5m/s	.03	-12	pre-	2.60×10^{8}
1589	AA,no CCN,5.0m/s	.03	-12	pre-	2.40×10^{8}
9489	AA,2.5m/s	.05	-11	pre-	1.35×10^{8}
7888	AA,2.5m/s	.07	-12.6	pre-	2.75×10^{8}
2089	AA,2.5m/s	.07	-12	pre-	1.90×10^{7}
2289	AA,no CCN,2.5m/s	.07	-12.6	pre-	2.45×10^{8}
1789	AA,5.0m/s	.07	-12.5	pre-	1.90×10^{8}
1689	AA,no CCN	.07	-12	pre-	2.85×10^{8}
2489	AA,2.5m/s	.07	-16	pre-	2.15×10^{8}
6187	AA,2.5m/s	.03	4.5	-4.3	2.00×10^{8}
7188	AA,2.5m/s	.07	0	-8	1.00×10^{8}
7288	AA,2.5m/s	.03	0	-8	1.20×10^{8}
7388	AA,2.5m/s	poly	0	-7.9	2.00×10^{8}
0589	AA,2.5m/s	.03	-10	-10.2	1.85×10^{8}
8087	AA,2.5m/s	.03	-6	-9.8	1.70×10^{7}
5787	AA,2.5m/s	.03	0	-10.5	1.00×10^{8}
2589	AA,2.5m/s	.03	0	-12	1.60×10^{8}
2689	AA,2.5m/s	.07	-8	-12	1.80×10^{8}

Table B2

NUMERICAL MODEL SIMULATION INITIALIZATION DATA

Expt. No.	Type	P(mb)	T(°C)	AH($g\ m^{-3}$)	"w"($cm\ s^{-1}$)	NO(cm^{-3}) (P = 1)	run time(s)	#inj	size(μm)	expt. time(s)
6087	AA	614	-5.1	2.85	250	500	600	1.40E8	.03	95
7987	AA	614	-5.1	3.00	250	2700	600	1.70E7	.03	0
12188	AA	614	-5.1	3.10	500	700	350	1.50E8	.03	205
14188	AAN	610	-5.0	3.20	250	1500	600	4.20E7	.03	115
5788	AAN	614	-5.1	2.70	250	2800	600	6.00E7	.03	405
6088	AAN	579	-10.1	1.95	250	300	400	4.30E7	.03	350
7788	AA	565	-10.0	1.97	250	700	300	1.50E8	.03	375
7888	AA	565	-10.1	2.00	250	1000	300	2.75E8	.07	495
8288	AAN	614	-5.1	2.85	500	1200	350	8.40E7.	.07	100
8488	AAN	614	-5.1	2.65	25	3000	500	5.50E7	.07	250
12988	AAN	614	-5.1	2.75	500	1200	300	3.60E7	.03	45
14088	AAN	610	-5.0	3.20	350	2300	530	7.20E7	.03	180
13888	AAN	610	-5.0	3.20	500	2000	300	6.70E7	.03	35
13788	AAN	614	-5.1	3.00	250	3200	600	1.30E8	.07	205
123288	AAN	610	-5.0	3.10	350	2500	530	1.55E8	.07	195
13488	AAN	610	-5.0	3.10	500	2500	300	1.10E8	.07	75
14388	AAN	579	-10.1	2.10	50	2500	200	3.10E7	.03	40
9388	AA	610	-5.0	3.20	250	700	600	1.62E8	.07	280
11188	AA	610	-5.0	3.20	350	700	450	1.60E8	.07	255
11388	AA	610	-5.0	3.10	500	750	300	1.90E8	.07	197
11588	AA	610	-5.0	3.30	350	1000	450	1.40E8	.03	245
11788	AA	610	-5.0	3.30	500	1000	320	3.00E8	.03	215
11288	AA	610	-5.0	3.25	150	800	600	2.00E8	.07	220
11688	AA	610	-4.0	3.50	150	750	600	1.70E8	.03	390
9188	AA	614	-5.1	2.80	250	1800	600	1.72E8	.07	220
9788	AA	614	-5.1	2.80	500	1500	300	1.68E8	.07	130
7988	AAN	672	1.0	5.00	250	3000	1100	3.10E7	.03	255
6488	AAN	672	1.0	5.00	250	5500	1100	1.55E8	.07	615
6688	AAN	672	1.0	5.00	250	5000	1100	2.50E8	poly	180
8088	AAN	660	-5.0	2.95	250	800	0/40/400	5.10E7	.03	-
8188	AAN	660	-5.0	2.95	250	800	90/40/400	8.80E7	.07	-
7588	AA	660	1.0	5.00	250	6000	1100	2.80E8	.07	165
7688	AA	660	1.0	5.00	250	5000	1100	1.80E8	.03	195
7188	AA	610	-5.0	2.95	250	1000	90/40/400	1.00E8	.07	945
7288	AA	610	-5.0	2.95	250	800	90/40/400	1.20E8	.03	870
7088	AA	610	-5.0	2.70	250	2800	600	1.00E8	.07	240
9588	AA	610	-5.0	2.75	250	2000	600	1.38E8	.03	95
9688	AA	610	-5.0	2.95	250	3200	600	1.74E8	.07	85
8988	AA	610	-5.0	2.65	250	1800	600	1.38E8	.03	295
1789	AA	565	-10.0	1.97	500	1500	200	1.90E8	.07	80
5988	AAN	579	-10.1	1.93	250	300	300	5.30E7	.07	210
9088	AA	614	-5.1	2.80	250	1800	500	1.54E8	poly	-
13388	AAN	614	-5.1	3.20	250	3000	500	1.55E8	poly	-
13088	AAN	614	-5.1	2.85	500	1200	350	2.10E8	poly	-
13188	AAN	614	-5.1	3.20	500	2500	350	9.00E7	poly	-
6788	AAN	614	-5.1	2.75	250	2000	500	1.80E8	poly	-
6888	AAN	579	-10.1	1.95	250	300	400	1.25E8	poly	-
7488	AA	660	1.0	5.00	250	5500	1000	3.20E8	poly	-
7388	AA	660	1.0	5.00	250	1000	90/40/400	2.00E8	poly	-